Deciphering the *in vivo* role of the *Drosophila* RNA-binding protein Imp in cell motility

Clare Alexandra Pritchard

January 2016

This thesis is submitted
for the Degree of Doctor of Philosophy

NOTICE OF SUBMISSION OF THESIS FORM:
POSTGRADUATE RESEARCH

DECLARATION

This work has not been submitted in substance for any other degree or award at this or any other university or place of learning, nor is being submitted concurrently in candidature for any degree or other award.

Signed …… (candidate) Date ……

STATEMENT 1

This thesis is being submitted in partial fulfillment of the requirements for the degree of PhD

Signed …… (candidate) Date ……

STATEMENT 2

This thesis is the result of my own independent work/investigation, except where otherwise stated. Other sources are acknowledged by explicit references. The views expressed are my own.

Signed …… (candidate) Date ……

STATEMENT 3

I hereby give consent for my thesis, if accepted, to be available for photocopying and for inter-library loan, and for the title and summary to be made available to outside organisations.

Signed …… (candidate) Date ……

STATEMENT 4: PREVIOUSLY APPROVED BAR ON ACCESS

I hereby give consent for my thesis, if accepted, to be available for photocopying and for inter-library loans after expiry of a bar on access previously approved by the Academic Standards & Quality Committee.

Signed …… (candidate) Date ……

To Mum & Dad

Acknowledgements

Firstly I would like to thank my supervisor Sonia López De Quinto for her invaluable guidance, enthusiasm, patience and unwavering faith in me throughout my PhD. It has been a pleasure to work for her over the last four years and I am grateful for all of her help, particularly during the difficult times. I would also like to thank our collaborator Prof. Will Wood at the University of Bristol for his help, providing fly lines and for making the many trips to his lab to carry out confocal imaging possible, which were essential to this project. I also owe a huge thanks to Kate Comber and other members of the Wood lab for training and advice. Thank you to Wynand Van der Goes van Naters for the hours he spent injecting fly embryos for my project and for training me to do it myself! I would also like to thank Helen White-Cooper for her advice and support over the years.

To all my colleagues in the fly labs past and present – Leanne, Alina, Gordon, Simona, Ryan, Karen, Jesús, David, Kevin and everyone else in W3.25 - thank you for your friendship, support and the many pints we've shared. For their endless faith in me and the many fun times we've spent together over the years I thank my good friends Nardiah, Leanne, Kirsty, Ellen, Charlie, Tom, Zoe, Ryan and Gordon. Thank you to Charlie for many hours of study dates. You kept me writing through the hard times with support, tea and marshmallows! I owe a huge thank you to Nardiah who has been there for me throughout all of the good and bad times. Felix, thank you for putting up with me and for all of your patience and support. You always believed in me whenever I doubted myself.

Lastly, but by no means least, thank you to my wonderful Mum and Dad, to whom I owe everything. Without your constant love and support over the years I would not be where I am now and so this thesis is dedicated to you.

Whilst studying for my PhD I was funded by the BBSRC.

Summary

Cultured motile cells show a highly enriched belt of actin at the tip of their lamellipodial protrusions, termed the leading edge. It is at this leading edge that researchers have uncovered pools of highly localized mRNAs encoding actin and actin-regulatory proteins, including β-actin, Profilin, Cofilin and all seven subunits of the Arp2/3 complex, whose local translation is then required for proper cell migration. The localization and local translation of these mRNAs are regulated by RNA-binding proteins, including Imp, which localizes *β-actin* mRNA at the leading edge. However, published studies have so far failed to determine if Imp is required to localize *β-actin* mRNA and/or other mRNAs at the leading edge of migratory cells *in vivo*.

Our examination of *Drosophila* embryonic macrophage migration *in vivo* revealed that actin is not enriched at the leading edge, compared with cultured macrophages, demonstrating that a single cell population employs different mechanisms of cytoskeletal arrangement when migrating *in vivo*, compared with an *ex vivo* migration along a 2D substrate. It is therefore not surprising that we did not observe Imp at the leading edge of macrophages *in vivo*. However, overexpression of Imp reduced both the velocity and directionality of macrophages and inhibited cell-to-cell contact inhibition, suggesting a defect in microtubule dynamics, although we have yet to establish a mechanism for this.

We show that Imp binds the 3'UTR of *β-actin*, *profilin*, and *β-integrin* mRNAs and reveal three sites of primary sequence that are required for Imp binding to *β-actin* mRNA. Our results suggest that, in contrast to cultured migratory cells, *β-actin* mRNA is unlikely to be localized to, and locally translated, at the leading edge of macrophages *in vivo*. However, cytoplasmic mRNA regulation is likely to play some kind of role in cell migration, as revealed by overexpression of Imp, which impairs macrophage motility. This thesis highlights a crucial requirement for studies to determine the mechanisms of cytoplasmic mRNA regulation in motile cells *in vivo*, which appear to be distinct from those employed in some cultured cells.

Contents

Abbreviations

2D	Two-dimensional
3D	Three-dimensional
4e-BP	Eukaryotic initiation factor 4E-binding proteins
Act42A	Actin42A
Act5C	Actin5C
APF	After puparium formation
ARP2/3	Actin-related protein complex 2/3
BSA	Bovine serum albumin
CBEP	Cytoplasmic Polyadenylation Element Binding Protein
CDS	Coding sequence
Chic	Chickadee
ConA	Concanavalin A
crq	*croquemort*
Ct	C-terminal
dsRNA	Double-stranded RNA
ECM	Extracellular matrix
EGF	Epidermal growth factor
eIF	Eukaryotic initiation factor
FA	Focal adhesion
FAC	Focal adhesion complex
FISH	Fluorescence *in situ* hybridization
FLP	Flippase
FRT	Flippase recognition target
GFP	Green Fluorescent Protein
GMA	GFP-moesin
GW	Gateway cassette
hnRNP	Heterogeneous Ribonucleoprotein
hsp	Heatshock Protein
IBE	Imp Binding Element
IGF-II	Insulin-like growth factor 2
Imp	Insulin-like Growth Factor 2 (IGF-II) mRNA-binding Protein
JAK/STAT	Janus Kinase and Signal Transducer and Activator of Transcription

KH	K-Homology
Khc	Kinesin heavy chain
LB	Luria-Bertani
MARCM	Mosaic analysis with a repressible cell marker
mCh	mCherry
MCP	MS2 coat protein
MLP1	Muscleblind-like Splicing Regulator 1
MT	Microtubule
MTD	Maternal triple Gal4-driver
MTOR	Mechanistic target of rapamycin
MTORC	Mammalian target of rapamycin complex
mys	*myospheroid*
MZT	Maternal-to-zygotic transition
NLS	Nuclear localization signal
Nt	N-terminal
Osk	Oskar
PATx	1% BSA, 0.1% Triton-X in PBS
PBS	Phosphate-buffered saline
pBS	pBlueScript
PBT	0.1% Triton-X in pBS
PCM	Pericentriolar material
PCR	Polymerase chain reaction
PDGF	*Platelet-derived Growth Factor*
PDGF/VEGF	Platelet-derived Growth Factor/Vascular Endothelial Growth Factor
PI3K	Phosphatidylinositol-4,5-bisphosphate 3-kinase
pMAT	Maternal tubulin Gal4-driver
pMat	Maternal tubulin promoter
PMY	Peptide-methionine-tyrosine
PTB	Polypyrimidine-tract Binding Protein
PVF	PDGF/VEGF ligand
PVR	PDGF/VEGF receptor
qPCR	Quantitative polymerase chain reaction
qRT-PCR	Quantitative reverse transcriptase polymerase chain reaction
RBP	RNA-binding protein
RIP	RNA-immunoprecipitation

RNA polII	RNA Polymerase II
RNP	Ribonucleoprotein
RRM	RNA-recognition Motif
RT-PCR	Reverse transcriptase polymerase chain reaction
S2	Schneider-2
S2R+	Schneider-2 receptor plus
SDM	Site directed mutagenesis
SDS-PAGE	Sodium dodecyl sulfate-polyacrylamide gel electrophoresis
slbo	*slow border cells*
srp	*serpent*
tdMCP	Tandem MS2 coat protein
ts	Temperature sensitive
tub	Tubulin
UAS	Upstream Activation Sequence
upd	*unpaired*
UTR	Untranslated region
VEGF	*Vascular endothelial growth factor*
VEGFR	*Vascular endothelial growth factor receptor*
VERA	VG1 RNA-binding protein
VNC	Ventral nerve cord
WAL20	pWALIUM20
WAL22	pWALIUM22
wt	Wildtype
YFP	Yellow Fluorescent Protein
IMP1	Zipcode-binding protein 1

Table of Figures

Chapter 1:

Introduction

1.1 Gene Expression Regulation

It is important that cells are able to regulate both the temporal and spatial expression of proteins, which can be controlled through the regulation of gene expression. Control of gene expression is a complex process that can be regulated at many levels, starting with transcriptional regulation in the nucleus, which defines the timing and quantity of transcripts generated. However, gene expression can also be regulated post-transcriptionally in both the nucleus and cytoplasm (Latchman 2010). The regulation of RNA splicing, capping and polyadenylation occurs in the nucleus before nuclear export of mRNAs into the cytoplasm (Kong & Lasko 2012). Once in the cytoplasm, gene expression can be regulated through control of mRNA localisation and translation (Besse & Ephrussi 2008). In this case, mRNAs are localised to a specific region of the cell, so that proteins are locally translated when and where they are required in the cell (Gebauer *et al*. 2012). mRNAs can also be targeting for degradation within the cytoplasm, to prevent protein expression at a time or cellular region when it is not required (Glisovic *et al*. 2008) (**Figure 1**).

1.1.1 Role of RNA-binding proteins

RNA-binding proteins (RBPs) play an instrumental role in post-transcriptional gene regulation and are the main players in RNA regulation, both within the nucleus and cytoplasm (Glisovic *et al*. 2008). Often referred to as master regulators of gene expression by binding hundreds of different RNA targets, they are involved in an extensive range of functions in RNA processing including RNA splicing, stability, processing of the pre-mRNA 3' end, polyadenylation, nuclear export, mRNA localisation, translational repression and activation (Dreyfuss *et al*. 2002; Bish & Vogel 2014) (Figure 1). However, despite their extensive and important functions, many of the mechanisms by which RNA-binding proteins regulate RNA processing remain largely uncharacterised (Carpenter *et al*. 2006).

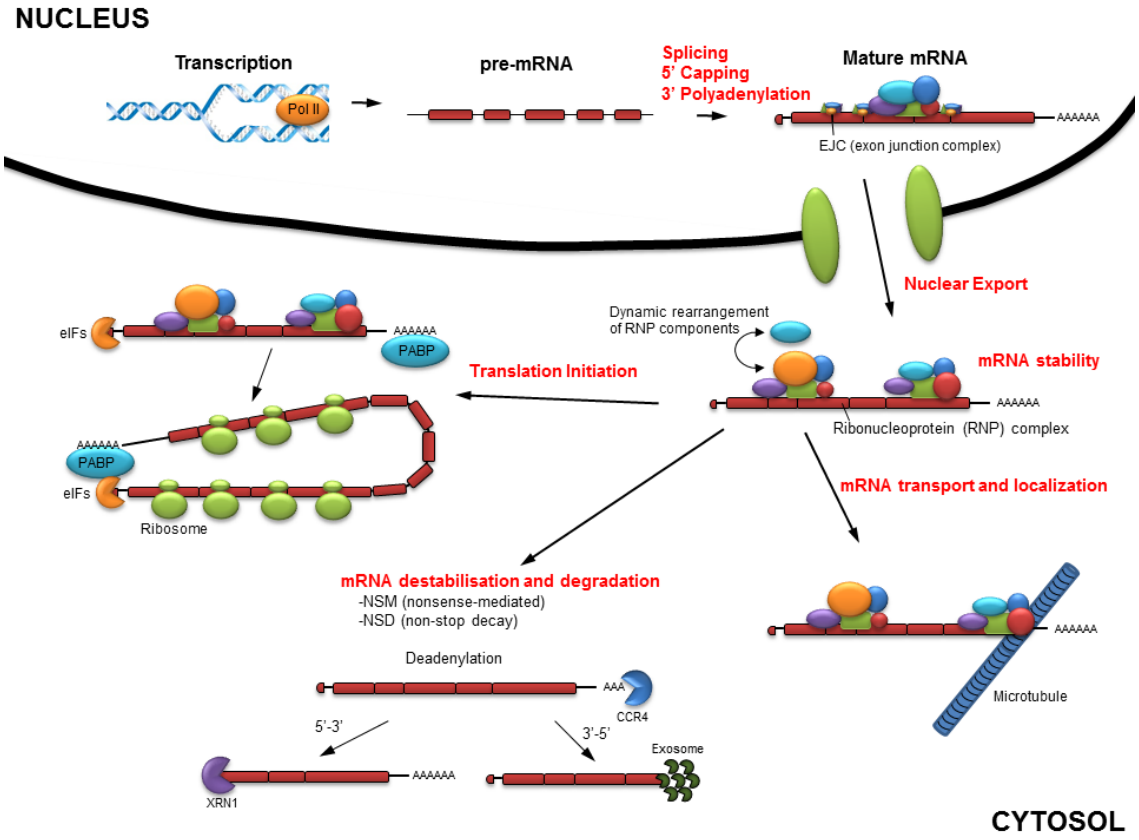

Figure 1. Five stages of gene expression regulation within the nucleus and cytoplasm.

Regulation of mRNA processing from transcription to translation is a complex process that is controlled through many stages. The processes (highlighted in red) that are used within the cell to regulate gene expression at the transcript level , including processing in the nucleus, nuclear export of mRNAs and control of mRNA localization, stabilization and translation to regulate both the spatial and temporal distribution of proteins within the cell.

RBPs are modular in structure and often contain several or a combination of RNA-binding domains, including RNA-recognition motifs (RRM), RGG (Arg-Gly-Gly) boxes and KH domains (Lunde *et al*. 2007). It has been proposed that by having a combination of RNA-binding domains which bind short sequences of RNA with low affinity, RBPs can bind many transcripts with high specificity compared with a single domain alone, as the short sequences are often non-unique. The relative position of these motifs to each other may also play a role in achieving RBP specificity (Lunde *et al*. 2007).

Heterogeneous ribonucleoproteins (hnRNPs) are a family of RNA-binding proteins that bind RNA transcripts both within the nucleus and cytoplasm to form RNP complexes (Carpenter *et al*. 2005). The distinction between hnRNPs and other classes of RBPs has become unclear as hnRNPs appear to share many of the same domains and functions as other RBP families (Dreyfuss *et al*. 2002). However core hnRNPs have been identified and partially

characterised (**Table 1**), although we still do not fully understand the mechanisms by which they regulate RNA processing (Singh & Valcárcel 2005).

Table 1. RNA-binding domains of core mammalian hnRNPs and the short RNA sequences to which they preferentially bind (Adapted from Singh & Valcárcel 2005).

hnRNPs	Domains	Preferred Sequences
A1	2x RRM, RGG	UAGGG(A/U)
A2/B1	2x RRM, RGG	(UUAGGG)*n*
C1/C2	1x RRM	U6
D	2x RRM, RGG	AU rich
E1/E2	3x KH	C rich
H/H'/F	3x RRM	GGGA
I (PTB)	4x RRM	UCUUC
K	3xKH, RGG	C rich
L	4xRRM	CA repeat
M	3xRRM	G or U rich (RRGGAGGRR)

1.1.2 Ribonuclearprotein complexes

From transcription to translation, the mRNAs within a cell are never naked, but are associated with several RBPs and bound into a large ribonucleoprotein (RNP) complex. However, mRNAs are never associated with a single type of RBP, but with a variety of different RBPs within these complexes (Müller-McNicoll & Neugebauer 2013). Many regulatory RNA-binding proteins also bind a variety of mRNA transcripts to regulate transcript-specific processing (Singh & Valcárcel 2005). One of the current challenges is to determine how this specificity is achieved. A large variety of RNA-binding proteins can bind a single transcript to form large RNP complexes, suggesting that a combination of proteins may aid in achieving transcript specificity (Van De Bor & Davis 2004). These complexes are formed within the nucleus to regulate RNA processing and can be re-modelled within the cytoplasm upon nuclear export (Van Dusen *et al*. 2010).

Many studies have carried out protein-complex immunoprecipitation assays to determine the composition of RNP complexes. However, these assays give little insight into the function of bound RBPs and although an RBP may be bound within a complex it may not necessarily play a direct role within that complex. For example, the *Drosophila* RNA-binding protein Imp (Zipcode binding protein 1 (IMP1) has been shown to bind *oskar* mRNA within the oocyte but

knock down of its expression has no effect on *oskar* mRNA processing, localisation or translation (Munro *et al*. 2006). It is therefore possible that although several RBPs may bind a single transcript, only a few are required for successful processing of the mRNA, or that they regulate only very specific events in the regulatory life of the RNA molecule (Shahbabian & Chartrand 2012).

The composition of RNP complexes is often very complex, containing many different RBPs, small non-coding RNAs, small nucleolar RNAs and microRNAs. As well as binding *cis*-acting elements in mRNAs, RBPs may be recruited through protein-protein interactions with other proteins contained in a complex, building up further specificity (Müller-McNicoll & Neugebauer 2013). Different RNA-binding proteins within a complex could act redundantly to ensure that RNA regulation is carried out in the absence of a single RBP (Dreyfuss *et al.* 2002). A study carried out using *Caenorhabditis elegans* oocytes has shown that the state of RNPs can be altered depending on the protein composition and developmental state of the oocyte (Hubstenberger *et al*. 2013). When the oocyte is in a developmentally quiescent state the RNP complexes contained within become tightly assembled (referred to as a solid state) so they cannot be re-modelled to ensure that mRNAs are translationally-silent. However, once actively developing, the RNP complexes with the oocyte become looser as the proteins bound within the complex relax their bonds (referred to as a liquid state), allowing bound RBPs to dissociate and new ones to associate with the complex to regulate RNA processing (Hubstenberger *et al*. 2013).

RNP complexes are consistently re-modelled as different factors dissociate or associate depending on the regulation required (Gebauer *et al*. 2012). It was often thought that RBPs which regulate the cytoplasmic localisation and/or translation of mRNAs bind to RNP complexes once they are exported from the nucleus. However, RBPs that regulate the cytoplasmic localisation and translation of mRNAs can be assembled onto these RNP complexes within the nucleus and remain during nuclear export, suggesting that the regulation of cytoplasmic localisation of an mRNA may even be set up in the nucleus directly after transcription (Müller-McNicoll & Neugebauer 2013).

Perhaps our greatest challenge is to decipher the so-called ‘mRNP code’ which would enable us to predict the RNP composition required to process specific mRNA transcripts (Singh & Valcárcel 2005). There is therefore a need to identify the entire protein and RNA compositions of individual RNP complexes, termed the ‘interactome’ to determine which RBPs are bound (Gebauer *et al*. 2012). However, this in itself represents a challenge as the composition of RNPs is so dynamic that the proteins bound could change depending on the state of the complex, its cellular position or depend on the events taking place within the cell.

Several groups have attempted to identify conserved RNA-binding domains within mRNAs. For example, a systematic analysis of transcripts containing RNA-motifs recognised by RBPs showed that there is high evolutionary conservation between motifs and identified new interactions between mRNAs and RBPs (Ray *et al*. 2013). These type of studies may also provide insight into the function of RBPs. For example, when transcripts containing many RNA-binding sites for a particular RBP were in high abundance and the transcript encoding that particular RBP was in low abundance, it was shown that the RBP tended to play a negative role in mRNA stability (Ray *et al*. 2013).

1.2 Role of mRNA localisation and local translation in the establishment and maintenance of cell polarity

1.2.1 Establishment of cell polarity

Intracellular localization of mRNA is one mechanism by which cells regulate gene expression in the cell cytoplasm, allowing local synthesis of proteins at their site of function (Meignin & Davis 2010). Importantly, mRNA localisation allows cells to generate and maintain cell polarity through the asymmetric localization and subsequent translation of proteins within a specific region of the cell (Medioni *et al*. 2012)

Cell polarity is an essential feature of eukaryotic cells. For example, stem cells often divide asymmetrically to produce another stem cell and a cell which becomes committed to lineage-specific differentiation (Nelson 2003). To achieve this asymmetric division, the dividing stem cell must become polarised as cell fate determinants are segregated into one of the two daughter cells (Knoblich 2008). Some eukaryotic cells are permanently polarised to enable them to carry out their functions, including columnar epithelial cells which show apical-basal polarity, fibroblasts and neurons which have exon-dendrite polarity. Motile cells, including immune cells such as monocytes and neutrophils, become highly polarised in response to extracellular migration cues, enabling them to migrate to sites where they are required (Du *et al*. 2007). Cell polarity is also required for correct axis formation during organism development, tissue development and cell proliferation (Mili & Macara 2009).

The establishment and maintenance of cell polarity requires the asymmetric localisation of cellular components including proteins, which could be achieved through changes in cytoskeletal organization, signalling pathways and reorganization at the cellular membrane Medioni *et al*. 2012). RNA localisation and localised translation to specific cellular compartments is one way in which the asymmetric distribution of proteins can be achieved, aiding the establishment of cell polarity. For example, in both *Xenopus* and *Drosophila*

oocytes the asymmetric distribution of maternal mRNAs is essential for establishing the body axis during embryonic development (Becalska & Gavis 2009; King *et al.* 2005). Examples of localized mRNAs have been known since the 1990s, including the mRNA of ASH1, an inhibitor of mating type switching in budding yeast, which is localised to the bud tip of a dividing yeast cell (Long *et al*. 1997; Takizawa *et al*. 1997).

1.2.2. Functions of RNA localisation

It is not fully clear why RNAs are localised within the cytoplasm. Different reasons have been proposed to explain why RNA is localized within cells. In some cases mRNA localisation may be preferable to transporting individual proteins. This is because localisation of mRNAs is considered more energetically favourable than protein localisation as single mRNA transcripts could produce many proteins, reducing transport costs (Du *et al*. 2007). Some RBPs also play a role in regulating the translation of mRNA by repressing or activating translation of pools of localized mRNA until the protein product is required. During transit localised mRNAs are often translationally silenced to ensure proper temporal and spatial protein expression, preventing protein malfunction (Meignin & Davis 2010). For example, the *Drosophila* protein Oskar is required at the posterior of the oocyte for correct establishment of the embryonic posterior axis. Delocalisation and ectopic expression of *oskar* mRNA to the anterior of the oocyte causes loss of the anterior axis in embryos due to mis-expression of Oskar protein (Ephrussi *et al*. 1992; Kim-Ha *et al*. 1995). The mRNA encoding Myelin Basic Protein is localized to and locally translated within the myelin compartment of oligodendrocytes, as this protein is extremely sticky and can have aberrant effects when expressed in other regions of the cell (Ainger *et al*. 1997).

Examples of localized mRNAs were first followed in large and highly polarized *Drosophila* and *Xenopus* oocytes (Kloc & Etkin 2005). However, it is now becoming clear that this may be a wider phenomenon than first anticipated. A large-scale fluorescent *in situ* hybridisation screen showed that 71% of 3370 genes in *Drosophila melanogaster* encode subcellularly localised mRNAs (Lécuyer *et al*. 2007) and mRNA localisation has been shown to regulate cell polarity in mammalian neurons, fibroblasts and epithelial cells (St Johnston 1995). This highlights that mRNA localisation is a widespread phenomenon and may therefore play an important regulatory function in a variety of cellular processes. However, much remains unknown about how and where RBPs bind mRNAs transcripts and how RNP complexes are able to regulate the localisation and local translation of many mRNAs (Mili & Macara 2009).

1.2.3. Mechanisms of RNA localisation

Pools of mRNAs can be localised to specific regions of the cell cytoplasm through a variety of different mechanisms while bound with RNP complexes. Active transport of mRNAs in RNP complexes is predicted to be the most common method of mRNA transport across the cell, along both actin filaments and microtubules with the assistance of molecular motors, such as Dynein, Kinesin or Myosin (Hirokawa 2006). For example, the mRNA of the pair-rule gene *hairy* is localised at the apical surface of the *Drosophila* syncytial blastoderm by minus-end directed transport with dynein along microtubules (Latham *et al*. 2001). Assisted by myosin, *β-actin* mRNA is actively transported along actin filaments to actin-rich regions such as the lamellipodial protrusions of migratory cells (Bullock *et al*. 2003).

mRNAs may also be selectively degraded in regions where the translated protein is not required. For example, *hsp38* mRNA is degraded throughout the *Drosophila* embryo by the RBP Smaug, but is protected from Smaug-mediated degradation at the posterior pole (Semotok *et al*. 2008). Other methods of cytoplasmic mRNA localisation include localised entrapment in which mRNAs diffuse through the cytoplasm and become anchored in the region of their requirement (Martin & Ephrussi 2009). For example, *cyclin B* mRNA diffuses throughout the *Drosophila* oocyte and becomes anchored within the pole plasm when it reaches the oocyte posterior (Raff *et al*. 1990).

1.2.4 mRNA localisation and cell migration

Motile cells show distinct cell polarity. The front of motile cells, termed the leading edge, is characterised by cytoskeleton actin protrusions termed lamellipodia or filopodia which drive directional cell movement (Lauffenburger & Horwitz 1996). Lamellipodia consist of branched actin filaments, while long, thin filopodia protrude from the lamellipodial extensions (Mattila & Lappalainen 2008). The rear of the cell, termed the lagging or rear edge, forms adhesions with the stroma or extracellular matrix to anchor the cell in position. These adhesions are broken when the cell becomes motile and actin microbundles at the rear edge contract to force the rear of the cell forwards (Ridley *et al*. 2003) (**Figure 2**).

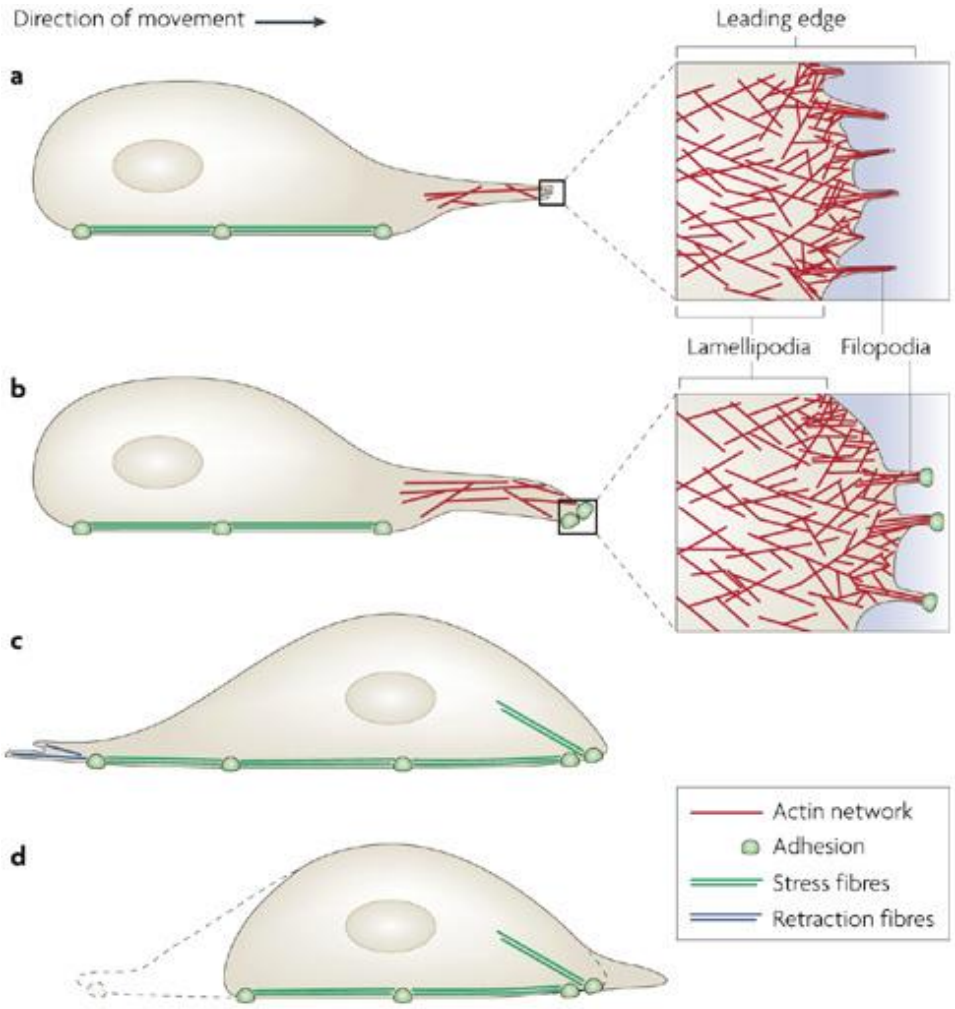

Figure 2. Motile cells show distinct polarity.

(**A**) The cell becomes highly polarized upon receiving extracellular migration cues and produces actin-rich lamellipodial and filopodial protrusions in the direction of migration, the tips of which are referred to as the leading edge. (**B**) New adhesions are formed between the substratum and the leading edge as the cell migrates forward. (**C**) This subjects the rear of the cell to contractile forces, which may help to propel the front of the cell forwards. (**D**) Dissolution of the adhesions at the cell rear releases the contractile forces and allows the rear of the cell to move forward. (Taken from Mattila & Lappalainen 2008 with permission).

Some actin-regulatory proteins have been shown to localise at sites of dynamic actin, such as the dendritic spines of neurons and the leading and lagging edge of migratory cells. For example, the actin regulatory protein Profilin has been shown to localise in lamellipodia at the leading edge of translocating rat fibroblasts (Buß *et al*. 1992) and migrating *Acanthamoeba castellanii* (Bubb *et al*. 1998). β-actin appears to be required at the leading edge of migratory cells for actin polymerisation and protrusion of lamellipodia (Yamazaki *et al*. 2005).

1.2.5 *β-actin* mRNA is enriched at the leading edge of cultured migratory cells

Importantly, apart from proteins, mRNAs encoding actin regulators have been shown to be localised in migratory cells. *β-actin* mRNA itself has also been shown to localise at the leading edge of cultured migratory cells by an RNA-binding protein called the Zipcode-binding protein 1 (ZBP1), also referred to as IMP1 (Insulin-like growth factor 2 mRNA binding protein 1). IMP1 binds to a conserved region termed the zip-code within the 3' UTR of *β-actin* mRNA (Ross *et al*. 1997; Shestakova *et al*. 2001; Oleynikov & Singer 2003). The zip-code, a sequence of 54 nucleotides within *β-actin* mRNA isolated from chicken, appears to be conserved across species as human *β-actin* mRNA is localised effectively within cultured chicken fibroblasts (Kislauskis *et al*. 1994; Ross *et al*. 1997).

IMP1 is required for *β-actin* mRNA localization, as well as its translational regulation. IMP1 represses translation of *β-actin* mRNA and upon phosphorylation of IMP1 by Src kinase, *β-actin* mRNA is translated (Hüttelmaier *et al*. 2005). Src kinase activity appears to be restricted to the cell periphery, although the signal that triggers Src kinase to phosphorylate IMP1 is currently unknown (Hüttelmaier *et al*. 2005). One interesting possibility is that extracellular migration cues play a role in triggering *β-actin* mRNA translation. Imp, the *Drosophila* homologue of IMP1, has been suggested to play a role in border cell migration, a group of 6-8 follicle cells which migrate from the anterior of the *Drosophila* egg chamber towards the oocyte (Munro *et al*. 2005 – unpublished) (see section 1.3.3).

1.2.6 *profilin* and *cofilin* mRNAs are enriched at the leading edge of cultured migratory cells

The actin-regulatory proteins, Cofilin and Profilin, are required for re-organization of the actin cytoskeleton upon formation of lamellipodial protrusions. Cofilin depolymerizes actin filaments to generate a pool of G-actin monomers and to increase the number of barbed ends of actin filaments at the leading edge (Wang *et al*. 2007). Depletion of Cofilin affects lamellipodia formation and directed cell migration. *cofilin* mRNA is localized at the leading edge of cultured migratory lung carcinoma cells by IMP1, which is mediated through the interaction of IMP1 with its 3'UTR (Maizels *et al*. 2015). Profilin is required for the formation of filamentous actin by binding G-actin monomers and presenting them to elongating actin filaments (Carlsson *et al*. 1977). The mRNA that encodes Profilin is enriched at regions of actin polymerization, including the periphery of lamellipodial protrusions, in mouse embryonic fibroblasts and is transported to these regions in RNP granules by transport along the microtubule cytoskeleton (Johnsson & Karlsson 2010).

1.2.7 mRNAs encoding the ARP2/3 complex subunits are enriched at the leading edge of cultured migratory cells

The Actin-related protein 2/3 complex (ARP2/3) consists of seven subunits and is required for regulating actin dynamics within motile cells through capping of actin filament pointed ends, assisting formation of a branched actin network (Machesky *et al*. 1997; Welch *et al*. 1997). The mRNA transcripts that encode all seven ARP2/3 subunits are also localised at the leading edge of cultured migratory cells by IMP1 (Mingle *et al*. 2005). The localised translation of a pool of individual protein subunits may allow efficient assembly of large complexes at a required site, such as the leading edge of a cell, overcoming the diffusion constraint of large complexes through the cellular cytoplasm (Mingle *et al*. 2005).

Disruption of both the actin and microtubule cytoskeleton caused a loss of *arp2/3* subunit mRNA at the leading edge, suggesting that the cytoskeleton is required for transport and/or anchoring of these transcripts (Mingle *et al*. 2005). Once localised, *arp2/3* subunit mRNAs may be locally translated at the leading edge in response to cell migration cues as association of *arpC2* mRNA with ribosomes is increased 31-fold in cells actively forming lamellipodia, compared to non-spreading cells, despite total *arpC2* mRNA levels remaining constant (Willett *et al*. 2013). To support this idea, ArpC2 protein co-localised with *arpC2* mRNA that was enriched at foci of active protein synthesis within lamellipodial protrusions (Willet *et al*. 2013). Arp2 depleted cells showed a loss of branched lamellipodia, with only multiple, narrow protrusions, an increase in net cell migration speeds and reduced directionality. While expression of a wildtype exogenous *arp2* transcript was able to rescue this phenotype, cells expressing exogenous *arp2* mRNA targeted to the perinuclear region formed normal lamellipodia but failed to restore normal directionality and cell migration speed (Liao *et al*. 2011). However, knockdown of the ARP2/3 complex in platelets and mouse embryonic fibroblasts did not inhibit lamellipodia formation, which may reflect differential regulation of cell migration and response to cell migratory cues in different cell types (Di Nardo *et al*. 2005).

The localisation of specific RNAs in lamellipodial protrusions appears to be a widespread phenomenon as suggested by a genome-wide screen which revealing that around 50 RNAs are significantly enriched in the pseudopodia of cultured fibroblasts (Mili *et al*. 2008). These RNAs encoded proteins involved in a range of functions including RNA metabolism, cytoskeletal organization, signalling, membrane trafficking and microtubule-based transport. However, little is known about the mechanism by which mRNAs, such as those of the individual *arp2/3* subunit transcripts, are localised at the leading edge and although it is

thought that other RBPs besides IMP1 play a role, their identity is currently unknown (Mingle *et al*. 2005; Gu *et al*. 2009).

1.2.8 mRNAs localised at the leading edge are then locally translated

The process of translation can be divided in three main stages; initiation, elongation and termination (Lengyel & Söll 1969). One major mechanism of gene expression regulation is the control of translational initiation (Sonenberg & Hinnebusch 2009). Eukaryotic initiation factors (eIFs) are assembled into a large multi-protein complex termed eIF4F which recruits transcripts to the ribosome. Competitive binding of eIF4E-binding proteins (4E-BPs) to the eIF4E subunit prevents eIF4F assembly (Preiss & Hentze 2003). The mTORC (mammalian target of rapamycin complex) modulates the binding of 4E-BPs to eIF4E and is required for translation initiation (Proud 2008).

Localised mRNAs must be locally translated to ensure that proteins are expressed where required within the cell. To support the idea that pools of mRNAs are localised to the leading edge and translated when required, (i.e. upon the cell receiving migratory cues), granules containing ribosomal subunits and translation initiation factors are enriched within the lamellipodia of spreading cultured cells (Chicurel *et al*. 1998; Willett *et al*. 2010; Willett *et al*. 2011).

Both eIF4E and eIF4G, as well as 40S and 60S ribosomal subunits, are co-localised in lamellipodia of spreading cells (Willet *et al*. 2010). The Peptide Methionine-Tyrosine (PMY) technique, in which PMY is incorporated into nascent polypeptides to terminate translation, which can then be detected by anti-PMY antibodies, showed that active translation was taking place at the leading edge of cultured migratory cells (Willet *et al*. 2011). Consistent with this result eIF4E, eIF4GI, mTORC and the 40s ribosomal subunit rpS6 were co-localised with PMY at sites of active translation.

Further research has shown that these translation initiation factors and ribosomal subunits are enriched in punctate foci at the distal edge of the lamellipodia which appear to co-localise with sites of focal adhesion complexes (FACs), shown by co-staining with β3-integrin (Chicurel *et al*. 1998; Willet *et al*. 2009). Interestingly, the recruitment of mRNA and ribosomes to FACs appears to be mediated by integrins, particularly integrin β1. Integrin binding to the ECM substrate and resulting tension moulding and mechanical restructuring of the intracellular actin cytoskeleton that follows appears to act as a trigger for mRNA and ribosome recruitment to FACs (Chicurel *et al*. 1998).

Loss of protein synthesis by inhibition of mTORC1 in cultured migratory fibroblasts led to decreased migration velocity and an increase in migration straightness, suggesting a loss of directionality (Willet *et al*. 2013). When migrating to wounds, these cells also failed to form lamellipodia and wound coverage was significantly reduced, suggesting that protein synthesis is required for protrusion formation and cell migration (Willet *et al*. 2013).

Research shows that transcription and/or RNA export from the nucleus are not required for RNA recruitment to the leading edge (Chicurel *et al*. 1998). When cells are required to rapidly polarise in response to extracellular migration cues, pools of localised proteins may be activated, for example by phosphorylation, at the leading edge. However, once this pool of protein is depleted, newly synthesised proteins will be required to replace them. Transcription and then subsequent translation of these proteins may require too long to replenish protein stores rapidly. Localisation of mRNA may therefore act as a middle-ground between transcription and protein synthesis, with translation of localised mRNA replenishing proteins required at the leading edge quickly (Chicurel *et al*. 1998).

Due to the enrichment of ribosomes and mRNA recruitment to the leading edge of migratory cells, it is logical to assume that RBPs play a role in transporting and regulating mRNA transcripts recruited to these ribosomes. To support this idea, CBEP (cytoplasmic polyadenylation element binding) protein, commonly required to activate mRNA translation, was co-localised with the cell-matrix adhesion marker talin at the leading edge of spreading cultured cells (Willet *et al*. 2009). Partial co-localisation of the RBP HuR was also observed with eIF4E at the leading edge (Willet *et al*. 2009). The hnRNP Polypyrimidine Tract Binding Protein (PTB) has been shown to transiently localise at FACs within the leading edge of mouse embryonic fibroblasts, where it associates with mRNAs that encode focal adhesion scaffolding proteins, including α-Actinin 4 and Vinvulin (Babic *et al*. 2009). Interestingly, PTB depletion in these cells resulted in a loss of cell spreading and reduced number of protrusions, a decrease in Vinculin protein at the cell periphery and significantly shorter focal adhesions (Babic *et al*. 2009).

Taken together, the studies summarized here suggest that mRNA localisation at the leading edge of migratory cells may be a widespread phenomenon to regulate cell motility. mRNAs must then be locally translated, requiring localisation of the translational machinery, including ribosomes and translation initiation factors, to regions containing localised transcripts.

1.2.9 mRNA localisation and metastatic potential

Further insight into the localisation of transcripts required for cell motility may have implications for cancer biology and immunology. PTB is frequently overexpressed in highly-

metastatic human glioma, which has been shown to increase non-directional migration in two human glioma cell lines. Down-regulation of PTB also inhibited migration of these cell lines (Cheung *et al*. 2009). It would be interesting to see if this is the result of mRNA delocalisation, which may be required for proper cell motility.

Microarray analysis of transcripts precipitated from IMP1-containing complexes in highly-metastatic MTLn3 cells revealed that *e-cadherin, β-actin and arp2/3* subunit mRNAs were highly associated with IMP1. Knockdown of IMP1 expression in these cells revealed that these mRNAs are sequestered within the nucleus, suggesting that IMP1 may be required for their nuclear export (Gu *et al.* 2012). *β-actin* mRNA is often delocalised in the highly-metastatic MTLn3 human cancer cell line, causing loss of a defined leading edge. This increases the cells' response to chemotactic signals concomitantly with an increased flexibility in their direction of migration (Shestakova *et al*. 1999). Delocalisation of *β-actin* mRNA may be caused by reduced expression of IMP1 in metastatic cells as IMP1 expression appears to be actively repressed in metastatic MTLn3 breast cancer cells (Gu *et al*. 2012). Knock-down of the RNA-binding protein HuR, which stabilises *β-actin* mRNA, also increased metastatic potential of the HeLa cancer cell line (Dormoy-Raclet *et al*. 2007). Mis-localization of *arp2* mRNA to the perinuclear region in human fibroblasts disrupted the formation of lamellipodia, resulting in an increase in cell motility and loss of directional cell migration (Liao *et al*. 2011).

Altogether, these findings suggest that delocalisation of mRNAs required for cell migration may increase the metastatic potential of tumour cells. However, it is important to note that these findings are based on *in vitro* analysis, which may not accurately predict the effect of mRNA localisation in cell motility within the context of a living organism. For example, the actin-regulatory protein Mena (Ena in *Drosphila*) is required to antagonise capping of barbed actin filaments and is localised at the leading edge of migratory cells. Studies carried out in tissue culture have shown that up-regulation of Mena in rat fibroblasts decreased cell motility (Philippar *et al*. 2008). Remarkably, a study carried out in migratory immune cells within *Drosophila* embryos *in vivo* showed the opposite effect: overexpression of Ena in haemocytes decreased their motility, which may be due to the spatial constraints placed on cells within the three-dimensional context of a living organism (Tucker *et al*. 2010).

To date, only a single study has attempted to study the localization of mRNAs implicated in cell motility in a living organism *in vivo* (Park *et al*. 2014). The group used the MS2 system to label endogenous *β-actin* mRNA within a live mouse model. Primary fibroblasts were then cultured from mouse embryos in culture media and were used for live-cell imaging within 48 hours of plating. Although imaging of endogenous *β-actin* mRNA in these cells showed that it

is enriched at the leading edge of fibroblast, it localized in a different manner to that of exogenously-labelled *β-actin* mRNA. Endogenous *β-actin* mRNA showed less directional movement and localized primarily through diffusion and trapping of individual mRNA particles, in contrast to exogenously-labelled mRNA that showed higher levels of directional localization by active transport to the leading edge. However, this study still required the investigation of mRNA localization in cells exposed to an artificial environment within a culture dish and so may not accurately reflect the localization of *β-actin* mRNA *in vivo*. The study also revealed that immortalised fibroblast cells lines and primary culture fibroblasts cultured over time lose the polarized distribution of *β-actin* mRNA localization, highlighting the importance of *in vivo* studies (Park *et al*. 2014).

The discovery that delocalisation of mRNAs required for cell migration may increase the metastatic potential of tumour cells could be used in cancer prognosis, in particular for predicting tumour invasiveness. However, before mRNA localisation and translation could be used in prognosis, or therapy studies against cell invasiveness, a suitable *in vivo* model system that recapitulates cell migration within a living organism should be established.

1.3 Models used to study cell motility *in vivo*.

Although several models have been established to study cell migration *in vivo* within a living organism, these studies are limited compared to those that have used *in vitro* cell culture systems to analyse the dynamics of cell motility. For example, cell migration has been studied partially *in vivo* in mammalian systems by dissecting transverse sections from the forelimb region of developing chick embryos. The sections continue to develop and the migration of muscle cell precursors from the somite to the developing limb bud can be observed (Knight *et al*. 2000). However, dissection of chick embryo could lead to defects in development of the sections, which may affect the migratory behaviour of migrating cells. The migration of immune cells from lymphoid organs to other tissues were imaged *in vivo* in whole mouse through use of a photoconvertible fluorescence protein (Tomura *et al*. 2008). However, the scope for *in vivo* imaging of migratory cells in mammalian models is limited due to their size and lack of genetic tractability.

Both zebrafish and killifish have been utilised as model organisms to study cell motility *in vivo* as they are small and the embryos are transparent, creating ideal conditions for imaging. The migration of stem cells *in vivo* has been studied by transplanting them into zebrafish embryos during development (Li & Zon 2011). However, the migration of exogenous cell population *in vivo* may not fully recapitulate the migration of endogenous cells. The regeneration of the zebrafish fin fold after amputation allows the migration of fibroblasts to be imaged *in vivo* to

the wound site (Mateus *et al*. 2012). Migrating mesenchymal cells have been followed in the pectoral fin bud of developing teleost embryos of the killifish *Aphyosemion scheeli* (Wood & Thorogood 1984). Migration of the primordial germ cells can also be observed in the zebrafish embryo, where they migrate to the developing gonad (Raz & Reichman-Fried 2006).

Drosophila embryos and the female ovary have also been used to study cell motility *in vivo*. A cluster of 6-10 cells termed the border cells, that are present in the female ovary at the anterior of the developing egg chamber, must collectively migrate to the anterior of the oocyte for successful oocyte development (Montell 2003). Dissection of the ovary from adult female flies allows the migration of these cells to be imaged *in vivo* (Cliffe *et al*. 2007; Prasad *et al*. 2007). The migration of a collective sheet of epithelial cells can be imaged *in vivo* during the last major event in *Drosophila* embryogenesis, in which a large hole is present in the embryos due to germ band retraction, is closed up by lateral migration of the epithelia on both sides of the hole (Millard & Martin 2008). This system allows not only the study of the general mechanisms of cell motility, but also to study how cells are able to migrate collectively as a single tissue.

Although cell migration has been well characterised in 2D tissue culture, more studies are now emerging in which cells are cultured on 3D matrices to more accurately recapitulate the conditions experienced by migratory cells *in vivo*. Extensive research has shown that the extracellular conditions experienced by migratory cells within different 3D matrix structures, generated with different materials, can affect the mechanism by which cultured cells polarise and migrate (Even-Ram & Yamada 2005; Gough 2010; Hakkinen *et al*. 2011; Petrie & Yamada 2012; Petrie *et al*. 2012). This finding suggests that the mechanisms of migration in motile cells *in vivo* may be even more varied due to the complex and varied nature of the extracellular environment experience *in vivo*.

All current evidence supports the need to study cell migration *in vivo* within a living organism. Within this project we have utilised both *Drosophila* embryonic macrophages (haemocytes) and *Drosophila* border cells to analyse the *in vivo* role that RNA regulation may play in regulating cell motility.

1.3.1 *Drosophila* haemocytes as an *in vivo* model system to study cell motility

Drosophila haemocytes, the equivalent of mammalian macrophages, are highly motile cells that play a critical role in both embryonic and larval development through phagocytosis of apoptotic cells, as well as in host defence against invading microorganisms (Wood & Jacinto 2007). Three distinct populations of haemocytes are specified during embryonic development

(Rizki 1978). These include plasmatocytes which make up 90-95% of the haemocyte populations with around 700 individual cells specified, with the remaining two types including crystal cells and lamellocytes (Holz *et al*. 2003). It is the plasmatocytes which are commonly described as professional phagocytes or macrophages (Rizki & Rizki 1980) and it is this population of haemocytes which will be the focus of this study and will hereupon be referred to as haemocytes.

Haemocytes appear approximately 8-10 µm in diameter and are highly polarised, migratory cells (Bernardoni *et al*. 1997; Lebestky *et al*. 2000) (**Figure 3**). Their dynamic leading edge ruffles as the actin filaments and microtubules are de-polymerised and re-polymerised to direct and drive cell motility (Lanot *et al*. 2001). *Drosophila* haemocytes play two important roles: i) including a developmental role in which they are required to secrete extracellular matrix proteins and engulf dead cells and debris generating during embryonic development (Fessler *et al*. 1994; Murray *et al*. 1995; Franc *et al*. 1996); ii) they also play a major role in innate immunity through the monitoring and destruction of pathogens and through signalling to the fat body, to induce the secretion of antimicrobial proteins (Tzou *et al*. 2002; Agaisse *et al*. 2003).

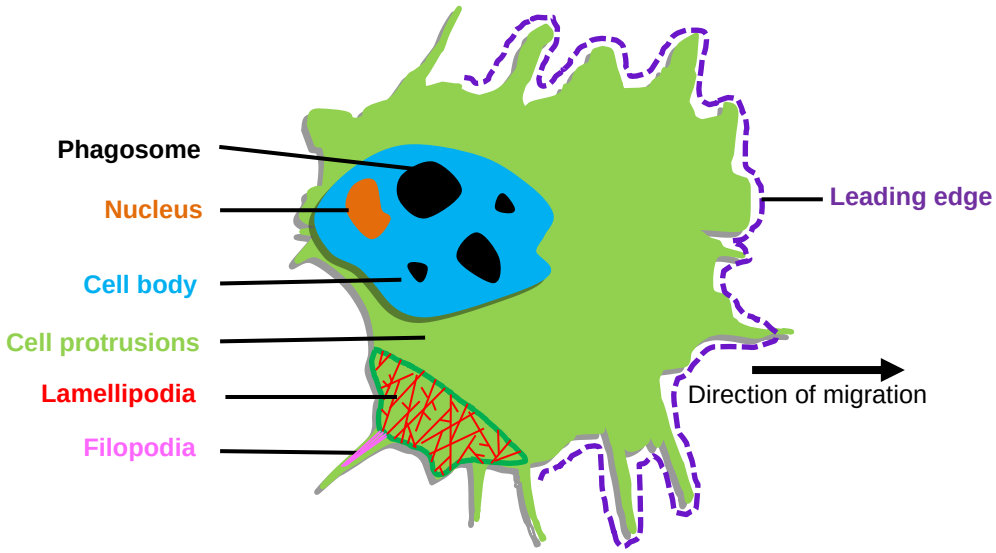

Figure 3. Basic structure of a migratory *Drosophila* macrophage (haemocyte).

The cell body contains the cytoplasmic organelles, including the nucleus, and is typically spherical in shape. Haemocytes are highly phagocytic and the cell body contains numerous phagosomes (also called vacuoles) which allows up-take and digestion of cellular debris within the embryo. The cellular protrusions extend in the direction of migration and consist of actin-rich, highly branched lamellipodia and long, spikey filopodia which extend from the edges of the lamellipodia. The leading edge is defined as the tips of the cellular protrusions, from which newly-formed lamellipodia and filopodia extend.

Haemocytes are first specified in the head mesoderm during stage 5 of embryonic development by the GATA transcription factor Serpent (*srp*), which is required for haematopoietic development (Tepass *et al*. 1994; Lebestky *et al*. 2000). Haemocytes then show a distinct developmental migration from stage 10 of embryonic development (Tepass *et al*. 1994; Wood *et al*. 2006). Haemocytes move into the retracting germ-band at the anterior of the embryo and are transported to the posterior during germ-band retraction at stages 11-12 of embryonic development. Haemocytes at both anterior and posterior ends then migrate along the ventral midline, where the future nerve cord is developing, until they line the entire ventral midline at stage 14 (Wood & Jacinto 2007). During embryonic stages 15-16 the haemocytes disperse throughout the entire embryo, although a pool of haemocytes remain at the ventral nerve cord and migrate laterally to form three parallel lines along the entire ventral surface of the embryo (Wood *et al*. 2006; Wood & Jacinto 2007) (**Figure 4**).

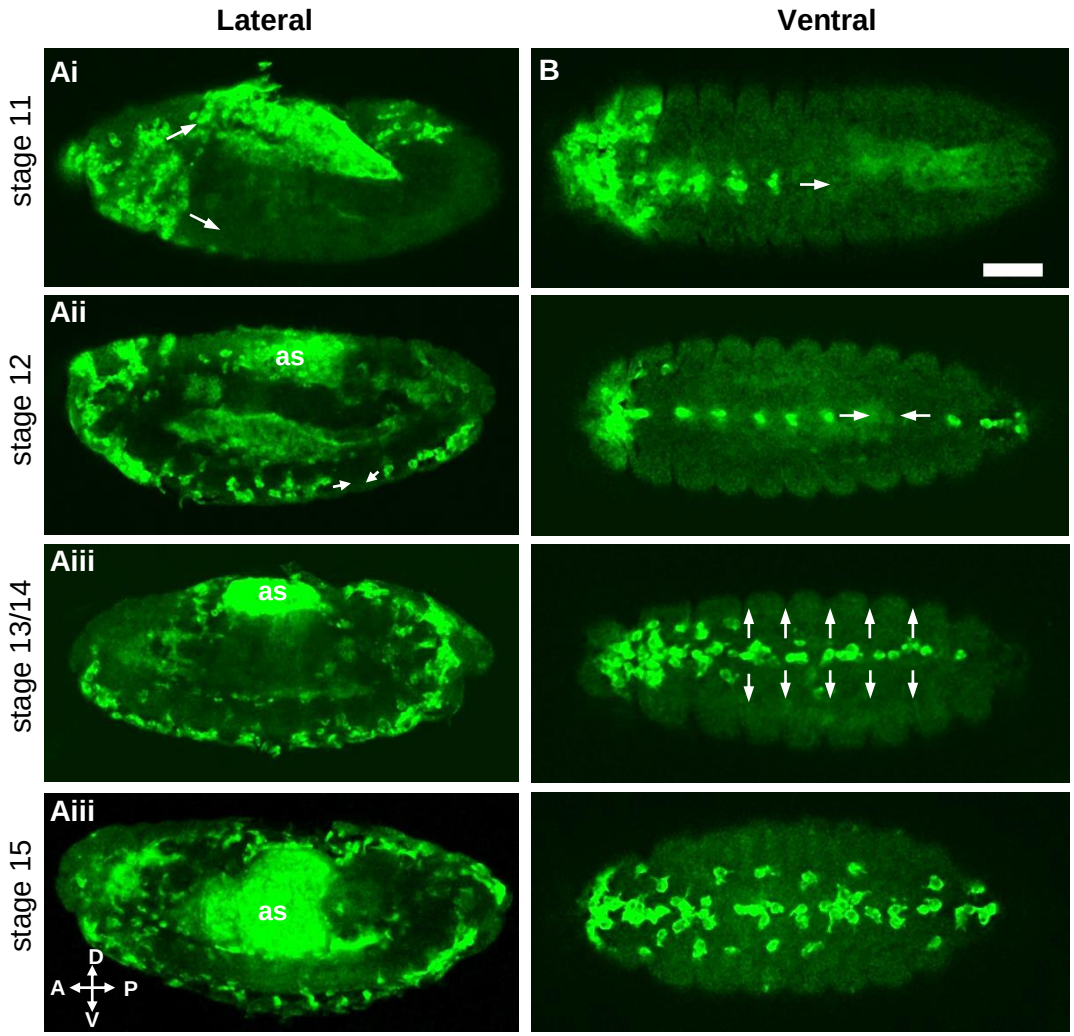

Figure 4. Developmental migration of haemocytes during stages 10-16 of *Drosophila* embryogenesis.

To label haemocytes UAS-GFP was expressed using the haemocyte-specific *srp*-Gal driver. *Drosophila* embryos were then fixed and immunostained with a primary antibody against GFP to visualize haemocytes and embryos of the various stages were selected for confocal imaging. (**A**) The haemocytes are specified in the head mesoderm (anterior) at stage 10 and a population of haemocytes are passively transported to the posterior within the retracting germband at stage 11 (**Ai**), before migrating anteriorly along the ventral midline at stage 12 (**Aii**). In addition to this population, two haemocyte populations migrate from the head mesoderm along either the ventral or dorsal surfaces of the embryo at stage 12 until they form lines across these regions (**Aii**). These haemocytes then disperse throughout the entire embryo at stages 15-16 (**Aiii** & **Aiiii**). (**B**) Demonstrates the characteristic migration of a population of haemocytes along the ventral midline where the future ventral nerve cord (VNC) will develop. Once they have undergone lateral migration at stage 14 of embryogenesis, haemocytes at the ventral surface migrate randomly (referred to as random migration).

1.3.2 Signalling pathways regulating *Drosophila* haemocyte migration

The developmental migration of haemocytes along the ventral midline is directed by the PDGF/VEGF ligands PVF2 and PVF3, which are expressed from embryonic stage 12 (Cho *et al*. 2002; Wood *et al*. 2006). PVF2 and PVF3 are received by PVR, the *Drosophila* homologue of the vertebrate platelet-derived growth factor (PDGF) and vascular endothelial growth factor (VEGF) receptors, which is expressed in haemocytes (Wood *et al*. 2006). At embryonic stages 15-16 expression of the PVF2 ligand is down-regulated along the ventral midline causing haemocytes to migrate laterally, forming three parallel lines that run anteriorly to posteriorly along the developing ventral nerve cord (Wood *et al*. 2006) (**Figure 4**). The role of haemocytes at these stages is to engulf and phagocytose apoptotic debris generated during development of the ventral nerve cord, as well as the production and secretion of several extracellular membrane molecules (Fessler *et al*. 1994).

Haemocytes are also subject to a second, distinct chemotactic migration to epithelial wounds, where they phagocytose any debris generated at a wound site (Stramer *et al*. 2005). Wound healing assays carried out in *Drosophila* embryos have revealed that haemocytes within a 40 µm radius of a wound will receive extracellular cues and rapidly re-polarise and migrate to the wound site within minutes (Stramer *et al*. 2005). PVR signalling is not required for this chemotactic migration, but instead requires phosphatidylinositol-3-kinase (PI3K) signalling (Wood *et al*. 2006). The mechanisms regulating haemocyte migration to wounds is therefore distinct from those controlling developmental migration. Interestingly, haemocytes fail to respond to wound cues until embryonic stage 15 as the PDGF/VEGF signalling pathway, activated by a gradient of PVF ligand, overrides haemocyte response to PI3K signalling (Wood *et al*. 2006).

The migratory behaviour of haemocytes, their characteristic lamellipodial protrusions, together with their ability to rapidly re-polarise makes them an ideal cell type to study cell motility. Formation of lamellipodial protrusions at the leading edge of haemocytes requires many of the same actin-regulatory proteins that have been shown to regulate the polarisation of fibroblasts and other migratory cell types in tissue culture. The developmental migration of haemocytes along the ventral midline at stage 15 of embryonic development can be studied through time-lapse imaging using confocal microscopy and wound-healing assays can also be carried out using an ablation laser to control chemotactic haemocyte migration to study cell migration within an *in vivo* system (Stramer *et al*. 2005).

Interestingly, many of the factors required for *Drosophila* haematopoiesis and subsequent regulation of haemocyte function are conserved within vertebrate haematopoiesis (Evans *et al*. 2003). The specification of both vertebrate blood progenitor cells and *Drosophila*

haemocytes requires expression of GATA transcription factors, including *serpent* (*srp*) in *Drosophila* and GATA1, GATA2 and GATA3 in mice (Fujiwara *et al*. 2003). Although not required for haemocyte specification, the PDGF/VEGF receptor, termed PVR in *Drosophila*, is required for the developmental migration of haemocyte (Cho *et al*. 2002). In mammals, the VEGFR signalling pathway induces B cell development and is required for maintenance and/or survival of haematopoietic stem cells (Gerber *et al*. 2002), with increased VEGF ligand expression often resulting in various haematological malignancies (Ferrara *et al*. 2003). Most relevant to this study is the fact that many of the key regulatory proteins shown to be essential for the polarisation and migration of cultured mammalian migratory cells are also required for migration of *Drosophila* haemocytes *in vivo* (Ridley *et al*. 2001). These include the small GTPases Rho, Rac and Cdc42, with a requirement of Rac to form lamellipodia, Rho for the dissolution of adhesions at the rear of haemocytes and Cdc42 to maintain haemocyte polarity (Stramer *et al*. 2005). Fascin and Ena are required to regulate the actin cytoskeleton during haemocyte migration (Zanet *et al*. 2009; Tucker *et al*. 2011) and SCAR/WAVE, a member of the WASp family, is required for proper haemocyte migration and efficient processing of apoptotic debris engulfed by haemocytes during phagocytosis (Evans *et al*. 2013).

The developmentally-hardwired migration of *Drosophila* embryonic haemocytes and their ability to directly migrate to epithelial wounds, regulated through two distinct signalling pathways, as well as their similarity to mammalian macrophages makes them an ideal system to study the role of RNA regulation in cell motility (Wood & Jacinto 2007; Evans *et al*. 2010). The high genetic-tractability and short lifecycle times of *Drosophila* also makes them an ideal model system.

1.3.3 *Drosophila* border cells as an *in vivo* model system to study cell motility

The border cells are a small cluster of 6-10 cells that migrate posteriorly from the anterior of the *Drosophila* female ovary (Montell 2003). Female *Drosophila* flies have two ovaries which each contain 12-16 ovarioles (King 1970). Each ovariole contains a string of developing egg chambers at various stages of maturity which undergo a process termed oogenesis (**Figure 5A**). Germline and somatic stem cells are contained at the apical end of the ovariole within the germarium (Büning 1994). Asymmetric germline stem cell division in the germarium produces a new stem cell and a cystoblast, which divides four times to produce 16 germline cells (Spradling 1993). One of these will form the developing oocyte, while the remaining 15 become polyploidy nurse cells that nurture the developing oocyte. The germline cells are surrounded by a monolayer of somatic follicular cells, forming the epithelium of the egg chamber (Spradling. 1993) (**Figure 5B**).

Two pairs of specialised follicular cells, termed polar cells, are positioned at each end of the egg chamber, termed polar cells (Margolis & Spradling 1995) (**Figure 5B**). Developing egg chambers bud off from the germarium, with the most mature egg chambers positioned at the distal end of the ovariole, which then bud off from the ovariole upon reaching maturity (King 1970) (**Figure 5A**). During oogenesis the nurse cells generate and load the developing oocyte with maternal mRNAs and proteins which are required for the mature egg to undergo the early stages of embryogenesis upon fertilisation, before the onset of zygotic transcription, termed the maternal-to-zygotic transition (MZT) (Lasko 2012). The development of the egg chamber is classified through a number of different developmental stages, reaching maturity upon stage 14 of oogenesis (Spradling 1993).

During early stage 9 of oogenesis a cluster of 6-10 somatic follicle cells, including the two anterior polar cells, delaminate from the uniform monolayer of follicle cells at the anterior epithelium of the egg chamber (Montell 2003) (**Figure 5Ci**). These cells, termed the border cell cluster, round up and migrate posteriorly between the nurse cells to the oocyte border (**Figure 5Cii & Ciii**). The two non-migratory polar cells form the centre of the cluster and are surrounded by the migratory outer cells, which aid polar cell migration (Han *et al*. 2000). The border cells are required to form a structure at the oocyte anterior called the micropyle. The micropyle contains a pore through which the sperm enters and so failure of border cell migration prevents fertilisation of the mature egg (Montell *et al*. 1992). Border cells are also required to express the gene *torso-like* which is required for patterning of the head and tail regions of the embryo (Savant-Bhonsale & Montell 1993).

The *slow border cells* (*slbo*) gene, a homologue of the mammalian transcription factor C/EBP, has been identified as essential for border cell migration as it is required for the expression of genes that enable the border cells to become motile (Montell *et al*. 1993). Targets of *slbo* required for border cell migration include E-cadherin, focal adhesion kinase (FAK) and myosin VI (Oda *et al*. 1997; Niewiadomska *et al*. 1999; Bai *et al*. 2000; Geisbrecht & Montell 2002). The JAK/STAT pathway is also required for proper migration. Expression of the JAK/STAT cytokine ligand *unpaired* (*upd*) is restricted at stage 9 of oogenesis to the pair of polar cells at each end of the egg chamber, which activates the JAK/STAT pathway in the outer cells of the border cell cluster (Beccari *et al*. 2002). Downregulation of *upd* expression in the polar cells alone results in failure of border cell migration, while *upd* downregulation in all ovarian cell types excluding the two pairs of polar cells allows efficient border cell migration (Silver & Montell 2001).

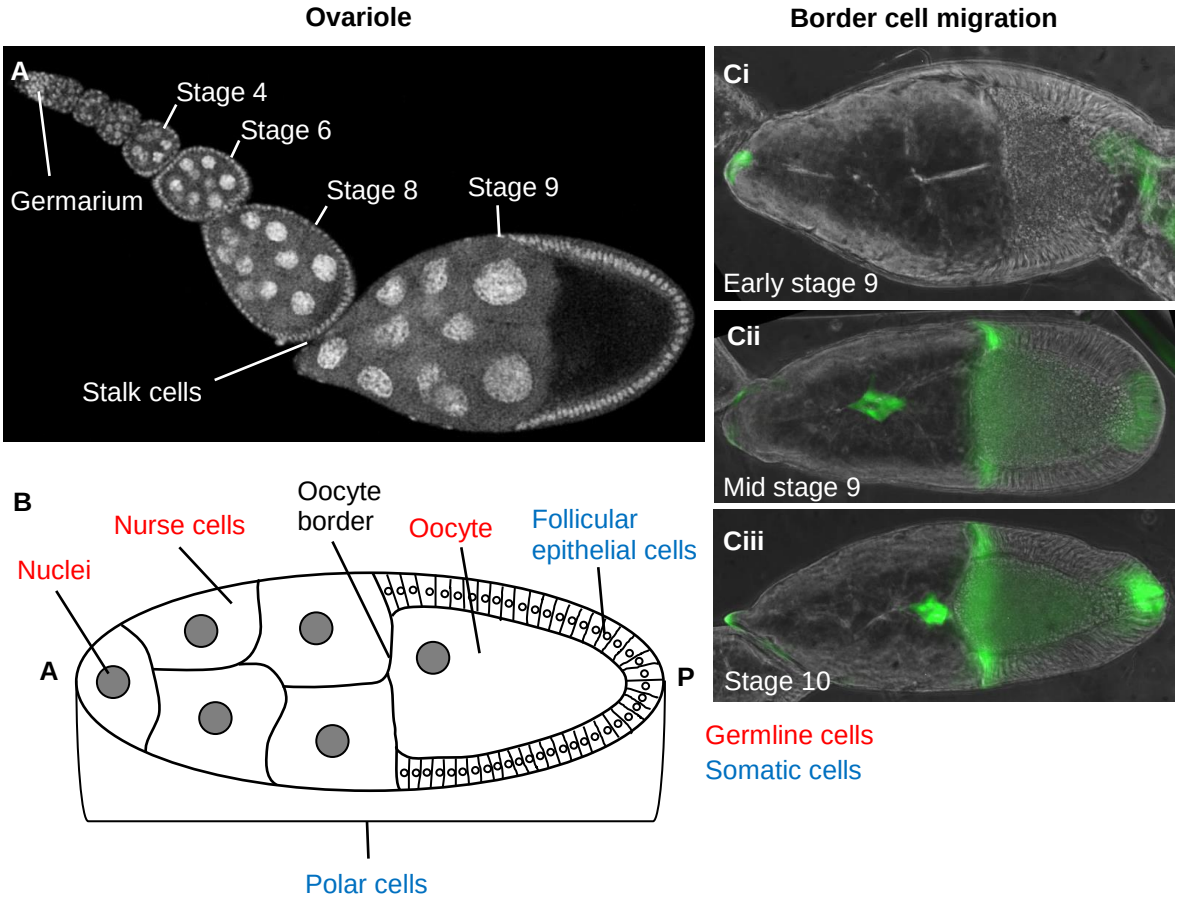

Figure 5. Border cell migration during *Drosophila* oogenesis

(**A**) A single ovariole contains a string of developing oocytes that are connected by stalk cells. The germarium, located at the apical end, contains germline and somatic stem cell populations that divide to produce 16 germline cells and somatic follicular cells. The most mature oocytes are located at the distal end of the ovariole and bud off upon reaching maturity at stage 14 of oogenesis. (**B**) A schematic representation of the structure of a stage 10 egg chamber. Cells of germline origin are highlighted in red, while somatic cells are highlighted in blue. (**C**) A cluster of 6-10 follicular epithelial cells delaminate from the epithelium at the egg chamber anterior (**Ci**) and migrate centrally through the nurse cells towards the posterior of the oocyte (**Cii**). Upon reaching the oocyte border (**Ciii**) the border cells remain at the border to later form the micropyle.

The timing of border cell migration is regulated by the Ecdysone hormone through the transcriptional co-activator protein *taiman* (*tai*), which binds to hormone receptors in the presence of a ligand (Bai *et al*. 2000). The border cells migrate centrally through the egg chamber by expression of a chemoattractant in the oocyte (Montell 2003). Evidence suggests that expression of both the VEGF/PDGF and EGF (Epidermal growth factor) signalling pathways may be required for border cell guidance during their migration (Duchek *et al*. 2001). For example, the Pvf1 ligand, a homologue of mammalian VEGF/PDGF, is expressed at high levels within the oocyte and knockout of its expression results in border cell migration failure in ~30% of egg chambers (Duchek *et al*. 2001). Interestingly the

VEGF/PDGF signalling pathway is also implicated in the developmentally-hardwired migration of embryonic haemocytes (Cho *et al*. 2002; Wood *et al*. 2006).

To delaminate from the epithelium the border cells must first down-regulate factors associated with cell-cell adhesion, while still maintaining contact with each other and the two polar cells (Montell 2003). The border cell cluster must then become polarised for migration to successfully occur, which includes maintaining both a tailing and leading edge (Prasad & Montell 2007). Long actin protrusions extend from the border cells at the leading edge of the cluster between the two most anterior nurse cells to initiate migration (Tekotte *et al*. 2007). These actin protrusions persist throughout border cell migration and it is thought that signals received by the guidance receptors of the VEGF/PDGF and EGF signalling pathways trigger and help maintain this polarity (Duchek *et al*. 2001).

Although the role of cytoplasmic RNA regulation has been studied extensively in the *Drosophila* oocyte, we are yet to identify examples of RNAs whose cytoplasmic regulation is required for the proper migration of border cells. However, there is emerging evidence to suggest that mRNA localisation and/or local translation may be required to regulate border cell migration, as border cells lacking expression of either of the RNA-binding proteins Virilizer (Vir) and Hrp48 failed to migrate, although the transcripts regulated by these RBPs in border cells have yet to be identified (Mathieu *et al*. 2007). Downregulation of the RNA-binding protein PTB (Polypyrimidine Tract Binding Protein) in border cells also causes migratory defects, suggesting that RNA regulation within these cells may be required for cell motility (Besse & López de Quinto - unpublished). Finally, downregulation of Imp, the *Drosophila* homologue of IMP1, prevents border cell migration as their actin-rich protrusions as lost (Munro *et al*. 2005 – unpublished) in border cells prevents their migration. Their migration may require the localization of *β-actin* mRNA by Imp as a pool of *β-actin* mRNA was present within these protrusions, to which Imp binds at the 3'UTR (Munro *et al*. 2005 – unpublished).

The *Drosophila* border cell cluster is an ideal system to study the role of cytoplasmic RNA regulation as the ovary is easily accessible through dissection and can be fixed for both immunohistochemistry and *in situ* hybridisation, which does not result in the loss of actin protrusions from the border cells. However, although migration of the border cells can be imaged live in dissected ovaries *in situ*, it can be difficult to maintain the conditions required for continued development of the ovary. Therefore, *Drosophila* embryonic macrophages will be utilised to image the live migration of individual cells, while *Drosophila* border cells will be used as a complementary system to study collective cell migration *in vivo*, in a fixed tissue.

1.4 Candidate RBPs to study the roles of RNA regulation in cell migration

This project will focus on the potential role of three candidate RBPs in the regulation of cell motility *in vivo*. These three candidates include the IMP1 homologue Imp, Polypyrimidine-tract binding protein (PTB) and a homolog of the hnRNP A/B family of RBPs called Hrp48. Our current knowledge of the biological roles of these proteins, and our rationale for their selection within this project are described below.

1.4.1 Insulin-like growth factor 2 (IGF-II) mRNA binding protein (Imp)

The Insulin-like growth factor II (IGF-II) family of RNA-binding proteins consist of several members, including the vertebrate proteins IMP1, Imp2 and Imp3 (Nielsen *et al*. 1999). This family of RBPs have been shown to regulate the transport and translation of many transcripts (Nielsen *et al*. 2001). IMP1, identified in chicken, is orthologous to IMP1 and was shown to localise *β-actin* mRNA at the leading edge of migratory cells (Ross *et al*. 1997). Another member of the family, *Xenopus* VG1 RNA-binding protein (VERA), regulates localisation of Vg1 mRNA to the vegetal pole of the oocyte (Deshler *et al*. 1998).

The three vertebrate Imp proteins were thought to arise from two gene duplications shortly before the divergence of vertebrates and share 69-95% amino acid identity. Imp homologues have been identified in both *Drosophila* and *Caenorhabditis elegans*, with a single Imp homologue in *Drosophila* showing 47% sequence identity to the vertebrate Imp proteins. The vertebrate Imp proteins consist of two RNA-recognition motifs (RRMs) and four KH-domains (Nielsen *et al*. 1999), while the *Drosophila* and *C. elegans* homologue contains only the four KH-domains (Nielsen *et al*. 2000). The RRM domains of IMP1 appear dispensable for assembly of the protein into RNP granules, as when only the RRM domains of IMP1 are expressed, they are diffuse and distributed throughout the cytoplasm. However, when only the KH domains are expressed they assemble in granules and show the same expression as full length IMP1. This suggests that the four KH domains are both necessary and sufficient for the cytoplasmic trafficking of IMP1 (Nielsen *et al*. 2002).

Many studies suggest that IMP1/dImp is required for the establishment of cell polarity and subsequent migration of motile cells. As previously mentioned, these studies include those showing that IMP1 is required to localise *β-actin* mRNA and the mRNAs of all seven ARP2/3 complex subunits at the leading edge of motile cultured cells (Ross *et al*. 1997; Shestakova *et al*. 2001; Oleynikov & Singer 2003; Mingle *et al*. 2005). To further support this, border cells within the *Drosophila* oocyte fail to form actin-rich protrusions and migrate in the absence of dImp expression (Munro *et al*. 2005 – unpublished conference abstract).

However, although in some cultured cells Imp has been shown to bind and localise the mRNA of *β-actin*, it was not bound to or regulated by Imp-2 in myoblasts or localised at the leading edge (Boudoukha *et al*. 2010). Similarly, a genome-wide screen to identify RNAs enriched in lamellipodial protrusions in NIH/3T3 fibroblast cells revealed that the mRNAs encoding β-actin and the ARP2/3 subunits were not enriched in these protrusions (Mili *et al*. 2008), possibly reflecting mechanistic differences among cell types.

Several studies have shown the both vertebrate IMP1 and *Drosophila* Imp are associated with microtubules. Within cultured mouse fibroblast cells, IMP1 has been shown to localise on polar microtubules in the midzone of the mitotic spindle during anaphase (Nielsen *et al*. 2002). Transport of Imp within the *Drosophila* oocyte requires microtubules and loss of the microtubule-associated molecular motors dynein or kinesin results in inhibited transport of Imp (Boylan *et al*. 2008). Similarly, in the developing embryonic nervous system, Imp is rapidly and bidirectionally transported in granules along microtubules (Boylan *et al*. 2008). Microtubule precipitation experiments have shown that while IMP1 is bound to microtubules, it does not directly associate with microfilaments or actin filaments and is not directly bound to microtubules through RNAs (Nielsen *et al*. 2002).

One interesting idea is that Imp not only requires the microtubule network for its transport, but can also indirectly regulate microtubule polymerization and stabilization. A study to identify potential RNA targets of Imp-2 suggests that it is required to regulate transcripts whose products are essential for the stabilization of microtubules, and therefore muscle cell motility (Boudoukha *et al*. 2010). In this study co-immunoprecipitation of Imp-2 from C2C12 myoblasts showed that 35% of transcripts co-precipitated with Imp-2 encoded proteins involved in cell motility, adhesion and cytoskeleton and membrane re-modelling. The down-regulation of Imp-2 in these cells led to changes in cell morphology and a dramatic decrease in cell motility. Specifically, it caused a decrease in two post-translationally modified forms of α-tubulin (Glu-tubulin and δ-2 tubulin) which are associated with stabilized microtubules. The mRNA of PINCH-2, a LM domain protein that partially dissociates focal adhesion complexes, was significantly up-regulated in Imp-2 knockdown myoblasts, causing large aggregations of focal adhesions (FAs) at the cell periphery, which are normally found within cytoplasmic regions. These FAs are suggested to be sites of stabilization for MTs and re-modelling of these FAs to the cell periphery, caused by over-expression of PINCH-2, decreases the number of stable MTs. Imp-2 appears to directly bind the 5’ end of PINCH-2 mRNA. Knockdown of PINCH-2 mRNA in Imp-2 depleted myoblasts significantly increased the number of stable microtubules observed and restored cell motility, suggesting that up-

regulation of PINCH-2 mRNA could account for the changes in cell morphology and loss of cell motility seen in Imp-2 depleted myoblasts (Boudoukha *et al*. 2010).

1.4.2 *Drosophila* Polypyrimidine-tract Binding Protein (PTB)

PTB, also referred to as heterogenous nuclear ribonuclearprotein I (hnRNP I), is a member of the hnRNP family of RNA-binding proteins and regulates many aspects of mRNA metabolism, including splicing, polyadenylation, mRNA stability and localisation and translation initiation (Sawicka *et al*. 2008). PTB is ubiquitously expressed and appears to regulate the processing of many different transcripts. It consists of four RNA-recognition motifs (RRMs) which bind to pyrimidine-rich elements in RNA (Singh *et al*. 1995; Sawicka *et al*. 2008).

PTB is required for the localisation of mRNA, whose local translation is essential for the establishment of polarity within both *Xenopus* and *Drosophila* embryos. Localisation and then local translation of Vg1 within the vegetal cytoplasm of *Xenopus* oocytes is mediated by the Vg1 RNP complex. PTB is required to remodel the interaction between the RBP Vg1/Vera and *vg1* RNA which is required for localisation of the Vg1 RNP complex (Lewis *et al*. 2008). The localisation and local translation of *oskar* mRNA at the posterior of *Drosophila* oocytes is essential for establishing the posterior pole of the future embryo. PTB is required for the translational repression of *oskar* mRNA during its transport within an RNP complex to prevent its translation within regions of the oocyte where Oskar protein would cause abhorrent effects (Besse *et al*. 2009).

Importantly, knockdown of PTB expression within Border cells, a population of cells which show a distinct migratory pattern within the *Drosophila* ovary, prevents their migration during oogenesis (Besse & López de Quinto - unpublished). PTB has also been shown to transiently localise at FACs within the leading edge of mouse embryonic fibroblasts, where it associates with mRNAs that encode focal adhesion scaffolding proteins, including α-Actinin 4 and Vinvulin (Babic *et al*. 2009). PTB depletion in these cells resulted in a loss of cell spreading and reduced number of protrusions, a decrease in Vinculin protein at the cell periphery and significantly shorter focal adhesions (Babic *et al*. 2009).

Axon growth in developing neurons has been shown to require RNA localisation and localised translation at the tip of the extending axon, including *β-actin* mRNA (Olink-Coux & Hollenbeck 1996). Cells of the PC12 rat cell line produce neurites when grown with appropriate stimulates in cell culture and PTB has been shown to bind *β-actin* mRNA in these growing neurites (Ma *et al*. 2007). In PC12 cells treated with RNAi to deplete PTB expression, neurite growth was severely inhibited and the localisation of *β-actin* mRNA at the

tip of the growing neurite was reduced (Ma *et al*. 2007). This suggested that PTB may also play a role in the localisation and/or local translation of *β-actin* mRNA at the leading edge of migratory cells.

PTB is frequently overexpressed in highly-metastatic human glioma, which has been shown to increase non-directional migration in two human glioma cell lines (Cheung *et al*. 2009). Down-regulation of PTB also inhibited migration of these cell lines (Cheung *et al*. 2009). It would be interesting to see if this is the result of mRNA delocalisation, which may be required for proper cell motility.

1.4.3 *Drosophila* hnRNP A/B homologue, Hrp48

The RBP Hrp48, also known as Hrb27, is a member of the hnRNPA/B family of proteins and contains two RRM domains at its N-terminus, as well as a C-terminal Glycine-rich domain (Matunis *et al*. 1992). Hrp48 is required for the localisation of *gurken* mRNA in the *Drosophila* embryo (Goodrich *et al*. 2004) and for translational repression of *oskar* mRNA within the *Drosophila* oocyte (Yano *et al*. 2004; Huynh *et al*. 2004). Regulation of these mRNAs is critical to establish polarity within the developing *Drosophila* embryo (Goodrich *et al*. 2004; Yano *et al*. 2004; Huynh *et al*. 2004). Loss of Hrp48 expression in border cells causes severe migratory defects (Mathieu *et al*. 2007), suggesting that RNA regulation by Hrp48 is required for migration.

Interestingly, Hrp48 has been previously implicated in phagocytosis as shown by genome-wide RNAi screens in *Drosophila* S2 cells. Knock-down of Hrp48 expression in S2 cells decreased the incidence of infection of the cytosolic pathogen *Listeria monocytogenes* (Agaisse *et al*. 2005). Hrp48 was also identified in an immunoprecipitation pull-down assay of the SCAR/WAVE complex (Gautier *et al*. 2011). SCAR (suppressor of cAMP receptor)/WAVE [WASP (Wiskott-Aldrich syndrome protein)-family verprolin homology protein] proteins are members of the conserved WASP family of cytoskeletal regulators and are required for activation of the Arp2/3 complex, while regulates actin dynamics (Ibarra *et al.* 2005). Down-regulation of SCAR/WAVE protein expression in *Drosophila* S2 cells results in spikey membrane protrusions at the cell periphery and a genome-wide RNAi screen revealed that knock down of actin-regulatory genes, such as Rac1, Cdc42 and components of the ARP2/3 complex produced a similar phenotype (Gautier *et al*. 2011). Knock-down of Hrp48 expression also produced a phenotype similar to that of SCAR/WAVE down-regulation, suggesting that Hrp48 may play a role in regulating transcripts whose products are required for lamellipodial formation (Gautier *et al*. 2011). Many actin-regulatory proteins required for lamellipodial formation at the leading edge also play a role in regulating actin dynamics required for phagosome formation

(Pearson *et al*. 2003), supporting the idea that Hrp48 may play a role in regulating transcripts required for cell motility and phagocytosis in haemocytes.

1.5 Aims & Objectives

Although current research has revealed that RNA localisation and local translation of asymmetrically enriched mRNAs play an important role in the regulation of cell motility in cultured cells, these observations await *in vivo* validation.

The overall aim of this project is to establish an *in vivo* model to study the role of cytoplasmic RNA regulation in cell motility. Tools will therefore be generated to follow *in vivo* the distribution of candidate mRNAs previously implicated in the regulation of cell motility, together with their regulatory RNA-binding proteins. Two complementary systems will be used: i) *Drosophila* embryonic haemocytes, as an example of individual cell migration and ii) *Drosophila* border cells, as an example of collective cell migration.

Fly embryonic haemocytes are highly amenable to live imaging, show a distinct pattern of migration during development and represent a good example of individual cell migration. As the mechanisms regulating cell motility and phagocytosis of *Drosophila* haemocytes are conserved with those operating in mammalian macrophages, our findings could have implications for vertebrate immunology and medicine. The use of a complementary *in vivo* system, such as the collective cell migration of ovarian border cells, will allow us to compare and contrast the mechanisms underpinning different types of cell migration *in vivo*.

To characterize these model systems, the following objectives were set:

1) Generate and characterize tools to follow the subcellular localization of candidate RNA-binding proteins (RBPs) and their potential mRNA targets. These will include flurophore-tagged Imp, Hrp48 and PTB proteins and components of the MS2 system, which will be used to follow the localization of candidate mRNAs *in vivo*.
2) Study the effects that overexpression and loss of function of regulatory RBPs could have on cell motility *in vivo*.
3) Identify and characterize potential mRNA targets of regulatory RBPs, whose regulation is required for cell motility

Chapter 2:

Materials & Methods

2.1 Molecular Biology

As part of this project, a number of new constructs were generated using standard Molecular Biology techniques (see section 2.2 for details; listed in Appendix 1). The next sections will describe the general cloning procedures used to generate these constructs, as well as other molecular biology techniques.

2.1.1 Cloning Vectors

Two UAS-based cloning vectors were used for expressing transgenic constructs in *Drosophila*. The pUAST vector contains the hsp70 promoter and SV40 terminator to drive expression within somatic tissues, but does not drive transgene expression within the germline. To drive expression within the germline a modified vector, termed pUASP, which contains the P transposase promoter and 3' UTR of the maternally expressed K10 gene was developed (Duffy 2002). We used a modified pUASp vector, referred to as pTiger, containing the attP site required for integration of plasmids by the PhiC31 system (Ferguson *et al*. 2012) (Appendix 3.1). To achieve higher levels of expression, a modified version of the pUASt-attB containing vector (Basler Lab, Zurich) was generated by SLQ, which contained 19 UAS sites compared to the original plasmid that contained 5 UAS sites (Appendix 3.2).

To build constructs from several stitched sequences, or for constructs used to generate RNA probes, the pBluescript (pBS) vector was used in either the SK+ or KS+ orientation (Stratagene) (Appendix 3.3 & 3.4). The pENTR-TOPO vector (pENTR™ Directional TOPO® Cloning Kit acquired from *Life Technologies*) was used to clone candidate mRNAs for the MS2 system (Appendix 3.5). The pJET1.2 vector (CloneJET PCR Cloning Kit by Thermo Scientific) was used for some PCR products as an intermediate cloning step before cloning into the final expression vector (Appendix 3.6).

2.1.2 Polymerase chain reaction (PCR) and reverse-transcription PCR (RT-PCR)

Standard PCR reactions were carried out using either plasmids or genomic DNA as templates, and different polymerases depending on the purpose. Briefly, 10-20 ng of plasmid DNA or 100-200 ng of genomic DNA was used in 20-50 µl reactions in the presence of 0.2 µM sense and antisense primers. For cloning purposes, a High-fidelity DNA polymerase (Q5 or Phusion from NEB, or HiFiTaq polymerase from PCR Biosystems) was used in the presence of custom synthesized primers (Sigma) designed to amplify specific regions of interest and to introduce restriction enzyme

sites compatible to those present in the specific cloning/expression vector (Appendix 2). Diagnostic PCR reactions for screening were performed using standard Taq polymerases (i.e. RedTaq from Sigma or Taq DNA polymerase form PCR Biosciences). Annealing temperatures, elongation times and buffer conditions were adjusted to the primers used, the length of the fragment and the specific enzyme, following the manufacturer's instructions. All PCR reactions were carried out in a BioRad MJ Mini Personal Thermal Cycler.

RT-PCR reactions were carried out using SuperScript® III One-Step RT-PCR System with Platinum® *Taq* DNA Polymerase (Life Technologies) in a 50 µl total reaction volume with 50-100 ng starting RNA template depending on the amplification.

For subsequent applications, amplified PCR fragments were purified from the PCR reactions using GeneJET PCR Purification kit (Thermo Scientific) following the manufacturer's instructions.

2.1.3 Oligo Primer Design

To determine primer melting temperature and assess the degree of potential secondary structure and hetero/homo-dimer formation, oligo primers to amplify products for subsequent cloning into vectors, or for generating templates for *in vitro* transcription reactions, were designed manually from the appropriate DNA sequence and analysed using the OligoAnalyzer 3.1 tool from Integrated DNA Technologies

Primer pairs for real-time quantitative PCR analysis were designed using the QuantPrime tool. Primers were designed to amplify specific products of between 80-150 nucleotides. All qPCR primer pairs were first tested by standard end-point PCR using genomic DNA template, and products separated by gel electrophoresis to ensure their specificity and efficiency.

2.1.4 Agarose Gel Electrophoresis

DNA or RNA fragments were separated by size using electrophoresis on agarose gels. Typically 1% (w/v) gels in TBE buffer (Tris base, Boric acid, 0.5 M EDTA[8]) and SYBR® Safe DNA gel stain (Life Technologies) was used to visualise DNA fragments. 6x DNA loading dye solution (Thermo Scientific) or 2x RNA loading dye solution (Thermo Scientific) were used with either DNA or RNA samples, respectively. GeneRuler™ 1 kb Plus DNA Ladder (Thermo Scientific) was used to size DNA fragments, while the RiboRuler High Range RNA Ladder (Thermo Scientific) was used to size RNA fragments. Gels were analysed in either a GelDoc-

It®-310 documentation system (UVP) using UV light, or a Dark Reader Transilluminator (Clare Chemical Research) to excise bands for cloning.

2.1.5 DNA Gel Extraction

DNA fragments separated by agarose gel electrophoresis were cut using a clean scalpel and a Dark Reader Transilluminator. The GeneJet Gel Extraction Kit (Thermo Scientific) was used to extract the DNA from gel fragments according to the manufacturer's instructions.

2.1.6 Restriction Enzyme Digestions

All restriction digests were carried out using FastDigest enzymes (Thermo Scientific) in Universal Buffer (allowing double digests to be carried out simultaneously) for 5 to 60 minutes at 37°C. Restriction digests to screen constructs prepared from a bacterial culture were carried out in a 10 µl volume. To digest vectors for subsequent cloning, 1 µg of vector was digested in a 30 µl reaction volume. To digest PCR products for cloning, 1 µg of PCR product was digested in a 150 µl reaction. When required for further steps, restriction enzymes were heat inactivated, or the DNA purified using a GeneJET PCR purification kit (Thermo Scientific).

Vectors used for subsequent cloning steps were de-phosphorylated with FastAP Alkaline Phosphatase (Thermo Scientific) after digestion.

2.1.7 Ligation

All ligation reactions were carried out in a 10 µl volume using the Rapid DNA Ligation Kit (Thermo Scientific) with a 3:1 insert to vector ratio. Ligations were performed at room temperature for one hour.

2.1.8 Bacterial Cultures and Agar Plates

Luria-Bertani (LB) agar plates were made by disolving pre-mixed LB-agar large granules (Thermo Scientific) in the appropriate volume of distilled water, followed by autoclaving to sterilise the solution. Ampicillin was then added and the media poured into 10mm petri dishes, left to set and stored at 4°C. Bacteria were grown in liquid LB broth, also prepared from LB broth large granules (Thermo Scientific), autoclaved and stored at 4°C.

2.1.9 Transformation of Competent Cells

DH5α competent bacteria were prepared using the Mix & Go *E.coli* Transformation Kit (Zymo Research). 50 µl aliquots of DH5α competent bacteria were stored at -80°C. When required, bacteria were thawed gently on ice and 1 µl of plasmid or ligation mixture was added and gently mixed. Bacteria were incubated on ice for five minutes and were then spread on LB-agar plates containing either Ampiciliin (100µg/ml) or Kanamycin (50µg/ml) antibiotics for selection. Agar plates were incubated at 37°C overnight in a bacteria incubator.

2.1.10 Plasmid Preparation from Bacterial Culture

To screen individual colonies for the presence of the correct construct, colonies were inoculated in 1.5 ml of LB media containing an appropriate antibiotic. Cultures were grown at 37°C overnight with 250 rpm shaking. On the following day, cultures were centrifuged for 2 minutes at 13,000 rpm in 1.5 ml eppendorfs to pellet the bacteria. The supernatant was removed and the plasmid purified from the pellet using the Thermo Scientific GeneJet Plasmid Miniprep Kit according to the manufacturer's instructions.

To prepare plasmids for microinjection for fly transgenesis, bacteria colonies were inoculated in 20 ml LB media, grown overnight as described above and pelleted by spinning at 3000 x g for 20 minutes. The plasmid was purified using an Endotoxin-free E.Z.N.A.® Plasmid Isolation Kits (Omega Bio-Tek) according to the manufacturer's instructions.

2.1.11 Genomic DNA extraction from single flies

A single fly was ground in 100 µl of lysis buffer (50 mM Tris-HCl$^{8.0}$, 50 mM KCl, 2.5 mM EDTA, 0.45% NP-50, 0.45% Tween-20) containing 1 µl of Proteinase K (20 mg/ml) (Thermo Scientific) by using a clean pipette tip. The fly was then incubated for 1 hour at 65°C with occasional vortexing to aid digestion. The reaction was spun for 5 minutes to collect the cell debris and the supernatant was then mixed with 100 µl of binding buffer from the GeneJet PCR purification kit (Thermo Scientific) and loaded into an NBS DNA purification spin column. The column was centrifuged at 13,000rpm for 1 minute and the flow through discarded. 750 µl of DNA wash solution (Thermo Scientific) was added to the column and centrifuged for 1 minute. The flow through was discarded and the empty column centrifuged for a further minute to remove residual wash solution. The genomic DNA was then eluted by adding 50 µl of elution

buffer to the column, which was incubated for 2 minutes before centrifuging it at 13,000 rpm for 2 minutes.

2.1.12 Total RNA extraction from *Drosophila* embryos, ovaries and S2R+ cells

Approximately 10 pairs of ovaries or 200 embryos were used for extraction of total RNA with the GeneJET RNA purification kit (Thermo Scientific). Ovaries and embryos were collected in PBS and RNA extraction was either carried out immediately or the material stored in RNAlater solution (Life Technologies) at 4°C. To extract RNA from embryos or ovaries, the PBS was removed and the material re-suspended in 300 µl lysis buffer supplemented with 6 µl β-mercaptoethanol. The material was then homogenised in a borosilicate tissue grinder using 20 strokes of the pestle and 600 µl of Proteinase K at the appropriate dilution (supplied with kit) was added. The homogenised material was briefly vortexed, incubated at room temperature for 10 minutes and centrifuged for 5 minutes at 13,000 rpm. The supernatant was collected, supplemented with 450 µl ethanol and added to the provided spin columns. RNA purification using the spin column was then carried out according to the manufacturer's instructions and RNA eluted from the column in 50 µl nuclease-free water.

Total RNA was extracted from S2R+ cells by counting using a Neubauer Chamber (see section 2.5.3), and collecting $1x10^7$ S2R+ cells in appropriate culture media. Cells were pelleted by centrifugation at 250 x g for 5 minutes. The culture media was removed and cells washed in PBS to remove excess media. PBS was removed and the cells re-suspended in 600µl lysis buffer, supplemented with 12µl β-mercaptoethanol, before vortexing for 10 seconds. As the lysis buffer did not become viscous and no cell debris was observed, 360 µl of ethanol was added and the material was placed in a spin column after mixing. The spin column RNA purification was then carried out according to the manufacturer's instructions and RNA eluted from the column in 50 µl nuclease-free water.

2.1.13 Genomic DNA removal from RNA preparations

To remove genomic DNA from RNA preparations, up to 1 µg of RNA was used in 10 µl reactions with 1x DNase I reaction buffer with $MgCl_2$ and 1 µl DNase I (Thermo Scientific). The reaction was incubated at 37°C for 30 minutes and 1 µl of 50 mM EDTA was added before the reaction was incubated at 65°C for 10 minutes to inactivate DNase I. To remove genomic DNA from larger volumes of RNA the reaction was scaled up accordingly.

2.1.14 cDNA Synthesis

The SuperScript® III First-Strand Synthesis SuperMix was used to synthesise cDNA from purified and DNase I treated RNA. Typically, 6 µl of RNA template was used in a 20 µl cDNA synthesis reaction in the presence of oligo$(dT)_{20}$. Reactions and thermal cycling parameters were set up according to the manufacturer's instructions.

2.1.15 Real time quantitative PCR

qPCR reactions were carried out using either the qPCRBIO SyGreen Mix Lo-ROX (PCR Biosystems) or Brilliant III Ultra-Fast SYBR® QPCR Master Mix (Agilent Technologies) with a Chromo4™ Real-Time PCR Detector (Bio-Rad) and Opticon Monitor™ software. Triplicate 20 µl or 10 µl reactions were set up in in 96 well plates according to the manufacturer's instructions. The concentration of cDNA used was adjusted according to the assay and diluted in Milli-Q water to the maximum volume allowed for each reaction to minimise pipetting error. Low retention tips were used to pipette reaction components to minimise pipetting error. For primer design see section 2.1.2. All primers used for qPCR (primers 76 to 96) are listed in Appendix 2. Thermal cycling conditions were set up according to the manufacturer's instructions and melting curve analysis was performed after quantification to analyse product homogeneity and primer efficiency and aid the identification of false positives.

2.1.16 RNA Probe Synthesis: *in vitro* transcriptions

Plasmid Digestion

To generate *digoxigenin*-labelled RNA probes for FISH (fluorescence *in situ* hybridization) and biotinylated-labelled RNA probes for RNA-affinity pulldown assays, linearized pBS-SK+ constructs (or pJET2.1 in the case of *myospheroid* coding region) containing the fragment of interest were used in *in vitro* transcription reactions. Around 6 µg of plasmid DNA was linearized in a 150 µl digestion reaction with the appropriate restriction enzyme and subsequently purified using phenol extraction or a PCR purification kit (Thermo Scientific).

In vitro transcription

To generate sense or anti-sense RNA probes, the TranscriptAid T7 High Yield (Thermo Scientific), HiScribe™ T7 High Yield (New England Biolabs) or MEGAscript® T3 (Ambion) Transcription Kits were used. 10 µl reactions containing at least 0.5 µg of linearized templates were set up according to the manufacturer's instructions in the presence of either Digoxigenin-11-UTP (Roche) or Biotin-11-UTP

(Roche) in an 8:1 ratio (unmodified UTP to modified UTP). The resulting reaction was incubated overnight at 37°C. On the following day DNase I was added and the reaction incubated at 37°C to digest plasmid DNA. The RNA was then precipitated by adding 40 µl of RNase-free water and 30 µl of Lithium Chloride before chilling it at -20°C overnight. To pellet the RNA, the reaction was centrifuged at 13,000 rpm for 15 minutes at 4°C, and the pellet washed with 75% ethanol before being air-dried and re-suspended in 50µl RNase-free water. The final concentration of RNA probe was estimated by measuring the optical density using a NanoDrop ND-1000 and running a small quantity of RNA probe (circa 1 µg) on a 1% agarose gel to test the RNA integrity and concentration. The RiboRuler High Range RNA ladder (Thermo Scientific) was used to estimate the size of the RNA probes.

2.1.17 Polyacrylamide Gel Electrophoresis (SDS-PAGE) and Western Blotting

Polyacrylamide gel electrophoresis and protein transfer

Protein samples were mixed with an appropriate volume of 2x SDS loading dye, heated at 92°C for 5 minutes and loaded into hand cast 8% polyacrylamide gels. The Precision Plus Protein™ Dual Color Standard protein ladder (Bio-Rad) was used to size proteins. Separated proteins were then transferred onto 0.2 µm PVDF (polyvinylidene difluoride) membrane using the Trans-Blot Turbo Transfer System and the Trans-Blot Turbo™ Mini PVDF Transfer Packs (Bio-Rad) according to the manufacturer's instructions.

Detection of the protein of interest

To detect proteins, membranes were blocked in 5% milk in PBT (0.1% Tween-20 in PBS) for 1 hour and then incubated in primary antibody diluted in blocking solution overnight at 4°C with shaking (see **Table 2** for antibody dilutions). Membranes were washed 3 times in PBT for 10 minutes and then incubated in HRP-conjugated secondary antibody diluted in blocking solution for 1 hour at room temperature with shaking. After 3 washes in PBT for 10 minutes, proteins were detected by chemiluminescence using either Clarity™ Western ECL Blotting Substrate (Bio-Rad) or Luminata™ Forte Western HRP Substrate (Millipore). Membranes were exposed to X-Ray films (Fujifilm Super RX X-Ray film, Thermo Scientific).

SNAP i.d.® 2.0 protein detection system

Alternatively, once proteins were transferred onto PVDF membranes, protein detection was carried out using the SNAP i.d.® 2.0 detection system (Millipore), which uses vacuum to draw solutions through the membrane, allowing these steps to

be carried out in under 30 minutes. Incubation and washing steps were carried out according to the manufacturer's instructions using 0.1% milk in PTB as blocking solution. Chemiluminescent substrate was then applied to the membrane and protein detection was carried out as described above.

Table 2: Antibodies used for Western Blotting

Target	Host	Dilution	Source
Actin	Mouse	1:500	Developmental Studies Hybridoma Bank (JLA20)
GFP	Rabbit	1:3000	Amsbio (TP401)
Imp	Rabbit	1:3000	Medioni *et al*. 2014
Kinesin Heavy Chain	Rabbit	1:10,000	Cytoskeleton (AKIN01)
βPS-integrin	Mouse	1:50	Developmental Studies Hybridoma Bank (CF.6G11)
PTB	Rabbit	1:5000	Besse *et al*. 2009
HRP-coupled Rabbit IgG	Goat	1:5000	Millipore (12-348)
HRP-coupled Mouse IgG	Sheep	1:3000	GE Healthcare (NA931)

2.2 Constructs to generate transgenic fly lines

A number of different constructs were generated as part of this project (see Appendix 1). In general, they can be divided in two groups: i) plasmids encoding for proteins and/or mRNAs used for the generation of transgenic flies; and ii) plasmids containing different gene fragments used as templates for *in vitro* transcriptions. Although described in detail in the following sections, in general, pre-existing plasmids, cDNA or gDNA were used as template for the amplification of the sequence of interest using primers designed to add restriction sites compatible with those present in the final expression vector. For a complete list of the primers used in this project, see Appendix 2. Vector maps of all UAS constructs generated in this project can be found in Appendix 4. Constructs and individual cloning strategies are described below.

2.2.1 MS2 System for *in vivo* visualisation of exogenous mRNA

The MS2 system was used to examine the *in vivo* distribution of candidate mRNAs. The RNA-binding coat protein (MCP) from the bacteriophage MS2, fused to a reporter fluorophore, is expressed within the tissue of interest along with the candidate mRNA fused to several copies of the MS2-hairpin RNA binding sites. In our case, the candidate mRNA consisted of the entire transcript, including both the 5' and 3' UTRs to include all regulatory sequences. The MCP should bind the MS2 hairpin binding sites at regions where the candidate mRNA is localised and the reporter will give a readout of the localization pattern (Bertrand *et al*. 1998; Forrest & Gavis 2003).

Two separate constructs must therefore be generated for the MS2 system to work. The first will encode the MS2-hairpin tagged candidate mRNA and the second encodes the GFP or mCherry-tagged MCP. Candidate mRNAs with 18 hairpin repeats of the MS2 binding sites were tagged at their 5' end (**Figure 6**). Two different MCP constructs were generated, the first consisting of a sequence encoding only a single copy MCP protein C-terminally tagged with either GFP or mCherry. The second construct, termed the tandemMCP (tdMCP), encoded an MCP fusion protein in which two copies of the MCP sequence were joined by a short linker region, followed by the sequence of either mCherry or GFP. Expression of this construct should increase the signal of MCP bound to candidate mRNAs as the MCP dimerizes within the cytoplasm, before binding to the MS2 hairpin binding sites (Wu *et al*. 2012). By using a tandem copy of the MCP twice the number of fluorescently-labelled protein will bind the candidate mRNA, generating a stronger signal than that from a single copy of the MCP alone (Wu *et al*. 2012). Both the single and tandem MCP transgenes contain an NLS to ensure that unbound MCP is sequestered within the nucleus to reduce cytoplasmic background (Forrest & Gavis 2003).

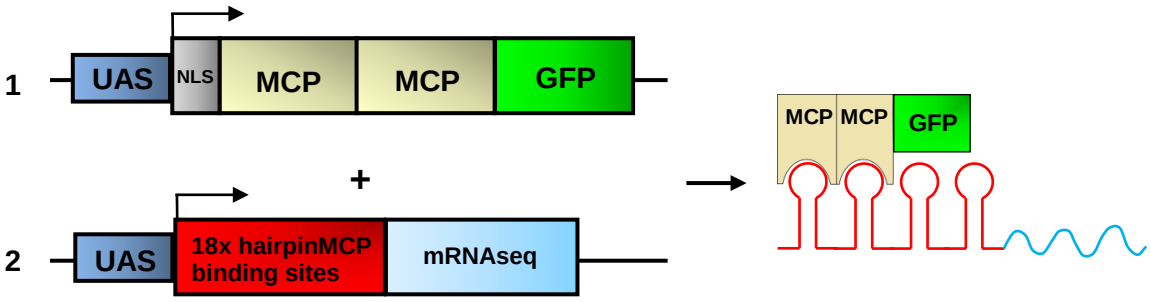

Figure 6. Schematic representation of the MS2 System. Two separate transgenes need to be co-expressed to visualise mRNA distribution within the cell of interest. Both transgenes are placed under the control of the UAS promoter to express them specifically within haemocytes or any other fly tissue using the GAL4/UAS system.

MS2 binding site & Gateway cassette construct

The pSL vector containing six repeats of the RNA hairpin specifically recognised by the MCP (Bertrand *et al*. 1998 – Addgene plasmid 27118) was used to generate a pSL vector containing 18 repeats of the MS2 RNA hairpin using the BglII (5') to EcoRI (3') restriction sites (generated in SLQ lab, unpublished). The MS2 hairpins were then digested from pSL with BglII and EcoRI restriction enzymes and ligated into the pTiger-attB (pUASp) expression vector, which was digested with BamHI (compatible with BglII) and EcoRI, resulting in the construct known as pTiger-MS2.

The Gateway Technology (Life Technologies) was used to quickly and systematically tag a number of mRNAs with the MS2 binding sites. To this end, a Gateway cassette was inserted downstream of the MS2 hairpin region in the pTiger-MS2 construct. The Gateway cassette contains the sequence required for the recombination of the mRNA sequences and the ccdB gene for selection. The Gateway cassette was amplified by PCR using the pUASt-Gateway-attB (donated by Konrad Basler Lab, Zurich) as template and primer pair 1 & 2 (see Appendix 2) that introduced a SphI restriction site at both the 5' and 3' ends. The resulting PCR fragment was gel purified and ligated into the pTiger-MS2 hairpin construct via SphI. The ligation reaction was transformed using competent ccdB-resistant bacteria. Both an EcoRI and NotI restriction digest were used to orient the Gateway insert within the pTiger-MS2 hairpin construct (Appendix 4.1).

pENTR TOPO cloning of candidate mRNAs

The entire genomic regions of *actin5C* (*act5C*), *actin42A* (act42A), *actin related protein 14D* (*arp14D*) and *actin related protein (arp66B)* were PCR amplified using genomic template DNA extracted from *Drosophila* ovaries using primer pairs 8 & 9 for *act5C*, 10 & 11 for *act42A*, 12 & 13 for *arp14D* and 14 & 15 for *arp66B* (see Appendix 2). The PCR fragments were purified by gel extraction and directionally cloned into the pENTR TOPO vector (pENTR™ Directional TOPO® Cloning Kit acquired from *Life Technologies*) by Topoisomerase activity (Appendix 3.4). The *oskar* genomic region was PCR-amplified using primer pair 16 & 17 (Appendix 2) and the pSP72-osk-genomic clone as template (Hachet & Ephrussi 2004). The PCR product was cloned into the pENTR-TOPO vector as described above. *act5C*, *act42A, arp14D, arp66B* and *oskar* were then recombined into the pTiger-MS2 hairpin construct (see above) through recombination with the Gateway cassette.

NLS-MCP-eGFP/mCherry

The MS2 coat protein (MCP), which contains an NLS at the 5' end, was PCR amplified from the pG14-MS2-GFP vector (Forrest & Gavis 2003) using primer pair 4 & 5 (see Appendix 2). A NotI restriction site was introduced at the 5' end of the MCP fragment 15bp upstream of an endogenous BamHI restriction site. An endogenous NotI site was amplified at the 3' end. Both the NLS-MCP fragment and pBluescript II KS+ (pBS) vector containing eGFP or mCherry (previously cloned into pBS via NotI (5') to BamHI (3')) were digested with NotI. NLS-MCP was ligated into both pBS-eGFP and pBS-mCherry via the NotI site and oriented using an EcoRI digest. The pBS-NLS-MCP-eGFP and pBS-NLS-MCP-mCherry constructs were then digested with BamHI and the inserts ligated into pTiger-attB, linearized with BamHI. NLS-MCP-mCherry was cloned from pTiger-attB into the pUAST-attB vector via the KpnI and XbaI restriction sites, which are present within the multi-cloning sites of both pTiger-attP (Appendix 4.2) and pUAST-attB.

The MCP was also cloned into both the pTiger and pUAST-attB vectors without the NLS for use as an unrelated RNA-binding protein control in immunoprecipitation assays. The MCP coding sequence was PCR amplified using primer pair 3 & 5 and the pG14-MS2-GFP vector (Forrest & Gavis 2003) as PCR template. A NotI and KpnI restriction site was introduced at the 5' end, while an endogenous NotI site was amplified at the 3' end. The PCR product was digested with NotI and ligated into both pBS-eGFP and pBS-mCherry via the NotI site. The MCP insert was oriented using an EcoRI diagnostic digest. The MCP-mCherry and MCP-GFP cassettes were then released from pBS-KS+ using KpnI and BamH, and ligated into pTiger and pUASt, which were opened with these restriction enzymes.

NLS-tandemMCP-eGFP/mCherry

Two copies of the MS2 coat protein (MCP) joined by a linker region (known as tdMCP) and containing an NLS at the 5' end, were PCR amplified from the UbC NLS-HA-MCP-YFP vector using primer pair 6 & 7 (see Appendix 2) (Grunwald *et al*. 2010 – obtained through Addgene plasmid 31230). Endogenous NotI sites were amplified at the 5' and 3' ends of the tandem MCP (tdMCP) fragment. Both the NLS-tdMCP fragment and pTiger vector containing eGFP or mCherry, previously cloned into pBS via NotI (5') to BamHI (3'), were digested with NotI. NLS-tdMCP was ligated into both pTiger-eGFP and pTiger-mCherry via the NotI site. Clones were screened using an NheI digest to determine the orientation of the NLS-tdMCP fragment in pTiger (Appendix 4.3).

2.2.2 *serpent*-GAL4::VP16

To express GAL4:VP16 under the control of the *serpent* (*srp*) promoter element, two genomic regions upstream and within the *srp* gene were PCR amplified from genomic DNA, as previously described (Brückner *et al*. 2004). Primer pair 18 & 19 amplified the first fragment, which introduced KpnI and XhoI restriction sites respectively, and primer pair 20 & 21 amplifed the downstream fragment, which introduced XhoI and SalI restriction sites respectively. The downstream *srp* fragment was cloned into pBS-SK+ from XhoI to SalI and the upstream *srp* fragment was subsequently cloned upstream of the downstream fragment via KpnI (5') and XhoI (3').

GAL4::VP16 was PCR amplified from gDNA extracted from flies expressing pMat-GAL4::VP16 using primer pair 22 & 23 (see Appendix 2), which introduced SalI-HindIII restriction sites. The SV40 terminator sequence, used to terminate transcription and promote polyadenylation of the GAL4 transcript, was amplified from the pUAST vector using primer pair 24 & 25 (see Appendix 2) which introduced an EcoRI restriction site at the 5' and amplified an existing BamHI site at the 3'. The SV40 terminator was cloned into the pBS-SK+ vector from EcoRI (5') to BamHI (3'). GAL4:VP16 was then cloned upstream of the SV40 terminator via SalI (5') to HindII (3'). The entire *srp* promoter region was released from pBS-SK+ via KpnI and SalI (3') and cloned upstream of GAL4:VP16 and the SV40 terminator to generate the entire *srp*-GAL4::VP16 cassette in pBS-SK+. This cassette was released by digestion with the KpnI and XbaI restriction enzymes and cloned into the fly expression vector pUASt-attB, from which the UAS sequence repeats and part of the *hsp70* promoter sequence were removed using PstI restriction digests (SLQ, unpublished) (Appendix 4.4).

2.2.3 UAS-Imp, UAS-Hrp48 and UAS-PTB

To C-terminally tag Imp, Hrp48 and PTB the coding regions of these genes, excluding the STOP codon, were amplified by PCR using cDNA template synthesised from *Drosophila* embryos. Primer pair 26 & 27 was used to amplify Imp and primer pair 28 & 29 to amplify Hrp48 (see Appendix 2). Primer pair 30 & 31 was used to amplify the coding region of PTB, using an existing PTB construct as template (Besse *et al.* 2009). The PCR primers introduced KpnI restriction sites at both the 5' and 3' ends of the Imp, Hrp48 and PTB coding regions. The PCR products were gel purified and digested with KpnI. The pTiger and pUASt vectors containing eGFP and mCherry, which were previously cloned into these vectors via NotI and BamHI, were digested with KpnI, which is situated upstream of mCherry and eGFP. The Imp,

Hrp48 or PTB coding regions were then ligated into pTiger-eGFP/mCherry and pUASt-eGFP/mCherry via KpnI. BamHI was used to screen/orient the Hrp48 and PTB clones, while PstI was used to validate the Imp clones (Appendix 4.5 – pTiger-Imp-GFP/mCherry).

To N-terminally tag PTB with eGFP the coding sequence of eGFP, excluding the stop codon, was amplified using primer pair 32 & 33 (Appendix 2), which introduced a KpnI site at the 5‘ and an SpeI site at the 3‘, using a pBS-eGFP clone as template. The PCR product was digested with KpnI and SpeI and ligated upstream of the PTB coding sequence, previously cloned into the pTiger vector using BamHI and XbaI sites (from the existing pUASp-GFP::PTB construct described in Besse *et al*. 2009).

2.3 pBS constructs to generate RNA probes

2.3.1 pBS-*actin42A* (*β-actin*)

To evaluate the distribution of *actin42A* mRNA in cultured haemocytes, the full length cDNA of *actin42A* was cloned to generate digoxigenin-labelled sense and antisense probes for an *in situ* hybridization. A primer pair containing a HindIII restriction site at the 5’ end (sense primer) and an XbaI restriction site at the 3’ end of the sequence (antisense primer) (primer pair 34 & 35 – see Appendix 2) were used in a PCR reaction together with cDNA from *Drosophila* embryos as template. The resulting PCR product was digested with HindIII and XbaI and ligated into the pBS-SK+ vector (Stratagene), which was also digested with HindIII and XbaI restriction enzymes. Colonies were screened for presence of the insert using a HindIII and XbaI diagnostic digest and positive clones were sequenced. To generate the antisense RNA probe, the construct was linearized with HindIII and *in vitro* transcription was carried out using the T3 promoter, while the sense probe was generated by linearization with XbaI using the T7 promoter (see Section 2.1.16).

2.3.2 pBS-*myospheroid* (βPS-integrin) clones

The 5’UTR, 3’UTR and coding sequence (CDS) of *myospheroid* (βPS-integrin) were individually cloned into the pBS vector to generate biotinylated RNA probes for use in RNA-affinity pulldown assays. Standard PCR using a high-fidelity polymerase was performed using cDNA from *Drosophila* embryos as template. Primer pairs amplifying the 5’ and 3’UTR regions introduced a KpnI restriction site at the 5’ and an XbaI restriction at the 3’ end of the sequences (primer pair 36 & 37 for 5’UTR and 40 & 41 for 3’UTR – see Appendix 2). The PCR products were digested with KpnI and XbaI

restriction enzymes and cloned into pBS-SK+, which was opened with these enzymes. Colonies were screened for presence of the inserts using a KpnI and XbaI double digest and positive colonies sequenced before final preparation.

The *myospheroid* CDS was amplified with primer pair 38 & 39 by introducing an EcoRI restriction site at the 5' and an XbaI site at the 3' end of the sequence (see Appendix 2). However, the *myospheroid* CDS contained an unannotated EcoR1 site which truncated the CDS when digested. The PCR product was blunt-end cloned into the pJet2.1 vector (Thermo Scientific). Positively oriented clones were linearized with XbaI and used for *in vitro* transcription from the T7 promoter present in pJet2.1.

2.3.3 *pBS-chickadee* (Profilin) & *actin42A* (β-actin) 3'UTRs

The 3'UTRs of *chickadee* (*chic*) and *actin42A* (*act42A*) were cloned into the pBS-SK+ vector (Stratagene) for generation of biotinylated RNA probes. Primer pairs were designed to amplify the 3'UTRs by introducing a KpnI restriction site at the 5' and XbaI restriction site at the 3' end of the sequences (primer pair 42 & 43 for *chic* 3'UTR and 44 & 45 for *act42A* 3'UTR – see Appendix 2). Standard PCR was carried out using cDNA template generated from *Drosophila* embryos. The PCR products were digested with the KpnI and XbaI restriction enzymes and ligated into pBS-SK+, opened with these restriction enzymes. Colonies were screened for presence of the *chic* or *act42A* 3'UTR with a KpnI and XbaI double restriction digestion. To generate biotinylated sense RNA probes the pBS-SK+ vector containing the *chic* or *act42A* 3'UTR was linearized with XbaI and *in vitro* transcription was carried out using the T7 promoter, as described in section 2.1.16.

Biotinylated RNAs were also generated against the 3'UTR of *oskar* and the coding sequence of *y14*, as previously described (Besse *et al*. 2009).

2.3.4 Site-directed mutagenesis (SDM) of Imp binding elements (IBEs)

The 3'UTR of *Drosophila act42A* contains 3 predicted IBEs (sequence UUUA(Y)) (**Figure 7**), which have not been validated as genuine Imp-binding sites. To determine if these IBEs in the *act42A* 3'UTR mediate binding to Imp in our RNA-affinity pulldown assay, we generated constructs in which either one, two or all three of the IBEs were mutated by site-directed mutagenesis (SDM).

pBS-act42A 3'UTR-ΔIBE1

To generate a construct in which the IBE1 alone was mutated, a sense mutagenic primer (primer 46 – Appendix 2) was designed to bind three nucleotides upstream of

the NsiI restriction site (ATGCAT) and nine nucleotides downstream of the IBE1 site. This primer contained the five mutated nucleotides of IBE1 from TTTAT to GGGCG. The pBS-*act42A* 3'UTR construct previously generated (section 2.3.1) was used as template in a PCR reaction with the mutagenic sense primer described above and T3 antisense primer (primer 48 – Appendix 2). The resulting PCR product was digested with NsiI, which cut upstream of the mutated IBE1 site (ΔIBE1) and just downstream of the IBE3 site. The wildtype pBS-*act42A* 3'UTR construct was digested with NsiI, ran on a 1% agarose gel to ensure the fragment containing the IBE sites was released, and the linearized vector gel purified. The digested PCR product was then ligated into the linearized pBS-*act42A* 3'UTR construct, restoring the full length *act42A* 3'UTR with the ΔIBE1 and wildtype IBE2-3 sites.

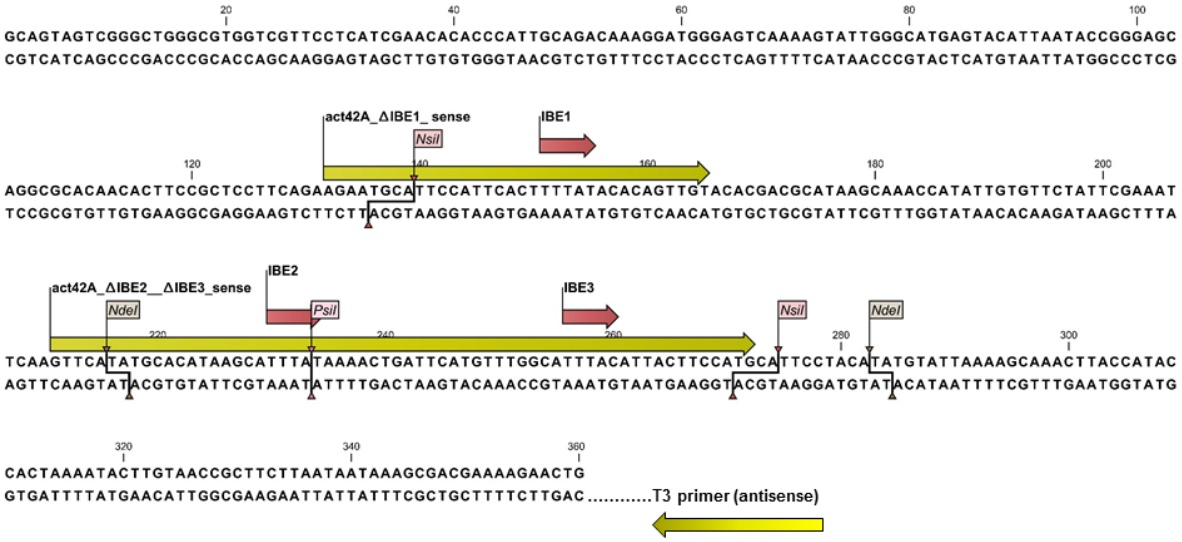

Figure 7. Annotated sequence of the *act42A* 3'UTR, highlighting the locations of the three predicted Imp binding elements (IBEs) (red arrows), the sense and antisense primers (yellow arrows), and the NsiI and NdeI restriction sites used for cloning of the mutated IBEs.

pBS-act42A 3'UTR-ΔIBE2-ΔIBE3

To generate a pBS-*act42A* 3'UTR construct with both the IBE2 and IBE3 sites mutated (ΔIBE2/3) a sense primer (primer 47 – Appendix 2) was designed to bind three nucleotides upstream of the first NdeI restriction site (CATATG) and extended downstream of the IBE3 site. The IBE2 site was changed from TTTAT to GAGCTC, while the IBE3 site was changed from TTTAC to GGGCG. T3 was used as an antisense primer (primer 48) and the pBS-*act42A* 3'UTR vector was used as PCR template. The PCR product was digested with the NdeI restriction enzyme, ligated

into the linearized pBS-*act42A* 3'UTR vector, lacking the wildtype NdeI 60 nucleotide fragment, to generate a construct containing ΔIBE2 and ΔIBE3. An NsiI diagnostic digest was used to screen colonies for the presence of the insert in the correct orientation.

pBS-act42A 3'UTR-ΔIBE1, ΔIBE2 + ΔIBE3

To generate a construct in which all three IBEs were mutated, the pBS-act42A 3'UTR-ΔIBE2-ΔIBE3 construct was digested with NdeI and the 60 nucleotide fragment containing both ΔIBE2 and ΔIBE3 was gel purified. The pBS-act42A 3'UTR-ΔIBE1 vector was digested with NdeI to release the wildtype IBE2 and IBE3 fragment and the linearized vector was gel purified. The ΔIBE2, ΔIBE3 fragment was ligated into the pBS-act42A 3'UTR-ΔIBE1 vector and the resulting colonies screened for presence of the insert within the correct orientation with an NsiI diagnostic digest.

All constructs were sequenced to ensure the IBE sites were correctly mutated. Each vector was then linearized with XbaI and used to generate biotinylated RNA probes by *in vitro* transcription, as described in section 2.1.16.

2.3.5 Sequencing of constructs

All constructs generated were sequenced (MWG Genomic Services) to ensure that fusion proteins were in frame and that no nucleotide substitutions, insertions or deletions had occurred. All pBS constructs were sequenced with the T3 and T7 primers provided by MWG. The pJet2.1-*myospheroid* CDS construct was sequenced with the M13 sense and antisense primers, also provided by MWG.

The pTiger constructs containing the MS2-hairpin binding sites with either the Gateway cassette, or recombined with the mRNA sequences, were sequenced with a sense primer that binds upstream of the multi-cloning site (MCS) and an antisense primer that binds downstream of the MCS (primers 49 & 50 – Appendix 2).

All UAS constructs containing coding regions tagged with either GFP or Cherry at the C-terminus (MCP, tdMCP, Imp, Hrp48 and PTB), were sequenced with a sense primer that binds upstream of the MCS (primer 49 for pTiger and primer 51 for pUASt) and an antisense primer that binds at the 5' of GFP (primer 52) or mCherry (primer 53) (see Appendix 2) to sequence the entire coding regions.

Several primers were designed to sequence the entire length of the *srp*-Gal4::VP16 construct. To sequence the beginning of the *srp*-Gal4::VP16 cassette we used a sense primer that binds upstream of the MCS in the pUASt-attB vector (primer 51).

Five sense primers (primers 54-59) were used to sequence the remainder of the cassette (see Appendix 2).

2.4 *Drosophila* Fly Work

2.4.1 General fly work

Flies were maintained in standard food vials containing yeast powder, corn flour, dextrose and plant agar. Nipagen (10% p-hydroxy benzoic acid methyl ester) and proprionic acid were added as anti-fungal and anti-microbial agents respectively. Established stocks were maintained at 18°C by changing the adult flies into fresh food vials every four weeks.

Virgin female and male flies for crosses and laying cages were collected by anaesthetisation with carbon dioxide emitted from a pad. These flies were collected in food vials and stored at 18°C until required.

To amplify fly stocks for laying cages, or to collect virgins or males for crosses, the stocks were kept at 25°C and tipped into fresh food vials regularly (every 2-3 days) until the required number of vials was obtained. The progeny were then collected from established vials for use in crosses or laying pots.

To set up crosses approximately 6-8 virgin female flies and 2-3 male flies were placed in a food vial with a small amount of dried yeast and tipped over into fresh food vials every 2-3 days. The progeny from old vials were either used to establish a new stock, set up subsequent crosses or collect virgin flies for laying cages.

2.4.2 GAL4-UAS System

The GAL4-UAS system was used to express proteins and RNAs within a specific tissue of interest, for example haemocytes. The yeast transcription activator GAL4 is expressed under the control of a tissue-specific promoter, allowing expression of the GAL4 protein only in the tissue of interest. The transgene of interest - for example a gene encoding a fluorescently labelled protein, or a short-hairpin RNAi construct - is placed under the control of an enhancer element termed the Upstream Activation Sequence (UAS), to which the GAL4 will bind, activating transcription of the transgene in a tissue-specific manner (Brand & Perrimon 1993) (**Figure 8**).

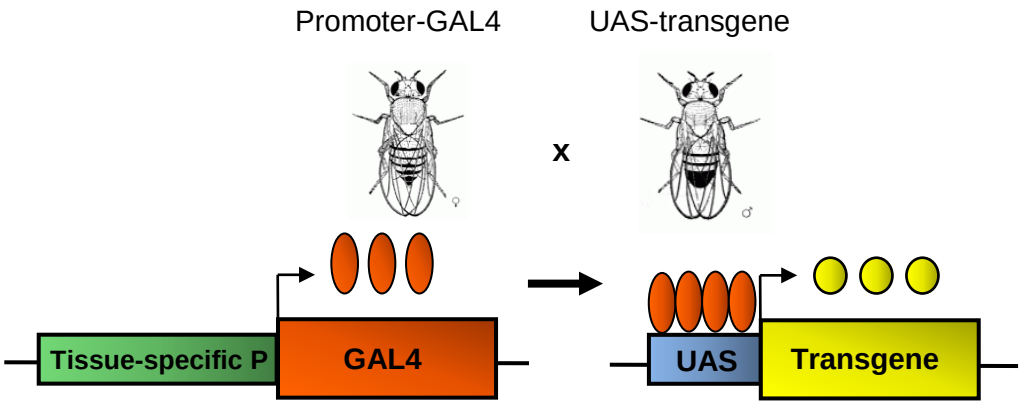

Figure 8. Schematic representation of the *Drosophila* GAL4/UAS. Flies expressing the GAL4 driver under the control of a tissue specific promoter are crossed to flies containing the UAS-transgene. In the progeny, the expression of the transgene of interest is restricted to the tissue of interest, defined by the tissue-specific promoter used to express the GAL4 driver.

2.4.3 Fly Stocks

A complete list of the fly stocks used in this project can be found in Appendix 5. A general description of these reagents can be found below. The w^{1118} fly strain was used as wildtype within this project.

Haemocyte-specific GAL4 Drivers

The GAL4-UAS system was used to specifically express fluorescently-labelled proteins within embryonic haemocytes using the haemocyte-specific promoters serpent and croquemort (Bruckner *et al*. 2004; Stramer *et al*. 2005). UAS-driven mCherry-moesin (Millard & Martin 2008) or GFP-moesin (GMA) (Dutta *et al*. 2002), consisting of only the actin-binding domain of moesin fused to either the mCherry of GFP fluorophores, were used to label the actin cytoskeleton. UAS-Clip-170-GFP (Stramer *et al*. 2010), containing only the microtubule binding domain of Clip-170, was used to label microtubules.

Upon imaging we observed that a single copy of a Gal4-driver was not sufficient to clearly visualize the fluorescent proteins. Therefore, we routinely used two copies of the haemocyte-specific *srp*-Gal4-driver to track and follow the haemocytes, or to express our proteins of interest.

Border cell-specific GAL4 drivers

The *slow border cells* (*slbo*) GAL4 driver line was used to drive UAS transgene expression in the border cells using the GAL4-UAS system (Rørth *et al*. 1998). *slbo*-GAL4 also drives expression within the stretched, posterior and columnar follicular

cells of the *Drosophila* egg chamber. To label the border cells we used either a *slbo*GAL4 fly line recombined with a UAS-CD8::GFP transgene (Rørth *et al*. 1998) or Lifeact::GFP directly fused to the *slbo* promoter to label the actin cytoskeleton (Riedl *et al*. 2008; Cai *et al*. 2014).

Maternal GAL4 drivers

Two maternal tubulin GAL4 drivers were used to drive expression of UAS transgenes in the female germline cells. These included the weaker *w; P(mat-tub-GAL4),mat67* driver located on chromosome II, and the stronger *P(mat-tub-GAL4),mat15* driver located on chromosome III (Bossing *et al*. 2002: Staller *et al*. 2013).

UAS Stocks

Most of the UAS constructs used were generated and tested as part of this project, including the fluorescently-labelled candidate RNA-binding proteins Imp, Hrp48 and PTB, as well as the MCP and candidate MS2-hairpin tagged mRNAs (listed in Appendices 1 & 5). To label border cells, UAS-CD8-GFP was previously recombined with the slboGal4 driver (Rørth *et al*. 1998). UAS-βPS integrin (Myospheroid) was used to overexpress β-integrin in haemocytes (Martin-Bermudo & Brown. 1996).

Protein Trap Stocks

To test the expression and distribution of endogenous proteins, YFP-exon-trap fusion protein fly lines from the Cambridge Protein Trap Insertion Consortium (CPTI lines – see http://www.flyprot.org) and GFP-exon-trap fusion protein fly lines from FlyTrap Project (see http://flytrap.med.yale.edu/) were used. These fly stocks were generated as part of protein-trap screen that relies on fluorescently-tagging of proteins by random mobilization of a GFP/YFP-containing transposable element in the genome (Morin *et al.* 2001).

RNAi Stocks

RNAi lines against PTB, Hrp48, Imp, Cdc42, Rac1 and Sexlethal were used within this project. The majority of RNAi fly lines used in this project were generated in the lab by Sonia López de Quinto using the hairpin sequences published by the *Drosophila* TRiP RNAi Project (see http://www.flyrnai.org/TRiP-HOME.html). TRiP RNAi lines express short RNA hairpins mimicking a miRNA precursor. All RNAi sequences were cloned into either the pWALIUM20 (WAL20) or pWALIUM22 (WAL22) vectors, as previously described for the TRiP RNAi constructs (Ni *et al*. 2009), which enabled them to be expressed under the control a UAS promoter to

drive RNAi in a specific tissue of interest. Longer RNAi hairpins from the Vienna *Drosophila* RNAi library were also used (Dietzl *et al.* 2007).

Mutant Stocks

Two *imp* mutant lines, recombined with a Flippase Recognition Target (FRT) – *w*-FRT19A imp^{7}/FM6 and *w*-FRT19A imp^{8}/FM6 (Medioni *et al.* 2014) – were used to generate *imp* border cell clones by Mosaic Analysis with a Repressible Cell Marker (MARCM).

2.4.4 Microinjection of Transgenic Constructs

PhiC31 integrase system

The PhiC31 integrase system was used to establish transgenic fly lines (Groth *et al*. 2004). This system enables non-random integration of transgenic constructs into the genome through expression of a serine-type recombinase within injected embryos (Bischof *et al*. 2007). This enzyme mediates sequence-specific recombination between an attachment site previously inserted into the genome, termed the attP landing site, and another attachment site termed attB, present in the injected plasmid. The Phic31 recombinase is expressed under the control of a germline-specific promoter (e.g. vasa or nanos). Two Phi31C fly stocks were used: the nanos-phiC31;;attP2 stock contains an attP insertion on the left arm of chromosome III (3L), and the nanos-phic31;attP40 stock contains an attP insertion at 2L (Markstein *et al*. 2008 – flies obtained from the Cambridge Stock Collection, stocks 13-18 and 13-20).

Preparing embryos for microinjection

PhiC31 fly stocks were placed in laying cages with apple juice agar plates at room temperature. One hour old embryos were collected from apple juice agar plates into an embryo collection basket and washed in 50% bleach for 1 minute to remove the chorion membrane. Embryos were then washed, transferred to a fresh apple juice agar plate, aligned for injection with a mounting needle and transferred onto a glue-coated coverslip. Embryos were then dried with silica beads for 17 minutes and coated in Halocarbon oil 700 (Sigma).

DNA preparation and injection

DNA constructs were prepared with an Endotoxin-free E.Z.N.A.® Plasmid Isolation Kit (Omega Bio-Tek) and diluted to a final concentration of 100-400 ng/µl. Injection needles were created with a p-97 Flaming/Brown Micropipette Puller and loaded with 2 µl of the DNA construct using a microloader tip (Eppendorf cat# 5242 956.003). A

Narishige IM-30 microinjector and Nikon Eclipse T5100 microscope was used to inject DNA into the posterior pole of single-cell embryos.

Screening and establishing transgenic flies

Surviving first instar larvae were collected and placed in food vials. Surviving adult flies were crossed to w^{1118} wildtype flies to screen for transgenic progeny by expression of the white mini-gene as a selection marker based on eye colour. Transgenic progeny were then crossed to appropriate balancer chromosomes. To ensure that the constructs had been integrated into the appropriate PhiC31 landing site, genomic DNA was extracted from individual flies of an established transgenic line. The gDNA was then used as PCR template to amplify a region spanning from just upstream of the attB integration site within the pTiger or pUAST expression vectors, to a region just downstream of the appropriate landing site (see Appendix 3.1 & 3.2 for vector maps) using primers 60-63 (Appendix 2). Amplification of a product indicated that the expression vector had integrated into the landing site successfully.

2.4.5 Crosses

MS2 System

To visualise *in vivo* MS2-labelled mRNA, virgin females of the genotype *w*; UAS-NLS-MCP-GFP/mCherry;TM2/TM6B*dfd* were crossed to the following males; *w*; *if*/CyO; UAS-18xMS2-*actin5C*, *w*;*if*/CyO; UAS-18xMS2-*actin42A*, *w;if*/CyO; UAS-18xMS2-*arp66B*, *w;if*/CyO; UAS-18xMS2-*arp14D* and *w;if*/CyO; UAS-18xMS2-*oskar*. Stocks of genotype *w*; UAS-NLS-MCP-GFP/mCherry; UAS-18xMS2-hairpin-mRNA/TM6B*dfd* were generated by crossing virgin females and males of *w*; UAS-NLS-MCP-GFP/CyO; UAS-18xMS2-mRNA/TM6B*dfd*. Identical cross schemes were carried out with the UAS-NLS-tdMCP-mCherry/GFP. While the MS2-hairpin tagged *actin5C*, *actin42A* and *oskar* mRNAs became homozygous, the *arp14D* and *arp66B* mRNAs did not.

To drive expression of the UAS-controlled MS2 system lines specifically in haemocytes *w*; UAS-NLS-tdMCP-GFP; UAS-18xMS2-mRNA/TM6B*dfd* males were crossed to virgin females of *w*; *srp*GAL4, UAS-mCherry-moesin; *crq*GAL4, UAS-mCherry-moesin. The TM6B*dfd* chromosome balancer fluorescently labels embryos from stage 13 through expression of YFP, which is driven by the *dfd* promoter and GMR enhancer element (Liang *et al*. 2006). As the hairpin-tagged *arp14D* and *arp66B* mRNA constructs were homozygous lethal, the TM6B*dfd* balancer was used

to select embryos positive for these hairpin-tagged mRNA by selecting against YFP fluorescent.

To test the MS2 system within *Drosophila* oocytes, virgin females from both maternal tubulin Gal4 drivers *w*; P(*mat-tub*-GAL4),mat67 and *w*;;P(*mat-tub*-GAL4),mat15 were crossed to UAS-NLS-MCP-mCherry; UAS-18xMS2-*actin42A* and UAS-NLS-MCP-mCherry; UAS-18xMS2-*oskar* males. Identical crosses were carried out to test the UAS-NLS-tdMCP-GFP constructs in the oocyte.

RNA-binding protein localization in Drosophila oocytes

To characterize the localization of Imp, Hrp48 and PTB in the germline of *Drosophila* oocytes, virgin females from both the maternal tubulin Gal4 drivers *w*; P(*mat-tub*-GAL4),mat67 and *w*;;P(*mat-tub*-GAL4),mat15 were crossed to UAS-Imp::GFP, UAS-GFP::Imp, UAS-Hrp48::GFP, UAS-PTB::GFP and UAS-GFP::PTB males. Ovaries were dissected from young (1-3 days old) resulting F1 females, which were fed on rich food for two days before dissection.

RNA-binding protein localization in haemocytes

To examine the distribution of Imp, Hrp48 and PTB in haemocytes, males or virgin females of the genotype: *w*; UAS-Imp::mCherry or UAS-Hrp48::mCherry lines were crossed to *w*; *srp*-GAL4, UAS-GMA; *crq*-GAL4, UAS-GMA. Virgin females or males expressing UAS-Imp::GFP or UAS-GFP::Imp were crossed to virgin females expressing *srp*-GAL4, UAS-mCherry-moesin; *crq*-GAL4, UAS-mCherry-moesin. To image the distribution of PTB in haemocytes, males containing the UAS-GFP::PTB transgene were crossed to virgin females containing *srp*-GAL4, UAS-mCherry-moesin; *crq*-GAL4, UAS-mCherry-moesin.

Overexpression analysis of Imp in haemocytes

To determine the effects of overexpressing Imp within haemocytes, homozygous fly stocks containing a double copy of the *srp*-GAL4 driver (which is significantly stronger than the *crq*-GAL4 driver) and UAS-Imp-mCherry were generated by crossing virgin females of genotype *w; srp*-GAL4, UAS-GMA; TM3*sb*/TM6B to *w; if*/CyO; UAS-Imp-mCherry males. Virgin females and males of *w*; *srp*-GAL4, UAS-GMA/CyO; UAS-Imp-mCherry/TM3*sb* were crossed to generate a homozygous stock. The same cross scheme was carried out with *w*; *srp*-GAL4, UAS-Clip170; *dp*/TM6B*dfd* flies to label microtubules in embryos over-expressing Imp. However, both the *srp*-GAL4, UAS-GMA and *srp*-GAL4, UAS-Clip170 constructs were homozygous lethal when crossed with UAS-Imp-mCherry, so to achieve a double copy of the *srp*-GAL4 driver, males of

these lines were crossed to virgin females expressing *w*; *srp*-GAL4; UAS-Imp-mCherry. Embryos with GFP-labelled haemocytes were then selected for imaging.

Protein-trap line imaging in haemocytes

To image the distribution of endogenous PTB in haemocytes, PTB protein trap lines in which a YFP cassette is inserted into the endogenous *hephaestus* (PTB) gene (see Duyk *et al.* 1990 for a description of the method), were first crossed to the *w*; *if*/CyO; TM3*sb*/TM6B balancer stock to generate *w*; *if*/CyO; PTB-GFP flies. Virgin females with the genotype *w*; *if*/CyO; PTB-GFP were then crossed to *w; srp*-Gal, UAS-mCherry-moesin; TM3*sb*/TM6B males to generate a homozygous *w*; *srp*-Gal, UAS-mCherry-moesin; PTB-GFP stock.

RNA-binding protein localization and overexpression in border cells

To examine the localization of Imp in border cells, virgin females of the genotype *w*; *slbo*GAL4/CyO, UAS-CD8-GFP were crossed to UAS-Imp-mCherry males. Homozygous stocks of the following genotype were generated; *w; slbo*GAL4/CyO; *slbo*::LifeAct-GFP, *w; slbo*GAL4/CyO; UAS-Imp-mCherry and *w; slbo*GAL4; *tubulin*GAL4, temperature-sensitive(ts) *tub*Gal80 for use in overexpressing RNA-binding proteins and driving expression of RNAi constructs. *slbo*GAL4 flies were first crossed to the double balancer fly line *w; if*/CyO;TM3*sb*/TM6B to generate a *w; slbo*GAL4/CyO; TM3*sb*/TM6B stock. This stock could then be crossed to both *w; if*/CyO; *slbo*::LifeAct-GFP, *w; if*/CyO; UAS-Imp-mCherry or *w; if*/CyO; *tub*GAL4, *tub*Gal80^{ts}.

To overexpress Imp in the border cells virgin females of the *w; slbo*Gal/CyO; *slbo*::LifeAct-GFP line were crossed to *w; slbo*GAL4/CyO; UAS-Imp-mCherry males. Virgin females of the genotype *w; slbo*GAL4/Cyo; UAS-Imp-mCherry were crossed to *w; slbo*GAL4/CyO; *tub*GAL4, *tub*Gal80^{ts} males.

RNAi in haemocytes

To ensure maximum gene knockdown specifically within haemocytes, fly crosses were used to establish homozygous stocks expressing a double copy of both the *w*; *srp*GAL4 driver or *srp*GAL4, UAS-GMA and the UAS-driven RNAi hairpins. The WALIUM22 RNAi hairpins were used to knockdown Imp and Hrp48 expression in haemocytes. Virgin females of genotypes *w*; *srp*GAL4, UAS-GMA; TM3*sb*/TM6B, and *w*; *srp*GAL4, UAS-GMA; TM3*sb*/TM6B were crossed to males expressing *w*; *if*/CyO; UAS-Imp RNAi or *w*; *if*/CyO; UAS-Imp RNAi. Homozygous stocks were then established through subsequent crosses. For imaging of haemocytes in RNAi

knockdown experiments *w*; *srp*GAL4; UAS-Imp RNAi or *w*; *srp*GAL4; UAS-Hrp48 RNAi virgin females were crossed to *w*; *srp*GAL4, UAS-GMA; UAS-Imp RNAi or *w*; *srp*GAL4; UAS-Hrp48 RNAi males to label the actin cytoskeleton of haemocytes, while ensuring maximal driver efficiency. For Imp RNAi knockdown experiments, flies were placed in laying cages at 29°C for live imaging of haemocyte migration.

RNAi in border cells

A *w; slbo*Gal/CyO; *slbo*::lifeAct-GFP stock was generated by crossing virgin female *w*; *slbo*GAL4/CyO; TM3*sb*/TM6B flies to *w*; *if*/CyO; *slbo*::lifeAct-GFP males. Virgin female *w; slbo*Gal/CyO; *slbo*::lifeAct-GFP flies were crossed to male flies containing RNAi transgenes. These included RNAi lines to target Cdc42 and Rac1 as positive controls, as knockdown of these genes are known to cause migratory defects, as well as an RNAi line against Sex Lethal, an unrelated RBP, as a negative control.

To determine if Imp, Hrp48 and PTB play any role in the regulation of border cell motility, their expression was reduced by RNAi using either short siRNA hairpins from the Transgenic RNAi Project (TRiP) or long dsRNA hairpins from the Vienna *Drosophila* Resource Center (VDRC) (**Table 3** and Appendix 5).

Table 3: RNAi lines used to deplete gene expression in *Drosophila* border cells

RNAi line	Gene depleted	RNAi Type
VAL20-Cdc42	*cdc42*	TRiP
VAL20-Rac1	*rac1*	TRiP
WAL22-Imp; WAL22-Imp	*imp*	TRiP
VAL20-Imp	*imp*	TRiP
Imp GD	*imp*	VDRC
VAL20-Hrp48	*hrp48*	TRiP
Hrp48 KK; Hrp48 GD	*hrp48*	VDRC
WAL20-PTB; WAL20-PTB	*hephaestus* (PTB)	TRiP

Mosaic analysis with a repressible cell marker (MARCM) stocks

Fly stocks to generate *imp* mutant border cell clones using MARCM were created by crossing *w*-FRT19A, *hs*-FLP, *tub*-GAL80 flies to the *w*-FM6/lethal; *sco*/CyO balancer stock to generate a *w*-FRT19A, *hs*-FLP, *tub*-GAL80; *sco*/CyO stock. *w*; *slbo*-Gal4, UAS-CD8-GFP flies were also crossed to *w*-FM6/lethal; *sco*/CyO balancer line to generate FM6/+; *slbo*-Gal4, UAS-CD8-GFP/CyO females, which were then crossed to *w*-FRT19A, *hs*-FLP, *tub*-GAL80; *sco*/CyO males. From this cross we established a *w*- FRT19A, *hs*-FLP, *tub*-GAL80; *slbo*-Gal4, UAS-CD8-GFP/CyO stock, which could then be crossed to *w*-FRT19A imp^{8} mutants to generate *imp* mutant border cell clones (see section 2.4.8).

2.4.6 Whole mount immunostaining of *Drosophila* embryos

Embryo Collection

To collect embryos for fixation, approximately 200 flies of the required genotype were placed in a plastic beaker (collection cage). If the embryos required were produced from a fly cross then ~60 virgin females and 20 male flies of the appropriate genotypes were placed in a collection cage and allowed to mate. A small blob of yeast paste (made from dried yeast and water to form a paste) was placed in the centre of an apple juice agar plate. The agar plate was then placed over the open top

of the collection cage and secured with an elastic band. Flies lay embryos into the agar, allowing these to be removed and collected.

Embryo Fixation

Drosophila embryos were transferred from apple juice agar plates to an embryo collection basket, dechorinated by submerging in bleach for 2 minutes, washed in distilled water to remove excess bleach and dried with tissue. The embryos were then transferred to an eppendorf tube and fixed in a 4% formaldehyde fixative solution (50 µl 36.5% formaldehyde (Sigma), 450 µl 1% PBS and 500 µl N-heptane) for 20 minutes with gentle shaking. The lower aqueous phase was removed and 500 µl of methanol was added to the upper heptane phase. After vortexing for 30 seconds to remove the vitteline membrane the devitellinised embryos were transferred to a fresh tube. The embryos were washed three times in methanol and stored at -20°C.

Immunostaining of embryos

Fixed *Drosophila* embryos were washed three times in 0.1% triton-X-100 in 1% PBS (PBT) and then three times for 20 minutes in 0.1% triton-X-100, 1% BSA in PBS (PATx) with shaking. Embryos were fixed and immunostained mainly to visualize haemocytes labelled with GFP using anti-GFP antibodies (**Table 4**). Primary antibody was removed and the embryos washed three times in PATx and a further three times in PATx for 20 minutes on a shaker. All secondary antibodies (Alexa Fluor® 488, Alexa Fluor® 555, Alexa Fluor® 633 – Life Technologies) were added at a 1:500 dilution and incubated on a shaker for 2 hours at room temperature. The embryos were washed in PATx three times to remove antibody and a further three washes for 20 minutes with shaking. If appropriate DAPI was added at a 1:1000 dilution in the first 20 minute wash in PATx following removal of secondary antibodies. Following the final wash step the PATx was removed and embryos were covered with 0.5 ml of mounting medium (2% propyl gallate, 80% glycerol in PBS) and stored at 4°C overnight for the embryos to settle.

Mounting of embryos

Stained embryos suspended in mounting medium were transferred to a watch glass and viewed under a Leica M210F fluorescent dissecting microscope. Embryos of appropriate stages were manipulated with level 4 dissecting forceps to the top of the watch glass and were taken up using a pipette tip. The embryos were then placed on a glass slide between two 22x22 mm coverslips stuck to the slide with nail polish. A

small volume of mounting medium was placed over the embryos and a 22x40 mm coverslip was placed over them and sealed with nail polish.

2.4.7 Whole mount immunostaining of *Drosophila* ovaries

Dissection and fixation of ovaries

Prior to ovary dissection, 6-15 newly eclosed female flies were prepared by placing them into a fresh food vial with dried yeast and 3-4 young male flies. The flies were kept at 22°C for 2-3 days to allow the ovaries to develop. Ovaries were then dissected in 1xPBS in a watch glass and transferred to a 1.5 ml Eppendorf using a glass Pasteur pipette. PBS was removed and the ovaries were fixed in 4% methanol-free formaldehyde (TAAB) or 3.7% formaldehyde with zinc (TAAB) for 20 minutes on a nutating shaker. The formaldehyde was then removed and the ovaries washed thrice in PBT (0.1% Triton-X-100 in PBS) for 20 minutes. DAPI counterstain was added to ovaries at a 1:3000 dilution in PBT for 5 minutes and removed. The ovaries were washed a final time in PBT for 5 minutes, removed and 50 µl Vectashield Hardset Mounting Medium (Vector Laboratories) was added. The ovaries were left in Vectashield overnight before mounting on glass slides the following day.

Immunostaining of ovaries

Ovaries were dissected and fixed for whole-mount immunostaining as described above. The ovaries were then washed twice in PBT, in which the ovaries were opened up by pipetting the tissue up and down several times through a 20-200 µl pipette tip (this ensures penetration of antibodies into individual egg chambers). The ovaries were then incubated in 1% Triton-X-100 in PBS for 60 minutes on a nutating shaker and then blocked in blocking solution (0.5% BSA, 0.1% Triton-X-100 in PBS) for 2 hours. They were then incubated in the appropriate primary antibodies diluted in blocking solution overnight at 4°C with shaking. On the following day the primary antibody was removed and the ovaries were washed twice in blocking solution for 20 minutes with shaking before blocking in 10% NGS, 0.1% Triton-X-100 in PBS for 2 hours. The 10% NGS solution was removed and appropriate Alexa Fluor® conjugated secondary antibodies diluted 1:500 in PBT were then added for 2 hours at room temperature with shaking. The ovaries were then washed once in PBT, counterstained with DAPI at 1:3000 dilution, washed once more in PBT and Vectashield mounting media added as previously described. They were then mounted on glass slides and imaged.

Mounting and imaging of ovaries

Ovaries were mounted onto glass slides in Vectashield and intact ovaries were broken up using cactus needles to ensure individual egg chambers could be isolated for imaging. A glass cover slip was then placed over the top. Ovaries were examined and imaged captured by either standard epifluorescence using an Olympus BX-50 microscope and Hamamatsu ORCA-05G digital camera, or by confocal microscopy using a Leica TCS SP2 AOBS spectral confocal system with a Leica DM6000B upright microscope with HC PL Fluotar 20x/0.50 and HCX PL APO 40x/1.25 oil objectives.

2.4.8 Mosaic analysis with a repressible cell marker (MARCM) in *Drosophila* border cells

MARCM was used to knockout the expression of Imp in border cells, which is otherwise homozygous lethal in flies. Briefly, MARCM allows the generation and positive selection of mutant clones of a gene of interest in specific cell types, which would otherwise be lethal in a whole organism (Lee & Luo. 2001).

Virgin female flies of the following genotype; FRT19A, imp^{8}/FM6 (Medioni *et al.* 2014) were crossed to FRT19A, *tubulin*-Gal80, *hsp*-FLP; *slbo-GAL4*, UAS-CD8-GFP/CyO males and allowed to generate progeny in a food vial before removal. Approximately 40 female progeny of the following genotype; FRT19A imp^{8}/FRT19A, *tubulin*-Gal80, *hsp*-FLP; *slbo*-GAL4, UAS-CD8-GFP/+ were selected upon eclosure and heat-shocked for 1 hour at 37°C in a water bath. After the heat shock was carried out females were placed in food vials with dried yeast (~20 females per vial), wildtype (w^{1118}) males were added and the ovaries dissected from females ~2-3 days later. The ovaries were fixed and counterstained with DAPI and then mounted on glass slides as previously described. Egg chambers that contained border cells that were GFP-positive were used for the analysis.

2.4.9 Real-time *in vivo* imaging of *Drosophila* embryonic haemocytes

Preparing embryos

Embryos expressing a haemocyte specific driver and a UAS-driven fluorescent protein (see Appendix 5 for a full list of UAS fly lines) were collected from apple juice agar plates into a mesh collection basket (Dutscher Scientific, 46-103) and dechorinated in 100% bleach for two minutes. Embryos were then washed in distilled water to remove all bleach and the mesh containing the embryos removed from the basket and placed onto a fresh agar plate for mounting and for keeping embryos

moist. A Leica M210F fluorescent dissecting microscope was used to stage and mount embryos. Embryos were staged according to gut morphology, as described in Campos-Ortega & Hartenstein 1985.

Mounting live embryos

Two 22x22 mm coverslips were stuck down onto either side of a glass slide with Scotch double-sided sticky tape. Embryos at stage 15 of embryonic development were mounted with the ventral side facing upwards onto the Scotch double-sided sticky tape, between the coverslips, by using level 4 dissecting forceps. A very small drop of Halocarbon oil 700 (Sigma) or voltalef oil (no longer commercially available) was placed over the embryo by using a tungsten needle to prevent over-drying of the embryo. A 32x22 mm coverslip was then placed over the embryos using forceps and stuck down on either side with nail varnish (**Figure 9**). Embryos were staged by examining head shape, germ-band position and the shape of the developing gut. Embryonic stage 15 was selected for live imaging as haemocytes are amenable to epithelial wounding at this stage.

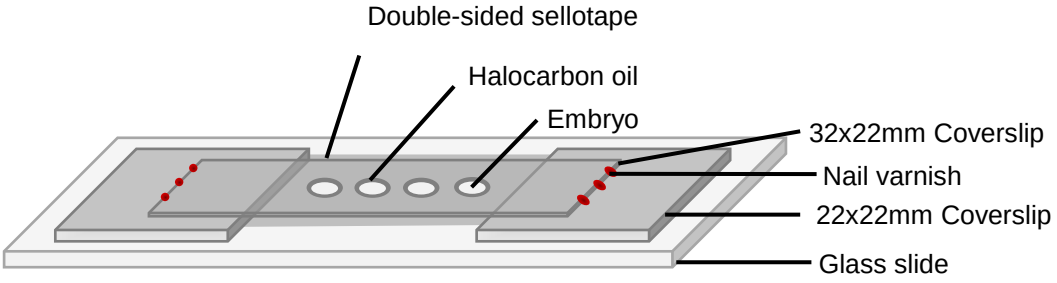

Figure 9. Schematic of mounting embryos prior to live imaging

Imaging embryos

Embryonic haemocytes were imaged using a PerkinElmer UltraVIEWVoX spinning disk scanning system with a Leica DMI6000B inverted microscope (laboratory of Prof Will Wood, University of Bristol) with a HCX PL APO 40X/1.30 or HCX PL APO 60x/1.4 oil immersion objective. The migration of haemocytes at the ventral surface of the embryo, dispersed along the developing nerve cord, was captured to analyse haemocyte developmental migration. To track the migration of individual haemocytes, images were captured over several Z-planes as haemocytes positioned along the ventral midline migrate dorsally away from the plane of focus (as well as towards either the anterior or posterior). Thus, 40 Z-stack series were created over

approximately a 20 µm section of the embryo ventral surface, with an image captured every 0.5 µm. An entire Z-stack was captured every 30 seconds.

Generating epithelial wounds

For wound healing assays, embryonic stage 15 embryos of the desired genotype were mounted as described above (**Figure 9**). The epithelium was then ablated dorsolaterally with respect to the ventral nerve cord using a nitrogen laser pumped dye laser (model no. VSL-337ND-S; Laser Science Inc.) connected to a PerkinElmer UltraVIEWVoX spinning disk confocal system using the Micropoint system (Andor Technology Ltd., Belfast, UK). Brightfield images of the epithelium were collected after wounding to determine and measure wound size. Z-sections of haemocytes were collected every 30 seconds for a total of one hour to capture haemocyte migration to epithelial wounds and phagocytosis of debris at the wound site. Wound-healing assays were performed at the Universities of Bath and Bristol, in the laboratory of Professor Will Wood.

2.4.10 Real-time *in vivo* imaging of *Drosophila* pupal haemocytes

Preparation and mounting of Drosophila pupae

Pupae expressing a haemocyte specific driver and fluorescent marker were collected from the sidewall of food vials 18-24 hours after puparium formation (APF) by gently lifting them with forceps. Pupae were gently wiped on tissue to remove food residue from the pupal case and were placed ventral side down on double-sided sticky tape on a glass slide. The operculum was then removed from the pupal case and the pupal case was gently slit along the lateral side towards the posterior using forceps. The pupal case was then gently lifted and stuck down onto the tape to expose the pupa. A 35mm glass bottom culture dish (MatTek Corporation) was coated with a thin layer of glue, made by soaking parcel tape in heptane. The exposed pupa was gently placed onto the culture dish lateral side down so that one of the developing wings was touching the cover glass. A small piece of wet tissue was placed in the culture dish to prevent drying of the pupa.

Imaging pupal haemocytes

Pupal haemocytes within the pupal wing disc were imaged using a Zeiss LSM 710 scanning laser confocal system with an Observer .Z1 inverted microscope. Patches of individual cells, rather than those clustered together, were selected for imaging. Time-lapse imaging was carried out by collecting a 20 µm Z-stack for 15-30 minutes at 1 minute intervals.

2.4.11 Analysis of *in vivo* imaging of *Drosophila* haemocytes

Calculating haemocyte velocity

The manual tracking plugin for ImageJ was used to track and calculate the distance travelled by individual haemocytes. To track individual haemocytes, the centre of the cell body was highlighted manually for each time point, and its coordinates used by the plugin to calculate the distance travelled between each. The total distance travelled by each haemocyte was then divided by the number of minutes over which its migration was tracked, to determine its average speed (µm/min).

To track haemocytes undergoing random migration during stage 15 of embryonic development, a Z-stack was captured every 30 seconds over a total period of 15 minutes. Individual haemocytes were tracked from the first to the last time-point and the total distance travelled divided by 15 to determine average speed.

To calculate the speed of haemocyte migration to wounds at embryonic stage 15, a Z-stack was captured every 30 seconds for one hour post-wounding. Tracking of an individual haemocyte began from the first time point that it began migrating towards the wound until its migration was halted at the wound edge. The number of minutes spent migrating by each haemocyte was calculated from the number of time points tracked for each individual.

Analysing contact inhibition

To study contact inhibition, a Z-stack was captured of haemocytes undergoing random migration at embryonic stage 15 every 30 seconds for a total of 15 minutes. The total number of time frames between the first, in which contact between two haemocytes was first seen, until the last time frame in which two haemocytes were in contact, was recorded. The total number of timeframes spent in contact was used to calculate the time frame of the contact event in minutes. Contact events in which haemocytes that were in contact within the first timeframe had not separated by the last, were recorded as over 15minutes. The data was then divided into four categories which included contact events lasting; <5 mins, 5.5-10 mins, 10.5-15 mins and 15 mins+.

Analysing haemocyte recruitment to wounds

To calculate the total number of haemocytes recruited to a wound over time at embryonic stage 15, a Z-stack was captured every 30 seconds for one hour post-wounding. The edge of the wound site was marked to help track individual haemocytes. The total number of haemocytes arriving at the wound edge was then

manually counted and recorded every 5 minutes, calculated from the number of timeframes (i.e. 5mins = 10 time frames), up to one hour.

The number of haemocytes recruited to a wound can vary depending on the wound size (i.e. a greater number of haemocytes are recruited to a larger wound) and, due to the nature of the laser, wound size was not always consistent between embryos. Therefore, the number of haemocytes recruited to a wound over time has to be normalized to the wound size. The area of the wound generated in each embryo was measured in ImageJ using the draw and measure function using Brightfield images of the epithelium and the wound area used to normalize the number of haemocytes to a wound size of 1000 μm^2, as wounds are usually between 500-1500 μm^2. To determine the mean number of haemocytes recruited to a wound of 1000 μm^2 in embryos of each genotype over time, the total number of haemocytes recruited every 5 minutes was averaged between each embryo.

2.5 Cell Culture: primary haemocyte culture and *Drosophila* S2R+ cells

2.5.1 Extraction and culture of larval haemocytes

Larval haemocytes were cultured through adaptation of the protocol described in Sampson and Williams, 2010. Larvae were collected from food vials or apple juice agar plates taken from laying cages and washed in distilled water to remove all food and debris. Ten third instar larvae were then selected for dissection. The lid of a 35 mm transparent cell culture dish was used as a dissection chamber. Larvae were dissected in 100 µl of Schneider's *Drosophila* medium (Sigma) containing 25% fetal bovine serum (FBS) (Sigma, F7524). Individual larvae were placed in the dissecting media with their dorsal side facing upwards and level 4 dissecting forceps were used to gently grip the anterior head end. A hooked tungsten needle was placed between the tracheae at the posterior end of the larvae and pulled away gently to puncture the epithelium, whilst keeping the gut intact. Approximately 0.5 µl of haemolymph is released from each larva.

Once ten larvae were dissected within the 100 µl of media, this was transferred to the well of a 24-well culture plate containing a 13 mm glass coverslip (VWR). A further 100 µl of dissecting media was added to the dissecting chamber to recover any remaining haemocytes and was then added to the well to supplement the cells already plated. Initially, coverslips were pre-treated with Concanavalin A (ConA) (Sigma, C5275) by incubating each coverslip with 10 µl of ConA solution (10 mg/ml) for an hour, before removing any remaining solution to allow coverslips to dry. The

24-well culture plate was then placed at 25°C for 1-2 hours, allowing the cells to adhere and spread to the coverslip before cells were fixed for immunostaining.

2.5.2 Maintenance of S2R+ cells

Drosophila S2R+ cells are an immortalized cell line isolated from wing discs of *Drosophila* embryos (Yanagawa *et al.* 1998). These cells share some parallels with haemocytes, including the ability to phagocytose and adhere to their substrate, and produce lamellipodial protrusions. The S2R+ cell line was kindly donated by Dr. Jilong Liu (Oxford University). S2R+ cells were maintained in either Shields & Sang M3 Insect Medium (Sigma Aldrich) or HyQ SFX-insect medium (GE Healthcare), both supplemented with 10% Fetal Bovine Serum (#F7524 Sigma Aldrich), at 25°C in either 25 cm^2 vented T-flasks or 92 mm plastic culture dishes (Nunclon). S2R+ cells were routinely passaged upon reaching confluency at a 1:10 dilution by detaching cells from the plastic using a sterile cell scraper and transferring to fresh media.

2.5.3 Calculating S2R+ cell density

S2R+ cells were counted using a Neubauer Chamber by re-suspending cells in media using a cell scraper. The glass coverslip was affixed to the chamber and 10 µl of cell suspension pipetted under the coverslip by capillary action. Cells were allowed to settle briefly and cell concentration calculated by counting total cell number in all four corners of the chamber and using the following calculation to determine the total number of cells:

$$\text{Total cells/ml} = \frac{\text{Total cell count} \times 10^4}{\text{Number of squares counted (4)}}$$

2.5.4 Immunostaining of cultured larval haemocytes and S2R+ cells

Cultured larval haemocytes and S2R+ cells were fixed and immunostained on sterilized 13 mm round glass coverslips (VWR) within 24-multiwell plates. Larval haemocytes were plated onto coverslips as described in section 2.4.1. To plate S2R+ cells, 500 µl insect culture media supplemented with 10% FBS was added to each well. Upon reaching subconfluency (~$1x10^7$ cells/ml) cells were re-suspended using a cell scraper and 20 µl of cell suspension (~$2x10^6$ total cells) was seeded into each well and mixed up pipetting up and down with a sterile Pasteur pipette and were allowed to settle for 1 hour at 25°C.

Cultured haemocytes and S2R+ cells were then fixed and immunostained by removing culture media and incubating the cells in 4% methanol-free formaldehyde

(TAAB) for 20 minutes with shaking. Cells were then washed thrice in 0.1% Triton-X, 1% BSA in PBS (PATx). Primary antibodies were diluted in 200 µl of PATx and incubated at 4°C overnight **(Table 4**). On the second day, cells were washed thrice in PATx and then with a further three 10 minute washes in PATx. Alexa Fluor® conjugated secondary antibodies were added at a 1:500 dilution and incubated with gentle shaking for 1 hour at room temperature. The secondary antibodies were washed out with three washes and three subsequent 10 minute washes, all with PATx solution. DAPI counterstain was added to the first 10 minute wash at a 1:1000 dilution. Alexa-fluor®-555 conjugated phalloidin (Life Technologies) was used to stain the actin cytoskeleton of S2R+ cells, which was added with secondary antibodies at a 1:200 dilution. The actin cytoskeleton of cultured haemocytes was visualized by expression of GFP-moesin within the cells and immunostaining with anti-GFP.

2.5.5 *In situ* hybridisation of cultured larval haemocytes

Cultured haemocytes were fixed directly on glass coverslips with 4% methanol-free formaldehyde (TAAB) for 20 minutes. The cells were then washed thrice in PBS and permeabilized by washing in 0.5% Tween-20 in PBS (PBT) for five minutes. The cells were then pre-hybridised in 200 µl hybridisation buffer (50% formamide, 5xSSC, 0.1% Tween-20, 50 µg/ml heparin, 100 µg/ml yeast tRNA) for 1 hour at 70°C and then incubated with appropriate dig-UTP-labelled RNA probes diluted in 500 µl hybridization buffer overnight at 70°C. On the following day the cells were washed extensively with five 10 minute washes in hybridization buffer and a further five 10 minute washes in PBT, all carried out at 70°C. The cells were incubated with a rhodamine-conjugated anti-DIG antibody (Roche) at a 1:200 dilution for one hour at room temperature. Alexa-fluor®-488 conjugated phalloidin (Life Technologies) was added at a 1:100 dilution to visualise the actin cytoskeleton. The cells were then washed three times in PBT to remove antibodies and were counterstained with DAPI at a 1:1000 dilution for 10 minutes. Two further 10 minute washes were carried out using PBT.

Table 4: Antibodies used for immunostainings

Primary antibodies			
Target	**Host**	**Dilution**	**Source**
Actin	Mouse	1:50	Developmental Studies Hybridoma Bank (JLA20)
Alpha-tubulin	Mouse	1:1000	Sigma (T9026)
GFP	Rabbit	1:1000	Amsbio (TP401)
Hrp48	Rabbit	1:200	Ephrussi Lab (EMBL – Germany)
Imp	Rabbit	1:1000	Medioni *et al*. 2014
Imp	Rat	1:1000	Medioni *et al*. 2014
PTB	Rabbit	1:200	Besse *et al*. 2009
PTB	Rat	1:200	Besse *et al*. 2009
βPS-integrin	Mouse	1:50	Developmental Studies Hybridoma Bank (CF.6G11)
Secondary antibodies & DNA/actin stains			
Alexa Fluor 488/555/633 anti-rabbit/mouse	Goat	1:500	Life Technologies (Invitrogen)
DAPI		1:1000 to 1:3000	Biotium (#40043; 10 mg/ml)
Alexa Fluor 488/555 Phalloidin		1:200 to 1:400	Life Technologies (Invitrogen)

2.5.6 Mounting

Glass coverslips were removed from the multiwell plates with level 4 dissecting forceps and placed facedown onto a single drop of ProLong® Gold Antifade Reagent (Life Technologies) on a glass slide. The slides were then placed at 4°C and left overnight to cure before imaging with a Leica TCS SP2 AOBS spectral confocal system with a Leica DM6000B upright microscope, using a HCX PL APO 100x/1.40 oil objective.

2.5.7 Double-stranded RNA (dsRNA) treatment of S2R+ cells

To knockdown expression of Imp and Myospheroid (βPS-integrin), dsRNA was generated for RNAi treatment of the *Drosophila* S2R+ cell line (Kao & Megraw. 2004; Rogers & Rogers.

2008). Cells were treated with dsRNA against GFP as negative control, while an untreated control was subject to the same conditions without addition of dsRNA.

Synthesis of dsRNA

To generate dsRNA, primers were designed to amplify a 500 nucleotide single exonic region of GFP, Imp or Myospheroid. To ensure the regions amplified were specific, BLAST searches against the *Drosophila melanogaster* genome were carried out using the FlyBase BLAST tool. The T7 promoter sequence was added to the end of both sense and antisense primers (primer pair 67 & 68 for Imp, 69 & 70 for GFP and 71 & 72 for Mys – Appendix 2), and standard PCR reactions were carried out using genomic DNA template. PCR products were ran on a 1% agarose gel to ensure only a single product was amplified and were PCR purified using the GeneJET PCR purification kit, according to the manufacturer's instructions and eluted in 50 µl of a 1:1 nuclease-free water, TE-buffer solution.

dsRNA was then synthesized by *in vitro* transcription (section 2.1.16) using the TranscriptAid T7 High Yield Transcription Kit (Thermo Scientific) and purified PCR product as template. The concentration and quality of RNA was tested by measuring the optical density using a NanoDrop ND-1000 and loading 1 µg of RNA on a 1% agarose gel, as previously described (section 2.1.16).

dsRNA treatment of S2R+ cells

Approximately $2.5x10^6$ S2R+ cells were seeded into 12-well plates in 500 µl culture media. Four conditions, including an untreated control and cells treated with dsRNA against GFP, Imp and β-integrin were carried out in triplicate (3 independent monolayers for each condition). The cells were allowed to settle and the media removed. 5 µg of dsRNA was added to 100 µl of serum-free media, which was then added to each well. 100 µl of serum-free media without dsRNA was added to each untreated control well. The cells were incubated in the dsRNA on a shaking platform for 30 minutes before 400 µl of media supplemented with 10% FBS was added to each well. This treatment was repeated once a day for a further two days, and the cells were then collected on the fourth day for Western blot and qPCR analysis.

Western blot analysis of dsRNA treatment

The total number of S2R+ cells per well was calculated (see section 2.5.3) and $1x10^7$ cells were collected from each monolayer, centrifuged at 2500 rpm for 5 minutes and the media removed. The cell pellet was then re-suspended in 20 µl of 2x SDS loading buffer and heated at 95°C for 5 minutes to lyse open the cells and 20 µl distilled water then added. The cell lysate was then split and two varying amounts – 10 µl or 30 µl – were loaded onto 8%

polyacrylamide gels and Western blots were carried out (see section 2.1.17) to immunoblot against Imp, Actin42A (β-actin) and βPS-integrin (see **Table 2** for antibodies).

Real-time qPCR analysis of dsRNA treatment

Total RNA was extracted from $1x10^7$ cells (see section 2.1.12) and used as template for cDNA synthesis (see sections 2.1.13-14). The optical density of cDNA in each condition was measured using a NanoDrop ND-1000 and 0.5ng of cDNA was added to each 20 µl qPCR reaction. qPCR was carried out as described in section 2.1.15 and was used to compare the mRNA levels of the ubiquitously-expressed control gene *rp49* and *imp*, *βPS-integrin*, *actin42A*, *profilin* and *arp2* in untreated and GFP-, Imp- and β-integrin-treated cells. See Appendix 2 for details of primers used for qPCR. All mRNA levels were normalized to the control gene *RNA polymerase II* (*polII*) and the percentage-change in mRNA levels in dsRNA-treated cells, compared with untreated controls, was then calculated.

2.6 Image and Data Analysis

2.6.1 Image processing

All confocal images were processed using ImageJ (NIH). mvd2 (Volocity) and lei (Leica) data files were opened using the Bio-Formats Importer plugin to import image metadata. Noise was removed by using Process; Noise; Despeckle and the image contrast was enhanced using Image; Adjust; Window/Level. Scale bars were added using Analyze; Tools; Scale Bar. To project Z-stacks Image; Stacks; Z-project was selected and Image; Color; Merge/Split Channels was used to view images within individual channels or to generate a merged image. To view images in grayscale Image; Type; 8-bit was used. After processing the images they were saved as both TIFF and JPEG images.

2.6.2 Measuring fluorescence intensity

The average fluorescence intensity of β-integrin and Imp immunostaining was measured in haemocytes cultured *ex vivo* using ImageJ. The drawing tool was used to draw around the entire cell, including the lamellipodial protrusions, and the Analyze; Measure tool was used to calculate the ‘mean gray value’, which gives a measure of sum of the gray values of all the pixels in the selection divided by the total number of pixels.

2.6.2 Statistical Analysis

All statistical tests carried out were student’s t-tests, except for the statistical test to determine if Imp overexpression rescues the overexpression of β-integrin in haemocytes, in which two-way ANOVA tests were performed. All statistical tests and graphs were generated using Prism 5 software.

2.7 Biochemistry

2.7.1 RNA-Affinity Pulldown Assay

An RNA-affinity assay was carried out to determine if Imp binds *myospheroid* (*β-integrin*) mRNA *in vitro*, as previously described (Besse *et al.* 2009). To briefly describe the procedure: a biotinylated RNA sequence of interest is generated and bound to streptavidin particles conjugated to magnetic beads. The biotinylated RNA-streptavidin bead complex is incubated in a soluble protein mixture and the beads are bound to a magnet. The beads are then washed to remove non-specific proteins. Bound proteins can then be released from the beads by heating in SDS buffer and specific proteins identified by immunoblotting.

Biotinylated RNA probes

Biotinylated RNA probes were generated for the 5'UTR, coding sequence and 3'UTR of *myospheroid* (*β-integrin*), as well as positive controls including the 3'UTRs of *oskar*, *chickadee* (*profilin*) and *actin42A* (*β-actin*). The coding region of *y14* was used as an unrelated negative control. See section 2.1.16 on the generation of RNA probes. The 3'UTRs of *chic* and *act42A*, as well as all regions of *myospheroid*, were cloned for this project (sections 2.2.4-5), while the 3'UTRs of *oskar* and coding region of *y14* were generated as previously described (Besse *et al.* 2009).

Preparing S10 embryonic protein extract

To prepare the S10 embryonic extract, ~3000 embryos (~200 µl volume) were collected from apple juice agar plates and de-chorinonated in 100% bleach for 2 minutes and rinsed in distilled water. The embryos were collected in an eppendorf tube using a paintbrush and were either flash frozen in liquid nitrogen and stored at -80°C, or used immediately. Frozen or fresh embryos were mixed by re-suspending in PBT (0.1% Triton-X-100 in PBS) in a single eppendorf and were then washed twice in PBT. The embryos were then washed once in cold hypotonic buffer (10 mM HEPES-KOH$^{7.4}$, 10 mM K-acetate, 1.5 mM Mg-acetate, 2.5 mM DTT) and a single time with hypotonic buffer containing protease inhibitors (Roche cOmplete Protease Inhibitor Cocktail tablets, EDTA-free). The embryos were then homogenised on ice in 200 µl hypotonic buffer containing protease inhibitors using a borosilicate tissue grinder with 20 strokes of the pestle. The homogenate was transferred to an Eppendorf, centrifuged at 10,000 rpm for 10 minutes at 4°C and the supernatant recovered, to which glycerol was added to a final concentration of 5%. The extract was kept on ice until required.

Binding of biotinylated RNA probes to magnetic beads

30 µl of magnetic beads conjugated to streptavidin particles were used for each biotinylated RNA point. The beads were washed three times in MB-TEN^{100} (10 mM Tris-HCl$^{8.0}$, 1 mM EDTA$^{8.0}$, 100 mM NaCl) and the washes were removed using the DynaMag™-2. The beads were then re-suspended in 250 µl MB-TEN^{100} and equimolecular amounts of biotinylated RNA were added to each point (typically ~1.5 µg). The bead-biotinylated RNA mixture was then incubated on a rotating wheel for 30 minutes at room temperature to bind the streptavidin and biotin particles and were then washed twice in MB-TEN^{1000} (10 mM Tris-HCl$^{8.0}$, 1 mM EDTA$^{8.0}$, 1 M NaCl) to remove unbound RNA. The RNA-bead mix was then washed twice in binding buffer (10 mM HEPES$^{7.9}$, 3 mM $MgCl_2$, 5 mM EDTA$^{8.0}$, 5% glycerol, 2 mM DTT, 0.5 % IGEPAL, 40 mM KCl).

Binding of proteins to biotinylated RNAs

The S10 embryonic extract was divided equally between each of the biotinylated RNA-bead complexes and the reaction was made up to 150 µl total volume with binding buffer containing heparin and yeast tRNA to reduce non-specific binding (10 mM HEPES$^{7.9}$, 3 mM $MgCl_2$, 5 mM EDTA$^{8.0}$, 5% glycerol, 2 mM DTT, 0.5% IGEPAL, 40 mM KCl, 3 µg/µl Heparin, 0.5 µg/µl tRNA). The RNA bead/S10 embryonic mix was then incubated at 4°C on a rotating wheel for 1 hour.

Elution and detection of bound protein

The unbound fraction was removed and the beads washed with binding buffer lacking heparin or tRNA but containing 150 mM KCl, which was designed to mimic physiological conditions within the cell. The bound proteins were then eluted from the beads by adding 20 µl of 2x SDS loading buffer and incubating at 90°C for 5 minutes. The SDS buffer was transferred to a clean eppendorf tube and 20 µl of distilled water was added to leave a 1x SDS final concentration. 15 µl of the bound extract was ran on an 8% polyacrylamide gel and immunoblotting was carried out to detect for the binding of Imp and PTB to the biotinylated RNAs. 10 µl of the unbound fraction was loaded and ran on an 8% gel to detect Kinesin heavy chain (Khc) as a loading control, to ensure an equal concentration of protein was added to each RNA.

2.7.2 RNA Immunoprecipitation from *Drosophila* embryos

RNA immunoprecipitation (RIP) was carried out to identify mRNAs bound to Imp-GFP in haemocytes. MCP-GFP was used as an unrelated RBP control, while wildtype embryos (e.g. no GFP expression) were used as a negative control. Wildtype embryos and those expressing Imp-GFP or MCP-GFP specifically in haemocytes were collected to generate

embryonic extracts, from which the GFP-tagged proteins were precipitated using GFP-nanotraps (Chromotek).

Embryo collection

Embryos were collected from apple juice agar plates in collection baskets and dechorionated in 100% bleach for 2 minutes. They were then rinsed in distilled water and dried with tissue. Dried embryos were collected in a 1.5 ml eppendorf, flash frozen in liquid nitrogen and stored at -80°C until enough embryos had been collected. For each condition approximately 1500 embryos (~100 µl volume in 1.5 ml eppendorf) were used.

Formaldehyde cross-linking

Embryos were placed in an embryo collection basket and washed in a continuous stream of 100% isopropanol for 20 seconds. They were then washed in a continuous stream of 100% heptane for 5 minutes and the excess then removed with tissue. Embryos were transferred to a 1.5 ml eppendorf and incubated in 500 µl of 0.2% formaldehyde (TAAB) for 5 minutes at 4°C on a nutating shaker. The cross-linking reaction was then quenched by addition of 500 µl 0.5 M glycine to a final concentration of 0.25 M. Glycine and formaldehyde were then removed with five washes (5 minutes each) in PBS. All above steps were carried out at 4°C.

Generating embryonic extract

Embryos were transferred in PBS to a borosilicate tissue grinder, which was placed on ice, and were then homogenized in 800 µl extraction buffer (25 mM Hepes$^{6.8}$, 50 mM KCl, 1 mM $MgCl_2$, 1 mM DTT, 125 mM sucrose, 0.2 mg/ml heparin, 10 µg/ml yeast tRNA, protease inhibitors (Roche cOmplete Protease Inhibitor Cocktail tablets, EDTA-free), RNase inhibitors (Thermo Scientific RiboLock RNase Inhibitor) by using 30 strokes of the pestle. The homogenate was centrifuged at 12,000 rpm for 5 minutes at 4°C to collect the supernatant. The supernatant was then re-centrifuged to remove any residual debris and was collected in a fresh eppendorf. 20 µl of the supernatant was retained for Western blot analysis and to generate cDNA for subsequent quantitative PCR analysis of the input material.

Immunoprecipitation

The embryonic extract (see above) was first incubated with uncoupled magnetic agarose beads (Chromotek) to reduce unspecific binding of proteins to antibody-coupled beads. The beads were first prepared by washing five times in 0.1% Triton-X in PBS and twice in wash buffer (25mM Hepes$^{6.8}$, 50 mM KCl, 1 mM $MgCl_2$, 1 mM DTT, 125 mM sucrose). The supernatant was added to 25 µl of uncoupled beads and incubated on a rotating wheel for 30 minutes at 4°C. The supernatant was then removed, using a magnet to trap beads, and added to 25 µl of anti-GFP-coupled magnetic agarose beads (GFP-Trap®-Chromotek) which

were prepared in the same way as the uncoupled beads. The supernatant was incubated with the beads on a rotating wheel for 1 hour at 4°C. The unbound fraction (remaining supernatant) was then removed and retained for Western blot analysis.

The beads were washed thrice in RIPA buffer (0.05 M Tris-HCl$^{7.4}$, 0.25%deoxycholic acid, 1% NP-40, 1 mM EDTA, 0.1% SDS) containing 150 mM NaCl and were washed a further three times in RIPA buffer containing 1M NaCl. The beads were then washed twice in wash buffer (25mM Hepes$^{6.8}$, 50 mM KCl, 1 mM $MgCl_2$, 1 mM DTT, 125 mM sucrose) and re-suspended in 200 µl wash buffer, which was split into two 100 µl halves. One half was used for RNA extraction, while the other was used for Western blot analysis.

RNA extraction of bound RNA from beads

To reverse the formaldehyde cross-linked, beads containing bound RNA-protein complexes were heated for 45 minutes at 75°C. To remove RNA from the beads, five equal volumes of TRIzol reagent (Invitrogen) was added to the 100 µl sample, mixed well and incubated for 5 minutes at room temperature. 100 µl chloroform was added and the mixture vigorously shaken for 15 seconds before incubation for 2-3 minutes at room temperature. The sample was centrifuged at 12,000 rpm for 15 minutes at 4°C and the colourless upper aqueous phase was collected. RNA purification was then carried out using the Quick-RNA™ MicroPrep (Zymo Research) by adding 600 µl of supplied RNA lysis buffer (supplied with kit)*. Column purification and in-column DNase treatment to remove genomic DNA was carried out according to the manufacturer's instructions. The RNA was eluted* in 10 µl nuclease-free water.

RNA extraction of unbound RNA

RNA was extracted from 10 µl of the unbound fraction using the GeneJET RNA Purification Kit (Thermo Scientific) by adding 600 µl of the supplied RNA lysis buffer, supplemented with β-*mercaptoethanol and carrying out column purification according to the manufacturer's instructions. The RNA was eluted in 50 µl of nuclease-free water and the optical density measured using a* NanoDrop ND-1000. Genomic DNA was removed from 1 µg of RNA using DNase I (RNase-free 1 U/µl – Thermo Scientific), according to the manufacturer's instructions.

Real-time quantitative PCR

Quantitative PCR was carried out to compare the levels of mRNAs precipitated from GFP-tagged embryonic extracts, to those from wildtype controls. cDNA synthesis and subsequent qPCR reactions were set up and carried out as described in sections 2.1.13-15. See Appendix 2 for a full description of all primers used for qPCR analysis. To control for

differences between conditions in the starting amount of the mRNAs tested, the amount of RNAs measured in the bound fraction were first normalized to their levels in the input fraction. These normalized values were then used to calculate the RNA fold-enrichments in the GFP-labelled RBP fractions, relative to wildtype.

Western blot analysis

Western blot analysis was carried out to ensure that GFP-labelled proteins were efficiently precipitated and determine the levels of these proteins remaining in the unbound fractions. 10 µl of 2x SDS loading buffer was added to 10 µl of the input and unbound fractions, representing approximately 2% of the total input and unbound fractions. The input and unbound samples were incubated at 95°C for 5 minutes and loaded on an 8% agarose gel.

To prepare the bound fraction, beads containing bound RNA-protein complexes were re-suspended in 40 µl 2x SDS loading and incubated at 95°C for 15 minutes to dissociate immunocomplexes. 40 µl of distilled water was then added to dilute 2x SDS loading buffer and 20µl was loading onto the gel, representing 25% of the total bound protein. SDS-PAGE and Western blotting was carried out as described in section 2.1.17 and GFP-labelled proteins were detected by blotting with anti-GFP antibodies (**Table 4**).

2.7.3 RNA Immunoprecipitation from *Drosophila* ovaries

RNA immunoprecipitation was carried out to identify candidate mRNAs bound to Imp-GFP and PTB-GFP in the germline of *Drosophila*. As for embryos, wildtype ovaries and those expressing MCP-GFP were used as control.

RNA immunoprecipitation from ovaries was carried out in the same way as immunoprecipitation from embryos. 70 pairs of either fresh or previously frozen ovaries – either wildtype or expressing Imp-GFP, PTB-GFP or MCP-GFP - were dissected from females and homogenized in 500 µl of extraction buffer. Formaldehyde cross-linking was not carried out. Subsequent immunoprecipitation steps, Western blot analysis, RNA extraction and qPCR analysis were carried out as described in section 2.7.2.

Chapter 3:

Establishing and testing an *in vivo* model system to investigate the role of RNA regulation in cell motility

3.1 *Drosophila* haemocytes as a model system to study *in vivo* mRNA localisation within migratory cells

This project was first started by establishing an *in vivo* model system to study the role of cytoplasmic RNA regulation in cell motility. *Drosophila* haemocytes, the *Drosophila* equivalent of mammalian macrophages, were chosen as these cells are highly polarised and display distinct lamellipodial protrusions at the leading edge (Wood *et al*. 2006). Haemocytes show a distinct developmental migration from stage 10 of embryogenesis when they are first specified (**Figure 4**) (Tepass *et al*. 1994). During embryonic stages 15-16 the haemocytes disperse throughout the entire embryo and a pool of haemocytes remain at the ventral nerve cord and migrate laterally to form three parallel lines along the entire ventral surface of the embryo (Wood & Jacinto 2007). These haemocytes then migrate randomly across the ventral surface, a process which we will refer to in this project as random migration. It is these ventrally-positioned haemocytes that will be imaged for the purposes of this project (Wood & Jacinto 2007) (**Figure 4**). From embryonic stage 15 onwards haemocytes respond to wound cues and migrate to the site of an epithelial wound to engulf any debris or invading pathogens at the wound edge, allowing the direction of migration to be controlled (Stramer *et al*. 2005). Random migration and directed migration of haemocytes to a wound site are regulated by two different signalling pathways which allows two distinct forms of migration to be utilised (Wood *et al*. 2006).

3.2 Haemocytes lose distinct polarity in fixed embryos

First we attempted to visualize fluorescently-labelled haemocytes in fixed *Drosophila* embryos. *Drosophila* embryos in which haemocytes were specifically labelled with GFP were fixed and immunostained with a primary antibody against GFP. Cytoplasmic GFP was expressed using two copies of the haemocyte-specific *srp*-Gal4 promoter and UAS-driven GFP. Haemocytes were imaged in stage 15 embryos by confocal microscopy. However, the methanol used within the fixation procedure kills the fluorescently signal so that the haemocytes could not be seen. We therefore decided to immunostain fixed embryos using either anti-GFP or anti-mCherry antibodies to visualize the haemocytes. Immunostaining allowed visualization of haemocyte positioning within embryos at various developmental stages (**Figure 10C**). However, upon fixation haemocytes were observed to lose their distinct morphology as the lamellipodial protrusions are disrupted during the fixing procedure (**Figure 10C**). Embryos were fixed in varying concentrations of 4%, 10% and 15% formaldehyde in an attempt to preserve haemocyte polarity. However, the lamellipodial protrusions were lost in haemocytes in all cases.

Loss of haemocyte lamellipodial protrusions in fixed samples limited the use of whole-mount immunostaining and *in situ* hybridisation to examine the cytoplasmic localisation of specific RBPs and mRNAs within haemocytes. However, immunostaining against GFP-labelled haemocytes was still used to reveal their position within the embryo and therefore analyse their migration from the head mesoderm, where they are specified, in embryos mutant for different regulatory proteins (dominant-negative assays or RNAi analysis).

The analysis of the cytoplasmic distribution of both RBPs and mRNAs, therefore, had to be performed on living embryos by live confocal imaging.

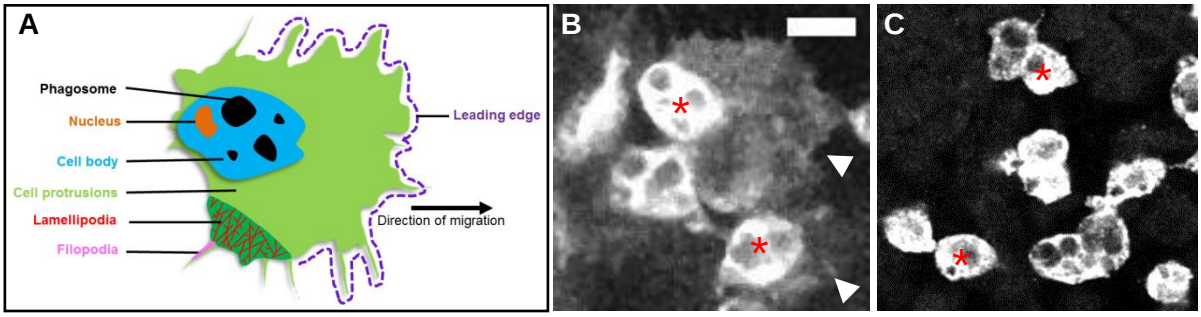

Figure 10. Visualization of haemocytes in fixed *Drosophila* embryos
(**A**) Schematic of a *Drosophila* haemocyte showing the cell body, which contains the nucleus and phagosomes/vacuoles, as well as the lamellipodial protrusions and filopodia which extend in the direction of migration. (**B**) Live confocal imaging of stage 15 *Drosophila* embryos expressing UAS-driven cytoplasmic GFP specifically within haemocytes using the haemocyte-specific *srp*-Gal4 driver. The lamellipodial protrusions of haemocytes are marked with white arrowheads, while the cell body is labelled with a red asterisk. (**C**) Stage 15 *Drosophila* embryos expressing UAS-driven cytoplasmic GFP specifically in haemocytes, using the *srp*-Gal4 driver, were fixed and immunostained with an anti-GFP antibody to image haemocytes. Although the haemocyte cell body can be clearly distinguished (asterisks), fixed haemocytes lose their lamellipodial protrusions. Increased exposure time failed to capture the presence of protrusions in fixed haemocytes. Scale represents 10 µm

3.3 Investigating the role of RNA regulation in haemocyte migration

Next we wanted to characterise *in vivo* the potential role that mRNA localisation may play in helping to establish cell polarity and aid migration in motile cells. To this end two distinct approaches were used. The first approach was to study the distribution of candidate mRNAs that may be enriched in the lamellipodial protrusions of haemocytes (or maybe other regions of the cell). The second approach was to study candidate RNPs, such as PTB, Hrp48 and Imp, which may play a role in the cytoplasmic regulation of mRNAs whose protein products are required for cell motility. The distribution of these RBPs was examined in haemocytes to determine where they are expressed and, if enriched in a specific region of the cytoplasm, what their role may be. We therefore started by generating transgenic flies expressing

fluorescently labelled candidate RBPs (Imp, Hrp48 and PTB) or the components of the MS2 system to follow the distribution of candidate mRNAs.

To characterize the fluorescently-labelled RNA-binding proteins generated in this project, we followed the same strategy for each. Firstly, we examined their localization in the *Drosophila* oocyte to ensure that they localized correctly when labelled, as the distribution of Imp, PTB and Hrp48 has been well documented in *Drosophila* ovaries, where they co-localize with *oskar* mRNA at the posterior of the oocyte (Yano *et al*. 2004; Munro *et al*. 2006; Besse *et al*. 2009). The posterior enrichment of these RBPs reflects their capacity to bind *oskar* mRNA or to incorporate into *oskar* RNP complexes so we used this as a readout of their functionality. Exon-trap lines (Duyk *et al*. 1990) or pre-existing validated transgenes directly driven by a maternal promoter were used for comparison of protein localization. Our labelled RNA-binding proteins were then expressed specifically in embryonic haemocytes using the GAL4/UAS system to examine their distribution within these cells *in vivo*. Finally, to confirm expression of our RBPs in haemocytes we examined the localization of endogenous Imp, PTB and Hrp48 in cultured haemocytes *ex vivo*, which also allowed us to compare contrast their distribution in both an *in vivo* and *in vitro* environment.

3.4 Imp is not enriched within the lamellipodial protrusions of haemocytes

The IMP1 RNA-binding protein, the mammalian homolog of Imp, has been shown to localise *β-actin* mRNA at the leading and lagging edge of both chicken and human fibroblasts in cell culture, which is required for proper directional motility and polarisation of these cells (Ross *et al*. 1997; Shestakova *et al*. 2001; Oleynikov & Singer 2003). To determine if this is also the case *in vivo,* we followed the distribution of two GFP-tagged Imp constructs: C-terminally (Ct)-tagged GFP/mCherry Imp (generated within this project) and N-terminally (Nt)-tagged GFP Imp (Medioni *et al*. 2014).

We first tested the localization of both the C-terminally and N-terminally tagged Imp-GFP transgenes within the *Drosophila* oocyte, where its localization has been previously characterised (Munro *et al*. 2006). The Nt-tagged GFP Imp was previously used in rescue experiments (Medioni *et al*. 2014), showing that this protein is functional. As a read out of endogenous Imp, we used a GFP exon-trap line (**Figure 11A**) (Quiñones-Coello *et al.* 2007). Both the Nt and Ct-tagged Imp transgenes localized normally in the oocyte and no major differences in their expression levels were observed **(Figure 11B&C**), suggesting that the GFP-tag does not affect the normal localization of the protein.

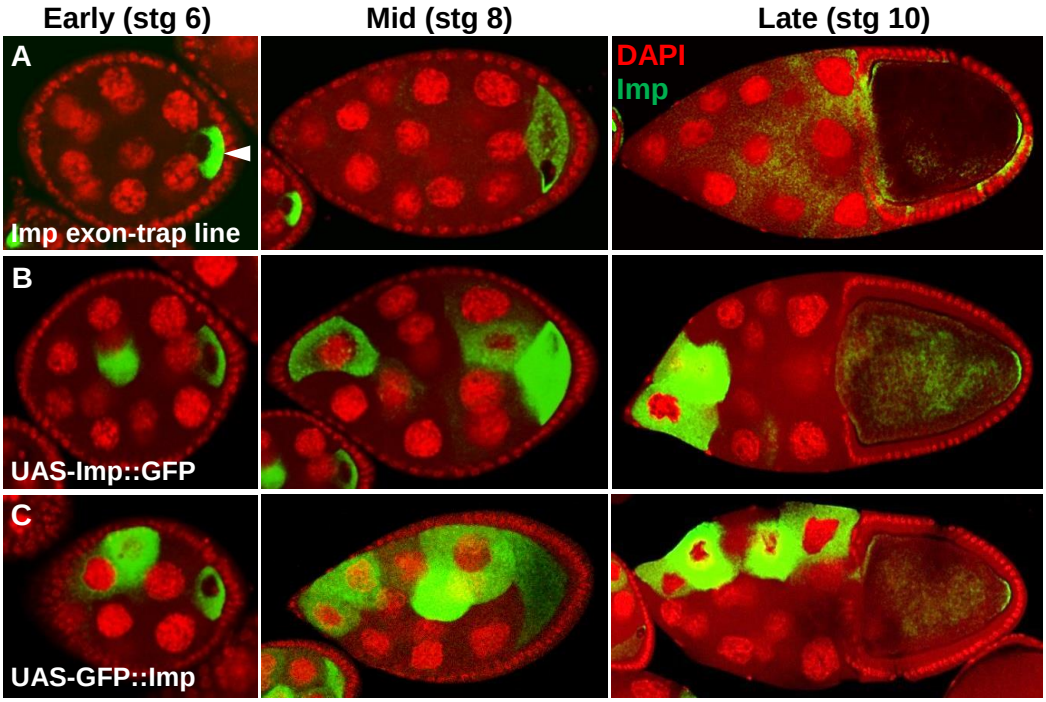

Figure 11. Testing the localization of Imp transgenes in the *Drosophila* oocyte
UAS-driven GFP-tagged Imp proteins were expressed specifically in *Drosophila* ovaries using the germline-specific maternal tubulin Gal4 (pMat-Gal4) driver. The ovaries were then dissected, fixed and counterstained with DAPI (red) to highlight nuclei and reveal the localization of Imp (green) in individual oocytes at different stages of oogenesis. (**A**) An Imp-GFP exon-trap line reveals the localization of endogenous Imp. (**B**) The distribution of an Imp transgene tagged with GFP at the C-terminus, compared with Imp tagged at the N-terminus (**C**). All GFP-labelled proteins localized as expected in a crescent at the oocyte posterior (white arrowhead) and also accumulate within the nurse cells.

3.5 Imp is not enriched within the lamellipodial protrusions of haemocytes

We followed the distribution of Ct-tagged Imp with GFP or mCherry in haemocytes *in vivo*, as well as the Nt-tagged Imp GFP, with comparable results. When expressed specifically in haemocytes Imp-mCherry was not present at the leading edge of the lamellipodial protrusions (**Figure 12**) but was distributed throughout the cell body. However, in contrast to findings in cultured migratory cells *in vitro* and migratory *Dictyostelium* cells, in which actin is enriched at the leading edge (DesMarais *et al*. 2002; Chang *et al.* 2000), we did not observe actin enrichments at the leading edge of haemocytes *in vivo*. Instead, a high concentration of actin was frequently observed at the edge of the cell body, specifically at a region from which the lamellipodial protrusions protrude (**Figure 12A** – red arrowheads). A long, narrow arm, which also showed a high actin concentration, frequently extended from this region of the cell body into the lamellipodial protrusions (**Figure 12A** – blue arrowheads).

Although Imp was not present at the periphery of lamellipodial protrusions we frequently observed Imp at the base of these arms of actin enrichment (**Figure 12** - yellow arrowheads).

The actin-rich protrusions, in which Imp was localized, could correspond to both actin or microtubules as microtubules and actin can be associated with each other within the lamellipodial protrusions, with microtubules extending along pre-existing tracks of actin-bundled filaments (Stramer *et al*. 2010). To determine if Imp could also co-localize with microtubules, we expressed the microtubule marker, Clip170-GFP, in haemocytes (**Figure 13**).

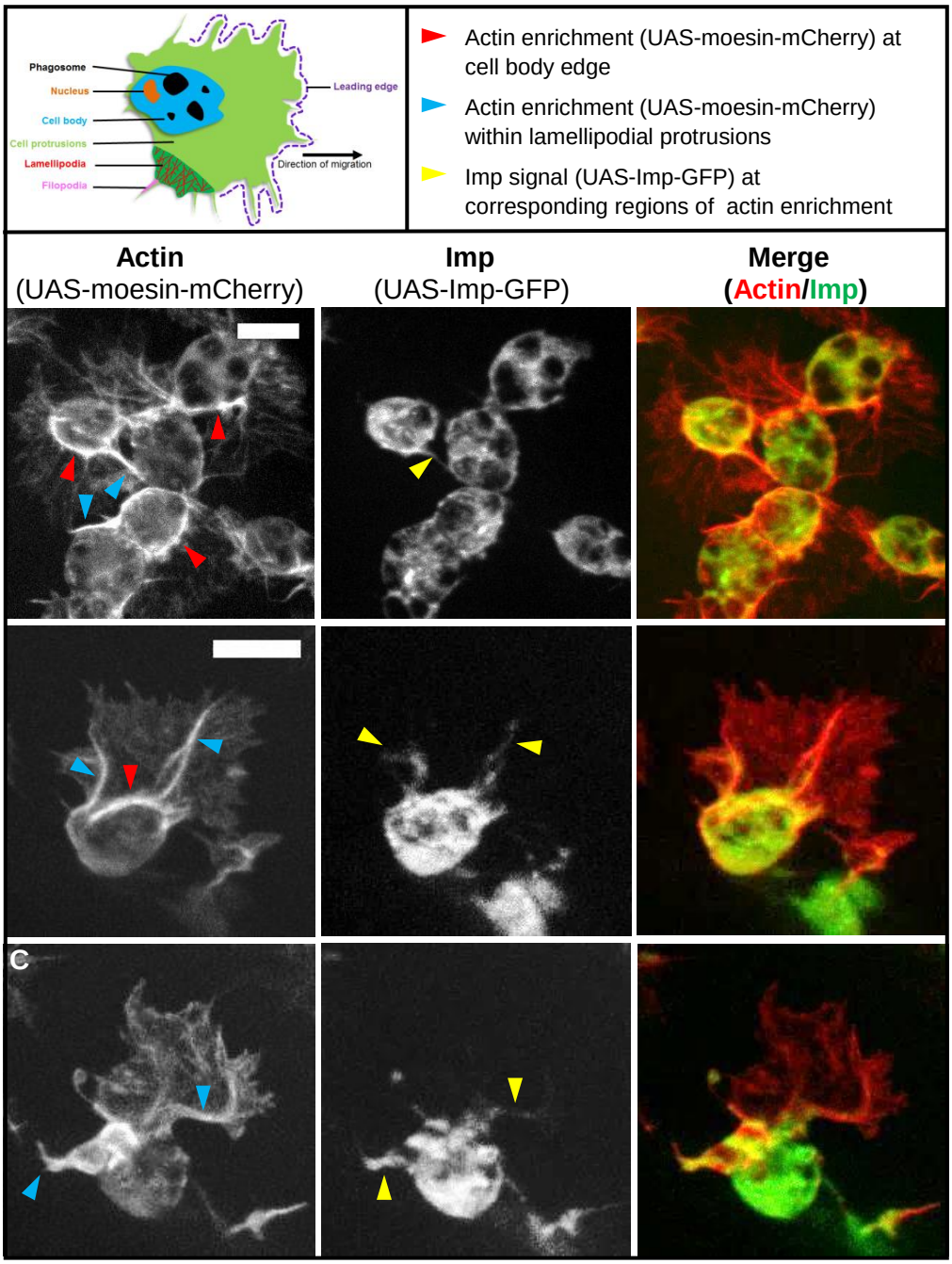

Figure 12. Live imaging of Imp distribution in *Drosophila* embryonic haemocytes *in vivo*

(**A**-**D**) Two copies of UAS-Imp-mCherry were expressed specifically in *Drosophila* embryonic haemocytes using the haemocyte-specific *srp*-Gal4 driver. Two copies of UAS-moesin-GFP were used to label the actin cytoskeleton. The distribution of Imp-mCherry in haemocytes was then imaged *in vivo* by live confocal microscopy of embryos at stage 15 of embryonic development. Red arrowheads highlight regions of actin enrichment located at the edge of the haemocyte cell body (see schematic for location of cell body). Blue arrowheads highlight regions of actin enrichment within the lamellipodial protrusions. Imp was not enriched at the leading edge of haemocytes, but was distributed throughout the entire cell body and was frequently observed in thin protrusions that extended from the cell body (yellow arrowheads). Imaging revealed that, in all cases, these Imp-containing protrusions (yellow arrowheads) co-localise with regions of actin enrichment (blue arrowheads). Scale bars represent 10 µm.

Migrating haemocytes form a structure, referred to as a microtubule arm, which consists of a tight bundle of lamellar microtubules that protrude from the haemocyte cell body in the direction of migration (Stramer *et al*. 2010). Imp was always present within the microtubule arm (**Figure 13A –** blue arrowhead) and was hard to detect in cellular protrusions when a microtubule arm was not formed (**Figure 13B**) (i.e. when the cell was repolarizing and a new microtubule arm was forming), suggesting that Imp primarily co-localizes with microtubules filaments in the lamellipodial protrusions. The actin cytoskeleton persists and then disassembles once the microtubule arm has been disassembled (Comber *et al*. 2010), so it is possible but unlikely that Imp co-localizes with actin in haemocyte protrusions as Imp fails to co-localize with persistent actin upon microtubule disassembly. However, as microtubules tend to extend along pre-existing tracks of actin, one can argue that Imp co-localizes with actin in these tracks when a new microtubule arm is formed.

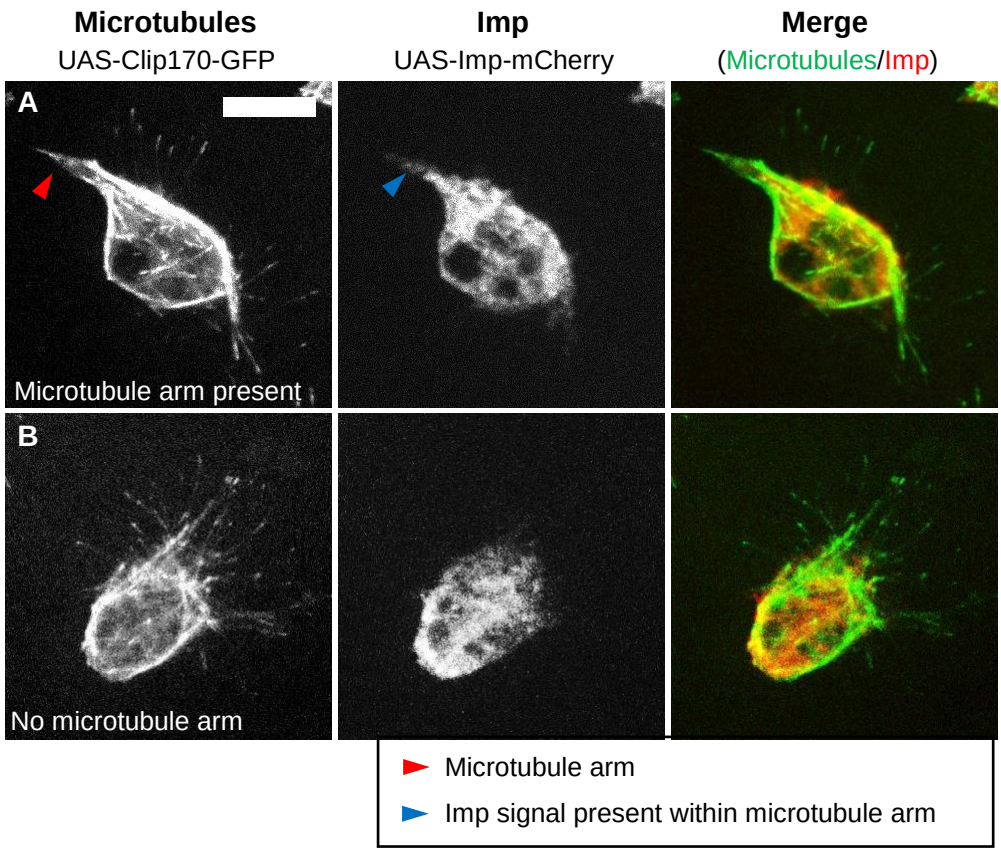

Figure 13. Co-localization of Imp distribution in *Drosophila* embryonic haemocytes *in vivo* with the microtubule marker Clip170

Two copies of the microtubule marker UAS-Clip170-GFP and UAS-Imp-mCherry were expressed in haemocytes using the haemocyte-specific *srp*-Gal4 driver and embryos were imaged by confocal microscopy at stage 15 of embryonic development. Haemocytes form a structure consisting of a bundled array of microtubules that protrude from the haemocyte cell body into the lamellipodial protrusions, termed the microtubule arm (Stramer *et al*. 2010). (**A**) When a microtubule arm was present (red arrowhead) Imp signal was always present within the base of it (blue arrowhead). (**B**) When no microtubule arm was formed (i.e. the microtubule arm was in the process of collapsing or re-forming) Imp signal was only observed in the cell body and not in the haemocyte protrusions, suggesting that Imp co-localizes primarily with microtubules and not the actin cytoskeleton. This is because the actin cytoskeleton persists and then disassembles once the microtubule arm has been disassembled – i.e. lamellipodial protrusions are still present when a microtubule arm is not. Scale bar represents 10 µm.

3.6 Comparing Imp localization in haemocytes *in vivo* and cultured cells

To confirm the expression of Imp in haemocytes and examine its localization *in vitro*, we used an *ex vivo* system. By culturing haemocytes we can compare and contrast the localization of Imp in both an *in vivo* and *in vitro* environment. Embryonic haemocytes have been cultured, although they fail to migrate within a culture dish and are unhealthy, forming only spindly projections (Tucker *et al*. 2011). *Drosophila* larvae contain the same haemocyte population as embryos, which can be bled from third instar larvae, cultured with a cell culture dish and induced to migrate by adding a pulse of ecdysone (Sampson & Williams 2012;

Sampson *et al*. 2013). Addition of ecdysone triggers larval haemocytes to polarize and produce lamellipodial protrusions. We therefore dissected third instar larvae to bleed out haemocytes, which were then cultured, fixed and immunostained against our proteins of interest.

Our first observation was that the morphology of cultured larval haemocytes was not uniform and the localization of Imp appeared to vary depending on the cellular morphology. Loosely, the different haemocyte morphologies included; cells that were highly spread with broad protrusions and cells that had shrunken around their nucleus and formed very few or no protrusions, which we refer to as 'shrunken rounded cells' (**Figures 14A & B**, respectively). Other morphologies included 'protrusive', in which clear lamellipodial protrusions were observed and 'large rounded', in which very few protrusions could be seen (**Figures 14C & D**, respectively). These different morphologies were observed at equal frequencies within the cell population.

The localization of Imp was highly variable in cultured haemocytes with different morphologies and even consistency of Imp localization in cells of similar morphologies was not observed (**Figure 14**). In highly spread haemocytes the localisation of Imp is mainly diffuse and granules of Imp enrichment are not prominent. Imp was mainly present in the central part of the cell, in a region that could correspond to the cell body (**Figure 14A**). In contrast, rounded-up cells show localization of Imp in distinct puncta (**Figure 14B & D**). Although immunostaining of Imp in cultured haemocytes failed to yield any information regarding a specific cellular localization, it confirmed that Imp is expressed in haemocytes.

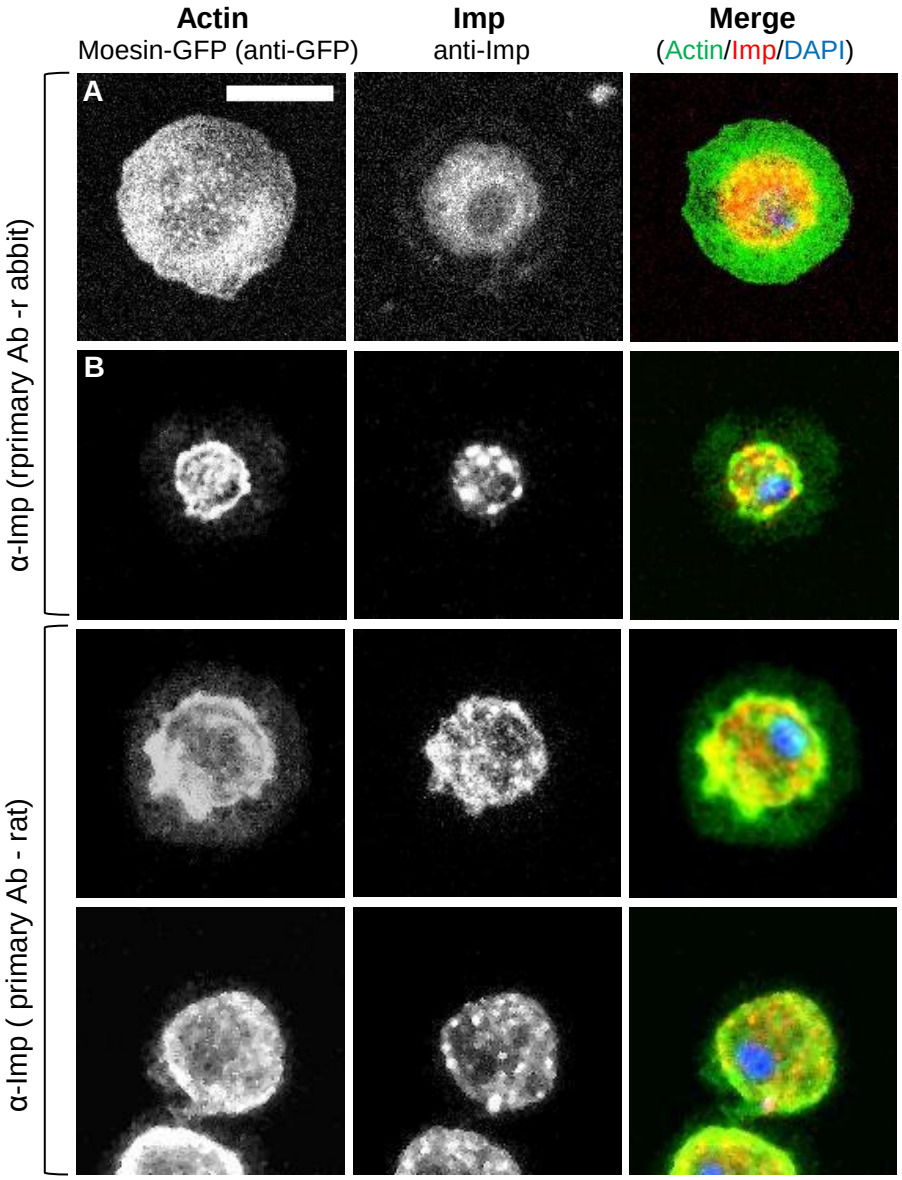

Figure 14. Immunostaining of Imp in *ex vivo* cultured *Drosophila* larval haemocytes revealed high variability in the morphology of cultured haemocytes

Haemocytes were dissected from third instar *Drosophila* larvae and cultured on uncoated glass before fixing and immunostaining with two distinct primary antibodies against Imp (red) raised in either (**A,B**) rabbit, or (**C,D**) rat. The actin cytoskeleton was labelled by anti-GFP immunostaining of haemocytes which expressed UAS-moesin-GFP, driven by two copies of the haemocyte-specific *srp*-Gal4 driver (green). Nuclei were counterstained with DAPI (blue). Haemocyte morphology was highly variable and a homogeneous population of cells was not observed. It was rare to observe cells that appeared identical in morphology although similar morphologies were seen. Haemocyte with different morphologies are shown, which we describe as (**A**) spread, (**B**) shrunken rounded, (**C**) protrusive rounded and (**D**) large rounded morphologies. These cells were observed at equal frequencies and various other morphologies were also seen (not shown). The localization of Imp was also varied in haemocytes with different morphologies and so it was not possible to conclude if Imp is localized to any specific cellular region in cultured haemocytes. However, Imp immunostaining reveals that Imp is expressed in haemocytes. Scale represents 10 µm.

We next analysed Imp localization in a haemocyte-like *Drosophila* cell line. The *Drosophila* S2R+ (Schneider-2 receptor plus) haemocyte-like cell line, which was isolated from the *Drosophila* wing disc, shows a characteristic spread morphology with extensive lamella when seeded on the lectin Concanavalin A (ConA) (Yanagawa *et al*. 1998). However, we found that addition of ConA to glass on which cells were seeded resulted in sequestering of antibodies to the glass surface, producing a high background (data not shown). We found that this background was significantly reduced in S2R+ cells seeded on non-coated glass. However, the morphology of S2R+ cells plated without ConA was variable, showing different degrees of spreading and different cellular shapes, including some that produced very few protrusions or none at all. We therefore compared the distribution of Imp in cells with varying morphology (**Figure 15**). Cells with different morphologies were observed at equal frequencies.

In S2R+ cells that show a spread morphology with branched lamella, as seen in cells seeded on ConA, Imp is present throughout the cellular cytoplasm with some patches of Imp signal observed in the cellular protrusions (**Figure 15A** – white arrowheads). Phalloidin staining showed that actin is enriched within regions of the lamella, as well as at the very tips of the lamellipodial protrusions. However, although Imp is enriched within regions of the lamella, it is not always associated with all actin enrichments (**Figure 15B**).

Some S2R+ cells show a rounded morphology with few or no actin protrusions (**Figure 15C & D respectively)**. Imp is localized in distinct puncta approximately 0.5 µm in diameter within these cells, as observed in rounded, cultured haemocytes. This appears most striking in cells undergoing division, which are unlikely to spread protrusions prior to cytokinesis (**Figure 15D**). When cytoplasmic extensions are present in these cells, Imp does not appear to be present within them (**Figure 15C**). Interestingly, this granular distribution of Imp is not observed in cells that are spread with lamella (**Figure 15A**) that is characteristic of S2R+ cells seeded on ConA (data not shown).

In summary, we show that Imp is not enriched at the periphery of cellular actin protrusions in haemocytes, both *in vivo* and *in vitro*, and is more highly concentrated within the cell body, than the protrusions. However, while the distribution of Imp was consistent in haemocytes *in vivo*, we observed variability of its localization in cultured haemocytes and S2R+ cells. Imp was enriched in distinct puncta of both haemocytes and S2R+ cells that were rounded up and formed few actin protrusions. While patches of actin enrichment were also observed in haemocytes *in vivo*, they were fewer in number and were not as distinct as those observed in cultured cells.

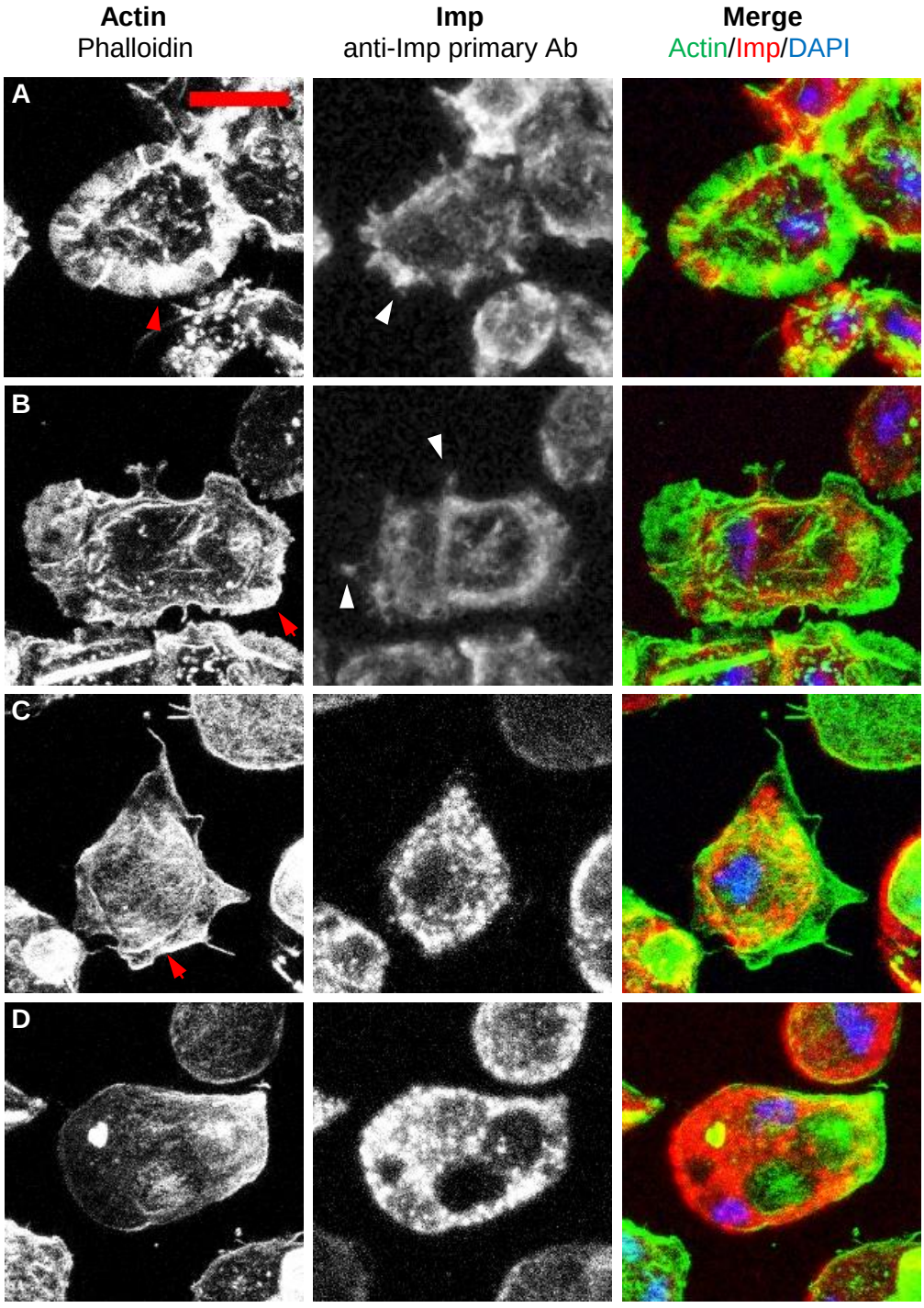

Figure 15. Immunostaining of an established *Drosophila* cell line reveals the distribution of endogenous Imp

Drosophila S2R+ cells were seeded on glass slides, fixed and immunostained with a primary antibody against Imp to reveal the distribution of Imp (red). Cells were stained with phalloidin to label the actin cytoskeleton (green) and DAPI to reveal nuclei (blue). S2R+ cells showed different morphologies when plated on uncoated glass and the localization of Imp in these cells was also shown to differ depending on cellular morphology. (**A**, **B**) A proportion of cells spread to form lamellipodial protrusions in which actin is enriched (red arrowheads). Imp is present in some regions of the lamellipodia (white arrowheads). (**C**, **D**) Some cells show a more polarised morphology, producing protrusions in only one direction (**C**) or fail to spread and show a rounded morphology (**D**). In these cells Imp is highly enriched in large granules, which are localised to the cytoplasmic region and are not present in lamellipodial protrusions, if formed. Scale represents 10 µm.

3.7 Characterizing the *in vivo* localization of PTB in haemocytes

The hnRNP I, PTB, has been shown to play a role in localising mRNAs required for generating focal adhesions (Babic *et al*. 2009), as well as a role in localising *β-actin* mRNA in the growing dendrites of developing neurons (Ma *et al*. 2007). Interestingly, knockdown of PTB expression in migratory border cells prevents their migration (Besse & López de Quinto, unpublished). Thus, we decided to examine the localization of a GFP-tagged PTB protein in live haemocytes to see if it is enriched within the lamellipodial protrusions of haemocytes or elsewhere in the cell that may be important for their migration.

As for Imp, we first tested the localization of both C-terminally (Ct) and N-terminally- (Nt) tagged PTB-GFP proteins in the *Drosophila* oocyte. PTB shows a highly nuclear localization in oocytes, but is also enriched in a crescent at the oocyte posterior, which reflects the binding of PTB to *oskar* mRNA (Besse *et al*. 2009) (**Figure 16A**). Both the Nt- and Ct-tagged PTB-GFP proteins (GFP::PTB and PTB::GFP respectively) localised in oocytes as expected, showing the crescent of PTB enrichment at the posterior (**Figure 16B & C**). However, Nt-tagged PTB appeared more active than the Ct-labelled protein, as the posterior enrichment of GFP::PTB could be clearly seen when expressed using the weaker pMat-Gal4 driver (**Figure 16B**).The posterior crescent of PTB::GFP was too weak when driven with the weaker pMat-Gal4 (data not shown) and could only be seen by driving expression with the stronger pMat-Gal4 (**Figure 16C**). This suggests that the Nt-tagged GFP::PTB binds *oskar* mRNA more efficiently than the Ct-tagged version and so we opted to express GFP::PTB in haemocytes.

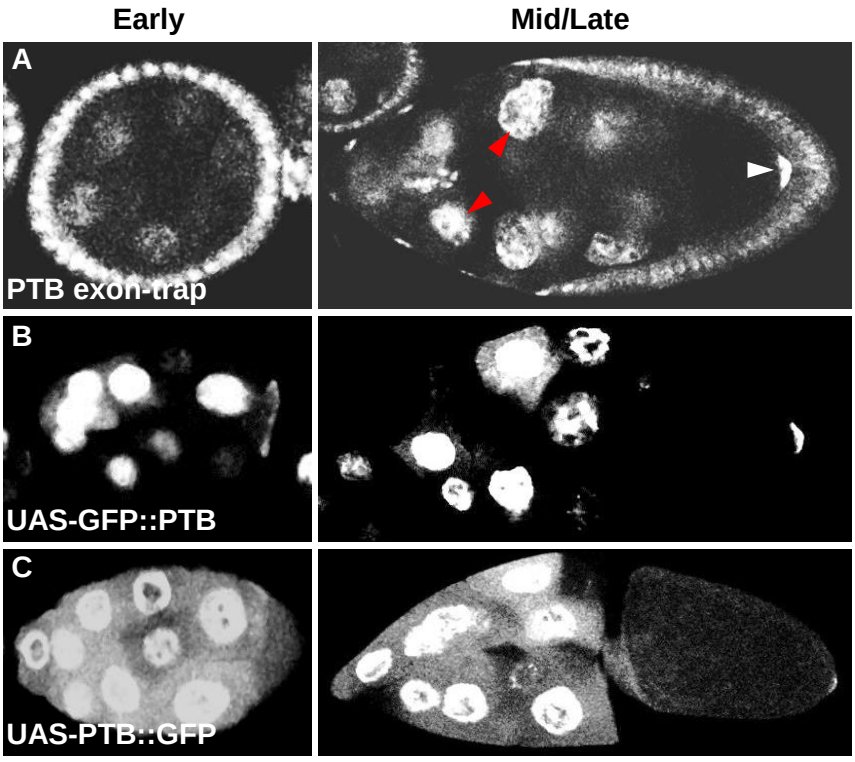

Figure 16. Distribution of different GFP-tagged PTB proteins within the *Drosophila* oocyte

UAS-driven GFP-tagged PTB proteins were expressed specifically in *Drosophila* ovaries using either a weak or strong germline-specific maternal tubulin Gal4 (*pMat*-Gal4) driver to compare their localization with a PTB-GFP exon-trap line that labels endogenous PTB. Ovaries were then dissected and fixed to examine the distribution of fluorescently-labelled PTB proteins at different stages of oogenesis by directly imaging GFP emission. (**A**) A PTB exon-trap lines reveals the localization of endogenous PTB, which is expressed in both germline and somatic cells (exon-trap line characterized in Besse *et al.* 2009). PTB is enriched in the germline nurse cell nuclei (red arrowheads) and in a crescent at the posterior (white arrowhead). (**B**) The localization of PTB tagged with GFP at the N-terminus was revealed using the weaker pMat-Gal4 driver. (**C**) Localization of PTB tagged at the C-terminus in a crescent at the posterior pole of oocytes could only be revealed by expression with the stronger pMat-Gal4 driver, suggesting that it binds mRNA localized at the posterior less efficiently than Nt-tagged GFP-PTB.

The localisation of PTB in haemocytes was tested in a variety of different ways, to follow both the distribution of the endogenous protein, and that of a fluorescently labelled PTB transgene. Firstly, the GFP-labelled PTB transgene (UAS-GFP::PTB), generated within this project, was expressed specifically in haemocytes using the GAL4/UAS system. PTB was weakly distributed throughout the cellular cytoplasm, including the lamellipodial protrusions, but showed a strong enrichment within a structure located in the cell body (**Figure 17A** – red asterisks), which we presume to be the nucleus, as PTB has well characterized nuclear functions (Sawicka *et al*. 2008).

We compared the distribution of wildtype PTB to that of a GFP-labelled PTB transgene lacking the nuclear localization signal (NLS) (UAS-GFP::PTB-ΔNLS) (Besse *et al*. 2009). The

strong enrichment of wildtype PTB observed within the cell body of haemocytes was not observed with GFP::PTB-ΔNLS, confirming the nuclear enrichment of wildtype PTB. However, the PTB-ΔNLS transgene was enriched in the haemocyte cell body in several granules (**Figure 17B** – blue arrowheads) not observed in the lamellipodial protrusions, which may be RNP granules enriched in PTB (**Figure 17B**). Interestingly, we occasionally observed a PTB enrichment at the leading edge (**Figure 17B** – yellow arrowheads).

We then compared the distribution of the exogenously-expressed PTB transgenes within haemocytes with the distribution of endogenous PTB using exon-trap lines, in which endogenous PTB protein is labelled through induction of a YFP cassette into the *hephasteus* gene (Lowe *et al*. 2014). Flies of the protein trap lines were crossed to *srp*-Gal4, UAS-mCherry-moesin flies to label and visualise the actin cytoskeleton within haemocytes. The PTB-GFP signal was very weak and as the protein trap line is expressed under the control of the endogenous promoter, the GFP-labelled PTB signal is present throughout the entire embryo and is not haemocyte specific, making it hard to resolve its distribution within haemocytes. Several large fluorescent particles could be seen within the cell body (**Figure 17C**- red asterisks). The majority of these large granules appeared to co-localize with phagosomes, suggesting that these are auto-fluorescent particles engulfed by haemocytes.

To determine if these particles were real PTB signal or autofluorescent particles, as well as examine the level of background auto-fluorescence in haemocytes (eg. without any GFP signal) we imaged embryos expressing only mCherry-moesin within haemocytes. Between two and three fluorescent particles of approximately 2 µm in diameter were often present in the cell body of haemocytes in the GFP channel (see **Figure 10A** for haemocyte morphology), although none were seen in the lamellipodial protrusions (**Figure 17D**). These observations suggest that the large particles observed in Figure 17D are likely to be auto-fluorescent debris engulfed by phagocytosis. However, no red background fluorescence was observed in embryos expressing only GFP-moesin (data not shown), which made mCherry-labelled proteins a better choice to examine protein distribution in haemocytes. PTB-mCherry constructs were not generated due to the time constraints of generating constructs and injecting them to generate transgenic flies.

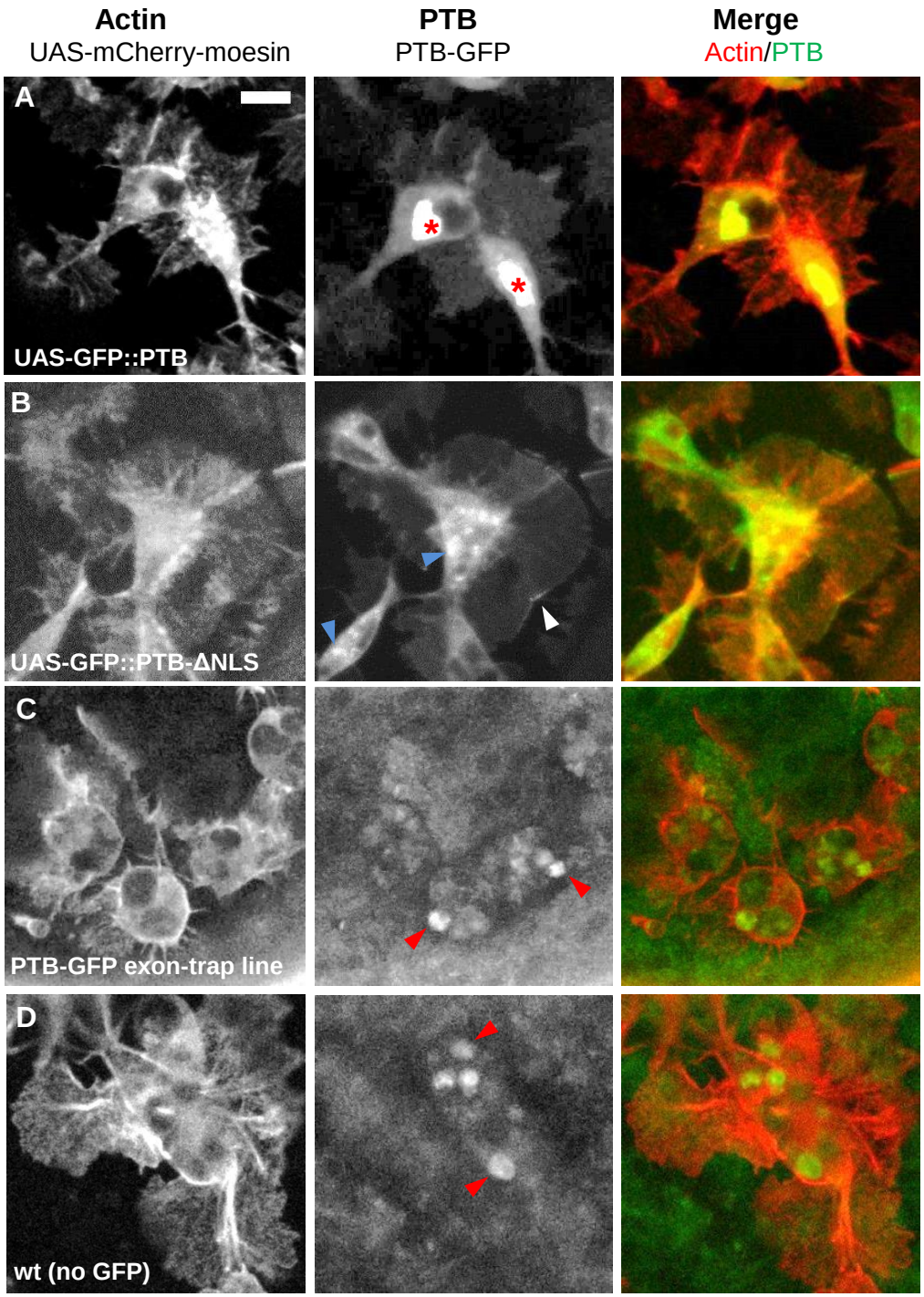

Figure 17. Localisation of PTB in live embryonic haemocytes *in vivo* using different approaches

The localization of PTB in haemocytes *in vivo* was examined by live confocal imaging of *Drosophila* embryos at stage 15 of embryonic development. The actin cytoskeleton was labelled with two copies of UAS-driven mCherry-moesin, which was expressed specifically in haemocytes using the *srp*-Gal4 driver. (**A**,**B**) Two UAS-driven PTB-GFP constructs were expressed specifically in haemocytes using the *srp*-Gal4 driver, including a wildtype PTB protein and a mutated version of PTB lacking the nuclear localization signal (PTB-ΔNLS), to compare the nuclear vs. cytoplasmic localization of PTB. (**A**) UAS-GFP::PTB shows strong enrichments in the cell body (red asterisks), which may be nuclear. (**B**) UAS-GFP::PTB-ΔNLS is expressed throughout the cytoplasm with granules in the cell body (blue arrowheads) and occasional enrichment at the leading edge (white arrowhead). (**C**) Endogenous PTB localization was examined using a PTB exon trap line (referred to as CPTI 30), in which endogenous

PTB is tagged with GFP. As endogenous PTB-GFP signal was weak it was compared with haemocytes lacking a GFP transgene (**D**) to distinguish real GFP signal from background green autofluorescence due to forced imaging conditions. Both images were taken with identical imaging conditions (e.g. same exposure time, etc.) (**D**) Large auto-fluorescent particles were present in the GFP channel of control live haemocytes negative for GFP expression (red arrowheads). Scale represents 5 µm.

3.8 PTB distribution in cultured larval haemocytes

The distribution of PTB was then examined in cultured larval haemocytes, to confirm its expression in haemocytes and compare and contrast its localization in both an *in vitro* and *in vivo* environment. We labelled endogenous PTB in cultured haemocytes firstly by using antibodies against PTB, and then by dissecting haemocytes from larvae of the PTB protein trap lines CPTI30 (Lowe *et al*. 2014) and CC00664 (Buszczak *et al*. 2007), which were fixed and stained with an antibody against GFP. This enabled the endogenous protein to be seen without the surrounding tissues.

We first observed that, unlike embryonic haemocytes *in vivo*, cultured larval haemocytes sometimes show enrichments of actin at the periphery of actin protrusions (**Figure 18**). Both the PTB exon trap lines revealed that PTB is present in small granules throughout the haemocyte cell body with a lower level of distribution within the lamellipodial protrusions (**Figure 18B-C**). Similarly to the pattern observed through live imaging, PTB was mainly spread though-out the whole cell body and was not enriched in any particular cellular compartment. However, we did not observe a strong nuclear enrichment of PTB, as we did not see any clear globular enrichments of PTB within the cellular cytoplasm at regions stained by DAPI (compare **Figures 17A & 18**). It is possible that nuclear enrichment of PTB was not observed in cultured haemocytes because the antibodies used failed to penerate the nucleus efficiently.

To confirm the pattern observed with the protein trap lines, we used antibodies to stain endogenous PTB. This assay showed that PTB was enriched in specific regions of the cell body and in the lamellipodial protrusions surrounding the cell body (**Figure 18D**). In the absence of ecdysone, haemocytes extended lamellipodial protrusions around the entire cell body and showed a round morphology. In this case, PTB was highly enriched in some large granules within the cell body and was also distributed throughout the cellular protrusions, with some small granules of enrichment (**Figure 18D**). In contrast, haemocytes plated with ecdysone were highly polarized and extended lamellipodial protrusions in a single direction. Actin was highly enriched in these protrusions compared with the protrusions of non-polarized haemocytes (**Figure 18E**). Interestingly, the localization of PTB in polarized

haemocytes appeared different, with rings of PTB enrichment in undefined structures within the cell that did not co-localise with enrichments of actin. PTB distribution appeared less granular in polarized haemocytes and it was enriched within some regions of the lamellipodial protrusions (**Figure 18E**). In conclusion, we did not reveal wildtype PTB enriched at the leading edge of live haemocytes *in vivo* or in cutured haemocytes.

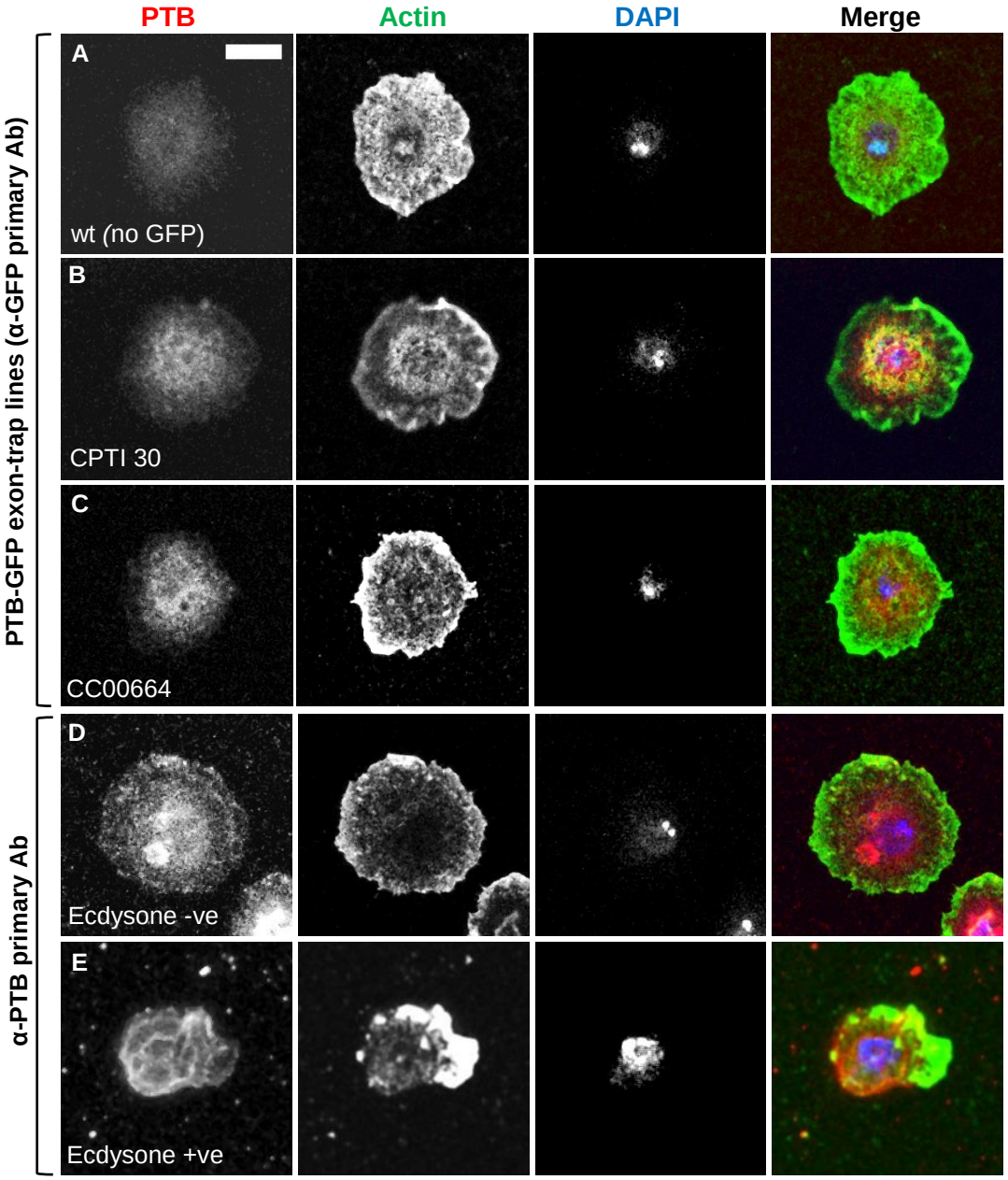

Figure 18. Immunostaining of PTB in cultured *Drosophila* larval haemocytes

Haemocytes were dissected out from third instar *Drosophila* larvae and cultured on glass before fixing and immunostaining to reveal the localization of endogenous PTB in cultured haemocytes (red). Haemocytes were stained with phalloidin to label the actin cytoskeleton (green) and DAPI to reveal nuclei (blue). In the case of anti-PTB immunostaining, haemocytes were cultured in the presence or absence of ecdysone, which is added to culture media to induce polarization of larval haemocytes. This allowed PTB localization to be compared in cultured haemocytes with different cytoskeletal

structures, including a rounded spread morphology (ecdysone absent) and a highly polarized morphology with a distinct leading edge enriched in actin (ecdysone present). (**A**) Wildtype haemocytes stained with an anti-GFP antibody to determine the level of background fluorescence. (**B,C**) Haemocytes isolated from two distinct PTB exon-trap lines (referred to as CPTI 30 & CC00664), in which endogenous PTB is labelled with GFP, were immunostained with anti-GFP primary antibody. (**D**,**E**) Endogenous PTB was visualized in wildtype haemocytes immunostained with a rabbit anti-PTB antibody in haemocytes seeded without (**D**) or with (**E**) the addition of ecdysone to induce polarization. Scale represents 10 µm.

In conclusion, PTB is distributed throughout the cell body and protrusions of haemocytes both *in vivo* and *in vitro*. However, the observed enrichments of PTB are variable between cultured haemocytes, with high levels of signal present in the lamellipodial protrusions of some cells, but not others (**Figure 18**). In contrast, the localization of PTB in haemocytes *in vivo* was highly consistent (**Figure 17A**) PTB was highly enriched in the nucleus of haemocytes *in vivo*, which was not observed in haemocytes *in vitro*, which may reflect a difference in the distribution of PTB, or the failure of our antibodies to penerate the nucleus efficiently.

3.9 Characterising Hrp48 distribution in haemocytes

We next decided to examine the localization of the RBP Hrp48 in haemocytes, as previous findings suggest that it may play a role in regulating cell migration (Mathieu *et al*. 2007). To follow the distribution of Hrp48 exclusively in haemocytes, we generated a UAS Hrp48 transgene that was tagged with GFP at the C-terminus. We first tested the localization of this Hrp48 transgene by expressing it in the ovary and compared it to the distribution of a Hrp48 transgene constitutively driven from a maternal promoter (**Figure 19A**). Both constructs behaved similarly and resulted in the accumulation of the tagged Hrp48 proteins at the posterior pole of the oocyte, as described for the endogenous protein (Huynh *et al*. 2004; Yano *et al*. 2004) Hrp48-GFP proteins localized as expected, when compared to immunostainings of endogenous Hrp48 (Yano *et al*. 2004), with an enrichment of Hrp48 forming a crescent at the oocyte posterior (**Figure 19B**).

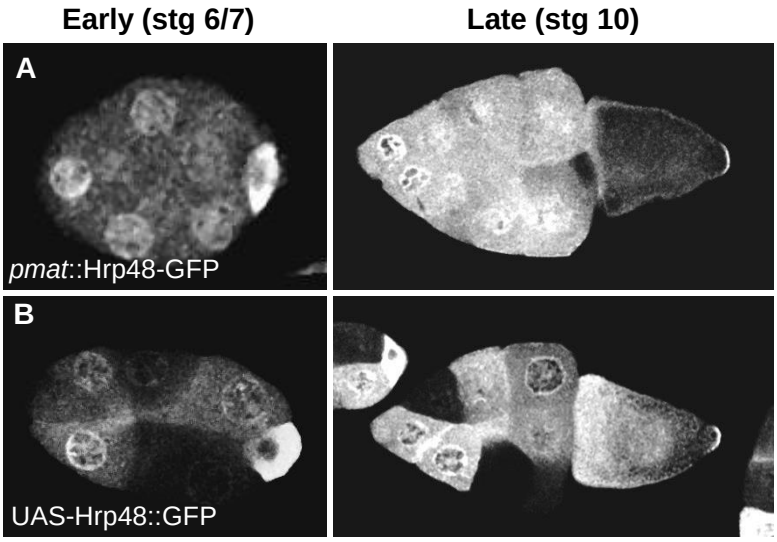

Figure 19. Testing the localization of Hrp48 transgenes in the *Drosophila* oocyte

A UAS-driven GFP-tagged Hrp48 protein was expressed specifically in *Drosophila* ovaries using the germline-specific maternal tubulin Gal4 (*pMat*-Gal4) driver to compare its localization with a GFP-tagged Hrp48 protein driven from a constitutive maternal tubulin promoter. Ovaries were dissected and fixed to examine the distribution of fluorescently-labelled Hrp48 at different stages of oogenesis. (**A**) The distribution of Hrp48-GFP, whose expression is driven by the maternal tubulin promoter. (**B**) The distribution of UAS-driven Hrp48 tagged with GFP at the C-terminus, which was generated in this project.

We then expressed the Hrp48 transgene in haemocytes and examined the localization of Hrp48-mCherry by live confocal imaging of stage 15 embryos. This revealed that Hrp48, in contrast to Imp and PTB, is mainly restricted to the cell body of haemocytes *in vivo* and is not present in the lamellipodial protrusions (**Figure 20A-B**). Hrp48 was sometimes co-localized with enrichments of actin at the edge of the cell body (**Figure 20A** – red arrowheads), although this only appeared in approximately 50% of haemocytes observed.

We confirmed that Hrp48 is expressing in haemocytes by staining cultured haemocytes with an antibody against Hrp48 (**Figure 20C**). Hrp48 was concentrated within the central region of cultured haemocytes, although it was present at the periphery of these cells at low levels (**Figure 20C**).

Overall, our analysis of Imp, PTB and Hrp48 distribution in haemocytes revealed that these proteins show different patterns of localization. Localization of these RBPs was consistent in haemocytes *in vivo*, with different cells showing similar patterns of RBP localization. However, this was not the case in cultured haemocytes, particularly for Imp, which showed different localization patterns in cells depending on their morphology. Interestingly, the morphology of cultured haemocytes was also varied, with some cells showing clear actin protrusions, while others formed few protrusions and showed a shrunken, rounded

morphology. We did not observe this in haemocytes *in vivo*, as all cells formed highly branched lamellipodial protrusions in the direction of migration.

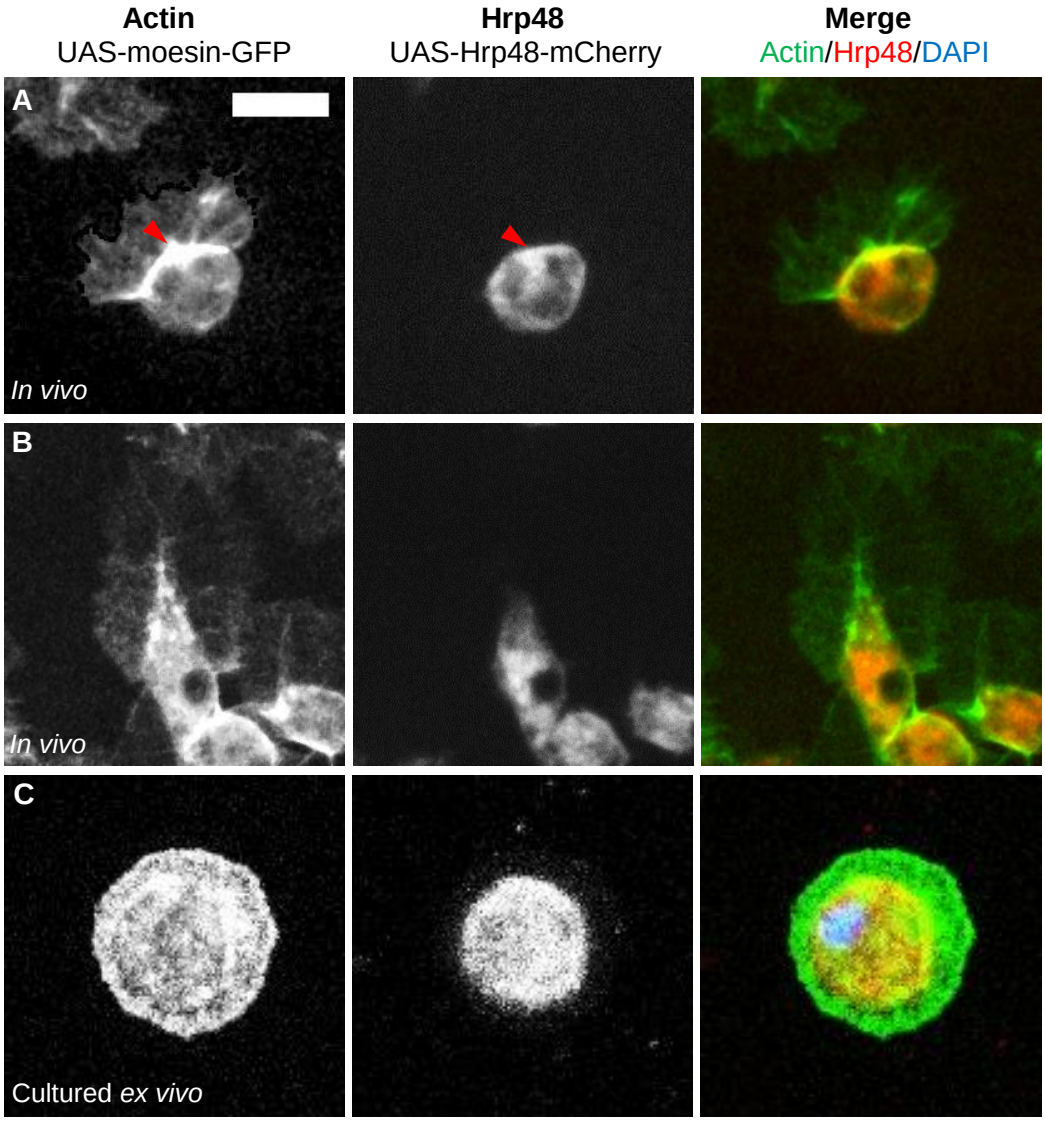

Figure 20. Comparison of Hrp48 distribution in live *Drosophila* haemocytes *in vivo* and cultured haemocytes

(**A**, **B**) UAS-driven Hrp48-mCherry was expressed in haemocytes using two copies of the haemocyte-specific *srp*-Gal4 driver (red). The actin cytoskeleton was labelled using two copies of UAS-driven moesin-GFP (green). The localization of Hrp48-mCherry was revealed by live confocal imaging of embryonic haemocytes *in vivo* in stage 15 embryos. (**A**) Hrp48 is not present within the lamellipodial protrusions, but is localized only to the haemocyte cell body. Hrp48 was occasionally enriched in some regions of actin enrichment within the cell body (red arrowheads), but this was not the case in the majority of haemocytes observed. (**C**) Larval haemocytes were dissected out and cultured on glass before subsequent fixing and immunostaining with a primary antibody against Hrp48 to reveal the localization of endogenous Hrp48 (red) in haemocytes cultured *ex vivo*. As for haemocyte imaging *in vivo*, the actin cytoskeleton was labelled by expression of UAS-driven GFP-moesin (green), which was then revealed by immunostaining with an antibody against GFP. Nuclei were counterstained with DAPI (blue). Immunostaining of endogenous Hrp48 in cultured larval haemocytes confirms that Hrp48 is expressed in haemocytes. Scale represents 10 µm

3.10 Analysis of MS2-tagged mRNAs in haemocytes using the MS2 system

As haemocytes lose their distinct polarity in fixed embryos, the distribution of candidate mRNAs in haemocytes could only be examined through live imaging. Thus, components of the MS2 system for visualizing the *in vivo* localization of mRNA were constructed and microinjected into embryos to create transgenic fly lines (see materials and methods). In brief, the system requires expression of two separate constructs; the first being a fluorescently-labelled RNA-binding MS2 coat protein (MCP) and the second an mRNA tagged to MS2 hairpin binding sites. The MCP binds the MS2 hairpin binding sites, which should allow the localization of the mRNA to be visualized (Bertrand *et al.* 1998; Forrest & Gavis 2003).

First, a single copy of the MCP C-terminally fused to mCherry, which contained a nuclear localization signal (NLS), was studied. We opted to use MCP-mCherry as a low level of auto fluorescence is present in the red channel in embryos, limiting the possibility of false-positive signal. As expected, the MCP labelled with mCherry showed a highly nuclear localization, with a very weak and diffuse signal in the haemocyte cell body (**Figure 21A**). No expression of this protein could be seen in the lamellipodial protrusions.

We then co-expressed the MCP-mCherry with the MS2-hairpin tagged *actin42A* mRNA, as *β-actin* mRNA, the mammalian homologue of *actin42A*, has been shown to localize at the leading edge of cultured migratory cells (Shestakova *et al*. 2001). However, we failed to see any change in the distribution of the MCP upon addition of MS2-tagged *actin42A* (compare **Figure 21A & B)**. It is possible that MS2-tagged *actin42A* is expressed at low levels, so cannot be detected above unbound MCP in the cytoplasm.

To boost the signal of the MCP, a construct containing two copies of the MCP sequence joined by a small linker region, referred to as the tandem MCP (tdMCP) was generated, as the MCP has to form homo-dimers within the cell cytoplasm before binding to any MS2 hairpin binding sites (developed in Wu *et al*. 2012). Although the level of transcript encoding the tdMCP will be comparable to the single version, when translated the tdMCP will not need to dimerize, doubling the levels of MCP dimer within the cytoplasm compared with expressing a single copy of the MCP.

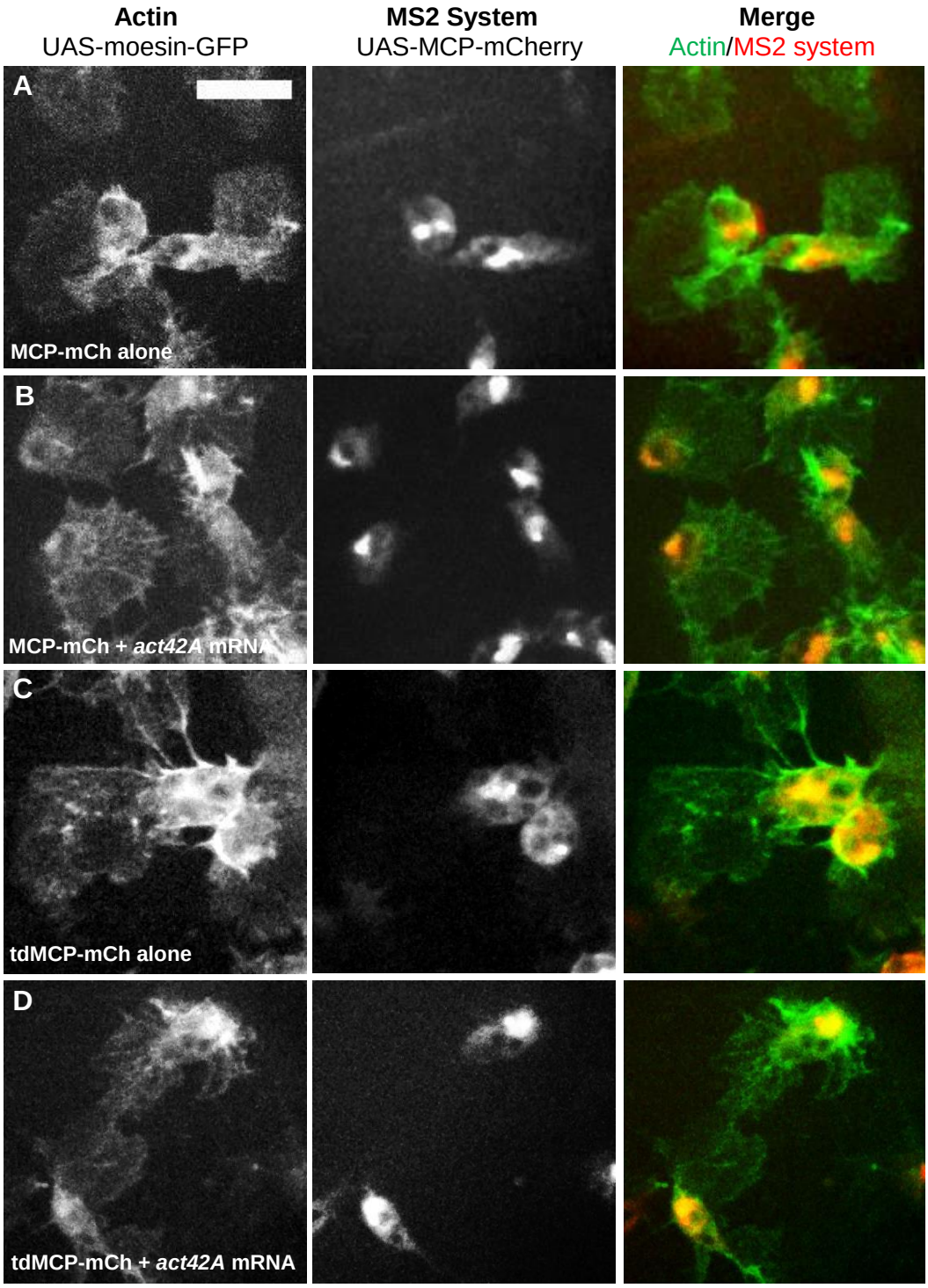

Figure 21. Analysis of *β-actin (Drosophila actin42A)* mRNA distribution using the MS2 system

UAS-driven MS2 system reagents, including both the single copy (MCP) and tandem copy (tdMCP) of the mCherry-tagged MS2 coat protein (MCP) and the MS2-tagged *actin42A* mRNA, were expressed in haemocytes using two copies of the haemocyte-specific *srp*-Gal4 driver (red). Actin42A is the *Drosophila* homologue of mammalian β-actin. The actin cytoskeleton of haemocytes was labelled using two copies of UAS-driven GFP-moesin (green). The distribution of mCherry-labelled MCP was revealed by live confocal imaging of haemocytes *in vivo* within embryos at stage 15 of embryonic development. (**A** & **C**) Control embryos expressing either (**A**) mCherry-fused MCP alone (MCP-mCh) or (**C**) the mCherry-fused tandem MCP (tdMCP-mCh) reveals the distribution of MCP protein in the absence of an MS2-hairpin tagged mRNA. Both the single and tandem MCP proteins contain an NLS

to sequester unbound MCP within the nucleus. (**B** & **D**) The localization of (**B**) MCP-mCherry and (**C**) tdMCP-mCherry when co-expressed with MS2-tagged *actin42A* mRNA. Scale represents 20 µm.

The tdMCP tagged with mCherry was expressed specifically in haemocytes using the Gal4/UAS system. The protein and was enriched in the nucleus, as it also contains an NLS, but was also weakly and diffusely distributed throughout the cell body (**Figure 21C**). This pattern of localization was identical to the single mCherry-fused MCP. However, when expressed with the MS2-hairpin tagged *actin42C* mRNA the distribution of MCP protein appeared identical to the distribution seen when expressed alone, without the tagged mRNA (compare **Figure 21C & D**). Similar results were obtained with the MS2-tagged *actin5C* (*β-actin* homologue) and *arp66B* (*arp3* homologue) mRNAs (data not shown), which have also been shown to localize at the leading edge of cultured motile cells (Shestakova *et al*. 2001; Mingle *et al.* 2005).

To test if endogenous *act42A* mRNA localises within the lamellipodial protrusions of haemocytes, fluorescence *in situ* hybridisation (FISH) was carried out on larval haemocytes, which were dissected and cultured *ex vivo,* as previously described. Both antisense and sense RNA probes were generated against *act42A* mRNA and used for FISH, which showed that *act42A* mRNA is diffusely localised throughout the entire haemocyte, including the lamellipodial extensions (**Figure 22A**). *act42A* mRNA appears more highly concentrated within the haemocyte cell body, with a lower concentration within the cellular protrusions. (**Figure 22A**). Enrichments of *act42A* mRNA were not observed at the leading edge of cultured haemocytes. This suggests that the level of *act42A* mRNA is lower in the lamellipodial protrusions than the cell body and so may not be detectable using the MS2 system. It also shows that, in cultured haemocytes, *act42A* mRNA is not enriched within any specific cellular compartment. This may make its distribution difficult to follow by the MS2 system in haemocytes *in vivo*, as the MCP alone is also diffusely distributed throughout the cell body of haemocytes. If this is the case, we may expect to see a depletion of MCP signal in the nucleus and an increase in the cytoplasm, which was not observed with either the single or tdMCP (**Figure 21**).

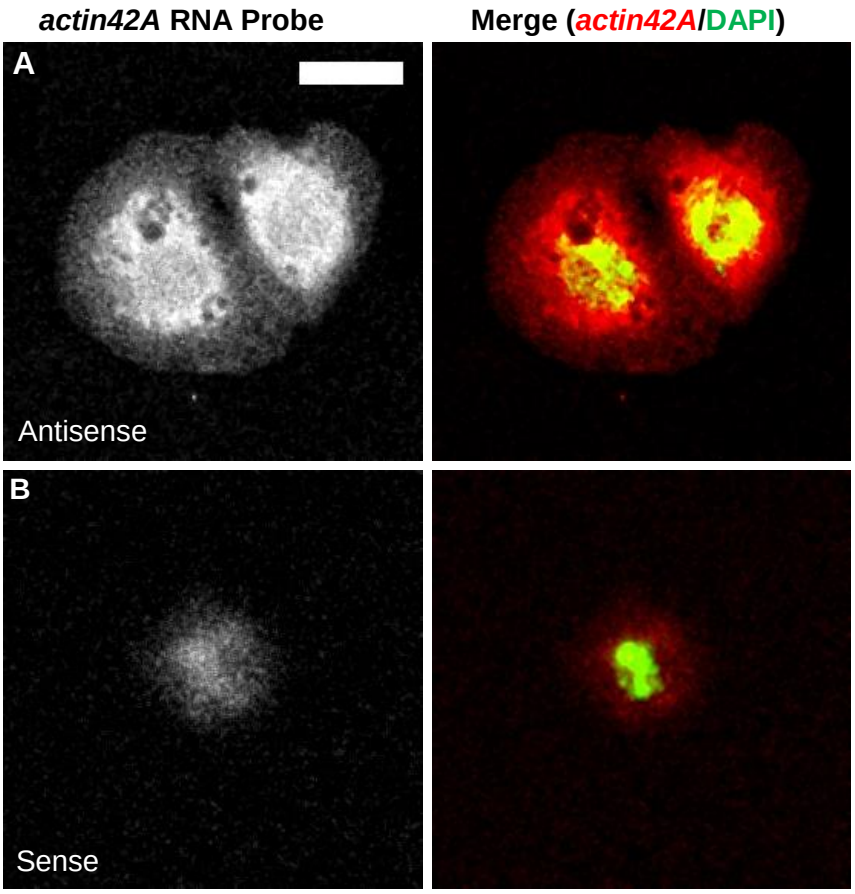

Figure 22. Localization of *actin42A* mRNA in *ex vivo* cultured *Drosophila* haemocytes using fluorescent *in situ* hybridization (FISH)

Drosophila larval haemocytes were dissected from third instar larvae and cultured on glass before fixation and fluorescent *in situ* hybridisation (FISH) was carried out using an antisense probe against *actin42A* (*act42A*) mRNA (red). The nuclei of cultured haemocytes were labelled with DAPI (green). (**A**) Antisense probe against *act42A* mRNA shows that the mRNA is present in lamellipodial protrusions, although it is found at a higher concentration within the cell body. There are no specific enrichments of the mRNA within haemocytes. (**B**) Sense probe control against *act42A* mRNA to reveal background fluorescence (red). Scale represents 10 µm.

To confirm that the *act42A* mRNA fused with the MS2 hairpin binding sites is expressed within haemocytes, RT-PCR was performed using RNA extracted from embryos expressing either the tandem-MCP alone or co-expressed with MS2-tagged *act42A* mRNA. Contaminating genomic DNA was first removed from the RNA. As a control, we decided to tag *oskar* (*osk*) mRNA with MS2 hairpins, using the same cloning strategy as that employed to tag *the β-actin* and *arp2/3* mRNAs. We chose *osk* mRNA as a positive control as this mRNA localizes to the posterior pole of the oocyte during mid to late oogenesis, which has been successfully visualized using the MS2 system (Zimyanin *et al*. 2008). We also extracted RNA from embryos expressing MS2-tagged *osk* mRNA to confirm its expression.

RT-PCR to specifically amplify the MS2 hairpin-tagged *act42A* (primer pair 64 & 65) or *osk* mRNAs (primer pair 64 & 66) (**Figure 23A**) showed that the mRNAs are expressed in these embryos, compared with embryos expressing the MCP alone (**Figure 23B**). Negative controls omitting the reverse transcriptase enzyme were carried out to ensure all genomic DNA was degraded. This suggests that either the MCP does not bind the *act42A* mRNA, or that *act42A* has a low cytoplasmic distribution which is not distinguishable from the signal of unbound MCP.

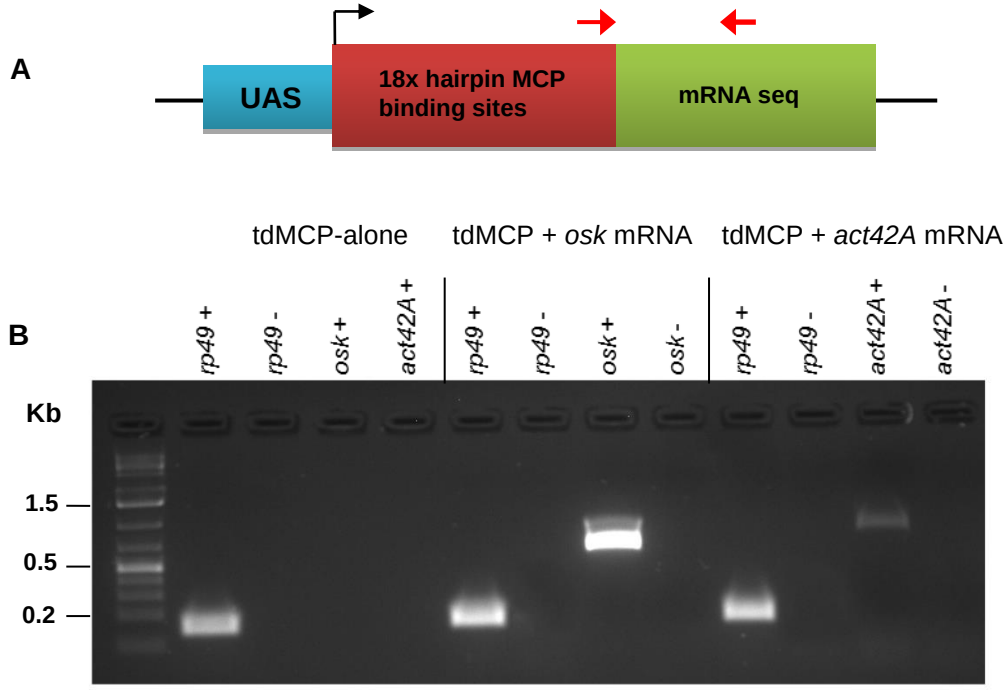

Figure 23. RT-PCR confirms MS2 hairpin-tagged mRNAs are expressed in *Drosophila* haemocytes

The expression of MS2-tagged *actin42A* (*act42A*) and *oskar* (*osk*) mRNAs in haemocytes was confirmed by extraction of RNA from embryos expressing the UAS-driven mRNAs specifically in haemocytes and subsequent RT-PCR analysis. (**A**) Region of hairpin-tagged mRNAs amplified by RT-PCR primer pairs (red arrows). (**B**) Gel electrophoresis to separate products generated by RT-PCR. Primers amplifying a region of *rp49* mRNA (encodes a ribosomal protein) was used as positive control (*rp49*+). Negative controls omitted reverse transcriptase enzyme from RT-PCR reactions to ensure no contaminating genomic DNA was present (*rp49*-, *osk*-, *act42A*-). Products of the expected size (*rp49*=0.15Kb, *osk*=0.9Kb, *act42A*=1.2Kb) were amplified for both *osk* and *act42A* mRNAs, confirming that they are expressed in *Drosophila* haemocytes (*osk*+, *act42A*+).

3.11 Testing the MS2 system in the *Drosophila* oocyte

The localization of several mRNAs within the *Drosophila* oocyte have been successfully revealed *in vivo* using the MS2 system, including *bicoid*, *gurken* and *oskar* mRNAs (Jaramillo *et al*. 2008; Weil *et al*. 2008; Zimyanin *et al*. 2008). To test the affinity of the MCP to the hairpin-binding sites used in our constructs, we expressed them within the *Drosophila* oocyte. This analysis should reveal whether the MS2 system fails to reveal tagged-mRNA localization only in haemocytes or if there is a fundamental problem with the system we constructed. MS2-hairpin tagged *oskar*, which is localized to the posterior, was expressed in the oocyte, together with both the single MCP-mCherry (data not shown) and tdMCP-GFP (**Figure 24**).

Two GAL4 drivers of varying strengths were used to express both the MCP-mCherry and tdMCP-GFP and hairpin-tagged mRNAs. The pMat-Gal4 driver inserted in the third chromosome (pMat (III)) is significantly stronger than the pMat-Gal4 driver inserted in the second chromosome (pMat (II)). Expression of the tdMCP alone reveals that it has a nuclear localisation as expected, with only weak, diffuse cytoplasmic background (**Figure 24A** – red arrowheads). Any cytoplasmic enrichment of tagged-mRNAs should therefore be revealed. However, when expressed under the control of the stronger pMat (III) driver the tdMCP alone caused oogenesis arrest; the egg chambers do not appear morphologically wildtype and mature oocytes fail to develop (**Figure 24C**). This suggests that expression of the tdMCP protein at high levels within the oocyte had a detrimental effect on oocyte development. Expression of the tdMCP from the weaker pMat (II) driver allowed oogenesis to proceed and mature oocytes were produced (**Figure 24A**).

The mRNA encoding Oskar protein is highly enriched at the posterior of the *Drosophila* oocyte (posterior region marked by white asterisk – **Figure 24A**). However, addition of MS2-hairpin tagged *oskar* mRNA revealed no difference in the pattern of expression in the oocyte compared with the tdMCP-GFP alone, with no clear posterior enrichment (**Figure 24B & D**). This was also observed for the single MCP-mCherry (data not shown). This suggests that the MS2 system does not successfully reveal MS2-binding site-labelled mRNA localisation in both the oocyte and haemocytes.

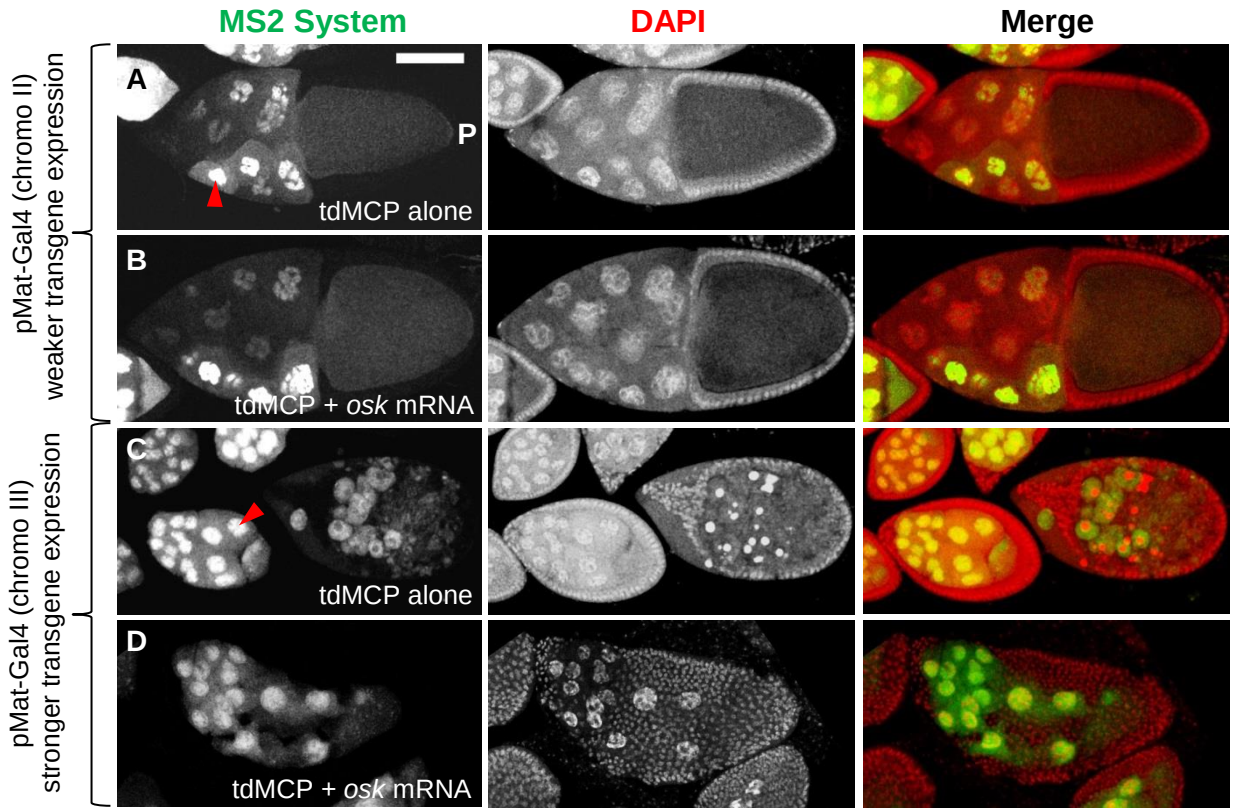

Figure 24. Testing the MS2 system in fixed *Drosophila* oocytes to reveal localization of *oskar* mRNA

The UAS-driven MS2 system reagents, including the tandem-MCP-GFP (td-MCP) and the genomic region of *oskar* (*osk*) mRNA tagged with MS2-binding sites, were expressed in *Drosophila* ovaries using maternal tubulin Gal4 drivers (pMat-Gal4). The ovaries were then fixed and counterstained with DAPI to reveal nuclei (red). *oskar* mRNA was used as its localization at the posterior of *Drosophila* oocytes has been well characterized (Besse *et al*. 2009). Individual oocytes were imaged by confocal microscopy to reveal the distribution of the tdMCP-GFP (green). (**A**) Control oocytes expressing tdMCP-GFP alone and (**B**) the tdMCP-GFP and *osk* mRNA together expressed under the control of the weaker pMat (II) Gal4 driver. (**C**) Oocytes expressing tdMCP-GFP alone and (**D**) the tdMCP-GFP and *osk* mRNA together expressed under the control of the stronger pMat (III) Gal4 driver. Oogenesis is arrested in oocytes expressing tdMCP-GFP with the stronger pMat-Gal4 driver, as shown by the morphology of the oocyte nuclei (red). Red arrows highlight the nuclear localisation of the tdMCP-GFP. *osk* mRNA should be enriched at the oocyte posterior, at the region labelled with 'P'. Scale represents 100 µm.

Chapter 4:

Role of the RNA-binding protein Imp in *Drosophila* haemocyte and border cell migration

4.1 Effect of different fluorescently-labelled markers in haemocyte migration velocity

Upon imaging the distribution of Imp in haemocytes *in vivo*, we observed that their speed appeared significantly reduced compared to haemocytes expressing only a haemocyte label, such as moesin-GFP. However, previous publications show that the average speed of haemocyte migration to wounds can vary, even between different strains of control embryos (Stramer *et al*. 2005; Stramer *et al*. 2010; Comber *et al*. 2013; Evans *et al*. 2013). To control for this, we used wound healing assays to compare the speed of migration of haemocytes expressing either cytoplasmic GFP, the actin-binding domain of Moesin fused to GFP (to label the actin cytoskeleton) or the microtubule-binding domain of Clip-170 fused to GFP (to label the microtubules) (**Figure 25A-C**). All three labels were expressed separately in haemocytes using two copies of the *srp*-Gal4 driver. Although the average speed of haemocyte migration to wounds varied significantly depending on the label expressed, the average speed was consistent between embryos expressing the same haemocyte label (**Figure 25D**).

While there was no significant difference between the migration speed of haemocytes expressing Clip170-GFP and cytoplasmic GFP (t-test, $p=0.079$), there was a significant different in speed between haemocytes expressing moesin-GFP and Clip170 (t-test, $p=0.0169$) and between moesin-GFP and cytoplasmic GFP expressing haemocytes (t-test, $p<0.001$) (**Figure 25D**). As it is not possible to track haemocyte speed without the use of a fluorescent label, it is not known which strain most closely resembles the migratory speed of haemocytes in wildtype (wt) flies that do not express a fluorescent label. These results need to be taken into account when comparing the behaviour of haemocytes with different genetic backgrounds (i.e. when expressing different fluorescent markers) and shows that, the effects of knockdown or overexpression of proteins in haemocytes should be analysed in haemocytes with the same genetic background.

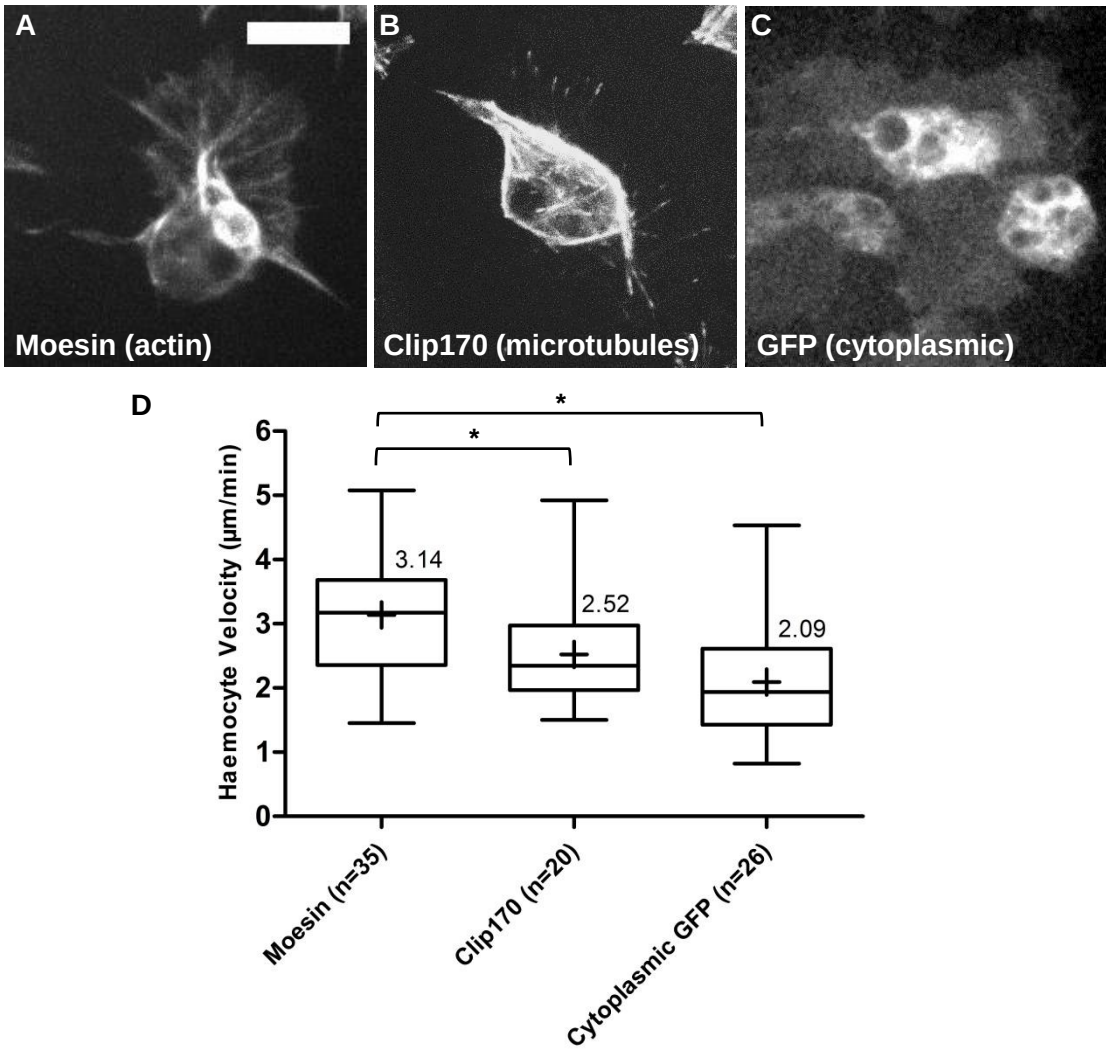

Figure 25. Effect of different fluorescently-labelled markers in haemocyte migration velocity

Three UAS-driven GFP-tagged proteins, commonly used within this project to label haemocytes during live confocal imaging, were expressed in haemocytes. Haemocytes expressing the markers were imaged by live confocal imaging of embryos at stage 15 of embryonic development. (**A**)The GFP-labelled actin-binding domain of moesin, (**B**) GFP-labelled microtubule-binding domain of Clip170 (**C**) and cytoplasmic GFP were expressed specifically in haemocytes using two copies of the haemocyte-specific *srp*-Gal4 driver. Scale represents 10 µm. (**D**) Epithelial wounds were generated in stage 15 embryo and time lapse imaging was carried out to calculate the speed of haemocyte migration to wounds, to identify any potential effects of the haemocyte markers on cell motility. Box shows median and interquartile range. Whiskers show the maximum range of migration speeds. Crosses and numeric values represent the mean. Asterisks and brackets represent statistically significant differences (t-test, $p<0.05$) in the speed of haemocyte velocity between different haemocyte markers.

4.2 Overexpression of Imp reduces the speed of haemocyte migration

When analysing the distribution of the C-terminally-tagged GFP and mCherry Imp constructs in haemocytes, we observed that haemocyte migration to wounds was impaired when compared to control haemocytes expressing a moesin-GFP label (**Figure 26A & B**). This effect was dosage sensitive as it was only evident when using two copies of the Gal4 driver.

In embryos containing a double copy of both the *srp*-Gal4 driver and Imp-mCherry, the speed of haemocyte migration to wounds was reduced to 1.94 µm/min (n=33) compared with 3.14 µm/min (n=35) in moesin-GFP labelled haemocytes. Similarly, when a double copy of the *srp*-Gal4 driver and a single copy of the Imp-mCherry were expressed, the speed of migration to wounds was reduced to 1.96 µm/min (n=24). However, when only a single copy of both the *srp*-Gal4 driver and Imp-mCherry were expressed, the speed was restored to control levels (3.04 µm/min, n=23) (**Figure 26C**).

We then compared the results described above using a Ct-tagged Imp with those obtained using a functional Nt-tagged Imp construct, previously shown to rescue the effects of Imp knockdown in *Drosophila* γ-neurons (Medioni *et al*. 2014). The velocity of haemocyte migration to a wound site in haemocytes expressing a double copy of *srp*-Gal4 and a single copy of either N-terminally or C-terminally labelled Imp were compared (**Figure 26D**). Velocity was significantly reduced in haemocytes expressing both Imp::GFP (1.96 µm/min, n=24) and GFP::Imp (1.87 µm/min, n=27) compared to the moesin control (3.14 µm/min, n=35) (t-test $p<0.05$). However, there was no significant difference in the velocity of haemocytes expressing either Imp::GFP or GFP::Imp ($p=0.691$) (**Figure 26D)**, suggesting that position of the GFP tag has no effect on the function of Imp, and therefore the reduction of haemocyte velocity. The directionality of haemocytes migrating to a wound site was also significantly reduced in haemocytes overexpressing Imp::GFP ($p=0.01$) (**Figure 26E**).

When an epithelial wound is generated, hydrogen peroxide is released from the wound site, which triggers haemocytes within approximately 40 µm to migrate directly to the wound (Moreira *et al*. 2010). As the size of the wound determines the total number of haemocytes recruited and the size of epithelial wounds can vary between embryos, to compare the number of haemocytes recruited to a specific wound in different genetic backgrounds the number of haemocytes were normalised to a wound size of 1000 μm^2. After one hour post-wounding, the total number of haemocytes recruited to a wound in embryos overexpressing Imp was reduced compared with the moesin control (t-test, $p=0.006$) (**Figure 26F**). This observation is consistent with the notion that migratory speed is reduced in Imp-overexpressing haemocytes; as the speed of haemocyte migration is reduced, the number of haemocytes arriving at the wound site over the course of an hour is also reduced in haemocytes overexpressing Imp.

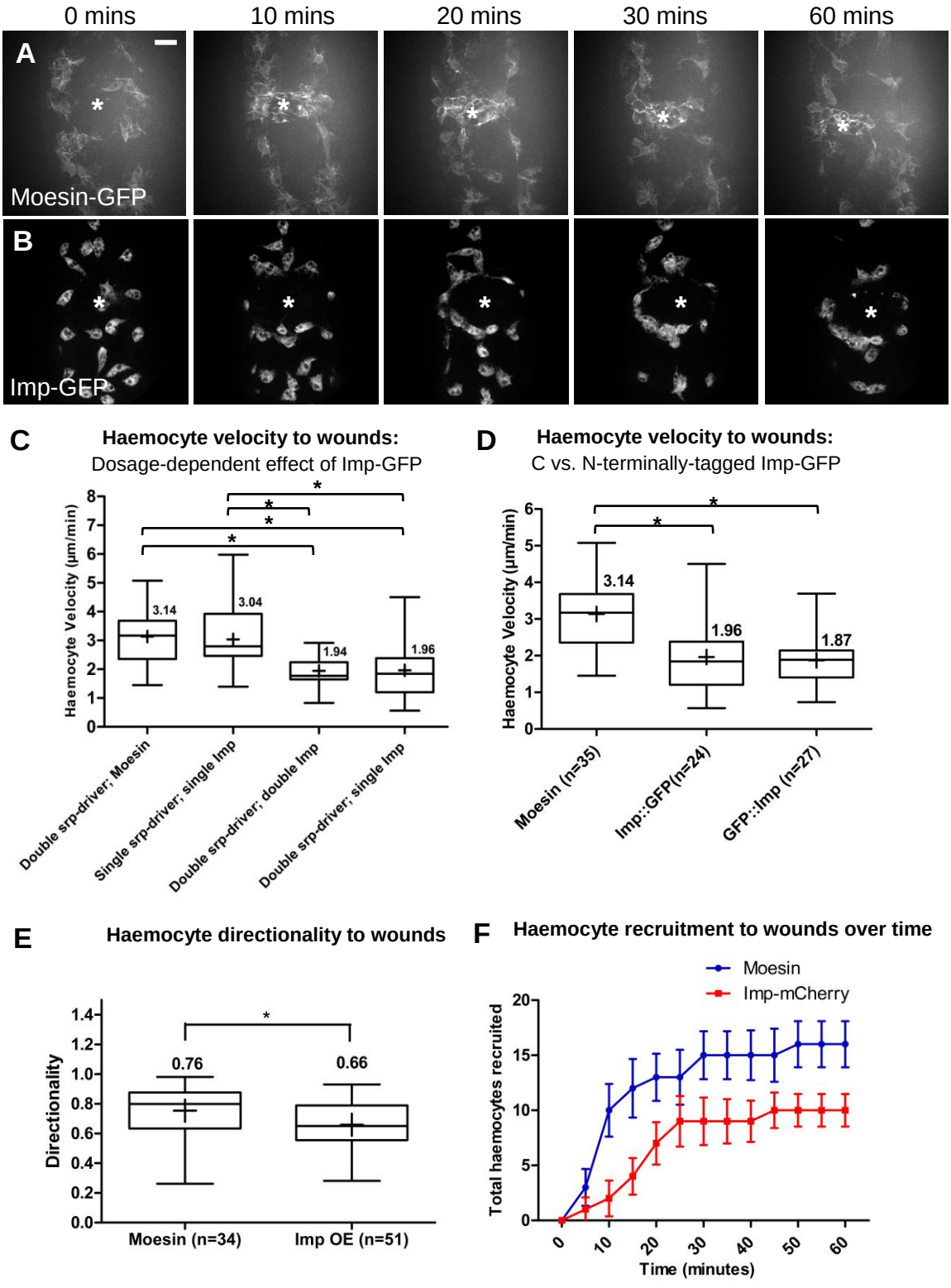

Figure 26. Imp overexpression compromises haemocyte migration and recruitment to wounds

Imp was overexpressed in haemocytes using two copies of both UAS-Imp-GFP and the haemocyte-specific *srp*-Gal4 driver. Epithelial wounds were generated in stage 15 embryos and haemocyte migration to the wound site tracked by live confocal microscopy to determine the effects of Imp overexpression on haemocyte motility. (**A,B**) Stills taken from live cell imaging of haemocyte migration to a wound site (asterisk). Haemocytes were labelled with two copies of either UAS-moesin-GFP (**A**) or UAS-Imp-GFP under the control of a double copy of the *srp*-Gal4 driver (**B**). Scale represents 20 µm. (**C**) Speed of haemocyte migration to a wound site was calculated by tracking individual

haemocytes with different combinations of either one or two copies of the *srp*-Gal4 driver and UAS-Imp-GFP construct to determine the effects of different dosages of Imp-GFP on haemocyte velocity to wounds. (**D**) Haemocyte velocity to wounds was reduced in haemocytes overexpressing either C-terminally- or N-terminally-tagged GFP-Imp, compared with UAS-moesin-GFP controls (t-tests, $p<0.001$), showing that the position of the GFP label does not affect the overexpression phenotype. (**E**) The directionality of haemocytes migrating to a wound is significantly reduced in haemocytes overexpressing UAS-Imp-GFP (t-test, $p=0.01$). The asterisks represent statistically significant different (t-tests, $p<0.001$) haemocyte velocities. Boxes show median and interquartile range. Whiskers show maximum range. Crosses and values represent the mean. (**F**) The total number of haemocytes recruited to a wound site over time was significantly reduced when haemocytes expressing UAS-Imp-mCherry were compared with a UAS-moesin-GFP control (t-test, $p=0.006$).

Apart from moving towards wounds, haemocytes display a characteristic developmental migration during embryogenesis (Tepass *et al*. 1994). At stages 12-13 of embryogenesis haemocytes migrate along the ventral midline to form a single line of haemocytes. From there, they migrate laterally to form a single line of haemocytes at stage 14. By embryonic stage 15, the haemocytes undergo random migration across the ventral surface within the constraint of the three line conformation (Wood & Jacinto 2007) (**Figure 27**). Haemocytes overexpressing Imp migrate normally across the ventral midline and undergo lateral migration to migrate randomly at embryonic stage 15. However, the speed of random migration is also significantly reduced in haemocytes expressing Imp either N-terminally or C-terminally tagged with GFP (**Figure 27A & B**) (t-test, $p<0.05$), compared with the moesin control (1.59, 1.45 and 2.46 µm/min respectively) (**Figure 27C**). There was no significant difference in the velocity of haemocytes expressing either C-terminally or N-terminally fused Imp ($p=0.135$).

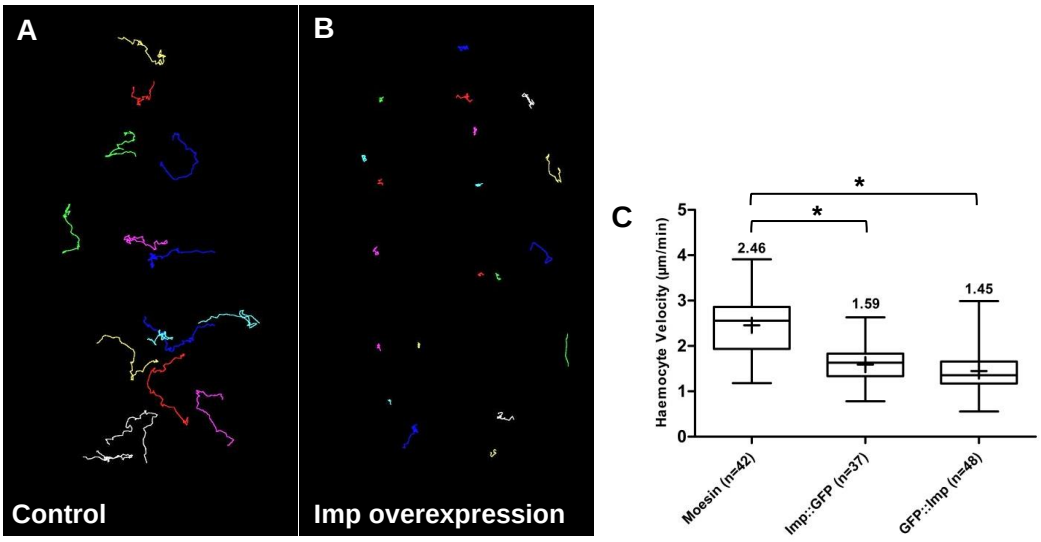

Figure 27. Random migration is reduced in haemocytes overexpressing Imp

Imp was overexpressed in haemocytes using two copies of UAS-Imp-GFP and the haemocyte-specific *srp*-Gal4 driver. Haemocyte velocity during random migration (developmental migration of haemocytes at the ventral midline of embryonic stage 15 embryos) was calculated by live confocal imaging of embryos over a 30 minute period. (**A**) Tracks of control haemocytes expressing two copies of the *srp*-Gal driver and a single copy of UAS-GFP-moesin over 30 minutes compared with (**B**) tracks of haemocytes expressing a double copy of both the *srp*-Gal4 driver and UAS-Imp-GFP and a single copy of UAS-GFP-moesin, reveals a reduction in haemocyte motility during random migration. (**C**) The speed of haemocyte motility during random migration was calculated by tracking individual haemocytes overexpressing either C-terminally-tagged or N-terminally-tagged Imp-GFP. Control haemocytes expressing UAS-GFP-moesin were tracked for comparison. Tracking revealed that the velocity of random haemocyte migration is significantly reduced in haemocytes overexpressing Imp, compared with the moesin control (t-test, $p<0.05$). Boxes represent median and interquartile range. Whiskers show maximum range. Crosses and values show mean. Asterisk and bracket represent a significantly statistic difference.

4.3 Overexpression of Imp causes loss of contact repulsion behaviour in haemocytes

Haemocytes undergoing random migration at embryonic stage 15 display contact repulsion, as individual haemocytes that come into contact rapidly repolarise and migrate away from each other (Stramer *et al*. 2010). As well as displaying slower migration during random migration, haemocytes overexpressing Imp spent longer in contact with each other when compared to embryos expressing the haemocyte markers moesin-GFP, Clip170-GFP and cytoplasmic GFP (**Figure 28A-D**). The majority of Imp-overexpressing haemocytes spent more than 15 minutes in contact with each other, whereas control haemocytes typically spend less than 6 minutes in contact (**Figure 28E**). Before repolarising and migrating away, haemocytes overexpressing Imp tended to stick together in clumps and migrated together very slowly. These haemocytes do not appear to re-polarise and migrate away from each other, although a few haemocytes are able to undergo normal contact repulsion.

Migrating haemocytes form a structure, referred to as a microtubule arm, which consists of a tight bundle of lamellar microtubules that protrude from the haemocyte cell body in the direction of migration (Stramer *et al*. 2010). Two haemocytes displaying contact inhibition will align their microtubules arms upon sensing that they will come into contact with each other if they continue on their current path of migration. Microtubule arm alignment lasts approximately three minutes before haemocytes re-polarize and migrate away from each other (Stramer *et al.* 2010). To determine if haemocytes overexpressing Imp were able to align their microtubule arms during contact repulsion, microtubule dynamics were examined in haemocytes expressing two copies of the *srp-Gal4* driver and Imp and a single copy of Clip170 fused with GFP to visualise microtubules. Haemocytes expressing a single copy of Clip170, driven by two copies of *srp-Gal4*, were used for comparison. While haemocytes were able to align their microtubules arms in embryos expressing only Clip170, this was not the case for the majority of haemocytes overexpressing Imp, which frequently remained in contact for over 15 minutes (**Figure 28F**).

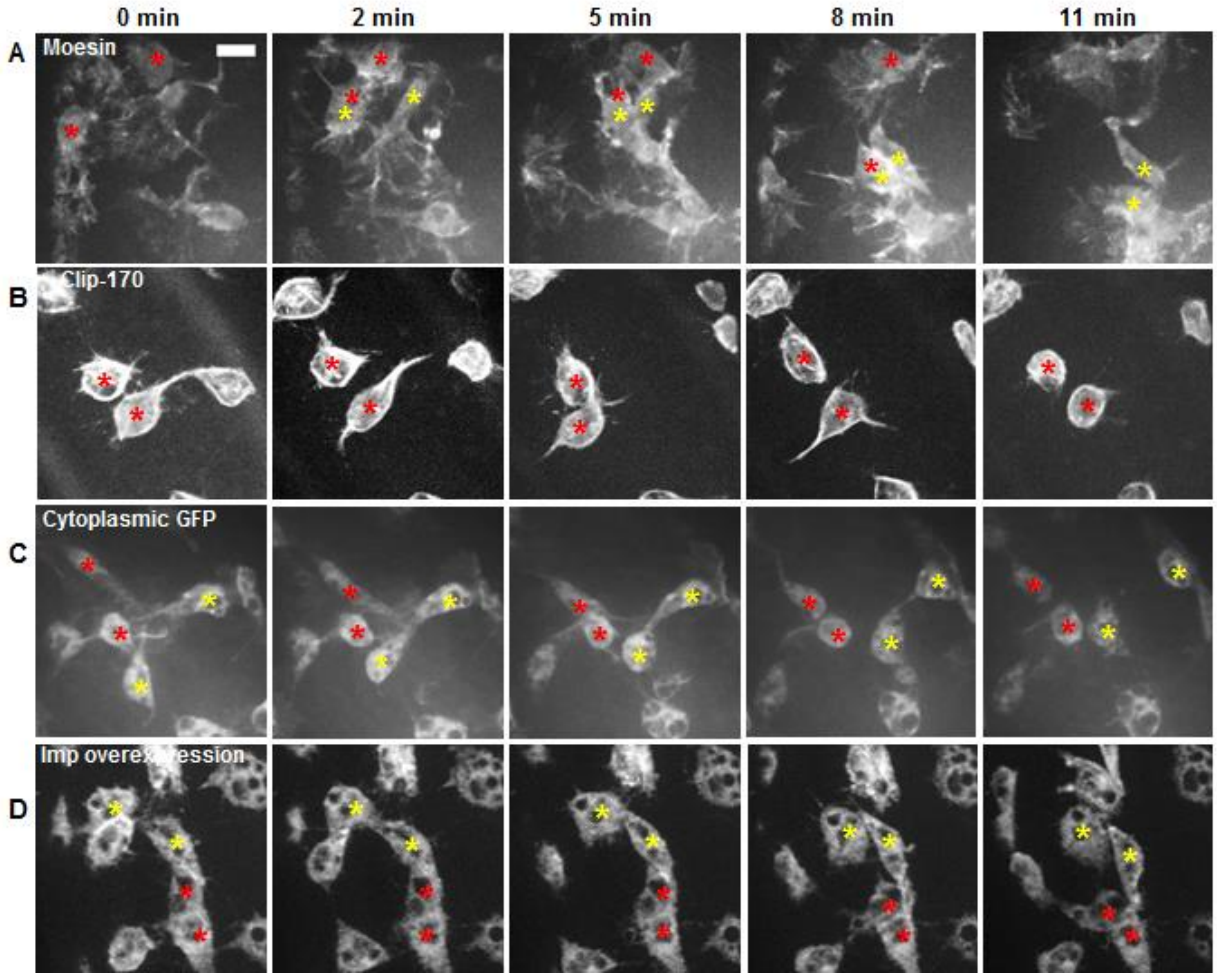
0 min
2 min
5 min
8 min
11 min
A
Moesin
B
Clip-170
C
Cytoplasmic GFP
D
Imp overexpression

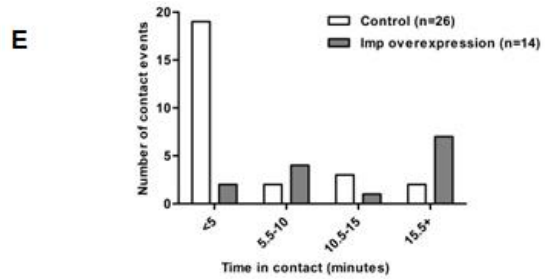
E
Control (n=26)
Imp overexpression (n=14)
Number of contact events
20
15
10
5
0
<5
5.5-10
10.5-15
15.5+
Time in contact (minutes)

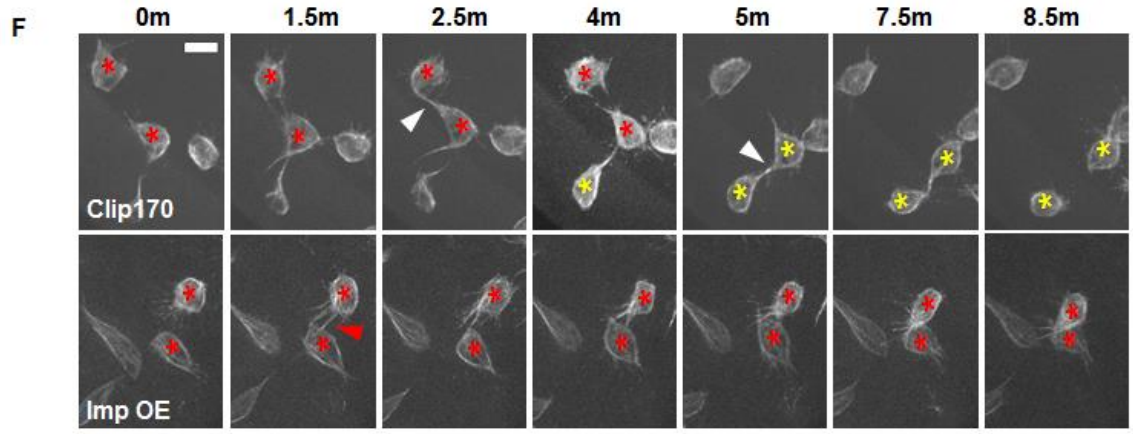
F
0m
1.5m
2.5m
4m
5m
7.5m
8.5m
Clip170
Imp OE

Figure 28. Live imaging of haemocytes overexpressing Imp *in vivo* reveals a loss of haemocyte contact inhibition behaviour

Imp was overexpressed in haemocytes by expressing two copies of both UAS-Imp-GFP and the haemocyte-specific *srp*-Gal4 driver and haemocyte contact inhibition behaviour, in which haemocytes that make contact re-polarize and migration away from eachother, was examined by measuring the total time spent in contact between two haemocytes. Control haemocytes expressing different UAS-driven markers (moesin-GFP, Clip170-GFP and cytoplasmic GFP) were used for comparison. (**A-D**) Stills taken from time-lapse imaging during random migration of embryonic stage 15 haemocytes expressing different markers. (**A**) Moesin-GFP, (**B**) Clip-170 and (**C**) cytoplasmic GFP expressing haemocytes contact and re-polarise in approximately 5 minutes (red and yellow asterisks show pairs of haemocytes undergoing a contact event). (**D**) Haemocytes overexpressing Imp-mCherry tend to stick together in clumps (red asterisk) or once contact has been made, remain in close proximity without touching (yellow asterisk). Scale represents 10 µm. (**E**) The time taken between the first contact and then separation of two haemocytes was calculated to determine the length of individual contact events. The number of contact events lasting 5 minutes or less is significantly higher in wildtype embryos, compared with those overexpressing Imp. The majority of contact events in embryos overexpressing Imp last over 15 minutes. (**F**) Time-lapse imaging of haemocytes expressing the microtubule marker Clip170-GFP alone or together with Imp using *srp*-Gal4. Haemocytes overexpressing Imp fail to align their microtubule arms upon microtubule contact with another haemocyte (red arrowhead), compared with haemocytes expressing Clip170 alone (white arrowheads). Asterisks mark contact events between two haemocytes over a time period of 8.5 minutes. Scale bars represent 10 µm.

4.4 Partial knockdown of Imp rescues the overexpression phenotype

To try rescuing the overexpression phenotype of Imp, an RNAi hairpin against Imp was co-expressed with the Imp-GFP transgene. Flies homozygous for both the *srp-Gal4*, UAS-GMA and UAS-Imp::GFP transgenes were crossed to flies homozygous for the *srp*Gal, UAS-GMA transgene and a UAS-Imp RNAi transgene so that the resulting embryos will contain a double copy of the *srp-Gal4* driver and a single copy of both the UAS- Imp::GFP and Imp RNAi transgenes. Embryos expressing a double copy of *srpGal*, UAS-GMA were used as a wildtype control, while embryos expressing two copies of *srp*Gal, UAS-GMA and a single copy of the UAS-Imp::GFP transgene were used as control for the Imp overexpression phenotype. To compare the expression level of Imp-GFP in control embryos and those co-expressing the RNAi hairpin against Imp, embryos were imaged at embryonic stage 15 after development at either 22°C or 29°C, using identical imaging conditions. The GFP signal in embryos expressing the RNAi hairpin was weak when compared with the control embryos at both 22°C and 29°C, even when subjected to a very high exposure level (Figure 29A & B). The GFP signal was weaker in embryos developed at 29°C, suggesting that the degree of knockdown is temperature-dependent, with the efficiency increasing at high temperatures, as expected for the GAL4/UAS system (**Figure 29B**).

The developmental migration of haemocytes was also examined in these embryos. In haemocytes overexpressing Imp::GFP alone haemocyte velocity was significantly reduced

compared with a moesin-GFP control (1.78 vs. 3.11 µm/min) as previously described and contact inhibition behaviour was severely inhibited (**Figure 28**). In haemocytes expressing both the RNAi hairpin and the Imp-GFP transgene contact inhibition behaviour was fully restored and the velocity of developmental haemocyte migration was partially rescued (2.5 µm/min), showing no significant difference compared with the controls (p=0.781, **Figure 29C**). This suggests that the RNAi reduces exogenous Imp-GFP levels to a level sufficient to rescue the Imp overexpression phenotype.

However, it was unclear if the rescue seen was a non-specific effect caused by adding in the additional UAS-Imp-RNAi transgene, effectively diluting the pool of GAL4 protein available to drive expression of UAS-Imp-GFP (see schematic representation - **Figure 29D**). To ensure that the rescue of the Imp overexpression phenotype is not due to dilution of GAL4 protein, the Imp-GFP transgene was co-expressed with an RNAi hairpin to targeting an unrelated RBP, Sexlethal (Sxl).

An immunoblot was carried out on an embryonic extract using an antibody against GFP to compare the levels of Imp-GFP in control embryos expressing a single copy of UAS-Imp-GFP and embryos co-expressing either UAS-Sxl-RNAi or UAS-Imp-RNAi alongside UAS-Imp-GFP. The blot showed that the level of exogenous Imp-GFP was only slightly reduced in embryos expressing Sxl-RNAi compared with controls, while those expressing RNAi against Imp showed a significant knockdown in the level of Imp-GFP (**Figure 29E**), demonstrating that the RNAi hairpin is effective against Imp and is a specific knockdown effect, rather than a non-specific dilution effect.

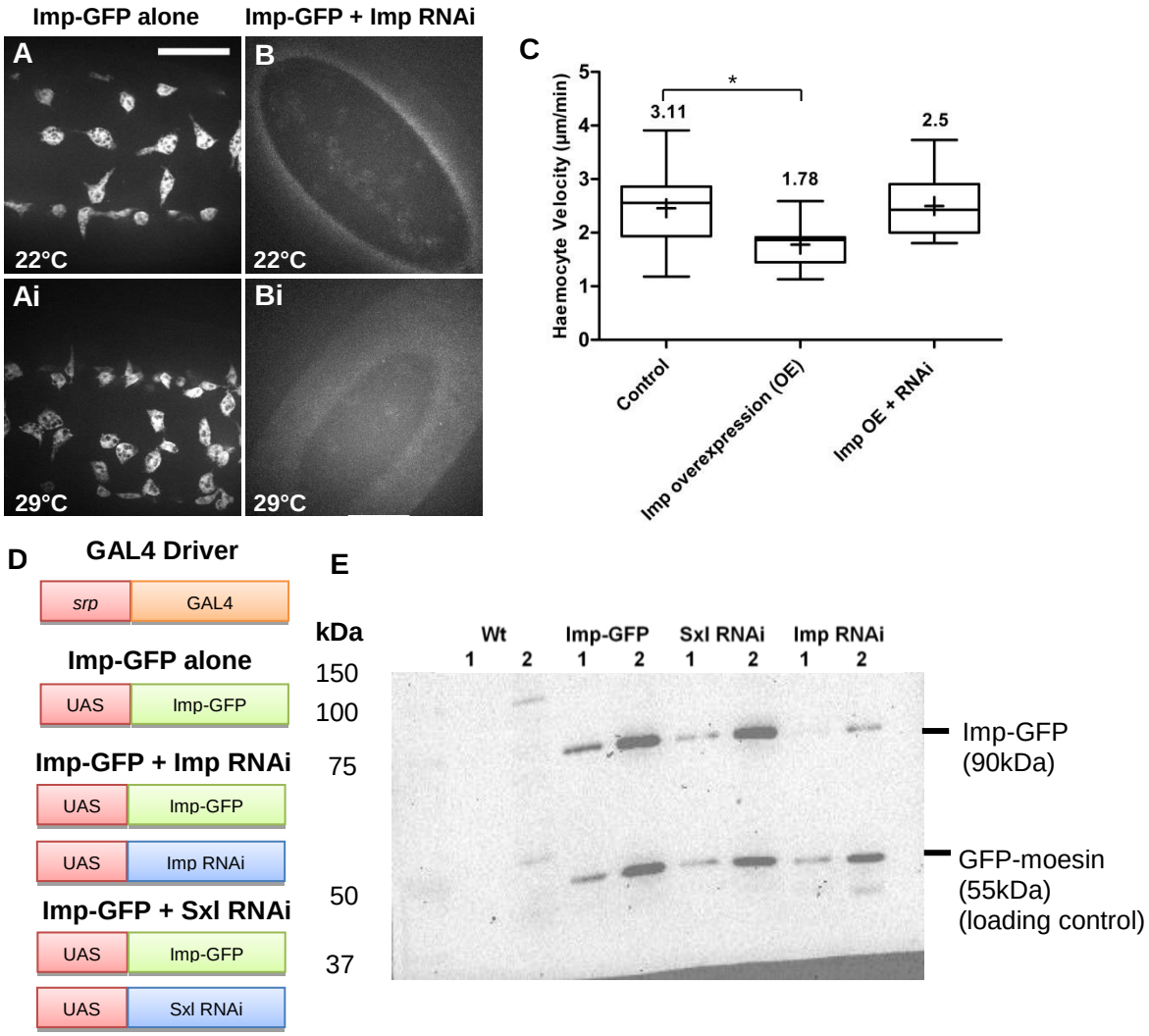

Figure 29. RNAi against Imp partially rescues the effects of Imp overexpression in live haemocytes

A UAS-driven RNAi hairpin against Imp was co-expressed with UAS-Imp-GFP, specifically in haemocytes, to determine if restoring Imp levels close to wildtype could rescue the Imp overexpression phenotype. (**A**,**B**) Images capture from (**A & Ai**) control embryos expressing Imp-GFP alone (*srp*-Gal4; UAS-Imp-GFP/+) and (**B & Bi)** embryos expressing Imp-GFP and Imp RNAi together (*srp*-Gal4; UAS-Imp-GFP/UAS-Imp-RNAi) at embryonic stage 15, which were developed at either 22°C or 29°C. Images were taken with the same exposure for direct comparison of the GFP signal. Scale represents 50 µm. (**C**) Expression of the RNAi against Imp, together with Imp-GFP, partially rescues the reduction of velocity seen in haemocytes overexpressing Imp-GFP alone (p=0.78). (**D**) Shows the number of UAS constructs present within each condition tested by Western blot. (**E**) A Western blot using anti-GFP shows that knockdown of Imp-GFP by RNAi is a specific effect, rather than a dilution effect of expressing an additional UAS transgene within haemocytes, as expression of RNAi against the unrelated RBP Sexlethal (Sxl) had little impact on Imp-GFP levels. Numeric values (1,2) represent two different concentrations of loaded protein.

4.5 Knockdown of Imp expression by RNAi has no effect on haemocyte behaviour

Our previous results indicate that overexpression of Imp impairs haemocyte behaviour. Thus, we decided to study the effect of reducing the levels of Imp in haemocyte motility. To this end, we used RNAi and expressed specifically in haemocytes a short-hairpin against Imp previously shown to rescue the Imp overexpression phenotype by reducing the overall levels of Imp (**Figure 29**). A fly stock containing two copies of both the *srp*-Gal4 driver and UAS-Imp RNAi were placed at 29°C and the resulting embryos used to image haemocytes, in parallel to controls containing two of the *srp*-Gal4 driver.

Haemocytes expressing Imp RNAi underwent developmental migration and were correctly positioned along the ventral midline of embryonic stage 15 embryos (**Figure 30D**). During random migration, the haemocytes migrated at speeds comparable to wildtype levels (t-test, p=0.093) (**Figure 30E**). These haemocytes also display normal contact repulsion behaviour when compared with wildtype haemocytes, with Imp RNAi haemocytes spending an average of 6 minutes in contact compared with 6.65 minutes for control haemocytes (**Figure 30F**). The speed of haemocyte migration to epithelial wounds was tracked in haemocytes expressing Imp RNAi, which showed that the RNAi treatment had no effect on the speed of haemocyte migration to wounds when compared with controls (t-test, p=0.798) (**Figure 30A-C**).

We also examined the motility of pupal macrophages expressing RNAi against Imp. In this case, the RNAi hairpin is expressed throughout embryonic and larval development and it has more time to accumulate and trigger *imp* mRNA degradation, compared with the short temporal window achieved during embryogenesis. We observed a high degree of variability in the speed of haemocyte migration among individual pupae, even in the controls (data not shown). Although we did not observe any dramatic effect in motility of pupal haemocytes expressing the Imp-RNAi construct (i.e. they migrated and were distributed normally, data not shown), the variability observed from pupae to pupae prevented us to conclude with confidence about any subtle changes in cell motility.

It is possible that, while Imp is knocked down efficiently, we fail to observe any haemocyte phenotype due to redundancy of Imp with other RBPs within functional RNP complexes. In conclusion, these results suggest that either Imp plays no role in haemocyte motility, that the RNAi against Imp is inefficient in reducing Imp levels below those required to impact on cell motility (i.e. residual Imp is able to carry out its normal function) or that other RBPs compensate for the loss of Imp, allowing RNP complexes to function as normal.

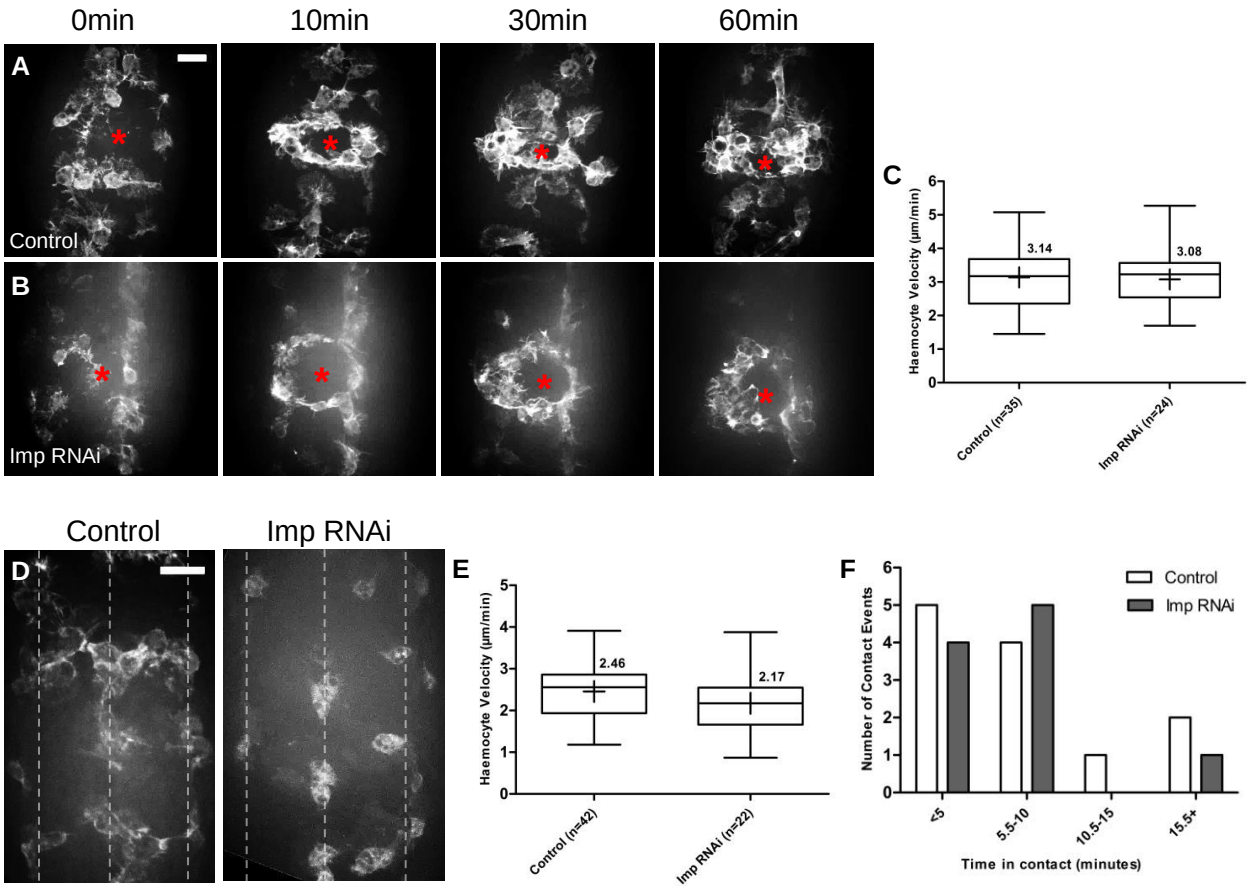

Figure 30. Reduction of Imp levels in haemocytes by RNAi results in no obvious phenotype

Two copies of an RNAi hairpin against Imp were expressed in haemocytes using two copies of the haemocyte-specific *srp*-Gal4 driver to determine the effects of Imp depletion on haemocyte motility and behaviour in live embryos at stage 15 of embryonic development. (**A**,**B**) Stills of time-lapse imaging carried out after generating epithelial wounds (marked with asterisk) in (**A**) control embryos (*srp-Gal4*, moesin-GFP), or (**B**) embryos expressing a copy of the short RNAi hairpin targeting Imp (*srp-Gal4*, UAS-moesin-GFP; Imp RNAi). (**C**) Speed of haemocyte migration to wounds of embryos shown in A & B. (**D**) The distribution of haemocytes at the ventral midline of embryonic stage 15 embryos appeared normal in embryos expressing Imp RNAi as three parallel lines (dashed lines) on haemocytes were observed in all embryos examined. (**E**) Haemocyte velocity during random migration was comparable to wildtype levels in Imp RNAi embryos at stage 15 of embryonic development (t-test, p=0.093). (**F**) The average time spent in contact between haemocytes during random migration was comparable in embryos expressing Imp RNAi (6 minutes average) to wildtype embryos (6.65 minutes average), suggesting no defects in contact inhibition behaviour as a result of Imp knockdown. Scale bars represent 20 µm.

4.6 Characterising the role of Imp in migratory border cells

After investigating the role of Imp in haemocytes, and to determine if the effects observed here are specific to this cell type, we decided to study the role of Imp in a different migratory cell type. *Drosophila* border cells are a cluster of 6-10 somatic cells that migrate collectively from the anterior of the female egg chamber, to a more posterior region termed the oocyte border, during oogenesis (Spradling 1993) (**Figure 5**). As border cells migrate collectively, this system allowed us to compare two different types of migration: collective migration (border cells) and individual cell migration (haemocytes). Furthermore, as the lamellipodial protrusions of border cells are retained upon fixation, and the progression of their migration through the egg chamber can be scored in fixed egg chambers, live imaging is not required to track border cell migration. Border cells are, therefore, an ideal complementary system to characterize the role of Imp in cell motility *in vivo* (Montell *et al*. 1992).

We first examined the localization of Imp in border cells using two different approaches. The first approach allowed us to examine the localization of endogenous Imp by using an exon-trap line inserted in the *imp* locus (Morin *et al*. 2001; Quiñones-Coello *et al*. 2007). The ovaries of females expressing endogenous Imp-GFP were dissected and fixed to examine the localization of Imp in border cells following GFP emission. The border cell cluster could be distinguished from the surrounding tissue, which was confirmed by DAPI counterstaining, to reveal the location of the border cell nuclei (**Figure 31A** – red arrowhead).

First, this analysis confirmed that Imp is expressed in border cells, as well as their surrounding tissue (e.g. nurse cells and oocyte) (**Figure 31A**). Imp appeared to be excluded from the border cell nuclei and seemed to be distributed throughout the cell cytoplasm without any enrichment at particular locations. However, Imp showed a speckled pattern of small granules, which may represent RNP complexes (**Figure 31B**). Interestingly, Imp decorates the cytoplasmic extensions projected by the leading cells of the cluster (**Figure 31C** – blue arrowhead), which have been shown to be enriched in actin protrusions (Prasad & Montell 2007). While Imp was present throughout the whole egg chamber, it appeared to be excluded from the region surrounding the entire border cell cluster, making the cluster easy to distinguish from the surrounding tissue (**Figure 31B & C** – white arrowheads).

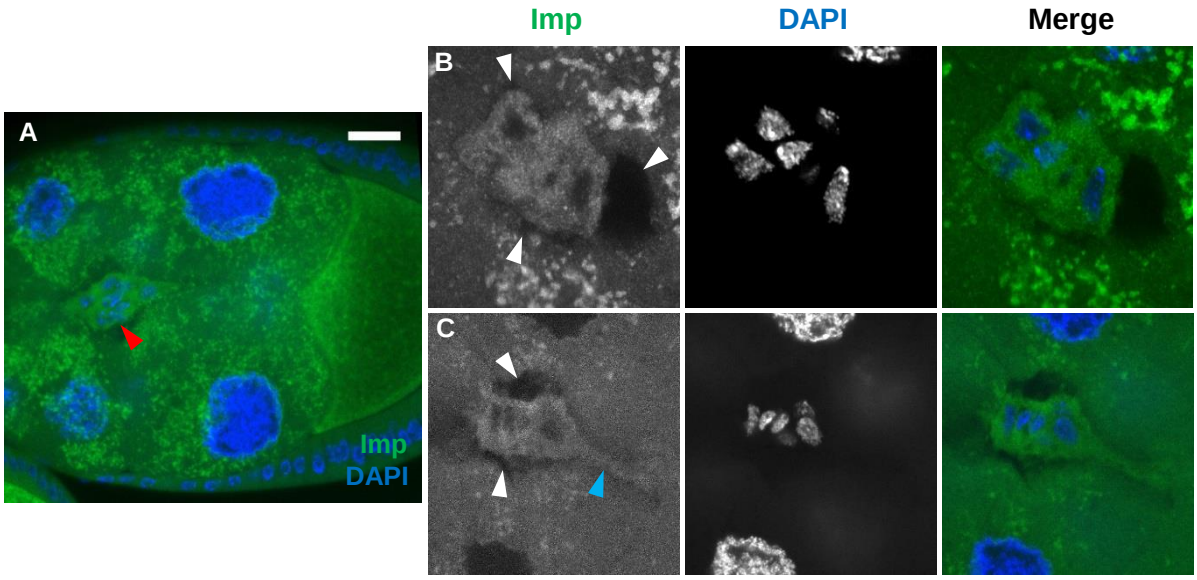

Figure 31. Localization of endogenous Imp in migratory *Drosophila* border cells

Ovaries were dissected from Imp exon-trap line females (referred to as G80 - Quiñones-Coello *et al.* 2007), in which endogenous Imp is labelled with GFP, to examine its localization within migratory border cells. After fixing, ovaries were counter-stained with DAPI (blue) and Imp-GFP (green) was imaged by detecting GFP emission. Individual oocytes were examined by confocal microscopy. (**A**) The border cell cluster can be identified from the surrounding tissue (red arrowhead (**B**, **C**) Imp does not show any specific enrichment within border cells, but is present throughout the cell cytoplasm. Imp appears to be present within the actin protrusions extended by the leading border cell(s) (blue arrowhead). Imp is not present in regions at the periphery of the border cell cluster (white arrowheads). Scale bar represents 50 μm.

Next, we compared the distribution of endogenous Imp (see above) with that of an Imp-mCherry fusion protein specifically expressed in border cells using the GAL4/UAS system. CD8-GFP, a cell surface marker, was used to label border cells. As for the exon-trap line, Imp was mainly present in the cell cytoplasm. However, there were some patches of Imp enrichment within the cytoplasm (**Figure 32Bi & Ci** – red arrowheads). Imp was also present within the cytoplasmic extensions of border cells, at both the rear and front of the border cell cluster (**Figure 32Bi & Ci** – white arrowheads). These regions have been described to contain actin structures important for cell motility (Prasad & Montell 2007).

Overall, our analysis shows that in both haemocytes and border cells, Imp is distributed throughout the main body of the cells: e.g. the region containing the cellular organelles (**Figures 19, 31 & 32**). In these two distinct migratory cell types, Imp is not clearly enriched at the leading edge, or in any other obvious cellular structure within the cytoplasm. In contrast to haemocytes, Imp decorates cytoplasmic actin-rich extensions at the periphery of those cells located at the rear and leading edges of the border cell cluster.

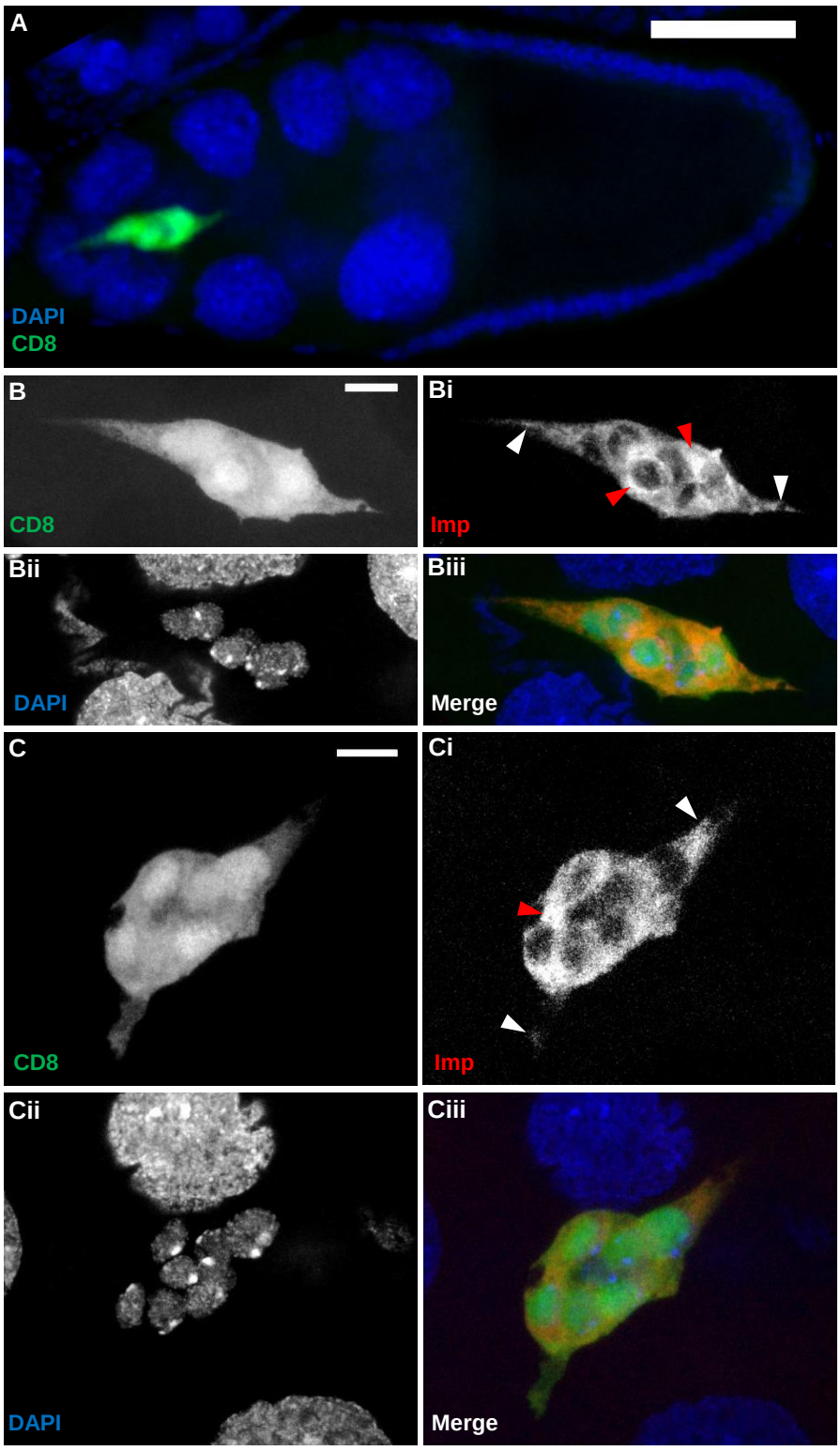

Figure 32. Localization of UAS-driven Imp-mCherry in migratory *Drosophila* border cells

The localization of Imp in border cells was examined by expressing UAS-Imp-mCherry (red) using the border cell specific *slbo*-Gal4 driver. UAS-CD8-GFP was used as a border cell label (green). Border cell nuclei were counterstained with DAPI (blue). (**A**) The position of migratory border cells can be seen in the context of the entire egg chamber, counterstained with DAPI to visualize nuclei (blue). Scale bar represents 50 μm. (**B, C**) Border cells were labelled with CD8 (green). (**Bi, Ci**) Imaging of UAS-Imp-mCherry reveals that patches of Imp enrichment are present in the cytoplasm (red arrowheads). Imp is present throughout cytoplasmic protrusions, at both the rear and front of the border cell cluster (white arrowheads). (**Bii, Cii**) DAPI counterstaining shows the nuclei of individual border cells (blue). Scale bars represent 10 μm.

4.7 Knockdown of Imp expression in border cells

To determine if Imp plays a role in border cell migration, we attempted to deplete Imp levels by expressing RNAi against Imp specifically in border cells. To ensure RNAi is effective in border cells, we also tested RNAi lines to knockdown expression of proteins known to prevent border cell motility, including Rac1 and Hrp48 (Murphy & Montell 1996; Mathieu *et al*. 2007), as well as PTB (*Besse &* López de Quinto - unpublished*).* All RNAi lines were crossed to flies expressing the *slbo*-Gal4 driver, as well as Lifeact-GFP driven from a constitutive *slbo* promoter to label the actin cytoskeleton of border cells. This ensured that our border cell marker did not deplete the pool of GAL4 protein available to drive expression of the RNAi hairpin.

We tested three different RNAi lines against Imp, including two short RNAi hairpins and a long RNAi hairpin (see Appendix 5). Similarly to haemocytes, we failed to observe any significant effect on border cell migration upon RNAi treatment against Imp (data not shown). However, we also failed to see border cell phenotypes when expressing RNAi hairpins against Rac1, PTB and Hrp48, all of which are known to be required for border cell migration. This suggests that our RNAi conditions are not effective enough to reveal border cell phenotypes.

To efficiently knockout expression of Imp in border cells, we next generated *imp* mutant border cells in an otherwise phenotypically wildtype egg chamber by using the mosaic analysis with a repressible cell marker (MARCM) technique (Lee & Luo 2001) and an *imp* null allele (Medioni *et al.* 2014). Briefly, MARCM uses FLP/FRT-based recombination to generate homozygous *imp* cells, which are GFP-labelled (see **Figure 33A** for a schematic representative of the fly crosses carried out to generate *imp* mutant border cells). GFP-positive border cells containing the FRT recombination site in an otherwise wildtype chromosome were used as controls (**Figure 33B**).

Although we did not observe any whole *imp* mutant border cell cluster, we analysed a large number of mixed clusters, in which *imp* was knocked out in up to three cells within the border cell cluster. These mixed border cell clusters were able to collectively migrate, even when mutant cells were leading the cluster, and we did not observe any defects compared with our controls (**Figure 33C**). Cell-to-cell contacts were maintained between both two mutant cells, as well as between wildtype and mutant cells, suggesting that loss of Imp does not affect the maintenance of cell-cell adhesions (**Figure 33C**). However, as we failed to achieve a full *imp* mutant border cell cluster, and due to the collective nature of border cell migration, we cannot exclude the possibility that wildtype cells within the cluster can compensate for any

defects present in mutant cells. Wildtype cells could indeed transport imp mutant cells, as the contacts between all cells, both wildtype and imp mutants, were maintained.

A **Mosaic analysis with a repressible cell marker (MARCM)**

F0 Control ♂ *w-FRT19A, hs-FLP, tub-GAL80* / *Y* ; *slbo-GAL4, UAS-CD8-GFP* / *CyO* x ♀ *FRT19A* / *FRT19A*

imp mutant ♂ *w-FRT19A, hs-FLP, tub-GAL80* / *Y* ; *slbo-GAL4, UAS-CD8-GFP* / *CyO* x ♀ *FRT19A, imp^{8}* / *FM6*

F1 ♀ *w-FRT19A, hs-FLP, tub-GAL80* / *FRT19A wt/imp^{8}* ; *slbo-GAL4, UAS-CD8-GFP* / + → **HEATSHOCK** ↓ DISSECT OVARIES

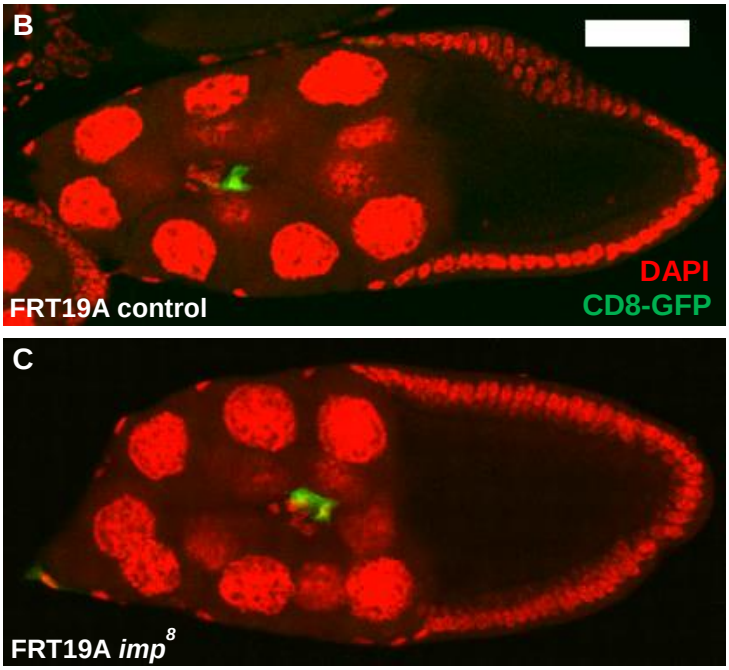

Figure 33. *imp* mutant border cells show no migratory defects with the *Drosophila* oocyte

imp mutant border cells were generated and analysed using a Mosaic analysis with a repressible cell marker (MARCM) approach to determine the effects of Imp knockout on border cell migration. (**A**) Outline of the MARCM protocol, including fly cross schemes, to generate mutant border cells. Crosses between *FRT19A* control or *FRT19A Imp^{8}* mutant virgin female flies for MARCM analysis. Ovaries were dissected from females after heat-shocking and were fixed and counterstained with DAPI to reveal nuclei (red). Imp mutant border cells are CD8-GFP positive and were imaged by detecting GFP emission through confocal microscopy (green). (**B**) Control GFP-positive border cells containing only the FRT19A recombination site were generated by MARCM. (**C**) GFP-positive *imp* mutant border cells were generated by MARCM using the FRT19A *imp^{8}* fly line. The progression of the border cell cluster within the egg chamber can be seen. DAPI was used to visualize unlabelled border cells, showing that GFP-positive cells in both the control and *imp* border cell clusters are located at the front of the cluster. Scale bar represents 50 µm.

Chapter 5:

Identification and characterization of Imp mRNA targets

5.1 Imp binds the 3'UTR of β-*integrin* mRNA

Our previous findings show that the overexpression phenotype of Imp phenocopies that of *myospheroid* (β-integrin) depletion in haemocytes (Comber *et al.* 2013). We therefore tested if *β-integrin* mRNA could be a target of Imp. In *Drosophila*, a short motif of primary sequence, consisting of five nucleotides (UUUAU/C) and termed the Imp binding element (IBE), has been shown to be required for the binding of Imp to the 3'UTR of *oskar* mRNA, which contains 13 IBEs within its 3'UTR (Munro *et al*. 2006).

Interestingly, we observed that *β-integrin* contains 13 IBEs, which were mainly concentrated in the 3'UTR region. To determine if Imp binds the 3'UTR of *β-integrin* we carried out an RNA affinity pulldown. Biotinylated probes were generated for the 3'UTR of *β-integrin*, as well as the 3'UTRs of *actin42A* (β-actin), *oskar* and *chickadee* (Profilin), all of which have been shown to bind Imp in different cell types and tissues (Medioni *et al*. 2014; Munro *et al*. 2006; Munro *et al*. 2005 – unpublished conference abstract). The coding sequence of *Y14* was used as negative control (Besse *et al*. 2009). Biotinylated RNAs were then bound to streptavidin particles conjugated to magnetic beads. An embryonic extract was generated to create a pool of soluble proteins, in which the RNAs were incubated. Biotinylated RNAs and any bound protein complexes were precipitated using a magnet and washed to remove unbound proteins. The binding of proteins to these RNAs were then analysed by Western blotting (**Figure 34A**).

We found that the strongest binding of Imp was to the 3'UTR of *profilin*. As expected, Imp also bound to the 3'UTRs of *act42A* and *oskar* (**Figure 34A**). Interestingly, this assay confirmed an interaction between Imp and the 3'UTR of *β-integrin*, which was comparable to that observed for the other known targets of Imp tested (**Figure 34A**).

For comparison, we also tested the interaction of these 3'UTR regions with PTB, another RBP known to bind and regulate *oskar* mRNA (Besse *et al*. 2009). PTB was observed bound to the 3'UTRs of *oskar*, *actin42A* and *β-integrin* with high affinity but, in contrast to Imp, showed a low affinity for the *profilin* 3'UTR (**Figure 34A**). This demonstrated that RBPs have different affinities for the RNA probes, and that a single RNA can interact with more than one RNA-binding protein, most likely in RNP complexes.

We next decided to map the binding of Imp to the entire *β-integrin* mRNA. To this end, we divided *β-integrin* mRNA into three regions; 5'UTR, coding sequence (CDS) and 3'UTR (see materials & methods section 2.3.2). Biotinylated probes were generated for the three regions and tested as previously described. We found that although Imp binds the 5'UTR and CDS, it

binds with much higher affinity to the 3'UTR (**Figure 34B**). Similarly, PTB also binds preferably to the *β-integrin* 3'UTR, compared to the 5'UTR and CDS.

Our analysis shows that the 3'UTR of *β-integrin* interacts with several RBPs, including Imp.

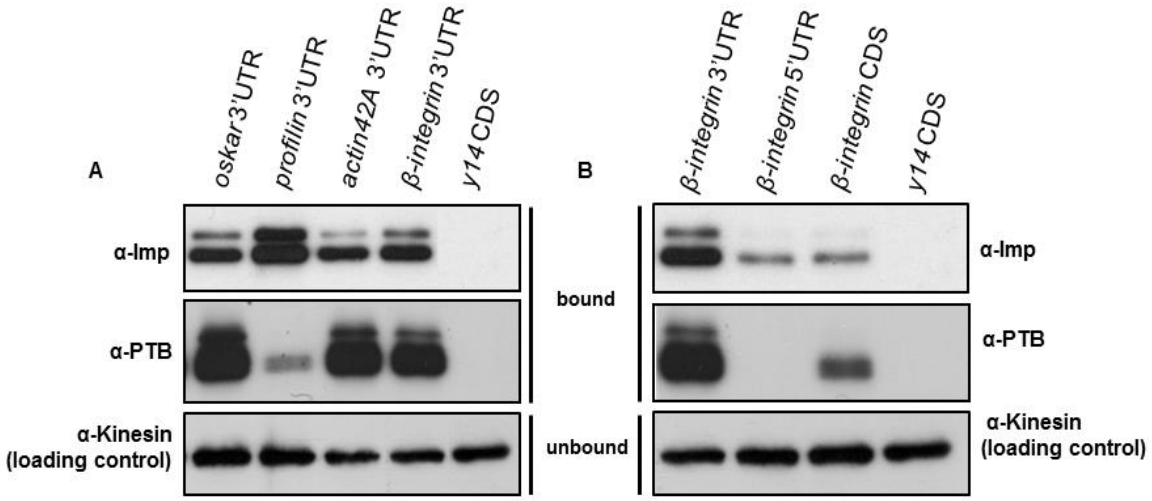

Figure 34. Imp binds with high affinity to the 3'UTR of *β-integrin* mRNA
RNA affinity pulldown assays were carried out using biotinylated RNAs to test and map the binding of Imp to *β-integrin* mRNA. For comparison, binding of the RNA-binding protein PTB was analysed. A *Drosophila* embryonic extract containing all soluble embryonic proteins was generated, in which biotinylated RNAs were incubated and subsequently precipitated. Western blots were carried out to determine binding of Imp and PTB to the different biotinylated RNAs tested (**A**) Imp binds with high affinity to the 3'UTR of *β-integrin*. The 3'UTRs of *oskar*, *profilin* and *actin42A* were used as positive controls, as they are known targets of Imp, while the coding region of *y14* as used as an unrelated RNA control. (**B**) Biotinylated RNAs that covered the entire *β-integrin* mRNA shows that Imp binds with higher affinity to the 3'UTR, compared with the 5'UTR and coding sequence (CDS). The name of the antibodies used for Western blotting are indicated on the sides.

5.2 Three predicted Imp binding elements (IBE) are required for Imp binding to the 3'UTR of *β-actin*

We next wanted to determine if the 13 IBEs required for Imp binding to the *oskar* 3'UTR (Munro *et al*. 2006) also mediate the binding of Imp to other transcripts, including *β-integrin*. Analysis of the *β-integrin* 3'UTR revealed the presence of 13 IBEs. Two main challenges were associated with the mutation of all 13 predicted IBEs: time constraints and the difficulty of introducing so many changes in the 3'UTR region without affecting other RNA-protein interactions. We therefore opted to mutate the three predicted IBEs contained within the 3'UTR of *actin42A*. *act42A* mRNA was an ideal candidate as we previously showed that Imp binds its 3'UTR with high affinity (**Figure 34A**) and, unlike its mammalian homologue IMP1,

the regions of the 3'UTR required for binding of Imp to *β-actin* (*actin42A*) mRNA have not been shown (Ross *et al*. 1997; Chao *et al*. 2010).

The positions of the three predicted IBEs within the *act42A* 3'UTR are shown in **Figure 35A**. Using site-directed mutagenesis we mutated all three IBEs, changing them from UUUAY to either GAGCTC or GGGCG, in the context of the entire 3'UTR. Biotinylated RNAs of the wildtype *act42A* 3'UTR and its IBE mutated versions were used in RNA-affinity pulldown assays against the *act42A* 3'UTR to test the binding capacity of Imp (**Figure 35A**). To determine if mutation of a single IBE or two IBEs has the same impact as mutation of all three together, we generated a subset of biotinylated RNAs which included the first IBE (ΔIBE1) mutated alone, the second and third IBEs (ΔIBE2+3) mutated alone, or all three mutated together (ΔIBE1+2+3).

The RNA pulldown revealed that mutation of either IBE1 alone, or both IBE2 and IBE3 had no obvious effect on Imp binding (**Figure 35B**). However, mutation of all three IBEs appeared to have a significant impact on the binding of Imp, with a clear reduction in the quantity of Imp bound to this transcript, compared to wildtype (**Figure 35B)**. These results suggest that all three IBEs mediate interactions with Imp (**Figure 35B**).

To determine if the IBE mutations could affect the binding of other RBPs to the *act42A* 3'UTR, we also tested the interaction of PTB with the wildtype and IBE mutated 3'UTR. While binding of PTB was slightly reduced to the *act42A* 3'UTR containing mutations in all three IBEs, this reduction did not appear as dramatic as that of Imp (**Figure 35B**), suggesting that mutation of these sites do not significantly perturb PTB binding.

In conclusion, the IBE changes introduced in the *act42* 3'UTR appear to affect the Imp interaction with more severity than the PTB interaction, suggesting that mutation of these three sites does not affect the secondary structure of this region so severely that all RBP interactions are impaired. However, secondary structure prediction analysis, and ultimately experimental structure analysis, is required to confirm this.

5.3 Analysis of the localization of Imp and β-integrin proteins in *Drosophila* haemocytes and border cells

After showing that Imp binds *β-integrin* mRNA (**Figure 34**), we examined the distribution of Imp and β-integrin proteins to see if they co-localize in different cell types. These proteins could not be co-localized in haemocytes *in vivo* as tagging β-integrin with a flurophore prevents its insertion into the cellular membrane, rendering it non-functional and unable to localize normally (personal communication – Comber & Wood, University of Bristol). We

therefore fixed and stained cultured larval haemocytes *ex vivo,* using antibodies against Imp and β-integrin, as well as moesin-GFP to label the actin cytoskeleton.

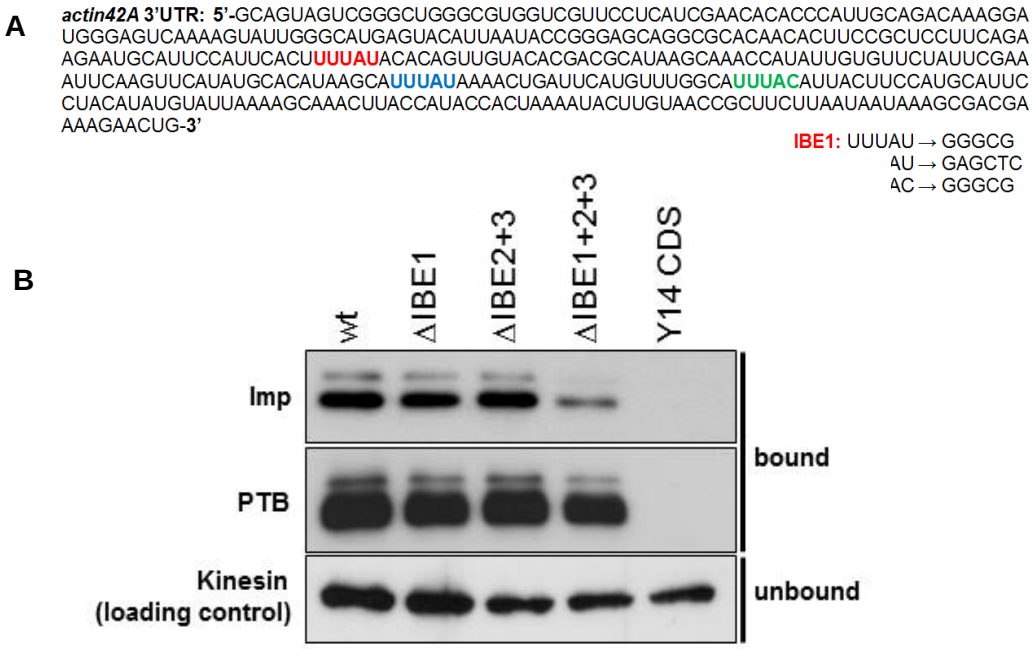

Figure 35. All three predicted Imp binding elements (IBEs) mediate Imp binding to the 3'UTR of *actin42A* (*β-actin*) mRNA

RNA affinity pulldown assays were carried out using biotinylated RNAs to test and map the binding of Imp to the 3'UTR of *actin42A* (*β-actin*) mRNA, in which different combinations of three predicted Imp binding elements (UUUAU/C) were mutated. For comparison, binding of the RNA-binding protein PTB was analysed. A *Drosophila* embryonic extract containing all soluble embryonic proteins was generated, in which biotinylated RNAs were incubated and subsequently precipitated. Western blots were carried out to determine Imp and PTB binding to the biotinylated RNAs tested. (**A**) *actin42A* 3'UTR sequence showing the location of the three predicted IBEs (UUUAU/C) and the changes introduced to their primary sequences. (**B**) Western blot analysis of RNA affinity pulldown assays using the biotinylated RNAs indicated above the immunoblots. Antibodies are shown on the left. The coding region of *y14* was used as an unrelated RNA control. Detection of Kinesin-heavy chain was used as a loading control.

As previously described for Imp (**Figure 14**), the localization of β-integrin also varies depending on cellular morphology. In highly spread cells with widespread protrusions, β-integrin shows a diffuse distribution throughout the entire cell, including the lamellipodia. Imp also appears diffusely distributed throughout the cell, but is present at much lower levels within the protrusions. In contrast, rounded cells with much smaller protrusions showed a punctate localization of both β-integrin and Imp, some of which co-localize within the cell body. However, fewer β-integrin granules are present, which are more defined and larger than the majority of smaller Imp-containing granules. Interestingly, haemocytes that are highly rounded and fail to form cellular protrusions contain a few, large granules of Imp, while β-integrin is spread diffusely throughout the cell with enrichments at the periphery, without

any clear granular enrichment. These results show that, as previously highlighted, the localization of Imp and β-integrin changes depending on cellular morphology. In this context, Imp and β-integrin partially co-localize to some cellular granules, depending on the morphology of the cell. However, they do not co-localize in the majority of haemocytes examined.

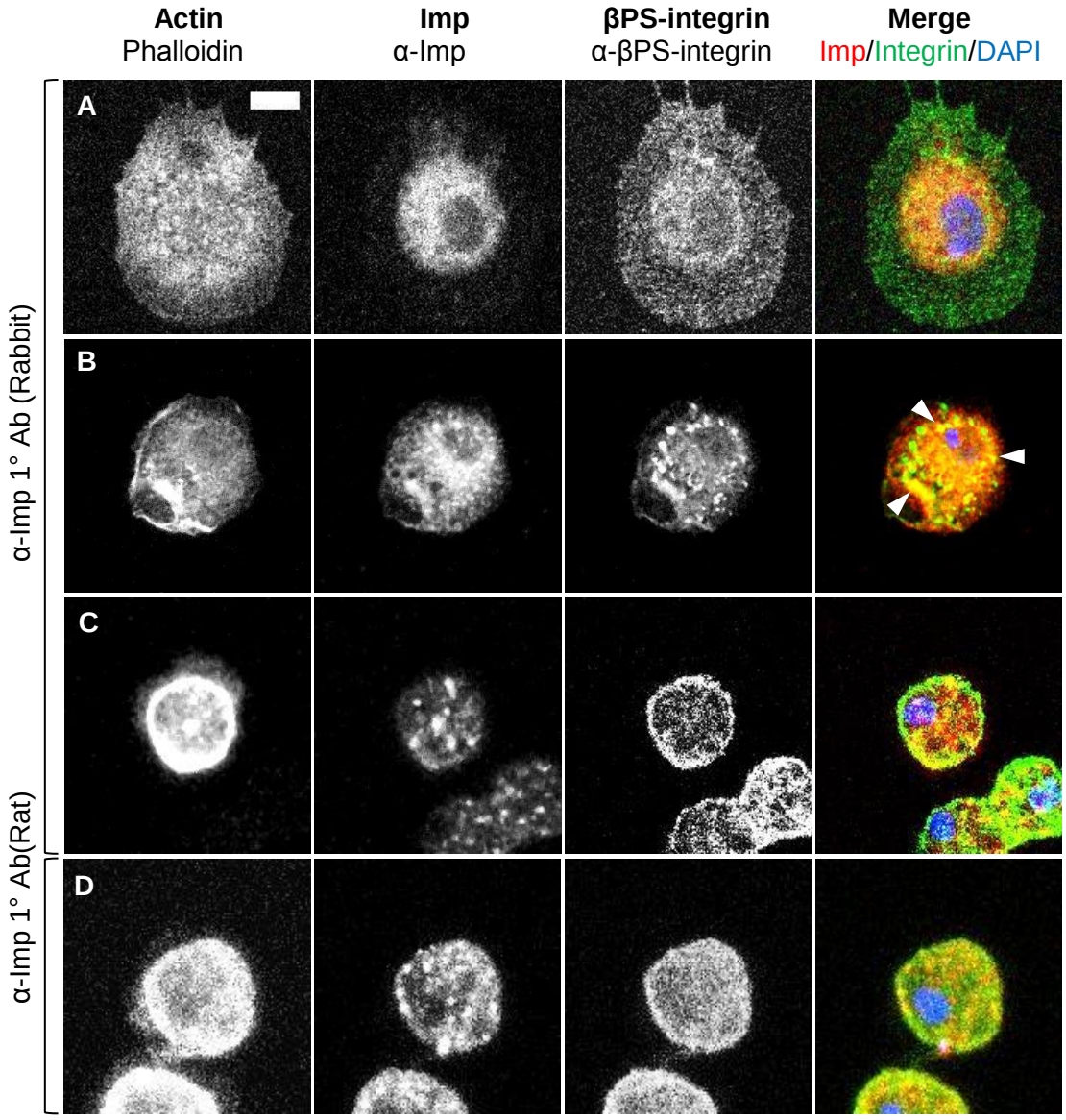

Figure 36. Co-localization of Imp and β-integrin in cultured *Drosophila* larval haemocytes

Larval haemocytes were dissected out from third instar larvae, cultured on uncoated glass, fixed and immunostained with primary antibodies against βPS-integrin and Imp to determine if these proteins co-localize in cultured haemocytes. Two distinct Imp antibodies were used, raised in either rabbit (**A & C**) or rat (**D**). Phalloidin staining was used to visualize the actin cytoskeleton, while nuclei were counterstained with DAPI (blue). Merged images contain βPS-integrin (green), Imp (red) and DAPI (blue). (**A**) In highly spread haemocytes the localization of βPS-integrin and Imp is diffuse. (**B**) βPS-integrin is enriched in a granular distribution, which co-localizes with some smaller granules containing Imp (white arrowheads). (**C & D**) In rounded haemocytes which do not form large protrusions, Imp is present in large granules, while βPS-integrin shows a more diffuse localization with some enrichment around the cell periphery. Scale bar represents 5 µm.

The localization of Imp and β-integrin was also examined in *Drosophila* border cells to investigate the localization of these proteins *in vivo*. Imp-mCherry was expressed specifically in border cells and was imaged directly by detection of mCherry emission, while endogenous β-integrin distribution was revealed with an anti-β-integrin antibody. Border cells also expressed the CD8-GFP marker.

Imp showed a diffuse distribution throughout the border cells, while β-integrin was localized in a granular pattern to the edges of the border cells (**Figure 37**). Imp and β-integrin appeared to show a different pattern of localization within border cells and did not significantly co-localize (**Figure 37**). In conclusion, Imp and β-integrin seem to be enriched in different cellular compartments in migratory cells, which may reflect the different roles these proteins perform.

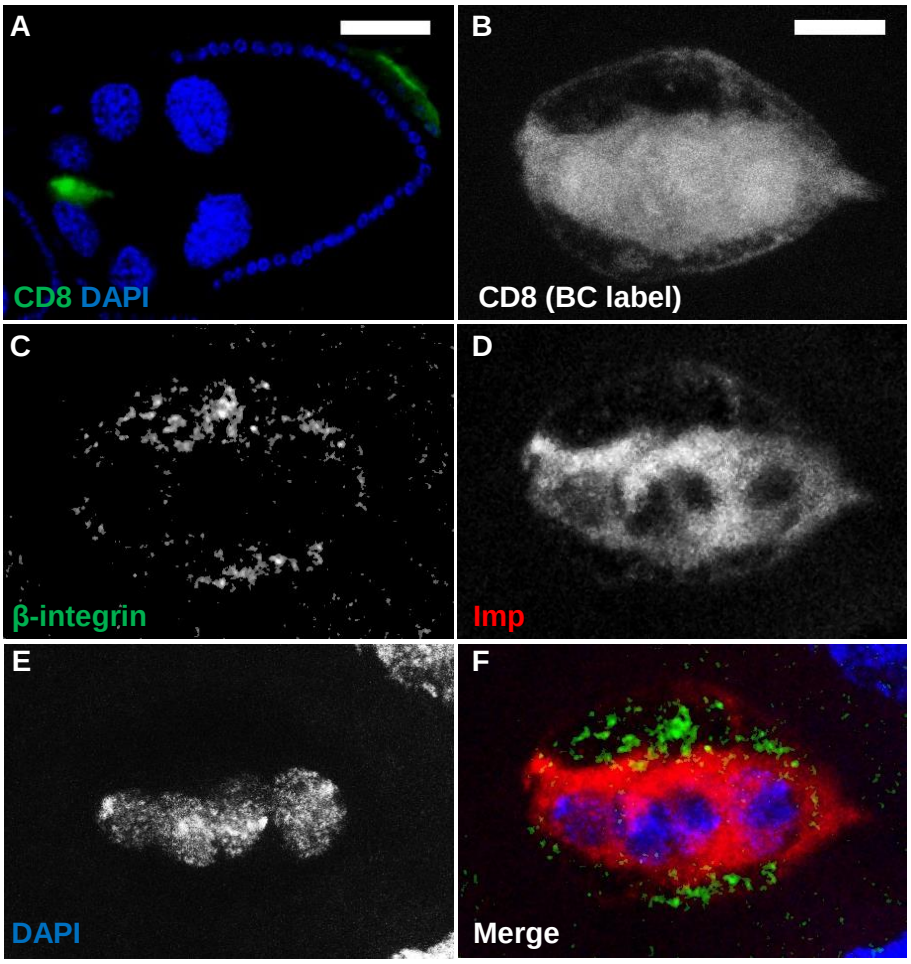

Figure 37. Co-localization of Imp and β-integrin in *Drosophila* border cells

To determine if Imp and β-integrin co-localize in migratory border cells within *Drosophila* oocytes, ovaries expressing UAS-Imp-mCherry specifically in border cells, using the *slbo*-Gal4 driver, were dissected and immunostained with anti-β-integrin (green). Imp-mCherry was imaged directly by visualizing mCherry emission using confocal microscopy (red). Border cells were labelled by expression of UAS-CD8-GFP and counterstained with DAPI to reveal nuclei (blue). (**A**) A migrating border cell cluster within the context of the entire egg chamber, seen by expression of the UAS-CD8-GFP label (green). Nuclei are counterstained with DAPI to reveal the surrounding egg chamber (blue) Scale represents 50 µm. (**B**) Border cells were labelled with CD8-GFP, (**C**) β-integrin antibody staining, (**D**) UAS-Imp-mCherry and (**E**) DAPI to highlight individual cells within the cluster. (**F**) The merged image contains Imp (red), β-integrin (green) and DAPI (blue). Scale represents 10 µm.

We next decided to analyse if depletion of Imp has any effect on the expression or localization of β-integrin. An RNAi hairpin against Imp was expressed specifically in haemocytes, which were then cultured and immunostained *ex vivo*. Two copies of the RNAi hairpin were expressed by both the *srp*-Gal4::VP16 and *srp*-Gal4 drivers for comparison. The actin cytoskeleton of these cells was labelled with anti-GFP as these haemocytes expressed moesin-GFP.

In general, we did not observe a significant difference in the localization of β-integrin between Imp RNAi and control cells, but the intensity of β-integrin appeared increased in haemocytes expressing RNAi against Imp (compare **Figure 38A-C**). To quantify changes in the levels of β-integrin and Imp the average fluorescence intensity of both β-integrin and Imp staining was measured in individual haemocytes expressing RNAi against Imp, and was compared to wildtype controls. Four repeats of the immunostaining were carried out on haemocytes expressing Imp RNAi under the control of the *srp*-Gal4::VP16 driver and two repeats using *srp*-Gal4 (n=20 haemocytes per assay). Haemocytes were isolated from a total of 20 larvae to control for differences between animals. We observed variable results across each repeat of the immunostaining assay, as the fluorescence intensity of Imp and β-integrin staining appeared to either increase or decrease relative to wildtype controls, suggesting a difference in the degree of knockdown achieved with the RNAi hairpin or in the efficiency of the immunostaining itself (**Figure 38D & E**).

However, the average fluorescence intensity of Imp and β-integrin staining was highly consistent between individual haemocytes within a single condition, as shown by calculating the standard error of the mean (SEM) (**Figure 38D & E**). This suggests that the sensitivity of staining was not that variable from cell to cell, but rather from assay to assay. We tried to use a more quantitative approach, but we were unable to achieve the numbers of isolated haemocytes required for carrying out Western blot analysis.

One important conclusion from these assays is the observation that the knockdown of Imp by RNAi is inefficient in haemocytes, as the average fluorescent intensities on Imp staining in RNAi treated haemocytes did not vary dramatically, compared with the controls in any of the assay repeats (**Figure 38D & E**). This is consistent with our *in vivo* observations (**Figure 30**).

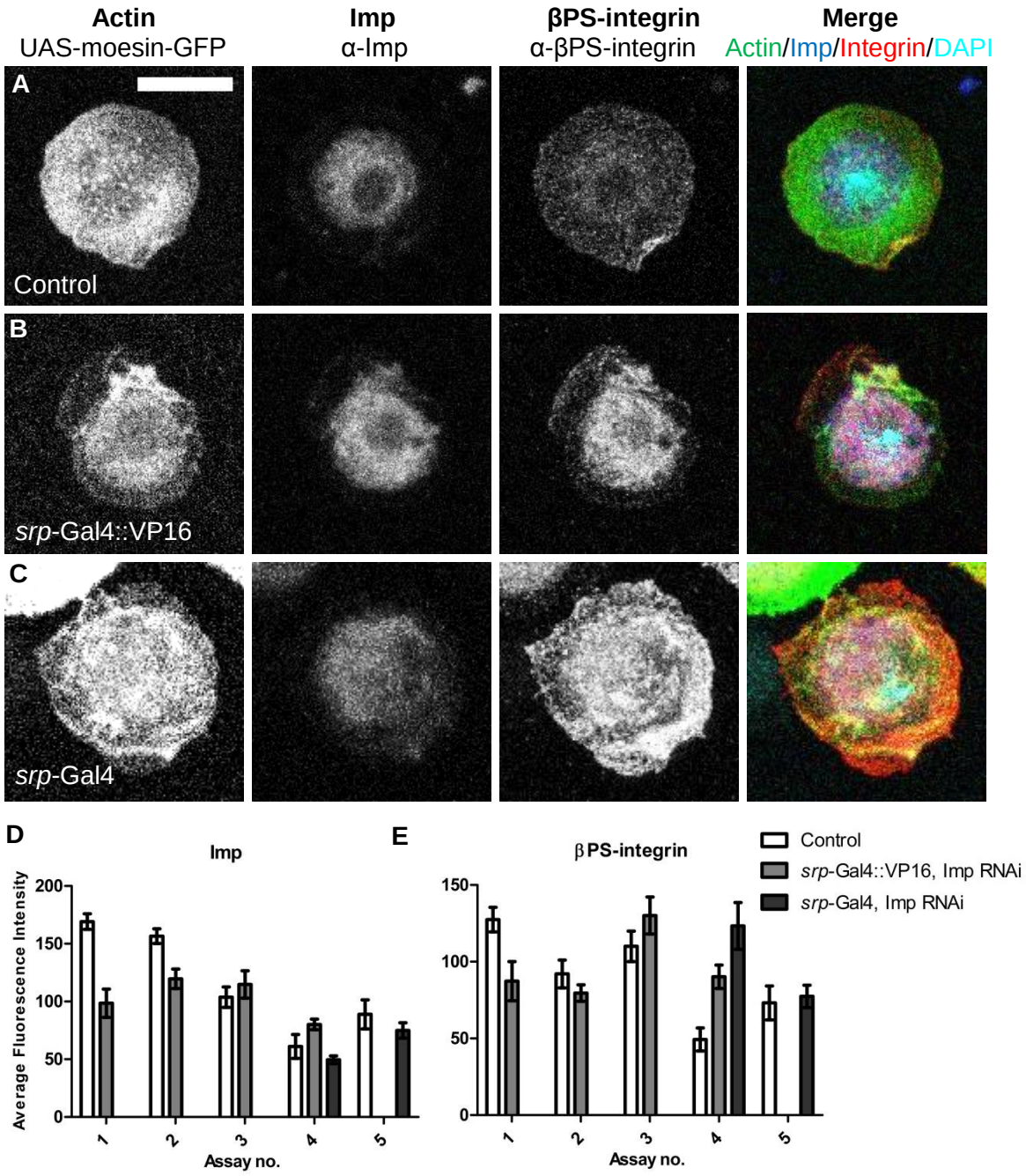

Figure 38. RNAi against Imp fails to efficiently knockdown Imp expression in cultured larval haemocytes

Larval haemocytes expressing a UAS-driven RNAi hairpin against Imp, expressed using either the *srp*-Gal4::VP16 or *srp*-Gal4 drivers, were dissected out of third instar larvae and cultured *ex vivo*. Cultured haemocytes were fixed and immunostained with antibodies against Imp (blue) and βPS-integrin (red). The level of Imp and βPS-integrin immunostaining was then quantified in individual cells by calculating the average fluorescent intensity, which was compared to wildtype controls to determine if Imp is efficiently knocked down by Imp RNAi, as well as identify any potential effects on β-integrin levels. The actin cytoskeleton was labelled by expressing UAS-moesin-GFP, driven by two copies of the haemocyte-specific *srp*-Gal4 or *srp*-Gal4::VP16 driver and staining haemocytes with anti-GFP antibody (green). Cultured haemocytes were counterstained with DAPI to reveal nuclei (cyan). Scale bar represents 10 µm. (**A**) Control haemocytes expressing only UAS-moesin-GFP. (**B**) Haemocytes expressing Imp RNAi under the control of the stronger *srp*-Gal4::VP16 driver, (**C**) or weaker *srp*-Gal4 driver. (**D-E**) Average fluorescent intensity values (mean gray value) of (**D**) Imp and (**E**) β-integrin staining in control vs. Imp RNAi haemocytes (n=20 haemocytes) across five repeats of

5.5 Depletion of Imp in *Drosophila* S2R+ cells by RNAi

In an attempt to reduce Imp levels more efficiently, we used the haemocyte-like S2R+ cell line, as treatment of *Drosophila* cell lines with double-stranded RNA (dsRNA) against the gene of interest produces a highly efficient knockdown (Kao & Megraw 2004; Rogers & Rogers 2008). As large numbers of cells can be treated, this would also allow us to perform Western blots.

We generated and treated S2R+ cells with dsRNA against Imp, using dsRNA treatment against GFP as a negative control. Western blot analysis confirmed that the knockdown of Imp was efficient (**Figure 39A**). Real-time quantitative PCR was then carried out to determine if the levels of candidate mRNA targets of Imp, including *β-integrin*, were affected by Imp depletion in S2R+ cells. All mRNA levels were compared to the control gene *RNA polymerase II* (*polII*) and then normalized to the mRNA levels of the untreated control. qPCR confirmed that in Imp-treated cells *imp* mRNA levels were reduced to 8% of the levels observed in untreated controls (**Figure 39B**). However, we did not observe any change in the levels of *β-integrin* mRNA in Imp-treated cells, suggesting that Imp does not regulate the levels of *β-integrin* mRNA (**Figure 39B**).

We also tested other candidate Imp target mRNAs, including *actin42A*, *profilin* and *arp2*, as well as mRNA encoding the ribosomal protein Rp49 as a negative control. The mRNA levels of all genes tested were increased by 20-28% in GFP-treated controls, compared to the untreated control, suggesting that uptake of dsRNA into S2R+ cells causes a general increase in the global level of mRNAs (**Figure 39B**). Although the mRNA levels of *β-integrin*, *rp49, actin42A* and *arp2* were increased in Imp-treated cells compared with GFP-treated controls (38%, 65%, 52% & 22% upregulated respectively), these appear within the error range of the assay, and so comparable to the GFP-treated control (**Figure 39B**). Consistent with this, we did not observe any change in the protein levels of Actin42A in Imp-treated cells, as shown by Western blot analysis (**Figure 39A**), despite a 52% increase in the *act42A* mRNA levels compared with GFP-treated controls (**Figure 39B**). We would therefore not expect to see changes in the levels of these genes at the mRNA level.

Interestingly, the levels of *profilin* mRNA levels are increased to 249% of GFP-treated controls in Imp-depleted cells, which suggests that Imp negatively regulates *profilin* mRNA stability and/or expression (**Figure 39B**). This is in contrast to the finding that overexpression of *profilin* in the γ-neurons of the *Drosophila* brain rescues the effects of Imp depletion, suggesting that Imp positively regulates *profilin* levels (Medioni *et al*. 2014).

In contrast, *profilin* mRNA was significantly downregulated in β-integrin-treated cells to 10% of GFP treated controls, suggesting that integrin signalling operates in a feedback loop to regulate *profilin* expression. β-integrin-treated cells also showed downregulation of *arp2* mRNA as these cells had 64% *arp2* mRNA levels compared with GFP-treated controls (**Figure 39B)**. The downregulation of *profilin* and *arp2* mRNA levels observed in β-integrin-treated cells appears to be a specific effect of β-integrin depletion, as we did not observe downregulation of any mRNAs in GFP-treated cells compared with untreated controls (**Figure 39B**).

Unfortunately, Western blot analysis to examine β-integrin levels in Imp-depleted cells was unsuccessful as a clear band of the correct size was not observed when blotting with the only known antibody available against *Drosophila* βPS-integrin (Appendix 6). However, several smaller bands were detected suggesting that β-integrin could be degraded. To determine if this was the case we depleted β-integrin in S2R+ cells by dsRNA treatment and compared this with untreated cells to see if the smaller bands observed were depleted. They were not, confirming that these bands are the result of non-specific antibody binding (Appendix 6).

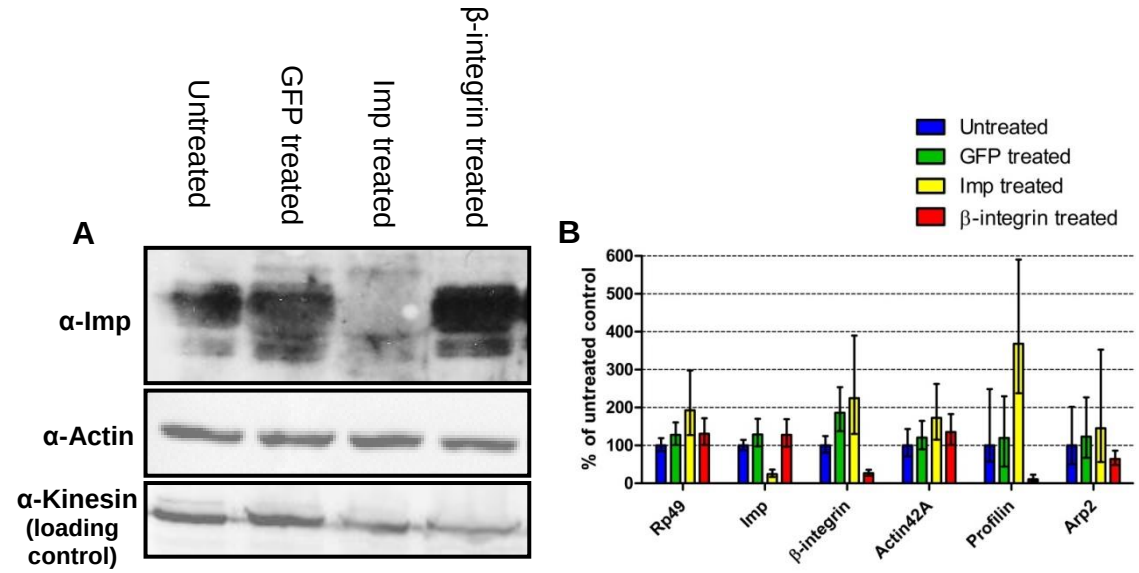

Figure 39. *profilin* mRNA levels are upregulated in Imp-depleted S2R+ cells

To determine if knockdown of Imp or β-integrin has any effects on the levels of β-actin or actin-regulatory mRNAs and/or proteins, *Drosophila* S2R+ cells were treated with dsRNA against Imp and β-integrin. Cells were treated with dsRNA against GFP as control. (**A**) Western blot analysis confirms that Imp protein is downregulated in S2R+ cells treated with dsRNA against Imp, while β-actin (Actin42A) protein levels are unaffected by Imp depletion. Kinesin was blotted against as a loading control. (**B**) Real-time quantitative PCR analysis of candidate mRNA targets of Imp in Imp and β-integrin-depleted cells by comparing to a control gene, RNA polymerase II (polII). Results represent an average of three independent repeats of dsRNA treatment and qPCR. Standard errors are calculated from reactions performed in triplicate.

5.6 Testing an *in vivo* interaction between Imp and β-integrin

Our finding that the overexpression of Imp phenocopies the knockdown of β-integrin in haemocytes and Imp binds to *β-integrin* mRNA *in vitro*, prompted us to test whether there may be a genetic interaction between Imp and β-integrin *in vivo*. Overexpression of β-integrin has a severe effect on haemocyte migration (**Figure 40B**). To determine if Imp plays any role in the regulation of β-integrin in haemocytes *in vivo* we overexpressed both Imp and β-integrin in haemocytes to see if Imp could rescue the negative effects of increased β-integrin levels.

We therefore expressed a UAS-βPS-integrin and UAS-Imp-mCherry transgene specifically in haemocytes and examined the migration of these cells to those expressing UAS-βPS-integrin alone (**Figure 40B & C**). Haemocytes expressing only cytoplasmic GFP, were used to label haemocytes and as control. Embryos were then fixed and immunostained with an antibody against GFP to label haemocytes. By embryonic stage 15 the *Drosophila* embryo is clearly divided into fourteen distinct segments, with two head, three thoracic and eight abdominal segments (**Figure 40A**). The progression of haemocyte migration was examining by scoring which embryonic segment haemocytes had reached by embryonic stage 15. The first two head segments were not taken into account as haemocytes are specified within this region, and so always occupy these segments.

We obtained a UAS-βPS-integrin transgene (Martin-Bermudo & Brown. 1996) which, when expressed specifically in haemocytes, revealed that overexpression of β-integrin in haemocytes has a severe effect on their motility *in vivo* (**Figure 6B**). While control haemocytes had migrated along the entire length of the developing ventral nerve cord by embryonic stage 15 (**Figure 40A**), haemocytes overexpressing β-integrin showed severe delays in their migration and had failed to migrate the full length of the embryo, often becoming stuck in the head mesoderm. We also failed to see haemocytes at the posterior of the embryo, which suggests that they fail to migrate from the head mesoderm to the germband, before it retracts at embryonic stage 12 (**Figure 40B**). Interestingly, we see the characteristic three line pattern of haemocytes in embryonic parasegments which are occupied by haemocytes, suggesting that haemocytes overexpressing β-integrin are able to complete lateral migration at embryonic stage 14. We therefore propose that haemocytes overexpressing β-integrin are able to respond normally to developmental migration cues, but do so at significantly reduced speeds.

Expression of Imp failed to rescue the overexpression phenotype of β-integrin as we observed no significant difference in the number of segments occupied by haemocytes ($p=0.91$) (**Figure 40D**). This suggests that either Imp does not negatively regulate the level of

β-integrin *in vivo*, or that an increase in Imp alone is not sufficient to rescue the effects of β-integrin overexpression.

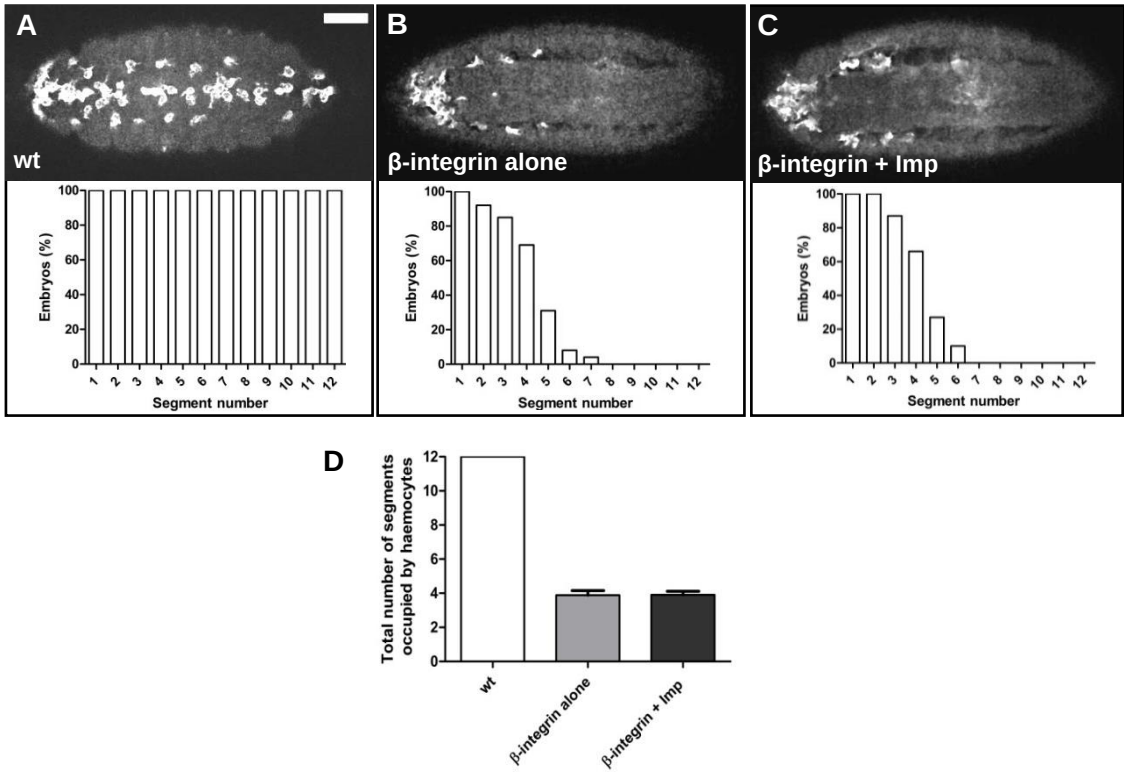

Figure 40. Imp fails to rescue the overexpression effects of β-integrin in *Drosophila* haemocytes

Overexpression of β-integrin in haemocytes prevents their migration from the head mesoderm of *Drosophila* embryos. Too determine if increased expression of Imp could rescue the overexpression phenotype of β-integrin, UAS-Imp-GFP and UAS-βPS-integrin were overexpressed in haemocytes using two copies of the haemocyte-specific *srp*-Gal4 driver. UAS-GFP was used to label haemocytes and *Drosophila* embryos were fixed and stained with an antibody against GFP. The progression of haemocyte migration along the ventral midline of *Drosophila* embryos was examined at embryonic stage 15. (**A**) In wildtype embryos haemocytes migrate from both the anterior and posterior along the entire length of the ventral midline and occupy all embryonic segments. (**B**-**C**) Haemocytes overexpressing (**B**) β-integrin alone and (**C**) both β-integrin and Imp fail to migrate along the entire length of the ventral midline (n= 30 embryos per genotype). (**D**) Shows the average number of embryonic segments occupied with haemocytes, which suggests that overexpression of Imp has no effect on the overexpression phenotype of β-integrin (two-way ANOVA, p=0.91). Scale bar represents 50 µm.

5.7 RNA immunoprecipitation (RIP) to identify mRNAs bound to Imp-GFP

To try obtaining evidence of an *in vivo* interaction between Imp and *β-integrin* mRNA, as well as other candidate mRNAs, we used immunoprecipitations of a GFP-tagged Imp and purified the associated RNAs. We first attempted immunoprecipitations from embryos expressing Imp-GFP specifically in haemocytes. As controls, we used both wildtype embryos that were negative for GFP expression, and embryos in which haemocytes expressed MCP-GFP as an unrelated RBP.

Western blot analysis was carried out to ensure that GFP-labelled proteins were present within the input and were successfully precipitated. Analysis of precipitated RNAs was carried out by real-time quantitative PCR (qPCR) to compare the levels of candidate mRNAs with the wildtype and MCP-GFP controls. The data gained from qPCR analysis is expressed as the fold-change in mRNA levels relative to wildtype, with all wildtype mRNAs normalized to 1 (**Figure 7**). The fold-change values obtained by qPCR can be seen in Appendix 7.

The immunoprecipitation was repeated three times without cross-linking proteins and RNA. However, although Western blot analysis showed that Imp-GFP was precipitated, we obtained variable results by qPCR as different levels of the RNAs analysed were precipitated with Imp-GFP in each repeat, when compared with the wildtype and MCP-GFP controls (data not shown). As the mRNA levels of each gene were normalized to the input levels, it is unlikely that the variability is due to differences in the amount of starting material.

It is possible that the RNP complexes, in which Imp is bound, are re-modelled after embryos are homogenized, as Imp-GFP expressed specifically in haemocytes is then exposed to the entire embryonic proteome. Formaldehyde cross-linking was then used on intact embryos to cross-link RNA and proteins within RNP complexes, preventing complex re-modelling. Western blot analysis showed that Imp-GFP and MCP-GFP are successfully precipitated (**Figure 41A**). However, after two repeats of cross-linking immunoprecipitation, the levels of candidate mRNAs precipitated with Imp were highly variable compared to wildtype and MCP-GFP controls, showing that cross-linking did not resolve this variability (compare **Figure 41B & C**).

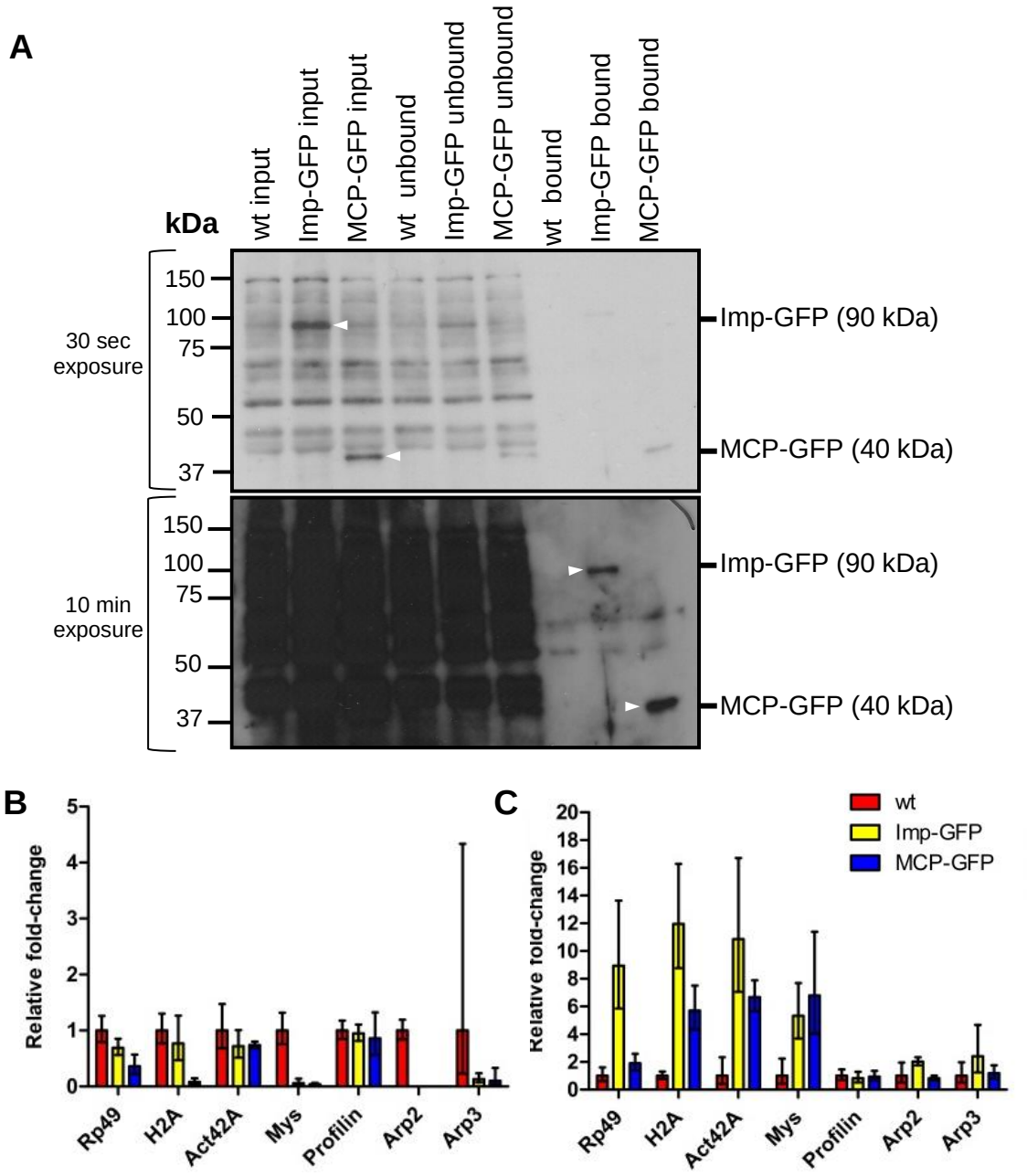

Figure 41. RNA precipitation to identify mRNAs associated with Imp in haemocytes

RNA immunoprecipitation was carried out to identify transcripts associated with Imp in *Drosophila* embryonic haemocytes. Imp-GFP was expressed specifically in haemocytes and precipitated from an embryonic extract, after cross-linking of RNAs and protein in intact embryos. MCP-GFP was precipitated as an unrelated negative control. (**A**) Western blot analysis shows that Imp-GFP and MCP-GFP are present within the input and are successfully precipitated in the bound fraction (white arrowheads). However, 2% of the total input and bound fractions were loaded compared with 50% of the total bound fraction, revealing that precipitation of Imp-GFP and MCP-GFP is inefficient. (**B**,**C**) Real-time quantitative PCR to detect candidate mRNAs precipitated with Imp-GFP, compared to the wildtype and MCP-GFP controls in two biological replicates. mRNA levels detected within the bound samples were first normalized to the levels of those detected within the input to control for differences in starting material. The levels of mRNAs precipitated with Imp-GFP and MCP-GFP were then compared relative to the levels of those mRNAs precipitated in the wildtype control. The results are expressed as fold-change relative to the wildtype control. Standard errors of the mean were calculated from reactions carried out in triplicate.

As a control for the RIP assays performed with embryos (see above), we attempted to identify mRNAs associated with both Imp and PTB in the *Drosophila* ovary, as mRNA targets of both these RBPs have been identified in the oocyte, including *oskar* and *gurken* mRNAs (Geng & Macdonald 2006; Munro *et al*. 2006; Besse *et al*. 2009; McDermott & Davis 2013). We therefore expressed both Imp-GFP and PTB-GFP in the germline of *Drosophila* oocytes and used wildtype ovaries, and those expressing MCP-GFP, as controls. However, formaldehyde cross-linking was not carried out on ovaries used for RIP assays.

Western blot analysis showed that all GFP-labelled RBPs were successfully precipitated (data not shown). Two distinct biological replicates of the RIP were performed and real-time quantitative PCR was then carried out, as described for embryos above. The RIP was carried out to test the levels of several mRNAs, including *oskar* and *gurken*, which are both known targets of Imp and PTB (Munro *et al*. 2006; Besse *et al*. 2009). As for RIPs from embryos, data gained from qPCR analysis was expressed as the fold-change in mRNA levels relative to wildtype, with all wildtype mRNAs normalized to 1 (**Figure 42**). The fold-change values obtained by qPCR can be seen in Appendix 7.

As expected, *oskar* mRNAs appeared highly enriched with PTB. *bicoid* mRNA was also highly enriched with PTB in both replicates (206-fold & 108-fold enriched, compared with wildtype controls), which suggests that *bicoid* is a target of PTB (**Figure 42**). However, *gurken* mRNA appeared highly enriched with PTB in only one of our replicates (136-fold increased vs. 12-fold increase compared to wildtype controls). This was also true for one of our negative controls *H2A*, which appeared enriched with both Imp and PTB in the first replicate (77 & 80-fold-change, respectively) compared with the second (7 & 3 fold-change, respectively). However, another negative control *rp49*, showed an 18-fold increase with PTB in the second replicate, compared with only a 7.5-fold change in the first replicate. Interestingly, *actin42A* mRNA appeared to be enriched with PTB in both replicates (75 & 16-fold change, respectively) (compare **Figures 42A & B**). However, it is difficult to determine if this is a real or non-specific enrichment, due to the fold-changes observed for the *rp49* and *H2A* controls, which are described above.

The above observations showed that fold-change of mRNAs associated with our RBPs was variable between biological replicates of the RIP and highlights the difficulties in determining if mRNAs that show a low fold-increase are non-specifically precipitated or are specifically associated with the RBP of interest. The overall levels of mRNA associated with both Imp and PTB, compared with wildtype controls, was higher in the first replicate (**Figure 42A**) compared with the second (**Figure 42B**). This suggests that either the overall level of total RNA was higher, or that more GFP-labelled RBP was precipitated in the first replicate. It is

also likely that some mRNAs could interact non-specifically with an RBP at a higher level in one replicate, compared with another, which may lead to false-positive enrichments. To control for this variability and ensure that we are detecting enrichments correctly, the global level of mRNAs precipitated with GFP-labelled RBPs, compared with wildtype, should be examined in in each biological replicate to set a minimum fold-change threshold, over which a specific mRNA is then considered enriched with an RBP. This threshold will be RIP-dependent and will vary in each independent biological replicate. At least three independent biological replicates of each RIP should also be carried out and compared to control for variability.

In conclusion, while RIP and subsequent qRT-PCR analysis of candidate mRNAs may be used to identify mRNAs that are highly enriched with RBPs of interest, such as *bicoid* and *oskar*, it is difficult to detect lower affinity mRNA-RBP interactions. To detect low affinity interactions, global mRNA levels should be compared between both the input and bound fractions, by either RIP-Chip or RNA-seq following RIP.

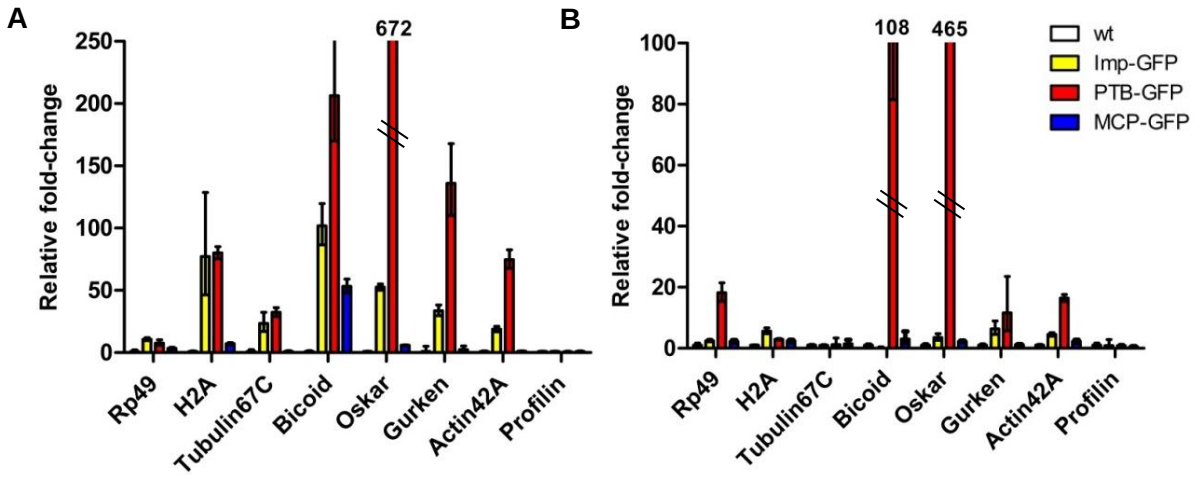

Figure 42. RNA precipitation to identify mRNAs associated with Imp and PTB in *Drosophila* oocytes

A number of mRNAs associated with Imp and PTB in *Drosophila* oocytes have been previously characterized, including *oskar* and *gurken* mRNAs. To determine the effectiveness of our RIP assay, Imp-GFP and PTB-GFP were expressed specifically in the germline of *Drosophila* oocytes and precipitated from an ovarian extract. qPCR was then carried out to establish if *oskar* and *gurken* mRNAs can be detected with Imp and PTB. MCP-GFP was precipitated as an unrelated negative control. (**A**, **B**) Real-time quantitative PCR to detect candidate mRNAs precipitated with Imp-GFP and PTB-GFP, compared to the wildtype and MCP-GFP controls in two biological replicates. mRNA levels detected within the bound samples were first normalized to the levels of those detected within the input to control for differences in starting material. The levels of mRNAs precipitated with Imp-GFP and MCP-GFP were then compared relative to the levels of those mRNAs precipitated in the wildtype control. The results are expressed as fold-change relative to the wildtype control. Standard errors were calculated from reactions carried out in triplicate.

Chapter 6:

Discussion

6.1 Analysis of the model systems and tools used to study the role of RNA regulation in cell motility *in vivo*

6.1.1 Evaluating the strengths and weaknesses of using *Drosophila* haemocytes as an *in vivo* model to study the role of RNA regulation in cell motility

Here we have established a model system to investigate the role of RNA regulation in cell motility *in vivo*. After attempting to fix *Drosophila* embryos it was established that the lamellipodial protrusions were destroyed within the fixation procedure (**Figure 10C**). Therefore, all analysis must be carried out using live imaging, placing a limitation on the use of the system, as transgenic flies must be generated to study the localization of proteins and mRNAs of interest.

Imaging of our GFP- and mCherry-labelled transgenes and the haemocyte labels (eg. moesin-GFP/mCherry) revealed that two copies of a GAL4 driver are required to drive these proteins at sufficient levels to be detected (data not shown). This limits the number of transgenes that can be expressed within haemocytes. The number of fly crosses required to achieve sufficient GAL4 drivers, a haemocyte marker and a transgene will also be significantly increased. We were able to improve the strength of the GAL4 drivers by generating a haemocyte-specific Gal4::VP16 driver, which did not remove the need for two drivers, but increased our capacity to overexpress RBPs, as well as knock down their expression by RNAi.

The use of protein trap lines to image the distribution of proteins within haemocytes is limited by the expression of the labelled protein in the surrounding tissues, making it difficult to establish if our proteins are expressed in the haemocytes themselves, particularly in the lamellipodial protrusions (**Figure 17C**). To overcome this problem, we constructed fluorescently-labelled RBPs that could be expressed specifically in haemocytes.

As previously shown, imaging showed that haemocytes are highly amenable to live imaging, as their polarisation and migration can be captured when imaging the ventral surface of the embryo (Stramer *et al*. 2005; Stramer *et al*. 2010). The available haemocyte labels also allow both the actin and microtubule structures to be clearly visualized, ensuring that any changes to the haemocyte cytoskeleton as a result of overexpression or knockdown of proteins of interest can be seen. The embryos can be easily staged, allowing animals of different stages to be selected, as well as ensuring reproducibility of assays. The developmental migration of haemocytes can be easily followed upon leaving the head mesoderm at embryonic stage 10, until their random migration across the ventral surface at embryonic stage 15, so that migratory defects at different stages would to be easily seen (Evans *et al*. 2010).

Wound healing assays are highly successful and allow the migration of haemocytes to be directed to a specific region of the embryo (Stramer & Wood 2009). Analysis of haemocyte velocity to wounds in embryos of different genetic backgrounds revealed that there is a high consistency in the average speed of haemocyte migration to wounds between different embryos of the same genetic background (**Figure 25D**). This makes them an ideal model to study cell motility as any changes in the speed of haemocyte migration, within haemocytes both depleted for or overexpressing proteins of interest, should be consistent between different embryos compared with controls, making any migratory defects easy to see and analyse.

6.1.2 Analysis of the MS2 system to study *in vivo* mRNA localisation in haemocytes

As fixed haemocytes lose their lamellipodial protrusions, *in situ* hybridisations could not be used to examine the distribution of mRNAs in migratory haemocytes. Instead, the MS2 system was used to follow the *in vivo* localisation of candidate mRNAs. Although several groups have utilised the MS2 system to visualise mRNA localisation, it has been mostly used to follow the mRNAs in cultured cells such as budding yeast (Bertrand *et al*. 1998; Hocine *et al*. 2013), primary cultures of mammalian fibroblasts (Lionnet *et al*. 2011) or bacteria (Golding & Cox 2004), as well as in whole tissues including *Drosophila* embryos, egg chambers and adult brain (Becalska and Gavis 2009; Forrest and Gavis 2003; Jaramillo *et al*. 2008; Ashraf *et al*. 2006; Belaya & St Johnston 2011; Lange *et al*. 2008). However, there are currently limited examples in which the MS2 system has been used to examine the localisation of an mRNA within a single cell *in vivo,* in the context of a whole living organism (JayaNandanan *et al*. 2011).

To test the MS2 system in haemocytes, several MS2 hairpin-tagged mRNAs, including the *Drosophila* homologues of *β-actin* and *arp3* mRNA *(actin5C, actin42A & arp66B)*, were tagged and expressed in haemocytes, as these transcripts have been shown to localise at the leading edge of migratory cultured cells (Shestakova *et al*. 2001; Mingle *et al*. 2005). However, the distribution of the MCP protein looked identical with or without co-expression of the *act5C*, *act42A* and *arp66B* mRNAs, suggesting that these mRNAs are not localised to the lamellipodia of haemocytes (**Figure 21** – *act42A*, data not shown for *act5C* & *arp66B*). However, other explanations are possible (see below). RT-PCR showed that the hairpin-tagged *actin42A* and *oskar* mRNAs are expressed in haemocytes, although their level of expression is unknown (**Figure 23B**).

The MS2 tools constructed in this project were tested in the *Drosophila* oocyte, as this system has been successfully used to study the localization of *oskar* mRNA (Zimyanin *et al*. 2008). However, we failed to see the previously characterised enrichment of *oskar* at the

oocyte posterior (**Figure 24B**), suggesting an issue with our MS2 system reagents/tools. Our MS2 binding sites were placed directly upstream of the 5'UTR of *oskar* mRNA, while the previous studies placed the binding sites within the full-length transcript, directly after the stop codon (Zimyanin *et al*. 2008). Similarly, to study the localisation of *nanos*, *bicoid* and *gurken* mRNAs within the oocyte, the MS2 binding sites were placed within the 3'UTR of all three transcripts (Forrest & Gavis 2003; Jaramillo *et al*. 2008; Weil *et al*. 2008).

The expression of the MS2 hairpin-tagged *oskar*, *bicoid*, *nanos* and *gurken* mRNAs were all able to successful rescue phenotypes caused by down-regulation of their products within the oocyte, revealing that these tagged transcripts are effectively translated (Forrest & Gavis. 2003; Jaramillo *et al*. 2008; Weil *et al*. 2008; Zimyanin *et al*. 2008). We therefore decided to place the MS2-binding sites at the 5' end of our candidate mRNAs to prevent their translation, as overexpression of the selected actin-related proteins in haemocytes is not likely to be innocuous. Although RT-PCR has shown that our transcripts are detectable when expressed in haemocytes (**Figure 23B**), their levels may be low or they may be rapidly degraded upon synthesis due to the presence of the MS2 hairpins at the 5'UTR. Alternatively, the MS2 hairpins may interfere with trafficking or localisation of the mRNA.

We also cannot exclude the possibility that the MCP protein does not bind the MS2 hairpin-binding sites and so, although present, the localisation of the candidate mRNAs cannot be seen. It is also possible that the candidate mRNAs selected are not specifically enriched in any region within haemocytes and so bound MCP is undistinguishable from the pool of unbound cytoplasmic MCP. However, if this were the case then the nuclear enrichment of MCP seen in haemocytes expressing the MCP proteins should appear diminished, which does not seem to be the case. The most likely explanation is that the MS2-hairpins at the 5' of the tagged mRNA trigger degradation. In this case, even if the MCP were able to bind the mRNA prior to degradation, it is likely that its localization would be changed compared with wildtype as mRNA targeted for degradation would be sequestered in P-bodies.

A study to test the resolution of the MS2 system in cultured fibroblasts for the application of tracking individual RNA molecules revealed that discrete particles of GFP-labeled mRNA were resolvable only when 24 MS2 binding sites were present in the reporter mRNA, and not in the presence of only 6 or 12 MS2 sites (Fusco *et al*. 2003). Although we originally attempted to generate MS2 hairpin-tagged mRNAs with 24 and 32 repeats of the MS2 sites, the repetitive nature of the DNA constructs caused degradation of the DNA when introduced into competent bacteria. The maximum number of MS2 hairpins we managed to introduce in our candidate mRNAs was 18 repeats, which may not be detectable above background level in both the oocyte and haemocytes.

We have recently acquired previously characterized fly lines containing an MS2-tagged *gurken* mRNA, as well as an extensively characterized MCP-mCherry fusion protein expressed under the control of a *nanos* promoter. We aim to test these reagents within the oocyte, with both our own MS2-tagged mRNAs and MCP proteins, to determine which part of our MS2 system is failing.

6.1.3 The RNA-binding proteins PTB, Hrp48 and Imp are differentially localized in haemocytes *in vivo*

The localization of the RNA-binding proteins PTB, Hrp48 and Imp was different upon expression in live haemocytes, suggesting that they may play functional different roles in this cell type. PTB was highly enriched in the nucleus (**Figure 17A**), which was not surprising as PTB has been well characterized as a nuclear regulator of RNA processing (Sawicka *et al*. 2008). PTB was also present at low levels throughout the lamellipodial protrusions, but was not enriched at any particular region within them (**Figure 17A**). In contrast, Imp and Hrp48 were not highly enriched in the nucleus, but diffusely localized throughout the cell body of haemocytes. While Hrp48 was exclusively restricted to the cell body (**Figure 20A**), Imp was present in some arm-like protrusions enriched for both actin and microtubules (**Figure 12 & 13**).

None of our RBPs were enriched at the leading edge of haemocytes, suggesting that either these specific RBPs are not required for localization of mRNAs at the leading edge, or that local RNA translation is not required for haemocyte migration. This idea is also in agreement with the observation that there are not enrichments of actin at the leading edge of haemocytes *in vivo* (**Figure 12A**). Immunostainings to reveal the localization of endogenous RBPs in cultured larval haemocytes supported our *in vivo* findings as PTB, Hrp48 and Imp were not enriched within, or at the periphery, of the actin protrusions (**Figures 14, 18 & 20C**).

6.1.4 Over-loading of proteins in migratory cells may cause migratory defects

Overexpression of Imp in haemocytes results in migratory defects as the speed of haemocytes is significantly reduced, during both random migration and directed migration towards an epithelial wound site. This effect appears to be dose-dependent as expression of a double copy of both the haemocyte-specific *srp*-Gal4 driver and Imp produces a more severe migratory defect, compared with expressing only a single copy of *srp*-Gal4 and Imp (**Figure 26C**).

These results should be taken with caution as the expression of different non-functional proteins in haemocytes can also cause variations in the speed of haemocyte motility (**Figure**

25D). It is possible, that despite being non-functional, the binding of moesin-GFP to actin filaments causes changes in actin dynamics and therefore the migratory behaviour of haemocytes. Equally, the binding of Clip170 to microtubules could prevent the binding of functional microtubule-binding proteins, causing the slower migration speeds observed. Alternatively, expression of cytoplasmic GFP, which diffuses throughout the entire cytoplasm of haemocytes, may also have an effect on haemocyte motility. Unbound cytoplasmic GFP may be targeted for degradation, increasing the phagocytic load of these haemocytes and diluting the pool of proteins required for efficient cell migration. Overexpression of proteins in haemocytes may also place a burden on the translational machinery, reducing the levels of proteins required for efficient migration.

The effects of markers used to track the migration of cells *in vivo* should be taken into account when analysing the effects of overexpression or depletion of a protein on interest on cell migration. It has been well documented that Imp is transported along microtubules by the molecule motors dynein and kinesin (Nielsen *et al*. 2002; Boylan *et al*. 2008). Overexpression of Imp in haemocytes could lead to an excess of Imp bound to microtubules, to transport it to regions of the cell where it is required. This could have a similar effect to Clip170 expression, resulting in a decrease in the speed of haemocyte migration. Therefore, the motility defects caused by overexpression of Imp may not be due to its functional role within the cell, but may instead be a by-product of overexpressing the protein itself.

6.2 Actin dynamics in haemocytes and implications for Imp function

6.2.1 In contrast to cultured haemocytes, actin is not enriched at the leading edge of haemocytes *in vivo*

We observed that, although actin was enriched at the periphery of lamellipodial protrusions in some cultured haemocytes *in vitro* (**Figure 18A**), this was not the case *in vivo*, using live imaging of embryonic haemocytes (**Figure 12A**). We examined the localisation of actin in haemocytes *in vivo* by following the distribution of the actin-binding domain of moesin fused to GFP (Dutta *et al*. 2002). This showed that actin is not enriched at the periphery of the lamellipodial extensions, also referred to as the leading edge (**Figure 12A & B**).

Addition of ecdysone to larval haemocytes cultured *ex vivo* triggered them to polarize and migrate across a 2D substrate (Sampson *et al*. 2013). Interestingly, in contrast to haemocytes *in vivo*, actin was highly enriched at the leading edge of a large proportion of cultured haemocytes treated with ecdysone (compare **Figure 19A & Figure 18E**). This suggests that cells migrating *in vivo*, within the context of a living organism, regulate their actin cytoskeleton in a different manner to those migrating across a 2D-surface.

Our understanding of the mechanisms governing cell motility is based on the haptokinetic model of fibroblast migration across a 2D substratum (Friedl & Weigelin 2008). The model is a cyclic process which first requires the polarization of the cells and the formation of actin protrusions. Various receptor complexes, including integrins, then cluster at sites within the protrusions to form adhesions with the substrata, termed focal adhesion complexes (FACs). Myosin motors assist in retraction of the cell body, which establishes a gradient of binding and traction forces between the front and rear of the cell to generate directional cell movement and dissolution of adhesion complexes (Friedl & Bröcker 2000). However, cultured cells migrating along a flat surface are likely to employ different mechanisms of migration compared with cells *in vivo*, migrating within the constraints of an extracellular matrix. Cells migrating along a flat surface do not encounter any mechanical resistance, unlike cells migrating within the constraints of a tissue (Friedl & Bröcker 2000) and assume a flat, spread morphology. However, motile cells such as fibroblasts assume different morphologies within a 3D matrix with a bi- or tri-polar morphology. They project cylindrical pseudopodia, unlike the flat, ruffling pseudopodia of fibroblasts within a 2D environment (Hakkinen *et al*. 2010). This difference in morphology means that arrangement of the actin cytoskeleton in likely to be different in cultured migratory cells versus those migrating within a tissue or 3D matrix.

Actin stress fibers are contractile actomyosin bundles that are required for adhesion of fibroblasts to the substrate and retraction of the rear edge (Hotulainen & Lappalainen 2006). Thick actin stress fibers are observed in fibroblasts cultured on 2D substrates, but when migrating within a 3D matrix they were not observed (Friedl & Bröcker 2000; Hakkinen *et al*. 2010). Migratory *Dictystelium* were also observed to lack stress fibers, indicating that they may not be required for certain types of cell migration (Rubino *et al*. 1984).

Stress fiber formation appears to inversely correlate with migration velocity as fibroblasts containing few or no stress fibers migrate on average 2.8 times faster than fibroblasts containing a higher density of stress fibers (Lewis *et al*. 1982). Fibroblasts within a 2D environment migrate at lower speeds, at an average of 0.2-0.4 µm/min (Ware *et al*. 1998; Hakkinen *et al*. 2010), while haemocytes *in vivo* show a much quicker migration speed of around 2.4 µm/min (**Figure 27C**), and are continually re-polarizing during migration. We did not observe a high density of actin stress fibers within haemocytes (**Figure 12A**), which are often found at the leading edge of cultured migratory cells. This could reflect the differences in the velocity of haemocytes, compared to cultured migratory cells. It is therefore likely that the regulation of actin dynamics within migratory cells *in vivo* are different to those migrating

on a 2D substrate *in vitro*, which may have an impact of the speed of their migration. This would explain the lack of actin enrichments at the leading edge of haemocytes *in vivo*.

Actin stress fibers are found in focal adhesion complexes (FACs) (Hotulainen & Lappalainen 2006). While the FACs formed in cells cultured on a 2D substrate are large and well-developed, the adhesions formed between migratory cells and a 3D matrix are much smaller and fewer are often formed (Friedl & Bröcker 2000). This is not surprising, considering the lack of actin stress fibers within migratory cells within a 3D matrix. Cultured haemocytes are sessile and so are likely to form strong actin-rich adhesions with the substrate on which they are cultured. FACs are formed between the substrate and the lamellipodial protrusions, particularly at the leading edge, and are mediated through integrin complexes at the cell membrane (Zaidel-Bar *et al*. 2004). This could account for the enrichments of actin that we observed at the tips of lamellipodial protrusions in cultured haemocytes (**Figure 14**). Meanwhile, highly motile cells *in vivo*, such as haemocytes, are less likely to form strong adhesions to the extracellular substrata due to the speed of their migration. This is supported by the fact that depletion of Zyxin in *Drosophila* pupal haemocytes, a protein required for the maturation of nascent adhesions into stable focal adhesions (FAs), significantly increased their *in vivo* migration (Moreira *et al*. 2013). Consistent with this, cultured fibroblasts form small, less developed adhesions with the substrate and show increased speeds of migration in a 3D matrix, compared with a 2D substrate (Friedl & Bröcker 2000; Hakkinen *et al*. 2010).

6.2.2 Local translation of *β-actin* mRNA at the leading edge is unlikely to play a role in haemocyte migration *in vivo*

Although actin was not enriched at the leading edge of haemocytes *in vivo*, we found that a belt of actin enrichment was frequently present at the edge of the cell body, in regions from which the lamellipodial protrusions would extend (**Figure 12A & B**). Frequently, an arm of actin would extend from this belt into the lamellipodial protrusions, which also showed a higher concentration of actin compared with the surrounding lamellipodia (**Figure 12A & B**). This pattern of actin enrichment has also been observed for other migratory cell types, such as Zebrafish primordial germ cells, which show an enrichment of actin at the edge of the region that houses the cellular organelles (cell body), from which lamellipodial protrusions extend (Blaser *et al*. 2005). The lamellipodial protrusions of these cells were not highly enriched with actin (Blaser *et al*. 2005). This suggests that there is a distinction between the cell body and the lamellipodial protrusions, which may be formed by a basket of microtubules formed around the haemocyte cell body (Stramer *et al*. 2010).

IMP1, the rat and chick homologue of Imp, has been shown to localise *β-actin* mRNA at the leading edge of cultured migratory cells, where actin protein also accumulates upon local translation at this region (Ross *et al*. 1997; Shestakova *et al*. 2001; Oleynikov & Singer 2003). Local translation of *β-actin* mRNA at the leading edge regulates cell motility *in vitro* (Hüttelmaier *et al*. 2005). However, as observed for actin, Imp was clearly not enriched at the leading edge of lamellipodial protrusions in haemocytes *in vivo* (**Figure 12**).Interestingly, Imp was present within the base of some arm-like protrusions that extend into the lamellipodia, which co-localized with the aforementioned arm of actin enrichment (**Figure 19**). Imp was present in the cytoplasmic extensions of migratory border cells (**Figures 31 & 32**). However, even in this case, we did not observe strong enrichments of Imp at the leading edge of border cell protrusions. Taken together, these findings suggest that Imp does not localise and regulate mRNAs at the leading edge of lamellipodial protrusions in haemocytes, although it may regulate mRNAs in other regions of the cell.

We have shown that the mRNA of *actin42A* (*β-actin*) is not enriched at the periphery or within any regions of the lamellipodial protrusions in cultured haemocytes *ex vivo* by *in situ* hybridization (**Figure 22**). Our observation that actin protein was also not enriched at the leading edge of haemocytes *in vivo* (**Figure 12**) suggests that *β-actin* mRNA may not be localized to, or locally translated, at the leading edge of these cells. To support this idea, recent studies have revealed that *β-actin* mRNA is not enriched within the cellular protrusions of motile cultured cells, when compared with the levels of mRNAs within the cell body (Mili *et al*. 2008; Thomsen & Lade Nielsen 2011; Jakobsen *et al*. 2013). These findings contrast to previous reports using *in vitro* cultured migratory fibroblasts (Ross *et al*. 1997; Shestakova *et al*. 2001; Oleynikov & Singer 2003), suggesting cell-type specific differences in the regulation of mRNAs and proteins required for cell motility. This highlights that a 'one rule for all' approach cannot be taken when investigating the mechanisms of cell motility, in both cultured cells and different migratory cell types *in vivo*.

One interesting possibility is that the enrichments of actin at the cell body edge, and in arms extending from this region, supply actin monomers to the continually re-polarizing lamellipodial protrusions. Actin monomers could be transported from these regions of actin enrichment and into the growing lamellipodial protrusions, ensuring a continual feed of actin to replenish actin stores at the leading edge. If this is the case, actin may be locally translated at these actin-rich structures, to which Imp is also localized (**Figure 19**). It would be interesting to examine the localization of the translational machinery in haemocytes, to determine if it is present or specifically enriched at the sites of actin enrichment.

6.3 Characterizing the role of Imp in motile cells

6.3.1 Imp may play a role in regulating microtubule dynamics in haemocytes

Although expression of cytoplasmic GFP, moesin-GFP or Clip170-GFP results in notable differences in the speed of haemocyte migration, haemocytes expressing these protein markers display comparable contact repulsion behaviour (**Figure 28A-C**). In contrast, haemocytes overexpressing Imp do not display normal contact repulsion but stick together in clumps and are often unable to re-polarise and migrate away from each other (**Figure 28D**). This suggests that the contact repulsion phenotype seen in haemocytes overexpressing Imp is a specific effect of increased Imp expression and therefore function, rather than an effect of simply overloading the haemocytes with a protein.

Migrating haemocytes form a structure, referred to as a microtubule arm, which consists of a tight bundle of lamellar microtubules that protrude from the haemocyte cell body in the direction of migration (Stramer *et al*. 2010). As haemocytes re-polarise, the microtubule arm will either be retained and re-orient if the change in the angle of migration is less than 40°. If the turn angle is greater than 40° the microtubule arm is dis-assembled and then re-assembled in the new direction of migration (Stramer *et al*. 2010). To undergo normal contact repulsion, haemocytes will align their microtubule arms upon contact for approximately three minutes before re-polarising and migrating away from each other. In the majority of cases, when the tip of a microtubule arm of one haemocyte comes into contact with another haemocyte, the haemocyte rapidly re-polarises before further contact is made (Stramer *et al.* 2010).

Examination of both microtubule and actin dynamics in *mys* (β-integrin) mutant haemocytes showed that while haemocytes were able to form a microtubule arm, this arm frequently collapses during random migration (Comber *et al*. 2013). Failure to maintain a microtubule arm prevents efficient contact repulsion, as assembly of a microtubule arm is essential to enable haemocyte to re-polarise upon contact (Stramer *et al*. 2010). Despite the ability of haemocytes overexpressing Imp to form a microtubule arm during random migration (**Figure 20**), the majority of haemocytes failed to align these microtubule arms or re-polarise upon contact with another cell (**Figure 28F**), suggesting that their ability to maintain a microtubule arm is impeded by an increase in Imp levels.

Interestingly, haemocytes that fail to form a microtubule arm can still migrate to wound sites, although they take longer to response to wound cues, take a less directional route to the wound site and show increased migratory speeds (Stramer *et al*. 2010). Although haemocytes overexpressing Imp formed a microtubule arm (**Figure 20**), the speed of their

migration and directionality was significantly reduced compared with controls (**Figure 26**). This suggests that Imp overexpression affects the ability of haemocytes to re-polarise, consistent with defects in microtubule arm formation. It would be interesting to fully examine the microtubule dynamics in haemocytes overexpressing Imp to determine if these haemocytes take longer to form a microtubule arm or once formed, fail to maintain it during migration.

In support of the idea that Imp may play a role in regulating microtubule dynamics, we observed co-localization of Imp and microtubules in haemocytes *in vivo*, with Imp always present in the base of the microtubule arm, without extending towards the tip (**Figure 20**). When haemocytes re-polarize, the microtubule arm is disassembled and re-formed in the new direction of migration (Stramer *et al*. 2010). In haemocytes that lacked a microtubule arm (e.g. in the process of disassembling and re-forming the microtubule arm), Imp was restricted to the cell body and we did not detect it within any protrusions (**Figure 20C**). This suggests that Imp is co-localized primarily to microtubules within haemocyte protrusions, rather than actin filaments. We propose that Imp may therefore regulate the localisation and/or translation of mRNAs that encode proteins required for microtubule dynamics. An alternative possibility is that Imp is transported in RNP granules along microtubule filaments, which has been observed in other cell types, and so Imp co-localization with microtubules is a result of Imp transport along the cytoskeleton (Nielsen *et al*. 2002; Medioni *et al*. 2014).

6.3.2 Changes in cellular morphology could trigger changes in the distribution of Imp

Interestingly, we observed that the localization of Imp in cultured haemocytes and the *Drosophila* S2R+ cell line varied in cells with different morphologies. Haemocytes and S2R+ cells that were spread and formed extensive lamellipodia showed a more diffuse distribution of Imp, while cells with a highly round morphology, which either failed to form lamella or produced very few cellular extensions showed a highly punctate distribution of Imp (**Figures 14 & 15**). This pattern was particularly pronounced in cells undergoing division (**Figure 15D**). This revealed the degree of heterogeneity in cells, even in culture conditions.

Plating of *Drosophila* S2R+ on different substrates induces changes in their morphology and it has been shown that some proteins, including the *Drosophila* βPS-integrin subunit, show different patterns of localization depending on the degree of spreading of the cells (Pereira *et al*. 2011). Similarly to our observations of Imp localization, in rounded up cells βPS-integrin (β-integrin) was localized in distinct puncta, indicative of FAC formation, while highly spread cells with branched lamellipodia showed a diffuse pattern of βPS-integrin, suggesting a lack of FACs (Pereira *et al*. 2011). Consistent with these findings, we also observed variations in

the localization of β-integrin in cultured haemocytes, with some cells containing distinct granules of β-integrin localization, while highly spread cells showed a diffuse distribution of β-integrin throughout the entire cell (**Figure 36**). However, Imp and β-integrin did not significantly co-localize when granules of Imp and/or β-integrin were observed (**Figure 36**), showing that the re-localization of β-integrin upon changes in cell morphology is distinct from the re-localization of Imp.

As granules of β-integrin are indicative of sites of FAC formation (Pereira *et al*. 2011), we presume that Imp is not localized to FACs in cultured haemocytes. Previous research has shown that integrin binding to the ECM substrate results in mechanical restructuring of the intracellular actin cytoskeleton, which acts as a trigger for mRNA and ribosome recruitment to FACs (Chicurel *et al*. 1998). This suggests that Imp does not play a role in recruitment of mRNAs to FACs upon integrin binding to the ECM. It would be interestingly to analyse the nature of Imp granules as mammalian IMP1 has been shown to associate with specific mRNAs in stress granules to positively regulate their stabilization during cellular response to stress (Stöhr *et al*. 2006). The rounded-up morphology of haemocytes and S2R+ cells could be indicative in a change in cellular morphology, due to cellular stress, which could trigger the localization of Imp into stress granules. However, characterization of the molecular composition of IMP1-containing granules in human embryonic kidney (HEK) cells showed that IMP-1 granules are distinct from stress granules or cytoplasmic foci containing the mRNA decay machinery, termed processing-bodies (P-bodies) (Jønson *et al*. 2007). This could be tested by co-localizing Imp with stress granule and P-body markers in haemocytes.

6.3.3 Lack of phenotype in *imp* loss-of-function haemocytes and border cells

Haemocytes expressing RNAi against Imp behaved as wildtype (**Figure 30**), suggesting that either knockdown of Imp expression has no effect on haemocyte motility/behaviour, or that our RNAi treatment was not effective enough to reveal a phenotype. We propose the latter, as we did not observe a dramatic reduction in the level of Imp staining in cultured haemocytes expressing Imp RNAi, and residual Imp protein was detectable (**Figure 38**). However, RNAi against Imp was effective at knocking down exogenous Imp-GFP, suggesting that the hairpin works, even if residual Imp-GFP was detectable at low levels (**Figure 29A & D**). Studies to characterize protein functions in haemocytes *in vivo* have utilized either dominant-negative proteins or mutants to generate a loss-of-function against the proteins of interest (Stramer *et al*. 2005; Stramer *et al*. 2010; Tucker *et al*. 2011; Evans *et al*. 2013; Evans *et al*. 2015), as RNAi hairpins against many different proteins appear ineffective at knocking down their targets (Will Wood – personal communication).

Haemocyte motility cannot be observed in *imp* null or hypomorphic mutant embryos as these embryos die before the onset of haemocyte specification (Boylan *et al*. 2008). Our attempts to generate *imp* mutant embryonic haemocytes by MARCM failed, which we attribute to the short time window available for haemocytes to express the GFP marker following heat shocks and subsequent recombination events. Therefore, to examine the effects of Imp depletion in haemocytes, MARCM analysis could be carried to generate *imp* mutant haemocyte clones in pupal haemocytes, as previously demonstrated (Moreira *et al*. 2013).

Similarly, we failed to observe border cell phenotypes by expression of RNAi against targets known to be required for border cell migration, including Rac1 and Hrp48 (Murphy & Montell 1996; Mathieu *et al*. 2007). It was therefore not surprising that we did not observe any effects on border cell migration by expression of an RNAi hairpin against Imp. A recent RNAi screen to identify regulators of border cell motility was successfully in identifying border cell phenotypes by co-expression of Dicer, which increases the efficiency of RNAi hairpin processing (Luo *et al*. 2015). Further attempts to knockdown Imp by RNAi could incorporate the expression of Dicer, to increase RNAi efficiency.

We cannot exclude the possibility that RNAi against Imp is effective and that depletion of Imp expression has no effect on haemocyte motilty. RBPs often function in large RNP complexes containing many different RBPs, some of which may act redundantly. Depletion of Imp levels, together with those from other components of such RNPs, may reveal the role of Imp within haemocytes. IMP1, the chicken homologue of Imp, represses the translation of *β-actin* mRNA at the leading edge of cultured migratory cells, until IMP1 is repressed upon phosphorylation by Src kinase (Hüttelmaier *et al*. 2005). If Imp is also functioning as a translational repressor in haemocytes, then although depletion of Imp may cause increased translation of specific mRNAs, the excess protein may not reach a level high enough to induce an aberrent effect on haemocyte motility. In contrast, overexpression of Imp could prevent the translation of mRNAs whose protein products are essential for cell motility, producing the effects seen in haemocytes overexpressing Imp. However our finding that levels of Actin42A (β-actin) protein, or mRNA, were not affected by Imp depletion in S2R+ cells (**Figure 39**) suggests that, at least *in vitro*, Imp does not regulate the stability or translation of *actin42A* mRNA (although this may not be applicable to haemocytes *in vivo*).

Knockout of Imp expression in migratory border cells did not appear to impede their migration through the egg chamber (**Figure 33C**), suggesting that Imp is not required for cell migration in this system. However, we failed to generate full mutant border cell clusters by MARCM, and so only examined downregulation of Imp in mixed clusters that contained 2-3 *imp* mutant cells in a cluster of 6-10 border cells (**Figure 33C**). Therefore, we cannot exclude

the possibility that, due to the collective nature of border cells, wildtype cells are able to compensate for the loss of Imp in mutant cells.

Border cells at the front of the cluster must extend protrusions to drive their migration through the nurse cells, to the oocyte border (Montell 2003). Mixed border cell clones containing *imp* mutant cells at the front of the cluster showed normal progression of migration through the egg chamber, suggesting that these cells were able to drive migration of the cluster. However, it has also been shown that border cells have the capacity to move around within the cluster, with cells at the front sometimes moving around the outside of the cluster to take up position at the rear (Prasad & Montell 2007). Thus we cannot confidently conclude that mutant cells at the front of the cluster are capable of driving migration, and are therefore functioning as wildtype.

We frequently observed clusters, in which two *imp* mutant border cell clones in direct contact were present at the front of the cluster. These cells were also able to maintain contact with each other throughout migration as we often observed *imp* mutant border cell clones in contact at the oocyte border, upon completing their migration. This finding suggests that Imp does not play a significant role in the establishment and maintenance of cell-to-cell contacts.

6.4 Identification of potential candidate mRNAs for regulation by Imp

6.4.1 Global levels of *β-actin* mRNA and protein are unaffected by downregulation of Imp in cultured cells

As previously discussed in section 6.2.1, our results suggest that the actin cytoskeleton of haemocytes *in vivo* is regulated in a different way to that of haemocytes cultured on a 2D surface. This suggests that the cytoplasmic regulation of *actin* mRNAs may also differ in motile cells *in vivo*, compared with cultured cells.

We showed that Imp binds the 3'UTR of *actin42A* (*β-actin*) mRNA (**Figure 34A**), indicating that it may indeed be a target of Imp. However, we did not observe a change in either global mRNA or proteins levels of *actin42A* in Imp-depleted S2R+ cells (**Figure 39**), consistent with recent reports (Hansen *et al*. 2015). Previous findings show that knockdown of the dImp orthologue IMP1 does not cause a change in *β-actin* mRNA or protein levels, but instead results in its de-localization and a subsequent loss of cell polarity (Ross *et al*. 1997; Shestakova *et al*. 2001; Oleynikov & Singer 2003). We may, therefore, not expect to see a change in the levels of actin upon Imp-depletion, but rather, a change in its cellular distribution.

We found that overexpression of Imp in haemocytes *in vivo* reduced the overall speed of their migration, both during random migration and directed migration to wounds, as well as inhibiting contact repulsion behaviour. Compared to control haemocytes, haemocytes overexpressing Imp re-polarized upon receiving a wound cue, despite exhibiting a significant reduction in directionality to the wound site (**Figure 26**). Previous studies of chicken embryonic fibroblasts (CEFs) show that overexpression of IMP1 causes a significant decrease in fibroblast speed, although their directionality was unaffected (Farina *et al*. 2003). *β-actin* mRNA was not de-localized in these cells (Farina *et al*. 2003). In contrast, treatment of CEFs with antisense oligos against the zipcode of *β-actin* mRNA, that prevent IMP1 binding, resulted in the delocalization of the mRNA. While the migratory speed of these cells was not affected, their directionality and persistence were significantly decreased (Shestakova *et al*. 2001).

We did not observe a significant change in the localization of actin in haemocytes overexpressing Imp, based on the distribution of moesin-GFP in haemocytes (**Figure 12**). However, as IMP1 acts as a translational repressor of *β-actin* mRNA (Hüttelmaier *et al*. 2005), we may expect that an increase in Imp levels in haemocytes could cause a decrease in the levels of *β-actin* protein. If this is the case, *β-actin* mRNA would be locally translated as expected, but at a reduced rate, which may impede the formation of lamellipodial protrusions. This could account for the reduction in haemocyte speed that we observed upon Imp overexpression, although we did not observe significant changes in the structure of lamellipodial protrusions (**Figure 12**).

6.4.2 Imp may alter actin dynamics by regulating the mRNAs of actin-regulatory proteins

Interestingly, Imp depletion caused a reduction in the amount of filamentous actin, and a subsequent increase in actin monomers, in S2 cells (Hansen *et al*. 2015). This finding suggests that Imp may play a role in the regulation of transcripts that encode proteins required for regulation of the actin cytoskeleton. A role for mammalian IMP1 in the regulation of mRNAs of actin regulatory proteins has been demonstrated. For example, the mRNA of the actin depolymerizing protein Cofilin is localized at the leading edge of cultured migratory cells by IMP1 (Maizels *et al*. 2015). Our observation that, in Imp-depleted S2R+ cells there is a change in the levels of the mRNA encoding Profilin, a protein required for the formation of filamentous actin, provides further evidence that Imp is likely to regulate the mRNAs of actin-regulatory proteins (**Figure 39**).

6.4.3 Characterization of Imp binding sites in the 3'UTR of *β-actin* mRNA

We showed that mutation of the three predicted Imp binding elements (UUUAU/C) (Munro *et al*. 2006) within the *actin42A* (*β-actin*) 3'UTR significantly reduced the interaction between Imp and *act42A* mRNA (**Figure 35B**). However, further qualitative assays are required to characterize the binding of Imp to these elements.

As mutation of the three IBEs in the *actin42A* 3'UTR resulted in only a slight reduction in PTB binding, compared with the significant reduction in the binding of Imp (**Figure 35B**), other regions in the 3'UTR should mediate the interaction with PTB. Consistent with this, we found polypyrimidine-rich regions, to which PTB binds, that were located outside of the IBE-containing region of the *act42A* 3'UTR. This shows that other regions of the *actin42A* 3'UTR, besides the three predicted IBEs, are required to mediate the binding of other RBPs, supporting the idea that 3'UTR regions function as a scaffold on which different RBPs assemble to form a ribonucleoprotein complex (RNP).

By aligning the 3'UTR of chicken *β-actin* and *Drosophila act42A* mRNAs we identified regions of conserved nucleotides within, and directly up- and downstream of, the 111 nucleotide region that contains the three predicted IBEs (**Figure 43** – IBEs highlighted in red). A 54 nucleotide sequence, which is located at the 5' end of the chicken *β-actin* 3'UTR, termed the zipcode, has been shown to mediate the binding of IMP1 to *β-actin* mRNA (Ross *et al*. 1997). Interestingly, no zipcode could be identified in the 111 nucleotide region containing the IBEs in the *act42A* 3'UTR. However, we identified a conserved region of seven nucleotides, CATTCCA, located seven nucleotides upstream of the first predicted IBE site in the *actin42A* 3'UTR (**Figure 43** – highlighted yellow).This short motif shared the highest level of nucleotide conservation observed between the sequences of the *β-actin* and *actin42A* 3'UTRs.

The 3'UTR of chicken *β-actin* contained two predicted IBEs, which are located 28 and 430 nucleotides downstream of the zipcode. Neither of these IBEs aligned with the 111 nucleotide region containing the 3 IBEs in the *actin42A* 3'UTR. However, although the IBEs themselves did not appear to be conserved, we did observe conserved sequences of either three or four nucleotides that were located in the regions downstream of each predicted IBE (**Figure 43** – highlighted in blue) Conservation of the region containing the three IBEs supports the idea that these sequences participate in the formation of conserved secondary structure that may assist in mediating Imp/IMP1 binding and it would be interestingly to carry out secondary structure analysis of this region, to determine the functionality of the conserved elements described here.

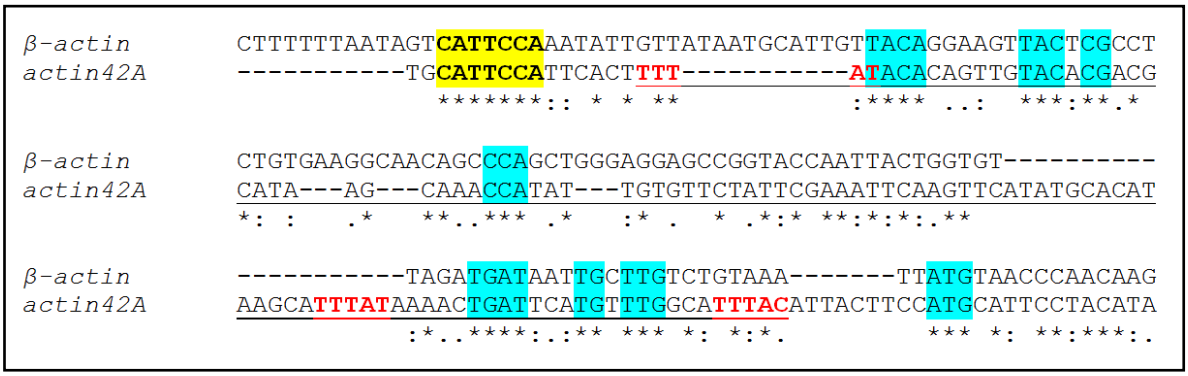

Figure 43: Conservation of primary sequence between chicken and *Drosophila actin* mRNAs Alignment of the 3'UTRs of chicken *β-actin* and its *Drosophila* homologue *actin42A* show that they contain regions of conserved primary sequence (highlighted in blue) around the three predicted Imp binding elements (IBEs) (highlighted in red), which includes a conserved motif of seven nucleotides (highlighted in yellow) located seven nucleotides upstream of the first IBE.

Since the discovery of the zipcode region in chicken *β-actin* mRNA, there have been several attempts to identify specific nucleotides within its sequence, that are required for IMP1 binding (Ross *et al*. 1990; Chao *et al*. 2010; Hafner *et al*. 2010; Pater *et al*. 2012). An ACACCC motif at both the 5' and 3' of the zipcode are required for IMP1 binding, as mutation of these motifs abolishes IMP1 binding (Ross *et al*. 1997). The third and fourth KH-domains of IMP1 were shown to recognize regions within the first 28 nucleotides of the zipcode, which is sufficient for IMP1 to *β-actin* mRNA (Chao *et al*. 2010). A CGGAC motif is required for binding of KH3 at the 5' of the zipcode, while a C/A-CA-C/U motif at the 3' was required for binding of KH4. Interestingly, the orientations of these two motifs within the 3' UTR are interchangeable within the 3'UTR (Pater *et al*. 2012). The secondary structure formed by both the rat and chicken zipcode is conserved, forming a well-defined stem loop structure, with the ACACCC motif residing in the terminal loop of the stem loop (Kim *et al*. 2015). IMP1 binding to the zipcode depends on this stem loop, showing that secondary structure is critical for IMP1 binding to *β-actin* mRNA (Kim *et al*. 2015).

Previous research has yet to determine if the zipcode of chicken *β-actin* is conserved in *Drosophila act42A* mRNA. We therefore attempted to identify any conservation among the zipcode of chicken *β-actin*, human *β-actin* and the 3'UTR of a*ctin42A* (**Figure 44A**). Two five nucleotide regions were highly conserved in all three, which included the ACACCC motif that has previously been shown to be required for IMP1 binding (Ross *et al*. 1997) and ACAAA, of which ACA has been shown to participate in binding of IMP1 (Chao *et al*. 2010) (**Figure 44B**). Although the ACACCC motif is conserved in the 3'UTR of *actin42A*, we showed that this motif alone, and the regions directly up- and downstream of it, are not sufficient for Imp to bind the *actin42A* 3'UTR with high affinity, as mutation of all three UUUA(Y) motifs

(predicted IBEs) within the 3'UTR, even if the ACACCC motif and the regions directly up- and downstream of the motif were wildtype, significantly decreased the binding of Imp (**Figure 35B**).

Chicken *β-actin* 3'UTR zipcode:

5'UAAACCGGACUGUUACCAACACCCCACACCCCUGUGAUGAAACAAAACCCAUAAAUGC 3'

Human *β-actin* 3'UTR zipcode:

5'TAGGCGGACTATGACTTAGTTGCGTTACACCCTTTCTTGACAAAACCTAACTTGCGCAGAAAAC
AAGATGAG 3'

***Drosophila actin42A* 3'UTR:**

5'GCAGUAGUCGG(G)CUGGGCGUGGUCGUUCCUCAUCG(A)ACACACCCAUUGCAGACAAAGG
AUGGGAGUCAAAAGUAUUGGGCAUGAGUACAUUAAUACCGGGAGCAGGCGCACAACACUUCC
GCUCCUUCAGAAGAAUGCAUCCAUUCACUUUUAUACACAGUUGUACACGACGCAUAAGCAAAC
CAUAUUGUGUUCUAUUCGAAAUUCAAGUUCAUAUGCACAUAAGCAUUUAUAAAACUGAUUCAU
GUUUGGCAUUUACAUUACUUCCAUGCAUUCCUACAUAUGUAUUAAAAGCAAACUUACCAUACC
ACUAAAAUACUUGUAACCGCUUCUUAAUAAUAAAGCGACGAAAAGAACUG 3'

Primary sequences implicated in ZBP1/Imp binding:

- ACACCC (Ross *et al.* 1997)
- ACA (Chao *et al.* 2010) ***β-actin* 3'UTR**
- CGGAC (Pater et al. 2012)
- C/A-CA-C/U (Pater *et al.* 2012)
- CAUA/U/C (Hafner *et al.* 2010)
- UUUAU/C (IBE) (Munro *et al.* 2006)

```
Chicken          TAAACCGGACTGTTACCAAC---ACCC---ACACCCCTGTGATGAAACAAAAC-------
Human            -TAGGCGGACTATGACTTAG---TTGCGTTACACC-CTTTCTT--GACAAAAC-------
Drosophila       ----CTGGGCGTGGTCGTTCCTCATCGAACACACCCATTGCA-G--ACAAAGGATGGGAG

                       **.*    :* ::    :      ***** .*   :    *****.

Chicken          CCAT---AAATG
Human            -CTA---ACTTG
Drosophila       TCAAAAGTATTG
                  *::   :.:**
```

Figure 44: Identification of conserved *β-actin* mRNA zipcode motifs in the 3'UTR of *Drosophila actin42A* mRNA

The 3'UTR of human and chicken *β-actin* mRNAs contain a conserved region of approximately 50 nucleotides, termed the zipcode, which contains elements required for IMP1 binding. The zipcodes of human and chicken *β-actin* mRNA and the entire 3'UTR of *actin42A* mRNA (*Drosophila β-actin* homolog) were aligned to identify conserved zipcode regions in the *act42A* 3'UTR. (**A**) Shows the location of motifs within the chicken and human zipcodes implicated in IMP1 binding, and the corresponding motif within the *actin42* 3'UTR, if present. (**B**) An alignment of chicken and human zipcodes, and the region containing conserved zipcode motifs within the *actin42* 3'UTR. Sequences conserved in only the human and chicken zipcodes are highlighted in yellow, while sequences conserved in all three are highlighted in red.

The RNA-binding protein Muscleblind-like splicing regulator 1 (MLP1), a human homologue of *Drosophila* Muscleblind, has been shown to regulate both *β-actin* and *integrin-α3* mRNAs by binding to the conserved zipcode within their 3'UTRs (Adereth *et al*. 2005). Deletion of the conserved ACACCC motif within the zipcodes of the *integrin-α3* and *β-actin* 3'UTRs, abolished MLP1 binding to both *β-actin* and *integrin-α3* (Adereth *et al*. 2005). However, the conserved ACACCC motif is not present within the 3'UTR of *Drosophila β-integrin* mRNA, or any of the five α-integrins (data not shown). Our observations that Imp binds the 3'UTR of *β-integrin* in the absence of the ACACCC motif (**Figure 34B**) suggests that either dImp binds to different RNA motifs to those characterized for IMP1, or that the ACACCC motif assists in the formation of conserved secondary structures that are achieved by different primary sequences in *Drosophila* transcripts.

Imp binds with high affinity to the 3'UTR of *β-integrin*, while only a residual binding was observed between Imp and the *β-integrin* 5'UTR and coding sequence (CDS) (**Figure 34B**). While the *β-integrin* 3'UTR contains 13 predicted IBEs, the 5'UTR does not contain any and the CDS contains only one IBE (data not shown). This suggests that a basal level of Imp binding exists to regions of RNA that do not contain predicted IBEs. Consistent with this idea, mutation of all three predicted IBEs in the 3'UTR of *act42A* reduced Imp binding to levels comparable to that of the *β-integrin* 5'UTR and CDS, suggesting that mutation of these sites reduces Imp binding to a basal level (compare **Figures 34B & 35B**). Reduction of Imp binding to a basal level, upon mutation of the three IBEs, supports the idea that the predicted zipcode, which appears to be located at the 5' end of the *act42A* 3'UTR, is not required for Imp binding (**Figure 35A**). However, to confirm that the region containing conserved zipcode nucleotides is not required for Imp binding to the *act42A* 3'UTR, these conserved nucleotides could be mutated to determine the effects on Imp binding.

6.4.4 Imp binds *β-integrin* mRNA but does not regulate its stability

Interestingly, overexpression of Imp produces a very similar phenotype to that observed upon depletion of the βPS-integrin subunit, encoded by *myospheroid* (*mys*) (herein referred to as β-integrin), in *Drosophila* haemocytes (Comber *et al*. 2013) (**Figures 26-28**). Integrins are cell surface receptors required for cellular adhesion to the ECM and for transducing extracellular signals to regulate cell motility, differentiation and proliferation (Giancotti & Ruoslahti 1999). As the β-integrin subunit forms hetero-dimers with all five *Drosophila* α-integrin subunits, removal of the β-integrin subunit disrupted the formation of the majority of integrin receptors within *Drosophila* (Comber *et al*. 2013). Zygotic knockout of β-integrin results in a significant reduction in the speed of both random and directed haemocyte migration to wounds, as well as a loss of contact repulsion behaviour (Comber *et al*. 2013),

similar to the effects observed in haemocytes overexpressing Imp (**Figures 26- 28**) (see section 6.3.1 for an evaluation of this phenotype).

We confirmed that Imp binds with high affinity to the 3'UTR of *β-integrin* mRNA, compared with the 5'UTR and coding regions (**Figure 34B**), which is consistent with the finding that Imp is associated with *β-integrin* mRNA in *Drosophila* S2 cells (Hansen *et al.* 2015). The effects of β-integrin knockdown in haemocytes are consistent with the effects that we observed upon overexpressing Imp, suggesting that Imp may play a role in the regulation of β-integrin by either destabilizating or translationally repressing *β-integrin* mRNA. We therefore attempted to rescue the motility defects caused by the overexpression of β-integrin in haemocytes, by overexpressing Imp. However, we observed no changes in the severity of β-integrin overexpression upon co-expression of Imp and β-integrin, suggesting that Imp does not destabilize or repress the translation of *β-integrin* mRNA in haemocytes in this assay (**Figure 40**).

Although we were unable to detect β-integrin protein levels in Imp-depleted cells by Western blot (Appendix 6), we show that knockdown of Imp has no effect on the level of *β-integrin* mRNA, compared with controls (**Figure 39**), supporting the findings of our *in vivo* genetic interaction assay (**Figure 40**). Upon knocking down β-integrin expression in S2R+ cells we observed that the cells became highly rounded, failed to produce lamellipodial protrusions and then detached from the substrate (data not shown). However, we did not observe any changes in the morphology of Imp-depleted S2R+ cells, demonstrating that Imp does not positively regulate β-integrin protein levels in these cells. Taken together, these findings suggest that Imp does not regulate the stability of *β-integrin* mRNA, which contrasts with assays showing that downregulation of IMP1 in human embryonic stem cells (hESCs) results in depletion of *integrin-β5* mRNA, due to an increased turnover of *integrin-β5* in the absence of IMP1 (Conway 2014). This supports the idea that Imp may play different roles in the regulation of transcripts in different cell types.

The result of our genetic interaction assay suggests that Imp does not regulate *β-integrin* mRNA in haemocytes, despite binding to its 3'UTR (**Figure 34B**). However, other alternative explanations are plausible. RBPs regulate mRNAs in functional RNP complexes, containing other RBPs (Martin & Ephrussi 2009). Overexpression of Imp alone may therefore not rescue the effects of β-integrin overexpression in haemocytes, due to a lack of other RBPs, in which to form a functional regulatory complex. It is also possible that the levels of Imp in haemocytes were too low to counter the effects of β-integrin overexpression. Alternatively, Imp may play a different role in the regulation of *β-integrin* mRNA. For example, it may mediate its localization within the cytoplasm. In all these cases, overexpression of Imp may

not have an impact on the migratory defects observed by overexpressing β-integrin in haemocytes, or *β-integrin* mRNA levels upon Imp depletion in S2R+ cells.

6.4.5 Imp may not be required for local translation of *β-integrin* mRNA in haemocytes

Interestingly, integrin mRNAs have been shown to be localized by other RBPs in other cell types. Human Muscleblind-like splicing regulator 1 (MLP1), a homologue of *Drosophila* Muscleblind, localizes *integrin α3* mRNA to the protrusions of human carcinoma cell lines *in vitro*, where it is locally translated (Adereth *et al*. 2005). Overexpression of MLP1 resulted in an increase in both *integrin α3* and *β-actin* mRNA and protein levels, as well as an increase in cell motility, while knockdown of MLP1 resulted in the loss of integrin α3 protein localization in cell protrusions (Adereth *et al*. 2005). This confirms that mRNAs encoding integrins have the potential to be localized and locally translated in the protrusions of cultured cells, although this may not be the case *in vivo,* or for other migratory cells. In contrast, we observed that overexpression of Imp *in vivo* decreased the motility of haemocytes (**Figures 26 & 27**) and show that this phenotype resemble the effects seen by knocking down expression of integrin complexes (Comber *et al.* 2013). However, compared with human carcinoma cell lines (Adereth *et al.* 2005), overexpression of β-integrin in haemocytes severely inhibits haemocyte motility (**Figure 40**), highlighting differences in the regulation of migration between these cell types. These findings suggest that if Imp does regulate the localization and/or translational of *β-integrin* mRNA, it does so in a different way to other RBPs that have been shown to localize *integrin* mRNAs in motile cells.

Previous studies showed that both *integrin α3* mRNA and protein co-localize in distinct granules with MLP1, which regulates the translation of *integrin α3* mRNA (Adereth *et al*. 2005). IMP1 and *β-actin* mRNA also co-localize at the periphery of cultured migratory fibroblasts, where the mRNA is locally translated (Hüttelmaier *et al*. 2005). Therefore, newly synthesized proteins from the pools of localized mRNA have the potential to co-localize with the regulatory RBP. If Imp plays a role in localizing *β-integrin* mRNA to regions of the cytoplasm in which it is locally translated, we would expect to see co-localization of Imp and β-integrin proteins in the regions in which *β-integrin* mRNA is localized and translated. However, we did not observe significant co-localization of Imp and β-integrin in either cultured haemocytes (**Figure 38A**) or migratory border cells (**Figure 37F**). While β-integrin was localized in distinct granules within the border cell cluster, Imp was not present in these granules (**Figure 37F**). If *β-integrin* mRNA is locally translated at regions of β-integrin protein enrichment, then it is unlikely that Imp plays a role in its translational regulation. However*, β-integrin* mRNA may not be locally translated, but the protein trafficked to regions of the cell where its function is required. It would be interesting to carry out *in situ hybridizations* to

detect the localization of *β-integrin* mRNA in both cultured haemocytes and border cells, to determine if it localizes with either Imp or β-integrin protein.

6.4.6 Depletion of Imp in *Drosophila* S2R+ cells suggests that Imp differentially regulates mRNAs targets, including *profilin*, in different cell types.

Our findings suggest that Imp may play a role in the stabilization of *profilin* mRNA, as *profilin* mRNA levels were increased in Imp-depleted S2R+ cells (**Figure 39B**). We also showed that Imp binds with high affinity to the *profilin* 3'UTR (**Figure 34A**), as previously reported by Medioni *et al*. 2014. Profilin is required for the formation of filamentous actin by binding G-actin monomers and presenting them to elongating actin filaments (Carlsson *et al*. 1977). Profilin also plays a role in promoting cell adhesion as knockdown of Profilin in S2 cells inhibits cell spreading on ConA and results in cell detachment (Rogers *et al*. 2003). Profilin increases the adhesiveness of cells in a variety of ways, including recruitment of integrin receptors to the cell surface (Moldovan *et al*. 1997), and increasing the expression level of R-cadherin in endothelial cells to aid adheren junction formation (Zou *et al*. 2009). It would be interestingly to determine if overexpression of Imp in haemocytes *in vivo* causes a decrease in Profilin levels, which could account for the observed reduction in velocity and loss of contact inhibition of these cells. This may be consistent with our observation that Imp overexpression in haemocytes phenocopies knockdown of β-integrin, as Profilin-depleted S2 cells show a loss of adhesion phenotype, identical to that of β-integrin knockdown (Rogers *et al*. 2003). Moreover, loss of Profilin in gastric carcinoma tissue caused a reduction in integrin-β1 levels (Cheng *et al*. 2015).

In addition, knockdown of Profilin expression in cultured *Drosophila* haemocytes increases their phagocytic activity, suggesting that Profilin negatively regulates phagocytosis (Pearson *et al*. 2003). The efficiency of phagocytosis in haemocytes overexpressing Imp *in vivo* could be analysed by acridine orange staining of live *Drosophila* embryos, to stain apoptotic bodies and examine their uptake in haemocytes (McCall & Peterson 2004; Evans *et al*. 2013). Alternatively, fluorescently-labelled bacteria could be injected into embryos to assess the phagocytic uptake of haemocytes (Vlisidou *et al*. 2009).

In contrast to our findings in S2R+ cells, a recent study showed that the levels of both *profilin* mRNA and protein are unaffected by Imp knockdown in *Drosophila* S2 cells (Medioni *et al.* 2014). We observed an increase in the level of *profilin* mRNA in Imp-depleted S2R+ cells, suggestive of an increase in Profilin protein levels. If this is the case, we would expect an increase in the level of filamentous actin in these cells. However, Imp depletion in S2 cells revealed a decrease in filamentous actin and no change in global mRNA levels (Hansen *et al*. 2015). This suggests that Imp may play distinct roles within S2 and S2R+ cells, which are

both derived from *Drosophila* embryos (Schneider *et al*. 1972). Although both S2R+ and S2 cells express haemocyte markers, characterization of their transcriptional profiles showed that they express different subsets of genes, so are molecularly different (Celniker *et al*. 2009; Cherbas *et al*. 2011). Their morphologies also differ, as S2R+ cells are more adherent and spread lamellipodial protrusions on glass, while S2 cells are more rounded and do not form protrusions unless plated on Concanavalin A (ConA) (Rogers & Rogers. 2008). *Drosophila* S2R+ cells express the Frizzled receptor, which acts as a receptor in the Wnt signalling pathway, while S2 cells do not (Yanagawa *et al.* 1998). Non-canonical Wnt signalling has been shown to activate actin-regulatory proteins including Rho1, Rac1 and Profilin (Komiya & Habas. 2008), which may reflect the observed differences in S2 and S2R+ morphology. The above studies suggest that S2R+ and S2 cells regulate their cytoskeleton in different ways. Given the differences between these two cell types, it is possible that regulation of *profilin* mRNA stability by Imp is required in S2R+ cells, but not in S2 cells. This finding has implications for the applicability of regulatory mechanisms identified in one cell type applying to another.

6.4.7 Low affinity mRNA-Imp interactions could not be identified by RNA-immunoprecipitation

We show that Imp-GFP protein was successfully precipitated from *Drosophila* embryos, using GFP-nanotraps (**Figure 41A**). However, we failed to detect any mRNAs that were significantly enriched with Imp (**Figure 41 B & C**). As controls, we tested if mRNAs known to associate with Imp and PTB in the oocyte could be identified in our RNA-immunoprecipitation (RIP) assay, including *gurken* and *oskar* mRNAs. (Geng & Macdonald 2006; Munro *et al*. 2006; Besse *et al*. 2009; McDermott & Davis 2013). We observed that *oskar* and *bicoid* mRNAs are significantly enriched with PTB in the two biological replicates performed.

While *oskar* mRNA has been shown to associate with PTB (Besse *et al*. 2009), *bicoid* had not previously been identified as PTB target so this result was surprising. PTB and *oskar* mRNA are highly enriched at the posterior of the oocyte (Besse *et al*. 2009) while, in contrast, *bicoid* mRNA forms a gradient with a high concentration at the oocyte anterior (St Johnston *et al*. 1989). One possibility is that, while the majority of *bicoid* mRNA is concentrated at the oocyte anterior, PTB may associate with residual *bicoid* mRNA at the posterior or during transport of this mRNA through the nurse cells, to repress its translation and ensure that mis-expression of Bicoid protein does not occur during transport. PTB is necessary to repress the translation of *oskar* mRNA during its transport to the oocyte posterior (Besse *et al*. 2009), showing that PTB has a translational repressor function.

Although *gurken* mRNA was enriched with PTB, it was present at much lower levels compared with *bicoid* and *oskar* mRNA (**Figure 41B & C**).

Our RIP from ovaries showed that, while high-affinity mRNA-protein interactions can be identified, it is difficult to identify lower-affinity interactions, or those interactions in which the mRNA is not significantly enriched with the RBP of interest. Other attempts to identify Imp-associated mRNAs by RIP show that the mRNAs associated with Imp were highly enriched. For example, the control mRNAs *rp49* and *GAPDH* were shown to be 4 fold and 8-fold enriched with Imp, respectively, compared with controls in the testis stem cell niche, while *unpaired* (*upd*) mRNA was ~208-fold enriched, as shown by RIP and subsequent qRT-PCR analysis (Toledano *et al*. 2012). Further analysis showed that *upd* mRNA is stabilized by Imp in the testis stem cell niche (Toledano *et al*. 2012).

A RIP and subsequent RT-PCR analysis to identify mRNAs associated with Imp in the *Drosophila* brain revealed that of *profilin*, *actin42A*, *arp2*, *arp3*, *rhoA* or *cofilin* mRNAs, only *profilin* was significantly enriched with Imp (Medioni *et al*. 2014). This is consistent with our finding that Imp binds the 3'UTR of *profilin* mRNA with higher affinity than other transcripts, including *act42A* (**Figure 34A**), and suggests that other Imp-mRNA interactions are not detectable or are washed out during the RIP procedure. A recent RIP and subsequent RNA-seq screen to identify mRNAs associated with Imp in *Drosophila* S2 cells also failed to detect *actin42A* (*β-actin*) mRNA (Hansen *et al*. 2015). However, when individual-nucleotide resolution cross-linking and Immunoprecipitation (i-CLIP) was carried out, in which RNAs and RBPs are cross-linked in RNP complexes prior to IP, *actin42A* mRNA was detected. However, it was not significantly enriched compared with other mRNAs including *profilin*, *Cdc42* and *Rho1*, suggesting that it is washed out in standard RIP protocols (Hansen *et al*. 2015). This suggests a low affinity association between Imp and *actin42A* mRNA, compared with other mRNA targets, and highlights difficulties in identifying low affinity mRNA-RBP interactions using standard RIP techniques.

While previous research shows that *profilin* mRNA is a target of Imp (Medioni *et al*. 2014; Hansen *et al*. 2015) and can be identified by RIP and subsequent RT-PCR analysis, we failed to detect an enrichment of *profilin* mRNA with Imp in all of our RIP assays (**Figures 41 & 42**). This was surprising, as we found that Imp binds the 3'UTR of *profilin* mRNA with high affinity (**Figure 34**) and *profilin* mRNA levels are increased in Imp-depleted cells (**Figure 39B**), which is suggestive of an interaction between *profilin* and Imp. Although Imp may not be associated with *profilin* mRNA in either haemocytes or the germline of the oocyte, we cannot exclude the possibility that we failed to reproducibly identify mRNAs enriched with Imp for technical reasons.

The possibility of complex re-modelling within the embryonic extract, and the potential loss of low affinity interactions during subsequent washing steps, led us to carry out formaldehyde-based cross linking on whole embryos (as described in Liu *et al*. 2009), prior to generating the embryonic extracts. After precipitation, the cross-linking was reversed by heating before subsequent RNA purification. However, it is possible that the crosslinking was not reversed, which could have interfered with RNA purification or subsequent PCR steps. Alternatively, the formaldehyde may have failed to penetrate intact haemocytes within embryos, leading to a loss of low affinity mRNA-Imp interactions. All wash steps of our initial RIPs, performed without cross-linking, were carried out with a low salt concentration (150 mM NaCl) to preserve low affinity interactions. However, upon the addition of cross-linking we performed all washes with a higher salt concentration (1 M NaCl), to reduce non-specific binding of transcripts. However, if cross-linking was not fully effective, low affinity mRNA-Imp interactions may have been washed out prior to RNA purification.

Although we show that Imp was successfully precipitated from embryos by RNA immunoprecipitation (**Figure 41A**), the level of bound Imp-GFP represented only a small fraction of the total Imp-GFP present in the embryonic extract (**Figure 41A** – Western blot shows 2% of total input and unbound protein vs. 50% of the total bound protein), suggesting that the pulldown may have been inefficient. Associated mRNAs may therefore not appear significantly enriched, compared with wildtype controls. Another possibility is that we are unable to identify mRNAs enriched with Imp because of a high level of background, caused by a large amount of non-specific binding of mRNAs to the mRNA-RBP-bead complex. High levels of non-specific mRNA binding may be due to the design of our assay, in which Imp-GFP is expressed in a small population of cells (~700) in the embryo and so, to acquire a sufficient level of Imp-GFP protein, a high number of embryos were used. This is likely to result in a very high concentration of total protein and mRNA, compared with total Imp-GFP. Non-specific binding of mRNAs could therefore mask the levels of mRNAs specifically associated with Imp-GFP.

In conclusion, the RIP assay requires optimization. While RIP and subsequent qRT-PCR analysis of candidate mRNAs appear successful in identifying mRNAs that are highly enriched with RBPs of interest, such as *bicoid* and *oskar*, it is difficult to detect lower affinity mRNA-RBP interactions. To detect low affinity interactions, global mRNA levels should be compared between both the input and bound fractions, by either RIP-Chip or RNA-seq following RIP, to set a minimum fold-change threshold, over which a specific mRNA is then considered enriched with an RBP.

Conclusions

1) Evaluation of haemocytes and border cells as model systems to study the role of RNA regulation in cell motility:

- Markers used to label cells and follow their *in vivo* migration could have an impact on cell motility, as we found that haemocytes expressing different markers migrated at different speeds. This highlights the importance of using appropriate controls when following motile cells overexpressing proteins of interest. This also demonstrates that even expression of non-functional proteins could disrupt normal functions within cells of interest.

- In contrast to current research carried out in cultured migratory cells, we found that actin was not enriched at the leading edge of haemocytes *in vivo*. As actin protein is not enriched at the leading edge, it is unlikely that *β-actin* mRNA is locally translated at this region in haemocytes *in vivo*. However, enrichments of actin were seen at the periphery of some haemocytes cultured *ex vivo*, particularly in those that were induced to polarize and migrate with the addition of ecdysone. This highlights striking differences in the regulation of the actin cytoskeleton in a single cell type when migrating *in vivo*, within the context of living organism, compared with an *ex vivo*, two-dimensional type of cell migration.

- We show that RNAi is inefficient in both haemocytes and border cells. Attempts to generate *imp* mutant border cells using MARCM showed that generation of whole *imp* mutant border cells was challenging. In contrast, dsRNA treatment of cultured cells resulted in highly efficient knockdown of the proteins of interest. This highlights the challenges faced when attempting to perform loss-of-function analysis *in vivo*, compared to *in vitro* approaches.

2) Analysis of tools generated to investigate RNA regulation in cell motility:

- Attempts to examine the localization of *β-actin* and *arp2/3* subunit mRNAs in haemocytes *in vivo* using the MS2 system failed. We confirmed that both components of the system required for detection of mRNAs are expressed in haemocytes. However, as their expression fails to highlight the localization of mRNAs previously characterized using this system, we conclude that either some of our MS2 transgenes do not work, or that the signal generated by the MCP bound to the MS2-tagged target remains under detection levels.

- The RBPs Imp, Hrp48 and PTB show distinct patterns of localization in *Drosophila* haemocytes, suggesting that they may play functionally different roles in the regulation of

RNAs in haemocytes. None of the above RBPs were enriched at the leading edge haemocytes, suggesting that they do not play a role in localizing mRNAs to this region.

3) Evaluating the association of Imp and *β-actin* mRNA:

- Our finding that actin is not enriched at the leading edge of haemocytes, and our observation that Imp was not present at the leading edge strongly suggests that, in contrast to findings in cultured cells, Imp does not regulate the localization and/or local translation of *β-actin* mRNA at the leading edge of haemocytes. Although Imp binds the 3'UTR of *β-actin* mRNA, depletion of Imp in cultured cells did not affect its mRNA or protein levels, showing that Imp does not regulate the stability and/or translation of *β-actin* mRNA in S2R+ cells. However, we cannot rule out the idea that Imp is required for localization of *β-actin* mRNA to specific regions of the cell.

- After confirming that Imp binds *β-actin* mRNA, we identified three sites spanning a 111 nucleotide region in the 3'UTR of *β-actin* (*Drosophila actin42A*) mRNA, that are required for binding of Imp. We show that the conserved ACACCC zipcode motif, which is required for binding of IMP1 to mammalian *β-actin* mRNA, is not sufficient for Imp binding to the *actin42A* 3'UTR.

- Overexpression of Imp in haemocytes results in a reduction of migration speed during development, as well as in directed migration to epithelial wounds, and causes a loss of contact repulsion behaviour. Loss of contact repulsion is indicative of microtubule regulatory defects, as haemocytes are unable to align microtubules arms. Consistent with this, we observed co-localization of Imp with microtubules filaments. We therefore propose that Imp may play a role in the regulation of mRNAs whose products are required to direct microtubule dynamics in haemocytes.

4) Other potential candidate mRNAs for regulation by Imp:

- Imp overexpression in haemocytes *in vivo* causes a similar phenotype to that of β-integrin loss-of-function. We found that Imp binds to the 3'UTR of *β-integrin* mRNA, although Imp and β-integrin do not significantly co-localize in cultured haemocytes, suggesting that either *β-integrin* mRNA is not locally translated at regions of β-integrin protein enrichment, or that Imp is not present in pools of locally translated *β-integrin* mRNA. As β-integrin is enriched at sites of FACs, we propose that Imp does not play a role in local translation of transcripts which may be localized to FACs. Finally, we showed that Imp does not regulate the stability of *β-integrin* mRNA in S2R+ cells.

- Our findings suggest that Imp may negatively regulate the stability of *profilin* mRNA, as *profilin* levels are increased in Imp-depleted cells. Interestingly, previous research shows that the effects of Profilin loss of function in cultured cells is consistent with those seen in β-integrin-depleted cells. As Imp overexpression in haemocytes produced a phenotype similar to that of β-integrin loss-of-function, it would be interesting to determine if the effects seen in haemocytes overexpressing Imp are caused by a reduction in *profilin* mRNA levels.

- Our attempts to confirm the association of Imp and candidate mRNAs *in vivo* by RNA-immunoprecipitation (RIP) and subsequent real time quantitative PCR analysis showed that this approach may be unsuitable for detecting low-frequency and/or low-affinity mRNA-RBP associations. To detect these interactions, global association of mRNAs with RBPs should be determined by RIP-Chip or RIP-seq. Alternatively, individual-nucleotide resolution cross-linking and immuno-precipitation (i-CLIP) could be carried out to preserve *in vivo* mRNA-RBP interactions. In conclusion, the RIP assay requires optimization.

Bibliography

Agaisse H., Burrack L. S., Philips J. A., Rubin E. J., Perrimon N. & Higgins D. E. (2005) Genome-wide RNAi screen for host factors required for intracellular bacterial infection. *Science.* 309(5738):1248-51.

Agaisse, H., Petersen, U.M., Boutros, M., Mathey-Prevot, B., and Perrimon, N. (2003). Signaling role of hemocytes in *Drosophila* JAK/STAT-dependent response to septic injury. *Developmental Cell* 5(3):441–450.

Ai E., Poole DS. & Skop AR. (2009) RACK-1 Directs Dynactin-dependent RAB-11 Endosomal Recycling during Mitosis in *Caenorhabditis elegans. Molecular Biology of the Cell. 20(6):1629-1638.*

Ainger K., Avossa D., Diana AS., Barry C., Barbarese E. & Carson JH. (1997) Transport and Localization Elements in *myelin basic protein* mRNA. *The Journal of Cell Biology*. 138(5):1077-1087.

Arias-Salgado E.G., Lizano S., Sarkar S., Brugge J.S., Ginsberg M.H. & Shattil S.J. (2003) Src kinase activation by direct interaction with the integrin β cytoplasmic domain. *PNAS*. 100(23):13298–13302.

Ashraf SI., Mcloon AL., Sclarsic SM. & Kunes S. (2006) Synaptic Protein Synthesis Associated with Memory is Regulated by the RISC Pathway in *Drosophila*. *Cell*. 124(1):191-205.

Babic I., Sharma S. & Black D.L. (2009) A Role for Polypyrimidine Tract Binding Protein in the Establishment of Focal Adhesions. *Molecular and Cellular Biology*. 29(20):5564-5577.

Bai J., Uehara Y. & Montell D.J. (2000) Regulation of invasive cell behaviour by Taiman, a *Drosophila* protein related to AIB1, a steroid receptor coactivator amplified in breast cancer. *Cell*. 103(7):1047-1058.

Bashirullah A., Halsell S.R., Cooperstock R.L., Kloc M., Karaiskakis A., Fisher W.W., Fu W., Hamilton J.K., Etkin L.D. & Lipshitz H.D. (1999) Joint action of two RNA degradation pathways controls the timing of maternal transcript elimination at the midblastula transition in *Drosophila* melanogaster. *The EMBO Journal*. 18(9):2610-2620.

Bateman J.R., Lee A.M. & Wu C.T. (2006) Site-specific transformation of *Drosophila* via phiC31 integrase-mediated cassette exchange. *Genetics*. 173(2):769-77.

Becalska A.N. & Gavis E.R. (2009) Lighting up mRNA localization in *Drosophila* oogenesis. *Developmen*t. 136(15):2493-2503.

Beccari S., Teixeria L. & Rørth P. (2002) The JAK/STAT pathway is required for border cell migration during *Drosophila* oogenesis. *Mechanisms of Development*. 111(1-2):115-123.

Belaya K. & St Johnston D. (2011) Using the mRNA-MS2/MS2CP-FP System to Study mRNA Transport During *Drosophila* Oogenesis. *Methods in Molecular Biology*. 714:265-283.

Bernardoni, R., Vivancos, V., and Giangrande, A. (1997). glide/gcm is expressed and required in the scavenger cell lineage. *Developmental Biology*. 191(1):118–130.

Bertrand E., Chartrand P., Schaefer M., Shenoy SM., Singer RH. & Long RM. (1998) Localization of *ASH1* mRNA Particles in Living Yeast. *Molecular Cell*. 2(4):437-445.

Besse F. & Ephrussi A. (2008) Translational control of localized mRNAs: restricting protein synthesis in space and time. *Nature Reviews Molecular Cell Biology*. 9(12):971-980.

Besse F., López de Quinto S., Marchand V., Trucco A. & Ephrussi A. (2009) *Drosophila* PTB promotes formation of high-order RNP particles and represses *oskar* translation. *Genes & Development*. 23(2):195-207.

Bhattacharjee S., Renganaath K., Mehrotra R. & Mehrotra S. (2013) Combinatorial Control of Gene Expression. BioMed Research International. Article ID: 407263.

Bianco A., Poukkula M., Cliffe A., Mathieu J., Luque CM., Fulga TA. & Rørth P. (2007) Two distinct modes of guidance signalling during collective migration of border cells. *Nature*. 448(7151)362-365.

Bischof J., Maeda RK., Hediger M., Karch F. & Basler K. (2007) An optimized transgenesis system for *Drosophila* using germ-line-specific phiC31 integrases. *Proceedings of the National Academy of Sciences in the United States of America*. 104(9):3312-3317.

Bish R. & Vogel C. (2014) RNA binding protein-mediated post-transcriptional gene regulation in medulloblastoma. *Molecules and Cells*. 37(5):357-64.

Blaser H., Eisenbeiss S., Neumann M., Reichman-Fried M., Thisse B., Thisse C. & Raz E. (2005) Transition from non-motile behaviour to directed migration during early PGC development in zebrafish. *Journal of Cell Science* 118(17):4027-4038.

Bossing T., Barros C.S. & Brand A.H. (2002) Rapid Tissue-Specific Expression Assay in Living Embryos. *Genesis*. 34(1-2):123-126.

Brand A.H. & Perrimon N. (1993) Targeted gene expression as a means of altering cell fates and generating dominant phenotypes. *Development*. 118(2):401-415.

Brückner K., Kockel L., Duchek P., Luque CM., Rørth P. & Perrimon N. (2004) The PDGF/VEGF Receptor Controls Blood Cell Survival in *Drosophila*. *Developmental Cell*. 7(1): 73-84.

Brückner K., Kockel L., Duchek P., Luque CM., Rørth P. & Perrimon N. (2004) The PDGF/VEGF Receptor Controls Blood Cell Survival in *Drosophila. Developmental Cell.* 7(1):73-84.

Bubb M.R., Baines I.C. & Korn E.D. (1998) Localization of actobindin, profilin I, profilin II, and phosphatidylinositol-4,5-bisphosphate (PIP2) in *Acanthamoeba castellanii. Cell Motility and the Cytoskeleton. 39(2):134-146.*

Bullock, S. L., Zicha, D. & Ish-Horowicz, D. (2003) The *Drosophila hairy* RNA localization signal modulates the kinetics of cytoplasmic mRNA transport. *EMBO Journal.* 22(10):2484–2494.

Büning J. (1994) The insect ovary: Ultrastructure, Previtellogenic growth and Evolution. Cornwall, UK: Chapman & Hall.

Buß F., Temm-Grove C., Henning S. & Jockusch B.M. (1992) Distribution of profilin in fibroblasts correlates with the presence of highly dynamic actin filaments. *Cell Motility and the Cytoskeleton*. 22(1):51-61.

Buszczak M., Paterno S., Lighthouse D., Bachman J., Planck J., Owen S., Skora AD., Nystul TG., Ohlstein B., Allen A., Wilhelm JE., Murphy TD., Levis RW., Matunis E., Srivali N., Hoskins RA. & Spradling AC. (2007). The Carnegie protein trap library: A versatile tool for *Drosophila* developmental studies. Genetics. **175(3)**:1505--1531.

Cai D., Chen S-C., Prasad M., He L., Wang X., Choesmel-Cadamuro V., Sawyer JK., Danuser G. & Montell DJ. (2014) Mechanical feedback through E-cadherin promotes direction sensing during collective cell migration. *Cell*. 157(5):1146-59.

Campos-Ortega JA. & Hartenstein V. (1985) Stages of *Drosophila* Embryogenesis. In: The Embryonic Development of *Drosophila melanogaster*. 1st ed. Berlin Heidelberg: Springer. pp. 9-84.

Carlsson L., Nyström LE., Sundkvist I., Markey F., & Lindberg U. (1977). Actin polymerizability is influenced by profilin, a low molecular weight protein in non-muscle cells. *Journal of Molecular Biology*. 115(3):465-483.

Carpenter B., MacKay C., Alnabulsi A., MacKay M., Telfer C., Melvin W. & Murray GI. (2006) The roles of heterogeneous nuclear ribonucleoproteins in tumour development and progression. *Biochimica et Biophysica Acta.* 1765(2):85-100.

Castellano F., Chavrier P. & Caron E. (2001) Actin dynamics during phagocytosis. *Seminars in Immunology.,* 13(6):347-355.

Celniker SE., Dillon LA., Gerstein MB., Gunsalus KC., Henikoff S., Karpen GH., Kellis M., Lai EC., Lieb JD., MacAlpine DM., Micklem G., Piano F., Snyder M., Stein L., White KP., Waterston RH.; modENCODE Consortium.(2009). Unlocking the secrets of the genome. *Nature*. 459(7249):927-930.

Chao JA., Patskovsky Y., Patel V., Levy M.,Almo SC. & Singer RH. (2010) IMP1 recognition of β-actin zipcode induces RNA looping. *Genes & Development*. 24(2):148-158.

Cheng Y., Zhu Z., Zhour J., Hu Z., Zhang J., Cai Q. & Wang L. (2015) Silencing profilin-1 inhibits gastric cancer progression *via* integrin β1/focal adhesion kinase pathway modulation. *World Journal of Gastroenterology*. 21(8):2323-2335.

Cherbas L., Willingham A., Zhang D., Yang L., Zou Y., Eads BD., Carlson JW., Landolin JM., Kapranov P., Dumais J., Samsonova A., Choi J., Roberts J., Davis C., Tang H., van Baren MJ., Ghosh S., Dobin A., Bell K., Lin W., Langton L., Duff MO., Tenney AE., Zaleski C., Brent MR., Hoskins RA., Kaufman TC., Andrews J., Graveley BR., Perrimon N., Celniker XE., Gingeras TR. & Cherbas P. (2011) The transcriptional diversity of 25 *Drosophila* cell lines. *Genome Research*. 21(2):301-314.

Cheung HC., Hai T., Zhu W., Baggerly KA., Tsavachidis S., Krahe R. & Cote GJ. (2009) Splicing factors PTBP1 and PTBP2 promote proliferation and migration of glioma cell lines. *Brain: A Journal of Neurology*. 132(8):2277-2288.

Chicurel ME., Singer, R. H., Meyer, C. J. and Ingber, D. E. (1998) Integrin binding and mechanical tension induce movement of mRNA and ribosomes to focal adhesions. *Nature*. 392(6677):730-733

Cho N.K., Keyes L., Johnson E., Heller J., Ryner L., Karim F. & Krasnow M.A. (2002). Developmental control of blood cell migration by the *Drosophila* VEGF pathway. *Cell* 108(6), 865–876.

Chung CY., Lee S., Briscoe C., Ellsworth C. & Firtel RA. (2000) Role of Rac in controlling the actin cytoskeleton and chemotaxis in motile cells. *Proceedings of the National Academy of Sciences.* 97(10):5225-5230.

Cliffe A., Poukkula M. & Rørth P. (2007) Culturing *Drosophila* egg chambers and imaging border cell migration. *Protocol Exchange.* doi:10.1038/nprot.2007.289

Comber K., Huelsmann S., Evans I., Sánchez-Sánchez, Chalmers A., Reuter R., Wood W. & Martín-Bermudo. (2013) A dual role for the βPS integrin *myospheroid* in mediating *Drosophila* embryonic macrophage migration. *Journal of Cell Science*. 126(15):3475-3484.

Deshler JO., Highett MI., Abramson T. & Schnapp BJ. (1998) A highly conserved RNA-binding protein for cytoplasmic mRNA localization in vertebrates. *Current Biology*. 8(9):489-496.

DesMarais V., Ichetovkin I., Condeelis J. & Hitchcock-DeGregori SE. (2002) Spatial regulation of actin dynamics: a tropomyosinfree, actin-rich compartment at the leading edge. *Journal of Cell Science*. 115(23):4649-4660.

Devenport D. & Brown NH. (2004) Morphogenesis in the absence of integrins: mutation of both *Drosophila* β subunits prevents midgut migration. *Development*. 131(21):5405-5415.

Di Nardo A., Cicchetti G., Falet H., Hartwig JH., Stossel TP. & Kwiatkowski DJ. (2005) Arp2/3 complex-deficient mouse fibroblasts are viable and have normal leading-edge actin structure and function. *Proceedings of the National Academy of Sciences of the USA*. 102(45):16263-16268.

Dietzl G., Chen D., Schnorrer F., Su K., Barinova Y., Fellner M., Gasser B., Kinsey K., Oppel S., Scheiblauer S., Couto A., Marra V., Keleman K. & Dickson BJ. (2007) A genome-wide transgenic RNAi library for conditional gene inactivation in *Drosophila. Nature.* 448(7150):151-156.

Dinkins MB., Fratto VM. & LeMosy EK. (2008) Integrin alpha chains exhibit distinct temporal and spatial localization patterns in epithelial cells of the *Drosophila* ovary. *Developmental Dynamics*. 237(12):3927-3939.

Dormoy-Raclet V., Menard I., Clair E., Kurban G., Mazroui R., Marco SD., von Roretz C., Pause A. & Gallouzi I.E. (2007) The RNA-Binding Protein HuR Promotes Cell Migration and

Cell Invasion by Stabilizing the β-*actin* mRNA in a U-Rich-Element-Dependent Manner. *Molecular Cell Biology*. 27(15):5365-5380.

Dreyfuss G., Kim VN. & Kataoka N. (2002) Messenger-RNA-Binding Proteins and the Messages they Carry. *Nature Reviews: Molecular Cell Biology*. 3(3):195-205.

Du T.G., Schmid M. & Jansen R.P. (2007) Why cells move messages: The biological functions of mRNA localisation*. Seminars in Cell & Developmental Biology*. 18: 171-177.

Duchek P., Somogyi K., Jekely G., Beccari S. & Rørth P. (2001) Guidance of cell migration by the *Drosophila* PDGF/VEGF receptor. *Cell*. 107:17-26.

Duffy J.B. (2002) GAL4 System in *Drosophila*: A Fly Geneticist's Swiss Army Knife. *Genesis*. 34:1-15.

Dutta D., Bloor JW., Ruiz-Gomez M., VijayRaghavan K. & Kiehart DP. (2002) Real-time imaging of morphogenetic movements in *Drosophila* using Gal4-UAS-driven expression of GFP fused to the actin-binding domain of moesin. *Genesis*. 34:146–151.

Duyk GM., Kim S., Myers RM. & Cox DR. (1990) Exon Trapping: a Genetic Screen to Identify Candidate Transcribed Sequences in Cloned Mammalian Genomic DNA. *Proceedings of the National Academy of Sciences*. 87(22):8995-8999.

Edgar B.A., Sprenger F., Duroni RJ., Leopold P. & O'Farrell P. (1993) Distinct molecular mechanisms regulate cell cycle timing at successive stages of *Drosophila* embryogenesis. *Genes & Development*. 8:440-452.

Ephrussi A. & Lehmann R. (1992) Induction of germ cell formation by oskar. *Nature*. 358(6385):387-392.

Evans CJ., Hartenstein V. & Banerjee U. (2003) Thicker Than Blood: Conserved Mechanisms in *Drosophila* and Vertebrate Hematopoiesis. *Developmental Cell.* 5: 673-690.

Evans IR., Ghai PA., Urbančič V., Tan K-L. & Wood W. (2013) SCAR/WAVE-mediated processing of engulfed apoptotic corpses is essential for effective macrophage migration in *Drosophila*. *Cell Death and Differentiation*. 20:709-720.

Evans IR., Rodrigues FS., Armitage EL. & Wood W. (2015) Draper/CED-1 mediates an ancient damage response to control inflammatory blood cell migration *in vivo*. *Current Biology*. 25(12):1606-1612.

Evans IR., Zanet J., Wood W. & Stramer BM. (2010) Live Imaging of *Drosophila* melanogaster Embryonic Haemocyte Migrations. *Journal of Visualized Experiments*. DOI: 10.3791/1696.

Even-Ram S. & Yamada KM. (2005) Cell migration in 3D matrix. *Current Opinion in Cell Biology*. 17(5):524-532.

Ferrara, N., Gerber, H.P., and LeCouter, J. (2003). The biology of VEGF and its receptors. *Nature Medicine*. 9: 669–676.

Fessler, L.I., Nelson, R.E., and Fessler, J.H. (1994). *Drosophila* extra-cellular matrix. *Methods in Enzymology*. 245:271–294.

Forrest KM. & Gavis ER. (2003) Live Imaging of Endogenous RNA Reveals a Diffusion and Entrapment Mechanism for *nanos* mRNA Localization in *Drosophila. Current Biology*. 13:1159-1168.

Franc, NC., Dimarcq, JL., Lagueux, M., Hoffmann, J., and Ezekowitz, R.A. (1996). Croquemort, a novel *Drosophila* hemocyte/macrophage receptor that recognizes apoptotic cells*. Immunity* 4:431–443.

Friedl P. & Bröcker EB. (2000) The biology of cell locomotion within three-dimensional extracellular matrix. *Cellular and Molecular Life Sciences. 57:41-64.*

Fujiwara, Y., Chang, AN., Williams, AM., and Orkin, SH. (2004). Functional overlap of GATA-1 and GATA-2 in primitive hematopoietic development. *Blood*. 103(2):583-585.

Garin J., Diez R., Kieffer S., Dermine JF., Duclos S., Gagnon E., Sadoul R., Rondeau C. & Desjardins M. (2001) The phagosome proteome: insight into phagosome functions. The *Journal of Cell Biology.* 152:165-80.

Gautier JJ., Lomakina M.E., Bouslama-Oueghlani L., Derivery E., Beilinson H., Faigle W., Loew D., Louvard D., Echard A., Alexandrova A.Y., Baum, B. & Gautreau A. (2011) Clathrin is required for Scar/Wave-mediated lamellipodium formation. The *Journal of Cell Science.* 124:3414-3427.

Gebauer F., Preiss T. & Hentze MW. (2012) From Cis-Regulatory Elements to Complex RNPs and Back. *Cold Spring Harbor Perspectives in Biology*. 4:a012245.

Geisbrecht ER. & Montell DJ. (2002) Myosin VI is required for E-cadherin-mediated border cell migration. *Nature Cell Biology.* **4**:616–620.

Gerber, HP., Malik, AK., Solar, GP., Sherman, D., Liang, XH., Meng, G., Hong, K., Marsters, JC., and Ferrara, N. (2002). VEGF regulates haematopoietic stem cell survival by an internal autocrine loop mechanism. *Nature.* 417:954–958.

Giancotti F.G. & Ruoslahti E. (1999) Integrin Signaling. *Science*. 285:1028-1032.

Glisovic T., Bachorik J.L., Yong J. & Dreyfuss G. (2008) RNA-binding proteins and post-transcriptional gene regulation. *Federation of European Biochemical Societies Letters*. 582(14): 1977-1986.

Goodrich J.S., Clouse K.N. & Schüpbad T. (2004) Hrb27C, Sqd and Otu cooperatively regulate *gurken* RNA localization and mediate nurse cell chromosome dispersion in *Drosophila* oogenesis. *Development*. 131:1949-1958.

Goswami S., Wyckoff J.B. & Lauffenburger D.A. *et al*. (2008). A Mena invasion isoform potentiates EGF-induced carcinoma cell invasion and metastasis. *Developmental Cell* 15: 813-828.

Gough NR. (2010) Moving in 2D Versus 3D. *Science Signaling*. 3(138):ec274.

Groisman I., Huang YS., Mendez R., Cao Q., Theurkauf W. & Richter JD. (2000) CPEB, maskin, and *cyclin B1* mRNA at the mitotic apparatus: implications for local translational control of cell division. *Cell.* 103:435-447.

Groth AC., Fish M., Nusse R. & Calos MO. (2004) Construction of transgenic *Drosophila* by using the site-specific integrase from phage phiC31. *Genetics*. 166(4): 1775-1782.

Gu W., Katz Z., Wu B., Park HY., Li D., Lin S., Wells AL. & Singer RH. (2012) Regulation of cell adhesion and motility-related mRNAs in breast cancer cells by IMP1/IMP1. *Journal of Cell Science*. 125:81-91.

Gu W., Pan F. & Singer RH. (2009) Blocking β-catenin binding to the IMP1 promoter represses IMP1 expression, leading to increased proliferation and migration of metastatic breast-cancer cells. *Journal of Cell Science*. 122:1895-1905.

Gupta T. & Schüpbach T. (2001) Two Signals Are Better Than One: Border Cell Migration in *Drosophila. Developmental Cell. 1(4):443-445.*

Hachet O. & Ephrussi A. (2004) Splicing of *oskar* RNA in the nucleus is coupled to its cytoplasmic localization. *Nature*. 428(6986):959-63.

Hafner M., Landthaler M., Burger L., Khorshid M., Hausser J., Berninger P., Rothballer A., Ascano Jr. M., Jungkamp A., Munschauer M., Ulrich A., Wardle GS., Dewell S., Zavolan M. & Tuschl T. (2010) Transcriptome-wide Identification of RNA-Binding Protein and MicroRNA Target Sites by PAR-CLIP. *Cell*. 141(1):129-141.

Hakkinen KM., Harunaga JS., Doyle AD. & Yamade KM. (2011) Direct Comparisons of the Morphology, Migration, Cell Adhesions, and Actin Cytoskeleton of Fibroblasts in Four Different Three-Dimensional Extracellular Matrices. *Tissue Engineering Part A*. 17(5-6):713-724.

Han DD., Stein D. &Stevens LM. (2000) Investigating the function of follicular subpopulations during *Drosophila* oogenesis through hormone-dependent enhancer-targeted cell ablation. *Development*. 127:573–583.

Hirokawa N. (2006) mRNA Transport in Dendrites: RNA Granules, Motors, and Tracks. *Journal of Neuroscience*. 26(27): **7139-7142.**

Hocine S., Raymond P., Zenklusen D., Chao JA. & Singer RH. (2013) Single-molecule analysis of gene expression using two-color RNA labeling in live yeast. *Nature Methods*. 10:119-121.

Hoehn M., Küstermann E., Blunk J., Widermann D., Trapp T., Wecker S., Föcking M., Arnold H., Hescheler J., Fleischmann B.K., Schwindt W. & Bührle C. (2002) Monitoring of implanted stem cell migration *in vivo*: A highly resolved *in vivo* magnetic resonance imaging investigation of experimental stroke in rat. *Proceedings of the National Academy of Sciences in the United States of America*. 99(25):16267-16272.

Hogan DJ., Riordan DP., Gerber AP., Herschlag D. & Brown PO. (2008) Diverse RNA-Binding Proteins Interact with Functionally Related Sets of RNAs, Suggesting an Extensive Regulatory System. *PLoS Biology*. 6(10):e255.

Holz A., Bossinger B., Strasser T., Janning W. & Klapper R. (2003) The two origins of hemocytes in *Drosophila*. *Development* 130:4955–4962.
Hotulainen P. & Lappalainen P. (2006) Stress fibers are generated by two distinct actin assembly mechanisms in motile cells. *The Journal of Cell Biology*. 173(3):383–394.

Hubstenberger A., Noble SL., Cameron C. & Evans TC. (2013) Translation Repressors, an RNA Helicase, and Developmental Cues Control RNP Phase Transitions during Early Development. *Developmental Cell*. 27:161-173.

Hüttelmaier S., Zenklusen D., Lederer M., Dictenberg J., Lorenz M., Meng XH., Bassell GJ., Condeelis J. & Singer RH. (2005) Spatial regulation of β-actin translation by Src-dependent phosphorylation of IMP1. *Nature*. 438: 512-515.

Huynh JR., Munro TP., Smith- Litière K., Lepesant JA. & St Johnston D. (2004) The *Drosophila* hnRNPA/B homolog, Hrp48, is specifically required for a distinct step in *osk* mRNA localization. *Developmental Cell*. 6(5):625-635.

Ibarra N., Pollitt A. & Insall RH. (2005) Regulation of actin assembly by SCAR/WAVE proteins. Biochemical Society Transactions. 33(6):1243-1246.

Iervolino A., Santilli G., Trotta R., Guerzoni C., Cesi V., Bergamaschi A., Gambacorti-Passerini C., Calabretta B. & Perrotti D. (2002) hnRNP A1 Nucleocytoplasmic Shuttling Activity is Required for Normal Myelopoiesis and BCR/ABL Leukemogenesis. Molecular and Cellular Biology. 22(7): 2255-2266.

Jakobsen KR., Sorensen E., Brondum KK., Daugaard TF., Thomsen R. & Nielsen AL. (2013) Direct RNA sequencing mediated identification of mRNA localized in protrusions of human MDA-MB-231 metastatic breast cancer cells. *The Journal of Molecular Signalling*. 8(1):9

Jaramillo AM., Weil TT., Goodhouse J., Gavis ER. & Schupbach T. (2008) The Dynamics of Fluorescently Labeled Endogenous *gurken* mRNA in *Drosophila*. *The Journal of Cell Science*. 121: 887-894.

JayaNandanan N., Gavis ER., Riechmann V. & Peptin M (2011) A genetic *in vivo* system to detect asymmetrically distributed RNA. *EMBO Reports*. 12(11):1167-1174.

Johnsson A. & Karlsson R. (2010) Microtubule-dependent localization of *profilin I* mRNA to actin polymerization sites in serum-stimulated cells. *European Journal of Cell Biology*. 89:394–401

Jønson L., Vikesaa J., Krogh A., Nielsen LK., Hansen Tv., Borup R., Johnsen AH., Christiansen J. & Nielsen FC. (2007) Molecular composition of IMP1 ribonucleoprotein granules. *Molecular and Cellular Proteomics*. 6(5):798-811.
Kao L. & Megraw TL. (2004) RNAi in Cultured *Drosophila* Cells. *Methods in Molecular Biology*, 247:443-457.

Kedersha N. & Anderson P. (2007) Mammalian stress granules and processing bodies. *Methods in Enzymology*. 431:61-81.
Kellogg D.R., Mitchison T.J. & Alberts B.M. (1988) Behaviour of microtubules and actin filaments in living *Drosophila* embryos. *Development*. 103: 675-686.

Kim H., Lee SJ., Gardiner AS., Perrone-Bizzozero NI. & Yoo S. (2015) Different motif requirements for the localization zipcode element of *β-actin* mRNA binding by HuD and IMP1. *Nucleic Acids Research*. doi: 10.1093/nar/gkv699.

Kim-Ha J., Kerr K. & Macdonald PM. (1995) Translational regulation of oskar mRNA by bruno, an ovarian RNA-binding protein, is essential. *Cell*. 81(3):403-412.

King M.L., Messitt T.J., Mowry K.L. (2005) Putting RNAs in the right place at the right time: RNA localization in the frog oocyte. *Biology of the Cell*. 97(1):19-33.

Kislauskis E.H., Zhu X. & Singer R.H. (1994) Sequences Responsible for Intracellular Localization of β-Actin Messenger RNA Also Affect Cell Phenotype. *The Journal of Cell Biology*. 127(2): 441-451

Kloc M. & Etkin LD. (2005) RNA localization mechanisms in oocytes. *The Journal of Cell Science*. 118(2):269-282

Kloc M., Wilk K., Vargas D., Shirato Y., Bilinski S. & Etkin LD. (2005) Potential structural role of non-coding and coding RNAs in the organization of the cytoskeleton at the vegetal cortex of Xenopus oocytes. *Development.* 132: 3445-57.

Knight B., Laukaitis C., Akhta N., Hotchin NA., Edlund M., Horwitz AR. (2000) Visualizing muscle cell migration *in situ. Current Biology. 10(10):576-585.*

Knoblich J.A. (2008) Mechanisms of Asymmetric Stem Cell Division. *Cell*. 132:583–597.

Kong J. & Lasko P. (2012) Translational control in cellular and developmental processes. *Nature Reviews Genetics*. 13(6):383-394.

Lange S., Katayama Y., Schmid M., Burkacky O., Brauchle C., Lamb DC. & Jansen RP. (2008) Simultaneous Transport of Different Localized mRNA Species Revealed by Live-Cell imaging. *Traffic*. 9:1256-1267.

Lanot R., Zachary D., Holder, F., & Meister M. (2001). Post-embryonic hematopoiesis in *Drosophila*. *Developmental Biology*. 230: 243–257.

Lasko P. (2012) mRNA Localization and Translational Control in *Drosophila* Oogenesis. *Cold Spring Harbor Perspectives in Biology.* 4(10): doi: 10.1101/cshperspect.a012294.

Latchman DS. (2010) Control of Gene Expression. *Gene Control*. New York: Garland Science. Chapter 8: 269-300.

Latham, VM., Yu, EH., Tullio, AN., Adelstein, RS. & Singer, RH. (2001) A Rho-dependent signaling pathway operating through myosin localizes β-*actin* mRNA in fibroblasts. *Current Biology.* 11(13):1010–1016.

Lauffenburger DA. & Horwitz AF. (1996) Cell Migration: A Physically Integrated Molecular Process. *Cell*. 84:359-369.

Lebestky, T., Chang, T., Hartenstein, V., and Banerjee, U. (2000).Specification of *Drosophila* hematopoietic lineage by conserved transcription factors. *Science.* 288:146–149.

Lécuyer E., Yoshida H., Parthasarathy N., Alm C., Babak T., Cerovina T., Hughes TR., Tomancak P. & Krause HM. (2007) Global analysis of mRNA localization reveals a prominent role in organizing cellular architecture and function. *Cell:* 131:174-187.

Lee T. & Luo L. (2001) Mosaic analysis with a repressible cell marker (MARCM) for *Drosophila* neural development. *Trends in Neurosciences*. 24(5):617-630.

Lengyel P. & Söll D. (1969) Mechanism of protein biosynthesis. *Bacteriological Reviews*. 33(2):264-301.

Lewis L., Verna JM., Levinstone D., Sher S., Marek L. & Bell E. (1982) The Relationship of Fibroblast Translocations to Cell Morphology and Stress Fibre Density. *The Journal of Cell Science*. 53:21-36.

Lewis RA., Gagnon JA, Mowry KL. (2008) PTB/hnRNP I is required for RNP remodeling during RNA localization in Xenopus oocytes. *Molecular Cell Biology*. 28(2):678-686.

Li P. & Zon LI. (2011) Stem cell migration: a zebrafish model. *Methods in Molecular Biology*. 750:157-168.

Liao G., Mingle L., Van De Water L. & Liu G. (2015) Control of cell migration through mRNA localization and local translation *WIREs RNA*. 6:1-15.

Liao G., Simone B. & Liu G. (2011) Mis-localization of Arp2 mRNA impairs persistence of directional cell migration. *Experimental Cell Research*. 317(6):812-822.

Lionnet T., Czaplinski C., Darzacq X., Shav-Tal Y., Wells AL., Chao JA., Park HY., de Turris V., Lopez-Jones M. & Singer RH. (2011) A transgenic mouse for *in vivo* detection of endogenous labeled mRNA. *Nature Methods*. 8(2):167-170.

Long RM., Singer RH., Meng X., Gonzalez I., Nasmyth K. & Jansen RP. (1997) Mating Type Switching in Yeast Controlled by Asymmetric Localization of *ASH1* mRNA. *Science*. 277(5324):383-387.

Lowe N., Rees JS., Roote J., Ryder E., Armean I. M., Johnson G., Drummond E., Spriggs H., Drummond J., Magbanua J. P., Naylor H., Sanson B., Bastock R., Huelsmann S., Trovisco V., Landgraf M., Knowles-Barley S., Armstrong JD., White-Cooper H., Hansen C., Phillips RG., Lilley KS., Russell, S. & St Johnston D. (2014) Analysis of the expression patterns, subcellular localisations and interaction partners of *Drosophila* proteins using a pigP protein trap library. *Development*. 141(20):3994-4005.

Lunde BM., Moore C. & Varani G. (2007) RNA-binding proteins: modular design for efficient function. *Nature Reviews: Molecular Cell Biology*. 8:479-490.

Luo J., Zuo J., Wu J., Wan P., Kang D., Xiang C., Zhu H. & Chen J. (2015) *In vivo* RNAi screen identifies candidate signaling genes required for collective cell migration in *Drosophila* ovary. *Science China Life Sciences*. 58(4):379-389.

Ma S., Liu G., Sun Y. & Xie J. (2007) Relocalization of the polypyrimidine tract-binding protein during PKA-induced neurite growth. *Biochimica et Biophysica Acta – Molecular Cell Research*. 1773(6):912-923.

Machesky, LM., Reeves, E., Wientjes, F., Mattheyse, FJ., Grogan, A., Totty, NF., Burlingame, AL., Hsuan, JJ. and Segal, AW. (1997). Mammalian actin-related protein 2/3 complex localizes to regions of lamellipodial protrusion and is composed of evolutionarily conserved proteins. *Biochemical Journal*. 328(1):105-112.

Maizels Y., Oberman F., Miloslayski R., Ginzach N., Berman M. & Yisraeli JK. (2015) Localization of *cofilin* mRNA to the leading edge of migrating cells promotes directed cell migration. *Journal of Cell Science*. 128:1922-1933.

Martin KC. & Ephrussi A. (2009) mRNA Localisation: Gene Expression in the Spatial Dimension. *Cell.* 136:719-730.

Martin-Bermudo MD. & Brown NH. (1996). Intracellular signals direct integrin localization to sites of function in embryonic muscles. *The Journal of Cell Biology*. 134(1):217–226.

Mateus R., Pereira T., Sousa S., Esteves de Lima J., Pascoal S., Saúde L. & Antonia J. (2012) *In vivo* Cell and Tissue Dynamics Underlying Zebrafish Fin Fold Regeneration. *PLoS ONE*. 7(12): e51766.

Mathieu J., Sung HH., Pugieux C., Soetaert J. & Rørth P. (2007) A sensitized PiggyBac-based screen for regulators of border cell migration in *Drosophila*. *Genetics*. 176(3):1579-1590.

Mattila PK. & Lappalainen P. (2008) Filopodia: molecular architecture and cellular functions. *Nature Reviews Molecular Cell Biology*. 9:446-454.

Mazzalupo, S., and Cooley, L. (2006). Illuminating the role of caspases during *Drosophila* oogenesis. *Cell Death & Differentiation*. 13:1950-1959.

McCall K. & Peterson JS. (2004) Detection of Apoptosis in *Drosophila*. *Methods in Molecular Biology*. 282:191-205.

Medioni C., Ephrussi A. & Florence B. (2012) *Drosophila* IMP1 controls axon growth and branching by regulating profilin mRNA *in vivo*. *The Embo Meeting 2012,* Nice. Abstract A007,p5.

Medioni C., Mowry K. & Besse F. (2012) Principles and roles of mRNA localization in animal development. *Development*. 139(18):3263-3276.

Medioni C., Ramialison M., Ephrussi A. & Besse F. (2014) Imp promotes axonal remodeling by regulating *profilin* mRNA during brain development. *Current Biology*. 24(7):793-800.

Meignin C. & Davis I. (2010) Transmitting the message: intracellular mRNA localization. *Current Opinion in Cell Biology*. 22(1):112-119.

Mili S. & Macara I.G. (2009) RNA localisation and polarity: from A(PC) to Z(BP*). Trends in Cell Biology*. 19(4):156-164.

Mili S., Moissoglu K. & Macara IG. (2008) Genome-Wide Screen Identifies Localized RNAs Anchored At Cell Protrusions Through Microtubules And APC. *Nature*. 453(7191):115-119.

Mili S., Moissoglu K. & Macara IG. (2008) Genome-wide screen reveals APC-associated RNAs enriched in cell protrusions. *Nature*. 453:115–119.

Millard TH. & Martin P. (2008) Dynamic analysis of filopodial interactions during the zippering phase of *Drosophila* dorsal closure. *Development*. 135:621–626.

Mingle LA., Okuhama NN., Shi J., Singer RH., Condeelis J. & Liu G. (2005) Localisation of all seven messenger RNAs for the actin-polymerization nucleator Arp2/3 complex in the protrusions of fibroblasts. *Journal of Cell Science*. 118: 2425-2433.

Moldovan NI., Milliken EE., Irani K., Chen J., Sohn RH., Finkel T., Goldschmidt-Clermont PJ. (1997) Regulation of endothelial cell adhesion by profilin. *Current Biology*. 7(1):24-30.

Montell D.J., Rørth P. & Spradling A.C. (1992) *slow border cells*, a locus required for a developmentally regulated cell migration during oogenesis, encodes *Drosophila* C/EBP. *Cell*. 71:51-62.

Montell DJ. (2003) Border-cell migration: the race is on. *Nature Reviews Molecular Cell Biology*. 4(1):13-24.

Moreira CGA., Jacinto A. & Prag S. (2013) *Drosophila* integrin adhesion complexes are essential for hemocyte migration *in vivo*. *Biology Open*. 2(8):795-801.

Moreira S., Stramer B., Evans I., Wood W. & Martin P. (2010) Prioritization of competing damage and developmental signals by migrating macrophages in the *Drosophila* embryo. *Current Biology*. 20(5):464–470.

Morin X., Daneman R., Zavortink M. & Chia W. (2001) A protein trap strategy to detect GFP-tagged proteins expressed from their endogenous loci in *Drosophila*. *Proceedings of the National Academy of Sciences in the United States of America*. 98(26):15050-15055.

Müller-McNicoll M. & Neugebauer KM. (2013) How cells get the message: dynamic assembly and function of mRNA–protein complexes. *Nature Reviews Genetics*. 14: 275-287.

Munro TP., Kwon S., Schnapp BJ. & St Johnston D. (2005) The *Drosophila* Orthologue of ZBP/Vera/Vg1RBP is essential for cell migration during oogenesis. *46th Annual Drosophila Research Conference, The Genetics Society of America*. San Diego, California. March 30–April 3, 2005. Abstract 256A.

Munro TP., Kwon S., Schnapp BJ. & St Johnston D. (2006) A repeated IMP-binding motif controls *oskar* mRNA translation and anchoring independently of *Drosophila melanogaster* IMP. *The Journal of Cell Biology*. 172(4):577-588.

Murphy AM. & Montell DJ. (1996) Cell type-specific roles for Cdc42, Rac, and RhoL in *Drosophila* oogenesis. *The Journal of Cell Biology*. 133(3):617-630.

Murray, MA., Fessler, LI., and Palka, J. (1995). Changing distributions of extracellular matrix components during early wing morphogenesis in *Drosophila*. *Developmental Biology*. 168:150–165.

Nelson W.J. (2003) Adaptation of core mechanisms to generate cell polarity. *Nature*. 422:(6933): 766-774.

Ni JQ., Liu LP, Binari R., Hardy R., Shim HS., Cavallaro A., Booker M., Pfeiffer B., Markstein M., Wang H., Villalta C., Laverty T., Perkins L., Perrimon N. (2009) A *Drosophila* Resource of Transgenic RNAi Lines for Neurogenetics. *Genetics*. 182(4):1089-1100.

Ni JQ., Zhou R., Czech B., Liu P., Holderbaum L., Yang-Zhou D., Shim HS., Tao R., Handler D., Karpowicz P., Binari R., Booker M., Brennecke J., Perkins LA., Hannon GJ. & Perrimon N. A genome-scale shRNA resource for transgenic RNAi in *Drosophila*. *Nature Methods*. 8(5):405-407

Nielsen FC., Nielsen J. & Christiansen J. (2001) A family of IGF-II mRNA binding proteins (IMP) involved in RNA trafficking. *Scandinavian Journal of Clinical and Laboratory Investigation*. 234:93-99.

Nielsen J., Christiansen J., Lykke-Andersen J., Johnsen AH., Wewer UM. & Nielsen FC. (1999) A Family of Insulin-Like Growth Factor II mRNA-Binding Proteins Represses Translation in Late Development. *Molecular and Cellular Biology*. 19(2):1262-1270.

Nielsen J., Nielsen F.C., Jakobsen R.M. & Christiansen J. (2000) The biphasic expression of IMP/Vg1-RBP is conserved between vertebrates and *Drosophila*. *Mechanisms of Development*. 96(1):129-132.

Niewiadomska P., Godt D. & Tepass U. (1999) DE-cadherin is required for intercellular motility during *Drosophila* oogenesis. *The Journal of Cell Biology*. 114:533–547.

Oda H., Uemura T. & Takeichi M. (1997) Phenotypic analysis of null mutants for DE-cadherin and Armadillo in *Drosophila* ovaries reveals distinct aspects of their functions in cell adhesion and cytoskeletal organization. *Genes to Cells* **2**:29–40.

Ohta S., Bukowski-Wills J., Sanchez-Pulido L., Lima Alves F., Wood L., Chen ZA., Platani M., Fischer L., Hudson D.F., Ponting C.P., Fukagawa T., Earnshaw W.C., Rappsilber J. (2010) The Protein Composition of Mitotic Chromosomes Determined Using Multiclassifier Combinatorial Proteomics. *Cell*. 142(5):810-821.

Oleynikov Y. & Singer R.H. (2003) Real-Time Visualization of IMP1 Association with β-Actin mRNA during Transcription and Localization. *Current Biology*. 13: 199–207.

Olink-Coux M. & Hollenbeck PJ. (1996) Localization and active transport of mRNA in axons of sympathetic neurons in culture. *The Journal of Neuroscience*. 16(4):1346-1358.
Paladi M. & Tepass U. (2004) Function of Rho GTPases in embryonic blood cell migration in *Drosophila*. *The Journal of Cell Science*. 117:6313–6326.

Park HY., Lim H., Yoon Y., Follenzi A., Nwokafor C., Lopez-Jones M., Meng X. & Singer RH. (2014) Visualization of Dynamics of Single Endogenous mRNA Labeled in Live Mouse. *Science*. 343(6169):422–424.

Pearson AM., Baksa K., Ramet M., Protas M., Mckee M., Brown D. & Ezekowitz, RA. (2003) Identification of cytoskeletal regulatory proteins required for efficient phagocytosis in *Drosophila*. *Microbes and Infection*. 5(10):815-824.

Pereira AM., Tudor C., Kanger JS., Subramaniam V. & Blanco EM. (2011) Integrin-Dependent Activation of the JNK Signaling Pathway by Mechanical Stress. *PLoS ONE*. 6(12):e26182.

Petrella LN., Smith-Leiker T., and Cooley L. (2007) The Ovhts polyprotein is cleaved to produce fusome and ring canal proteins required for *Drosophila* oogenesis. *Development*. 134:703-712.

Petrie RJ. & Yamada KM. (2012) At the leading edge of three-dimensional cell migration. *Journal of Cell Science*. 125(24):1-10.

Petrie RJ., Gavara N., Chadwick RS. & Yamada KM. (2012) Nonpolarized signalling reveals two distinct modes of 3D cell migration. *The Journal of Cell Biology*. 197(3): 439-455.

Philippar U., Roussos ET., Oser M., Yamaguch, H., Kim HD., Giampieri S., Wang Y., Ridley AJ., Schwartz MA., Burridge K., Firtel RA., Ginsberg MH., Borisy G., Parsons J.T. & Horwitz A.R. (2003) Cell Migration: Integrating Signals from Front to Back. *Science*. 302:1704- 1709.

Philippar U., Roussos ET., Oser M., Yamaguch, H., Kim HD., Giampieri S., Wang Y., Goswami S., Wyckoff JB., Lauffenburger DA., Sahai E., Condeelis JS. & Gertler FB. (2008) A Mena invasion isoform potentiates EGF-induced carcinoma cell invasion and metastasis. *Developmental Cell.* 15(6):813-828.

Prasad M. & Montell DJ. (2007) Cellular and Molecular Mechanisms of Border Cell Migration Analyzed Using Time-Lapse Live-Cell Imaging. *Developmental Cell*. 12(6):997-1005.

Prasad M., Jang AC., Starz-Gaiano M., Melani M. & Montell DJ. (2007) A protocol for culturing *Drosophila melanogaster* stage 9 egg chambers for live imaging. *Nature Protocols*. 2:2467-2473.

Preiss T. & Hentze MW. (2003) Starting the protein synthesis machine: eukaryotic translation initiation. *BioEssays*. 25(12):1201-1211.

Proud C. (2008) mTOR signalling and human disease. *Journal of Medical Genetics*. 45: S33-S43.

Quiñones-Coello AT., Petrella LN., Ayers K., Melillo A., Mazzalupo S., Hudson AM., Wang S., Castiblanco C., Buszczak M., Hoskins RA. & Cooley L. (2007) Exploring Strategies for Protein Trapping in *Drosophila*. *Genetics*. 175(3):1089-1104.

Raff J.W., Whittlefield W.G.F. & Glover, D.M. (1990) Two distinct mechanisms localise cyclin B transcripts in syncytial *Drosophila* embryos. *Development.* 110(4):1249–1261.

Ramet M., Manfruelli P., Pearson A., Mathey-Prevot B. & Ezekowitz RA. (2002) Functional genomic analysis of phagocytosis and identification of a *Drosophila* receptor for *E. coli*. *Nature.* 416**:** 644-8.

Ray D., Kazan H., Cook KB., Weirauch MT., Najafabadi HS., Li X., Gueroussov S., Albu M., Zheng H., Yang A., Na H., Irimia M., Matzat LH., Dale RK., Smith SA., Yarosh CA., Kelly SM., Nabet B., Mecenas D., Li W., Laishram RS., Qiao M., Lipshitz HD., Piano F., Corbett

AH., Carstens RP., Frey BJ., Anderson RA., Lynch KW., Penalva LO., Lei EP., Fraser AG., Blencowe BJ., Morris QD., Hughes TR. (2013) A compendium of RNA-binding motifs for decoding gene regulation. *Nature*. 499(7457):172-177.

Raz E. & Reichman-Fried. (2006) Attraction rules: germ cell migration in zebrafish. *Current Opinion in Genetics & Development*. 16(4):355–359.

Ridley AJ., Schwartz MA., Burridge K., Firtel RA., Ginsberg MH., Borisy G., Parsons JT. & Horwitz AR. (2003) Cell migration: integrating signals from front to back. *Science.* 302(5651):1704-1709.

Riedl J., Crevenna AH., Kessenbrock K., Haochen Yu J., Neukirchen D., Bista M., Bradke F., Jenne D., Holak TA., Werb Z., Sixt M. & Wedlich-Soldner R. (2008) Lifeact: a versatile marker to visualize F-actin. *Nature Methods*. 5(7):605-607.

Rizki TM. (1978). The circulatory system and associated cells and tissues. In The Genetics and Biology of *Drosophila*, M. Ashburner and T.R.F. Wright, eds. (New York, London: Academic Press).

Rizki TM., and Rizki, RM. (1980). Properties of the larval hemocytes of *Drosophila* melanogaster. *Experientia.* 36:1223–1226.

Rogers SL. & Rogers GC. (2008) Culture of *Drosophila* S2 cells and their use for RNAi-mediated loss-of-function studies and immunofluorescence microscopy. *Nature Protocols*. 3(4):606-611.

Rørth P. (1998). Gal4 in the *Drosophila* female germline. *Mechanisms of development*. 78(1-2):113-118.

Rørth P., Szabo K., Bailey A., Laverty T., Rehm J., Rubin GM., Weigmann K., Milán M., Benes V., Ansorge W. & Cohen S. (1998) Systematic gain-of-function genetics in *Drosophila. Development*. 125(6):1049-1057.

Ross A.F., Oleynikov Y., Kislauskis E.H., Taneja K.L. & Singer R.H. (1997) Characterization of a β-actin mRNA Zipcode-Binding Protein. *Molecular and Cellular Biology*. 17(4): 2158-2165.

Rubino S., Fighetti M., Unger E. and Cappuccinelli P. (1984) Location of actin, myosin, and microtubular structures during directed locomotion of *Dictyostelium amebae*. *The Journal of Cell Biology*. 98**:** 382–390.

Sampson CJ. & Williams MJ. (2012) *Rho GTPases: Methods and Protocols, Methods in Molecular Biology* 827: DOI 10.1007/978-1-61779-442-1_23

Sampson CJ., Amin U. & Couso J. (2013) Activation of *Drosophila* haemocyte motility by the ecdysone hormone. Biology Open. doi: 10.1242/bio.20136619

Savant-Bhonsale S. & Montell D.J. (1993) torso-like encodes the localized determinant of *Drosophila* terminal pattern formation. *Genes & Development*. 7:2548-2555.

Sawicka K., Bushell M., Spriggs KA. & Willis AE. (2008) Polypyrimidine-tract-binding protein: a multifunctional RNA-binding protein. *Biochemical Society Transactions.* 36(4):641–647.

Schneider I. (1972) Cell lines derived from late embryonic stages of *Drosophila melanogaster. Journal of Embryology & Experimental Morphology*. 27(2):353-365.

Semotok JL., Luo H., Cooperstock RL., Karaiskakis A., Vari HK., Smibert CA., Lipshitz HD. (2008) *Drosophila* maternal Hsp83 mRNA destabilization is directed by multiple SMAUG recognition elements in the open reading frame. *Molecular Cell Biology*. 28(22):6757–6772

Shahbabian K. & Chartrand P. (2012) Control of cytoplasmic mRNA localization. *Cellular and Molecular Life Sciences*. 69: 535-552.

Shestakova EA., Singer RH & Condeellis J. (2001) The physiological significance of *β-actin* mRNA localization in determining cell polarity and directional motility. *PNAS*. 13: 7045-7050.

Shestakova EA., Wyckoff J. & Jones J. (1999) Correlation of *β-Actin* Messenger RNA Localization with Metastatic Potential in Rat Adenocarcinoma Cell Lines. *Cancer Research*. 59:1202-1205.

Silver D.L. & Montell D.J. (2001) Paracrine signalling through the JAK/STAT pathway activates the invasive behaviour of ovarian epithelial cells in *Drosophila*. *Cell*. 107:831-841.

Singh R. & Valcárcel. (2005) Building specificity with nonspecific RNA-binding proteins. *Nature Structural & Molecular Biology*. 12: 645-653.

Singh R., Valcarel J. & Green MR. (1995) Distinct binding specificities and functions of higher eukaryotic polypyrimidine tract-binding proteins. *Science*. 268(5214):1173-1176.

Sonenberg N. and Hinnebusch, A. G. (2009) Regulation of translation initiation in eukaryotes: mechanisms and biological targets. *Cell*. 136(4):731-745

St Johnston D. (1995) The intracellular localization of messenger RNAs. *Cell*. 81(2):161-170.

St Johnston D., Driever W., Berleth T., Richstein S. & Nusslein-Volhard C. (1989). Multiple steps in the localization of *bicoid* RNA to the anterior pole of the *Drosophila* oocyte. *Development*. 107:S13-19.

Stöhr N., Lederer M., Reinke C., Meyer S., Hatzfeld M., Singer RH. & Hüttelmaier S. (2006) IMP1 regulates mRNA stability during cellular stress. The Journal of Cell Biology. 175(4):527-534.

Stramer B. & Wood W. (2009) Inflammation and wound healing in *Drosophila*. *Methods in Molecular Biology*. 571:137-149.

Stramer B., Moreira S., Millard T., Evans I., Huang CY., Sabet O., Milner M., Dunn G., Martin P. & Wood W. (2010) Clasp-Mediated Microtubule Bundling Regulates Persistent Motility and Contact Repulsion in *Drosophila* Macrophages *In vivo*. The *Journal of Cell Biology.* 189: 681-689.

Stramer B., Wood W., Galko MJ., Redd MJ., Jacinto A., Parkhurst SM. & Martin P. (2005) Live imaging of wound inflammation in *Drosophila* embryos reveals key roles for small GTPases during *in vivo* cell migration. The *Journal of Cell Biology.* 168: 567-73.

Stroschein-Stevenson SL., Foley E., O'Farrell P.H. & Johnson A.D. (2006) Identification of *Drosophila* geneproducts required for phagocytosis of Candida albicans. *PLoS Biology.* 4: e4.

Stroschein-Stevenson SL., Foley E., O'farrell P.H. & Johnson A.D. (2009) Phagocytosis of Candida albicans by RNAi-treated *Drosophila* S2 cells. *Methods in Moecular Biology.* 470**:** 347-58.

Stuart LM. & Ezekowitz RA. (2005) Phagocytosis: elegant complexity. *Immunity.* 22: 539-50.

Stuart LM., Boulais J., Charriere GM., Hennessy EJ., Brunet S., Jutras I., Goyette G., Rondeau C., Letarte S., Huang H., Ye P., Morales F., Kocks C., Bader J.S., Desjardins M. & Ezekowitz R.A. (2007) A systems biology analysis of the *Drosophila* phagosome. *Nature.* 445: 95-101.

Tadros W. & Lipshitz HD. (2009) The maternal-to-zygotic transition: a play in two acts. *Development* 136: 3033-3042.

Takizawa PA., Sil A., Swedlow JR., Herskowitz I. & Vale RD. (1997) Actin-dependent localization of an RNA encoding a cell-fate determinant in yeast. *Nature*. 389(6646):90-93.

Tekotte H., Tollervey D. & Davis I. (2007) Imaging the migrating border cell cluster in living *Drosophila* egg chambers. *Developmental Dynamics*. 236(10):2818-2824.

Tepass U., Fessler L., Aziz LI. & Hartenstein V. (1994) Embryonic origin of hemocytes and their relationship to cell death in *Drosophila*. *Development.* 120(7):1829-1837.

Tepass, U., Fessler, LI., Aziz, A., and Hartenstein, V. (1994). Embryonic origin of hemocytes and their relationship to cell death in *Drosophila*. *Development.* 120: 1829–1837.

Thomsen R. & Lade Nielsen A. (2011) A Boyden chamber-based method for characterization of astrocyte protrusion localized RNA and protein. *Glia*. 59:1782–1792.

Toledano H., D'Alterio C., Czech B., Levine E. & Jones DL. (2012) The *let-7*-Imp axis regulates ageing of the *Drosophila* testis stem-cell niche. *Nature*. 485(7400):605-610.

Tollis S., Dart AE., Tzircotis G. & Endres RG. (2010). The Zipper Mechanism in Phagocytosis: Energetic Requirements and Variability in Phagocytic Cup Shape. *BMC Systems Biology.* 4:149.

Tomura M., Yoshida N., Tanaka J., Karasawa S., Miwa Y., Miyawaki A. & Kanagawa O. (2008) Monitoring cellular movement *in vivo* with photoconvertible fluorescence protein ''Kaede'' transgenic mice. *PNAS*. 105(31):10871-10876.

Tracey WD., Ning X., Klingler M., Kramer SG. & Gergen, JP. (2000). Quantitative analysis of gene function in the *Drosophila* embryo. *Genetics*. 154:273-284.

Tucker PK., Evans IR. & Wood W. (2011) Ena drives invasive macrophage migration in *Drosophila* embryos. *Disease Models & Mechanisms*. 4:126-134.

Tzou, P., De Gregorio, E., and Lemaitre, B. (2002). How *Drosophila* combats microbial infection: a model to study innate immunity and host-pathogen interactions. *Current Opinions in Microbiology*. 5:102–110.

Van De Bor V. & Davis I. (2004) mRNA localisation gets more complex. *Current Opinion in Cell Biology.* 16(3): 300-307.

Van Doren, M., Williamson, A.L., and Lehmann, R. (1998). Regulation of zygotic gene expression in *Drosophila* primordial germ cells. *Current Biology*. 8(4):243-246.

Van Dusen C.M., Yee L., McNally L.M. & McNally M.T. (2010) A Glycine-Rich Domain of hnRNP H/F Promotes Nucleocytoplasmic Shuttling and Nuclear Import through an Interaction with Transportin 1. *Molecular and Cellular Biology*. 30: 2552-2562.

Vlisidou I., Dowling AJ., Evans IR., Waterfield N., ffrench-Constant RH. & Wood W. (2009) *Drosophila* Embryos as Model Systems for Monitoring Bacterial Infection in Real Time. PloS Pathogens. 5(7):e1000518. doi: 10.1371/journal.ppat.1000518.

Wang W., Eddy R. & Condeelis J. (2007) The cofilin pathway in breast cancer invasion and metastasis. *Nature Reviews Cancer*. 7:429-440.

Weil T.T., Forrest K.M. & Gavis E.R. (2006) Localization of *bicoid* mRNA in late oocytes is maintained by continual active transport. *Developmental Cell*. 11(2):251-262.

Welch, MD., DePace, AH., Verma, S., Iwamatsu, A. and Mitchison, T.J. (1997). The human Arp2/3 complex is composed of evolutionarily conserved subunits and is localized to cellular regions of dynamic actin filament assembly. *The Journal of Cell Biology*. 138(2):375-384.

Willet M., Brocard M., Pollard H.J. & Morley S.J. (2013) mRNA encoding WAVE–Arp2/3-associated proteins is co-localized with foci of active protein synthesis at the leading edge of MRC5 fibroblasts during cell migration. *Biochemical Journal*. 452(1):45-55.

Willett M., Brocard M., Davide A. and Morley S.J. (2011) Translation initiation factors and active sites of protein synthesis co-localize at the leading edge of migrating fibroblasts. *Biochemical Journal*. 438(1):217-227.

Willett, M., Pollard, H. J., Vlasak, M. and Morley, S. J. (2009) Localisation of ribosomes and translation initiation factors to talin/β3-integrin-enriched adhesion complexes in spreading and migrating mammalian cells. *Biology of the Cell*. 102(5):265-276.

Wood A. & Thorogood P. (1984) An analysis of *in vivo* cell migration during teleost fin morphogenesis. *The Journal of Cell Science*. 66:205-222.

Wood W. & Jacinto A. (2007) *Drosophila melanogaster* embryonic haemocytes: masters of multitasking. *Nature Reviews: Molecular Cell Biology*. 8(7):542-550.

Wood W., Faria C. & Jacinto A. (2006) Distinct mechanisms regulate hemocyte chemotaxis during development and wound healing in *Drosophila melanogaster*. The *Journal of Cell Biology.* 173(3):405-16.

Wu B., Chao JA. & Singer RH. (2012) Fluorescence fluctuation spectroscopy enables quantitative imaging of single mRNAs in living cells. *Biophysical Journal*. 102(12):2936-2944.

Wu JS. & Luo L. (2006) A protocol for mosaic analysis with a repressible cell marker (MARCM) in *Drosophila*. *Nature Protocols*. 1(6):2583-2589.

Xue Y., Zhou Y., Wu T., Zhu T., Ji X., Kwon Y., Zhang C., Yeo G., Black DL., Sun H., Fu X. & Zhang Y. (2009) Genome-wide Analysis of PTB-RNA Interactions Reveals a Strategy Used by the General Splicing Repressor to Modulate Exon Inclusion or Skipping. *Molecular Cell*. 36(6):996-1006.

Yamazaki D., Kurisu S. & Takenawa T. (2005) Regulation of cancer cell motility through actin reorganization. *Cancer Science*. 96(7):379-386.

Yanagawa S., Lee JS. & Ishimoto A. (1998) Identification and characterization of a novel line of *Drosophila* Schneider S2 cells that respond to wingless signaling. *The Journal of Biological Chemistry.* 273(48):32353-9.

Yano T., López de Quinto S., Matsui Y., Shevchenko A., Shevchenko A. & Ephrussi A. (2004) Hrp48, a *Drosophila* hnRNPA/B Homolog, Binds and Regulates Translation of oskar mRNA. *Developmental Cell*. 6(5):637-648.

Zaidel-Bar R., Cohen M., Addadi L. & Geiger B. (2004) Hierarchical assembly of cell–matrix adhesion complexes. *Biochemical Society Transactions*. 32(3):416-419.

Zanet J., Stramer B., Millard T., Martin P., Payre F. & Plaza S. (2009) Fascin is required for blood cell migration during *Drosophila* embryogenesis. *Development.* 136(15):2557–2565.

Zhang D., Grode K.D., Stewman S.F. *et al* (2011) *Drosophila* Katanin is a microtubule depolymerase that regulates cortical-microtubule plus-end interactions and cell migration. *Nature Cell Biology*. 13(4):361-370.

Zimyanin V.L., Belaya K., Pecreaux J., Gilchrist M.J., Clark A., Davis I. & St Johnston D. (2008) *In vivo* imaging of *oskar* mRNA transport reveals the mechanism of posterior localization. *Cell*. 124(5):843-853.

Zou L., Hazan R. & Roy P. (2009) Profilin-1 overexpression restores adherens junctions in MDA-MB-231 breast cancer cells in R-cadherin-dependent manner. *Cell Motility and the Cytoskeleton*. 66(12):1048-1056.

Appendices

Appendix 1: A) Constructs generated and tested for fly transgenesis

Table showing the constructs generated and tested for fly transgenesis in this project, the vectors into which they were cloned, whether the construct expresses a protein or an mRNA, and the PhiC31 landing site into which the transgene was integrated during fly transgenesis. A map of the vectors used for cloning can be found in Appendix 3.

Construct	UAS Plasmid(s)	Protein or mRNA expressed	PhiC31 landing site
Fluorescently-labelled RNA-binding proteins			
UAS-Hrp48-mCherry	pTiger (pUASP-14xUAS)	Protein	Attp2
UAS-Hrp48-GFP	pTiger	Protein	Attp2
UAS-Imp-mCherry	pTiger & pUASt-attB	Protein	Attp2
UAS-Imp-GFP	pTiger & pUASt-attB	Protein	Attp2
UAS-PTB-GFP	pTiger	Protein	Attp40
UAS-GFP-PTB	pTiger	Protein	Attp40
MS2 system Reagents			
UAS-MCP-GFP (No NLS)	pTiger & pUASt-attB	Protein	Attp40, Attp2
UAS-NLS-MCP-mCherry	pTiger & pUASt-attB	Protein	Attp40
UAS-NLS-MCP-GFP	pTiger & pUASt-attB	Protein	Attp40
UAS-NLS-tandemMCP-mCherry	pTiger	Protein	Attp40
UAS-NLS-tandemMCP-GFP	pTiger	Protein	Attp40
UAS-18x hairpin MS2 binding sites-*actin42a*	pTiger	mRNA	Attp40
UAS-18xMS2-actin5c	pTiger	mRNA	Attp2
UAS-18xMS2-*arp14D*	pTiger	mRNA	Attp3
UAS-18xMS2-*arp66B*	pTiger	mRNA	Attp2
***serpent*-Gal4::VP16 driver**			
serpent-Gal4::VP16	pUAST (NO UAS sites)	Protein	Attp40, Attp2

Appendix 1: B) Constructs generated for the synthesis of RNA probes

Table showing the constructs generated in this project for *in vitro* transcription of RNA probes. The restriction enzyme used for template linearization is shown, together with the promoter used for *in vitro* transcription, the orientation of the probe and the type of assay in which the probe was used.

Construct	Linearized with	Promoter/ Probe	Purpose
Biotinylated RNA Probes			
pBS-*myospheroid*-5' UTR	XbaI	T7/Sense	RNA-affinity pull down assays
pBS-*myospheroid*-3' UTR	XbaI	T7/Sense	RNA-affinity pull down assays
pJET2.1-*myospheroid*-coding sequence	XbaI	T7/Sense	RNA-affinity pull down assays
pBS-*chickadee*-3' UTR	XbaI	T7/Sense	RNA-affinity pull down assays
pBS-*actin42A*-3'UTR	XbaI	T7/Sense	RNA-affinity pull down assays
pBS-*actin42A*-3'UTR-ΔIBE1	XbaI	T7/Sense	RNA-affinity pull down assays
pBS-*actin42A*-3'UTR- ΔIBE2-ΔIBE3	XbaI	T7/Sense	RNA-affinity pull down assays
DIG RNA Probes			
pBS-actin42A-cDNA(*β-actin*)	HindIII	T3/Antisense	*In situ* hybridization (FISH)
pBS-actin42A-cDNA (*β-actin*)	XbaI	T7/Sense	*In situ* hybridization (FISH)

Appendix 2: Table of primer sequences used for PCR amplification, cloning and sequencing of constructs.

Nº	Primer Name	Primer Sequence	Purpose
MS2 System			
1	GW_SphI_Fwd	5'AAAAAGCATGCGGTATACAAGTTTGTAC 3'	Cloning of Gateway cassette into pTiger
2	GW_SphI_Rev	5'AAAAAGCATGCTTACGTCACCAC 3'	Cloning of Gateway cassette into pTiger
3	MS2_NotI_KpnI_Fwd	5'CCATGCGGCCGCCGGTACCATGGCTTCTAAC 3'	Cloning of MCP (No NLS) into pTiger/UASt
4	NLS_MS2_NotI_ BamHI_Fwd	5'GTCGGCGGCCGCGATAAGCTTG 3'	Cloning of NLS-MCP into pTiger/UASt (Endogenous BamHI site further down in sequence)
5	MS2_NotI_Rev	5' GAAGCGGCCGCCGTAGATG 3'	Cloning of both MCP (No NLS) & NLS-MCP into pTiger/UASt
6	tdMCP_NotI_Fwd	5'AAAGGTACCGCTGTGATCGTCACTTGG	Cloning of NLS-tdMCP into pTiger-GFP/mCherry (Endogenous NotI site further down in sequence)
7	tdMCP_NotI_Rev	5'AAAGCGGCCGCCGTAGATGCCGGAGTTTG 3'	Cloning of NLS-tdMCP into pTiger-GFP/mCherry
8	Act5C_gDNA_Fwd	5'CACCACTTTCAGTCGGTTTATTCCAG 3'	Cloning of *actin5C* genomic region into pENTR-TOPO
9	Act5C_gDNA_Rev	5' GTGTGTGGAATGGCAGAATATG 3'	Cloning of *actin5C* genomic region into pENTR-TOPO
10	Act42A_gDNA_Fwd	5'CACCACTTTAACTCGAAAAAGTAGGCG 3'	Cloning of *actin42A* genomic region into pENTR-TOPO
11	Act42A_gDNA_Rev	5'CATGCCAGCCAAATGCTAGC 3'	Cloning of *actin42A* genomic region into pENTR-TOPO
12	Arp14D_gDNA_Fwd	5'CACCGCCGATAGTATCGAATATGCA 3'	Cloning of *arp14D* genomic region into pENTR-TOPO
13	Arp14D_gDNA_Rev	5'GCATTCACTTACATAATTGGCATTCCAC 3'	Cloning of *arp14D* genomic region into pENTR-TOPO
14	Arp66B_gDNA_Fwd	5'CACCGCGAATGTGTGTGTGAC 3'	Cloning of *arp66B C* genomic

			region into pENTR-TOPO
15	Arp66B_gDNA_Rev	5'CGAAAGCGACGAAAGTGTTTGAG 3'	Cloning of *arp66B* genomic region into pENTR-TOPO
16	Oskar_gen_Fwd	5'CACCGGATCCAAGAATATTGGATCAC 3'	Cloning of *oskar* genomic region into pENTR-TOPO
17	Oskar_gen_Rev	5'AAGCTTAGAGCAAACAAAATCATTG 3'	
serpent-Gal4::VP16 Cassette			
18	*Srp*_Frag1_KpnI_Fwd	5'AGAGGTACCCTACTGCTTCCCACTC TAAG 3'	Cloning upstream fragment of *serpent* promoter
19	*Srp*_Frag1_XhoI_Rev	5'AAACTCGAGGGCAATGCCCCACCC CTTG 3'	
20	*Srp*_Frag2_XhoI_Fwd	5'AAACTCGAGCAGCGGGAGCAACAG GATCAA 3'	Cloning downstream fragment of *serpent* promoter
21	*Srp*_Frag2_SalI_Rev	5'AAAGTCGACTATGGGATCCGTGCTG GGGTAG 3'	
22	Gal4:VP16_SalI_Fwd	5'AAAGTCGACATGAAGCTACTGTCTT CTATCGAAC 3'	Cloning Gal4::VP16
23	Gal4:VP16_HindIII_Rev	5'AAAAAGCTTCATATCCAGAGCGCCG TAG 3'	
24	SV40_EcoRI_Fwd	5'AAAGAATTCTTGTTTATTGCAGCTTA TAATGGTTAC 3'	Cloning SV40 terminator region from pUAST
25	SV40_BamHI_Rev	5'AAAGGATCCAGACATGATAAGATA CATTGATG 3'	
UAS-Imp, Hrp48 & PTB			
26	Imp_KpnI_Fwd	5'AAAGGTACCATGGCATCCGAACTGG ATCAATTCG 3'	Cloning of Imp coding region into pTiger & pUASt-attB
27	Imp_KpnI_Rev	5'AAAGGTACCCTGTTGTGAGCTCGCC AGCTG 3'	
28	Hrp48_KpnI_Fwd	5'AAAGGTACCATGGAGGAAGACGAG AGGGG 3'	Cloning of Hrp48 coding region into pTiger & pUASt-attB
29	Hrp48_KpnI_Rev	5'AAAGGTACCGGACAGCCTGCGAGG TTGC 3'	

30	PTB_KpnI_Fwd	5'AAAGGTACCATGATGTCCTGCCCCATTC 3'	Cloning of PTB coding region into pTiger (PTB::GFP)
31	PTB_KpnI_Rev	5'AAAGGTACCCGATGTTCGACTTCGAGAAGCTTAC 3'	
32	GFP-PTB_KpnI_Fwd	5'AAAGGTACCATGGTGAGCAAGGC 3'	Cloning of PTB coding region into pTiger (GFP::PTB)
33	GFP-PTB_SpeI_Rev	5'AAAACTAGTCTTGTACAGCTCGTCCATG3'	
pBS clones to synthesize digoxigenin **probes for *in situ* hybridization**			
34	Act42A_HindIII_Fwd	5'AAAAAGCTTGTCGTTCCTCATCGAA33CACAC 3'	Cloning full-length cDNA of actin42A into pBS-SK+ to generate an RNA probe for *in situ* hybridization
35	Act42A_XbaI_Rev	5'AAATCTAGACGGTTACAAGTATTTTAGTGGTATGG 3'	
pBS clones to synthesize biotinylated RNA probes			
36	Mys_5'UTR_KpnI_Fwd	5'AAAGGTACCACATTGACTGTTGTTCCACCCCCTG 3'	Cloning 5'UTR of *myospheroid* (β-integrin) into pBS-SK+
37	Mys_5'UTR_XbaI_rev	5'AAATCTAGAGGCUUUGGCGGUUAGCGGUU 3'	
38	Mys_CDS_EcoRI_fwd	5'AAAGAATTCATGATCCTCGAGAGAAACCGG 3'	Cloning CDS of *myospheroid* into pBS-SK+
39	Mys_CDS_XbaI_rev	5'AAATCTAGACUAUUUGCCCGCAUA 3'CAUGGG	
40	Mys_3'UTR_KpnI_fwd	5'AAAGGTACCATTCGCTAACTAACTAAACATTAG 3'	Cloning 3'UTR of *myospheroid* into pBS-SK+
41	Mys_3'UTR_XbaI_Rev	5'AAATCTAGAAUUUUACUAAAAUUAGCGUCAAAC 3'	
42	Chic_3'UTR_KpnI_Fwd	5'AAAGGTACCTAGGAGAATAGATCAACAC 3'	Cloning 3'UTR of *chickadee* (Profilin) into pBS-SK+
43	Chic_3'UTR_NotI_Rev	5'AAATCTAGACGTGTGGATTTATGTACG 3'	
44	Act42A_3'UTR_KpnI_Fwd	5'AAAGGTACCGCAGTAGTCGGGCTGGGC 3'	Cloning 3'UTR of *actin42A* (β-actin) into pBS-SK+
45	Act42A_3'UTR_XbaI_Rev	5'AAATCTAGACAGTTCTTTTCGTCGCTTTATTATTAAGAAGC 3'	

Site directed mutagenesis (SDM) – *actin42A* 3'UTR			
46	Act42A_3'UTR _**NsiI**_**ΔIBE1**_ Fwd	5'AGA**ATGCAT**TCCATTCACT**GGGCG** ACACAGTTGT 3'	Site-directed mutagenesis of Imp binding site 1 (IBE1)
47	Act42A_3'UTR_**NdeI**_**ΔIBE2**_**ΔIBE3**	5'GTT**CATATG**CACATAAGCA**GAGCT** CAAAACTGATTCATGTTTGGCA**GGGC** GATTACTTCCATG 3'	Site-directed mutagenesis of Imp binding sites 2 and 3 (IBE2 & IBE3)
48	T3	5'ATTAACCCTCACTAAAGGGA 3'	Antisense primer for site-directed mutagenesis
Sequencing			
49	pTiger_seq	5'CCGCATAGGCCACTAGTG 3'	Sequence the 5' of all UAS constructs
50	pTiger_down	5'TCAAAGGCAGAAATGTTTACTCTTG ACC 3'	Sequence the 3' of the pTiger-18x MS2 hairpin-Gateway/mRNA constructs
51	pUASt_fwd	5'CAACTACTGAAATCTGCCAAG 3'	Sequence the 5' of UAS constructs and *srp*-Gal4::VP16 cassette
52	GFP_Rev	5'GTCCAGCTCGACCAGGATG 3'	Sequence the 3' of all C-terminally-tagged GFP constructs
53	mCherry_Rev	5' CACCCTTGGTCACCTTCAGC 3'	Sequence the 3' of all C-terminally-tagged GFP constructs
54	*Srp*_700bp_Fwd	5' CAGCCCATTAAAAGTGCCCCAG 3'	Sequence the entire *srp*-Gal4::VP16 cassette
55	*Srp*_1400bp_Fwd	5' ACCACAAGGCATCTTCCGGAC 3'	
57	*Srp*_2500bp_Fwd	5'CTCTCGCTCTATCTGTGCCAG 3'	
58	*Srp*_3280bp_Fwd	5' GCTTGCTTAGCGCCTGAGATC 3'	
59	Gal4_vp16_500bp_Fwd	5' AGACGATTTCGATCTGGACATG 3'	
Transgenic fly screening			
60	pTiger_attB_fwd	5'ACCAGCTCTTCGGCTTG 3'	Screen for insertion of pTiger constructs into appropriate PhiC31 landing site
61	pUAST_attB_fwd	5'CACTGCATTCTAGTTGTGGTTTGTCC AAAC 3'	Screen for insertion of pUAST constructs into appropriate PhiC31 landing site

62	Attp40_3'_rev	5'GCGGAGAGTACGTGGTAAACAACATC 3'	Screen for insertion of constructs into Attp40 landing site
63	Attp2_3'_rev	5'GAATACAATTGGCTTACGTAAGCC 3'	Screen for insertion of constructs into Attp2 landing site
Screening for MS2-binding site mRNA expression in haemocytes			
64	MS2_mRNA_Screen_fwd	5'GATCTGCTACCGGTATACAAGTTT 3'	PCR screen for expression of MS2-binding site labelled *actin42A* and *oskar* mRNAs
65	*act42A*_screen_rev	5'CCGGAGTGTTGAAGGTTTCAAAC 3'	
66	*oskar*_screen_rev	5'GCGCACCTCACTATCTATATCGGG 3'	
Generate PCR template for dsRNA synthesis			
67	Imp RNAi_T7_Fwd	5'TAATACGACTCACTATAGGGCACTGTCAGCTCTATCAACGACATC 3'	Generate PCR template for synthesis of dsRNA against *imp*
68	Imp RNAi_T7_Rev	5'TAATACGACTCACTATAGGGCCGGTGTGCCAACAATCGTC 3'	
69	GFP_RNAi_T7_Fwd	5'TAATACGACTCACTATAGGGGCCAGATACCCAGACCACAT 3'	Generate PCR template for synthesis of dsRNA against *gfp*
70	GFP_RNAi_T7_Rev	5'TAATACGACTCACTATAGGGATTGGGGTGTTCTGCTGGTA 3'	
71	Mys_RNAi_T7_Fwd	5'TAATACGACTCACTATAGGGTGTGCATCGAAGGAAAAGTGTCACAC 3'	Generate PCR template for synthesis of dsRNA against *myospheroid* (*β-integrin*)
72	Mys_RNAi_T7_Rev	5'TAATACGACTCACTATAGGGTACTCTTCGTATCCGCTGGCGG 3'	
Real-time quantitative PCR Primers			
73	Rp49_fwd	5'GCTAAGCTGTCGCACAAATGGCG 3'	Quantify *rp49* mRNA levels (qPCR)
74	Rp49_rev	5'TCCGGTGGGCAGCATGTG 3'	
75	H2A(CG31618)_fwd	5'CCGTGCCGGTCTTCAATTCCCTG 3'	Quantify *H2A* mRNA levels (qPCR)
76	H2A(CG31618)_rev	5'CGAGAACCTCAGCGGCCAGAT 3'	
77	RNA polII_fwd	5'TGGTGGTTCGGCCAAGAAT 3'	Quantify RNA polII levels (qPCR)
78	RNA polII_rev	5'CCACACAAGCAATAACCTGGGA 3'	
79	Act42A_RT_PCR_fwd	5'GATGAGGCACAGAGCAAACGTGG 3'	Quantify *actin42A* (*β-actin*) mRNA levels (qPCR)
80	Act42A_screen_rev	5'CCGGAGTGTTGAAGGTTTCAAAC 3'	

81	Imp_pPCR_fwd	5’TCGAGAAGATGCGCGAAGAAGG 3’	Quantify *imp* mRNA levels (qPCR)
82	Imp_qPCR_rev	5’AATGATACGGCCCACCTGAGAG 3’	
83	Mys_fwd	5’GCTGCTCACTACGATCCACGATC 3’	Quantify *myospheroid* (*β-integrin*) mRNA levels (qPCR)
84	Mys_rev	5’CCCGCATACATGGGGTTCTTGAAGG 3’	
85	Profilin_fwd	5’GAGCTCTCCAAACTGATCAGCGG 3’	Quantify *chickadee* (*profilin*) mRNA levels (qPCR)
86	Profilin_rev	5’GTCTTCATGCAGTGCACTCCGCT 3’	
87	Arp2_fwd	5’GGATCTGATGGTCGGCGATGAG 3’	Quantify *arp14D* (*arp2*) mRNA levels (qPCR)
88	Arp2_rev	5’GTGTTCGTCGGATCGATGTCCATC 3’	
89	Arp3_fwd	5’CGATGTGCGGCGTCCTCTATAC 3’	Quantify *arp66B* (*arp3*) mRNA levels (qPCR)
90	Arp3_rev	5’GCGTCCCTCGGACAAATTCTCGC 3’	
91	Oskar_fwd	5’GCA ACT ATA TAT CCG TGC GCG 3’	Quantify *oskar* mRNA levels (qPCR)
92	Oskar_rev	5’CCC GTC AGT TTT CGA TAT TCA C 3’	
93	Tub67C_fwd	5’GGC AGC CTG AAG ACC AAG GAG GAG 3’	Quantify *tubulin67C (tub67C)* mRNA levels (qPCR)
94	Tub67C_rev	5’CAC TGC TCT GCG ATC TTC TGC 3’	
95	Bicoid_fwd	5’GAC CT GCG CCA TCG CCG TT 3’	Quantify *bicoid* mRNA levels (qPCR)
96	Bicoid_rev	5’ACC CTT CAA AGG CTC CAA GAT CTG TAG C 3’	
97	Gurken_fwd	5’CCC GCG CTT GCT GCT C 3’	Quantify *gurken* mRNA levels (qPCR)
98	Gurken_rev	5’CAC ACT TGC ATC TCC TTG TGG 3’	

Appendix 3: Maps of empty vectors used to clone constructs listed in Appendix 1

Appendix 3.1: Map of pTiger (pUASP-attB-14X UAS) expression vector

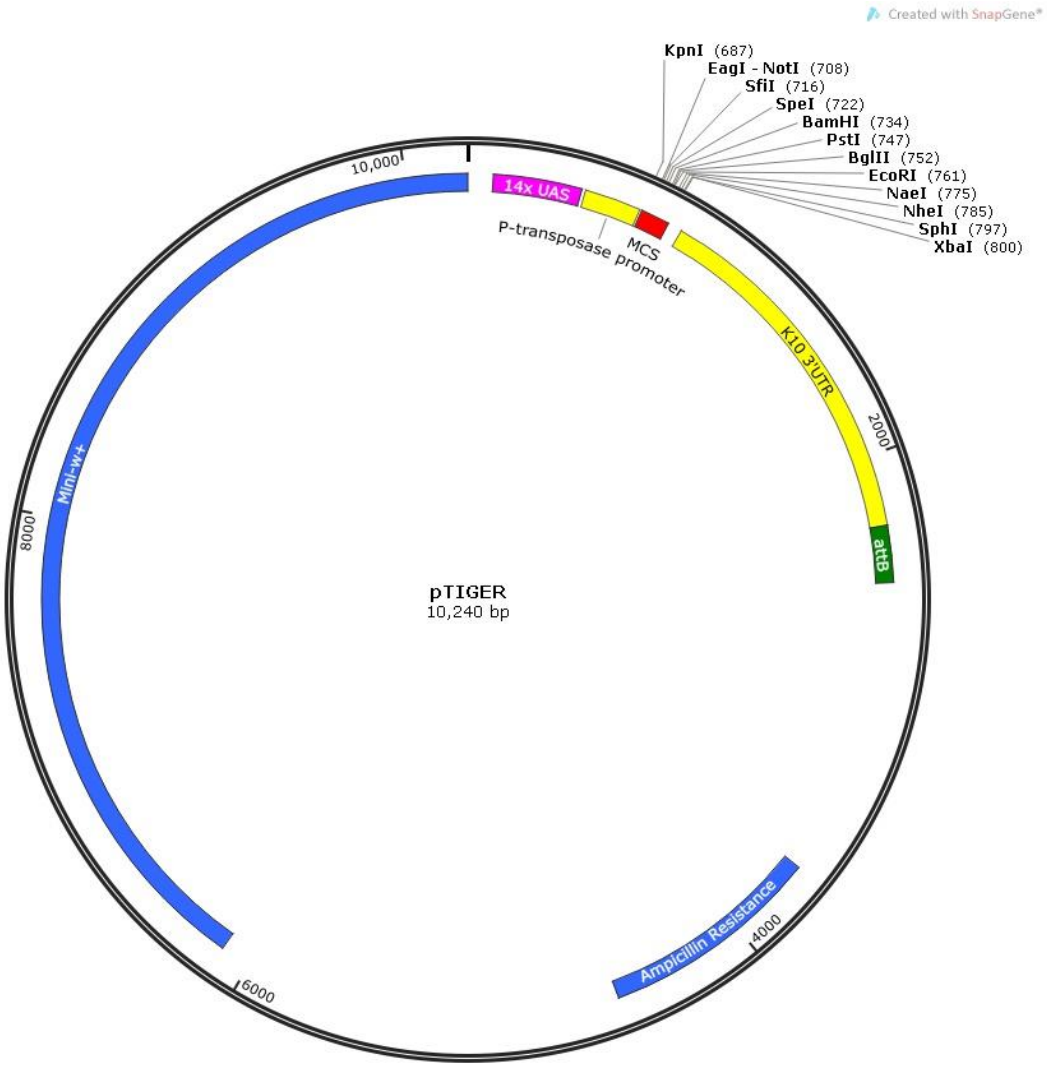

pTiger was designed to express constructs primarily within the germline of flies. The pTiger vector contains 14 UAS sites upstream of the multi-cloning site (MCS) to drive transgene expression using the GAL4/UAS system. The P-transposase promoter aids expression in the germline. The K10 3'UTR ensures transcription termination and polyadenylation of the transgene cloned into the MCS. The attB site allows the vector to be integrated into attP landing sites within the fly genome through the PhiC31 system (materials & methods). The mini *white* gene (w+) encodes an eye pigment transporter that restores eye colour in flies lacking the white gene, to screen adult flies for positive integration events. The β-lactamase ampicillin resistance gene allows for bacteria positive selection. pTiger was constructed by Scott B. Ferguson and described in Ferguson *et al*. 2012.

Appendix 3.2: Map of the pUAST-attB-19XUAS expression vector.

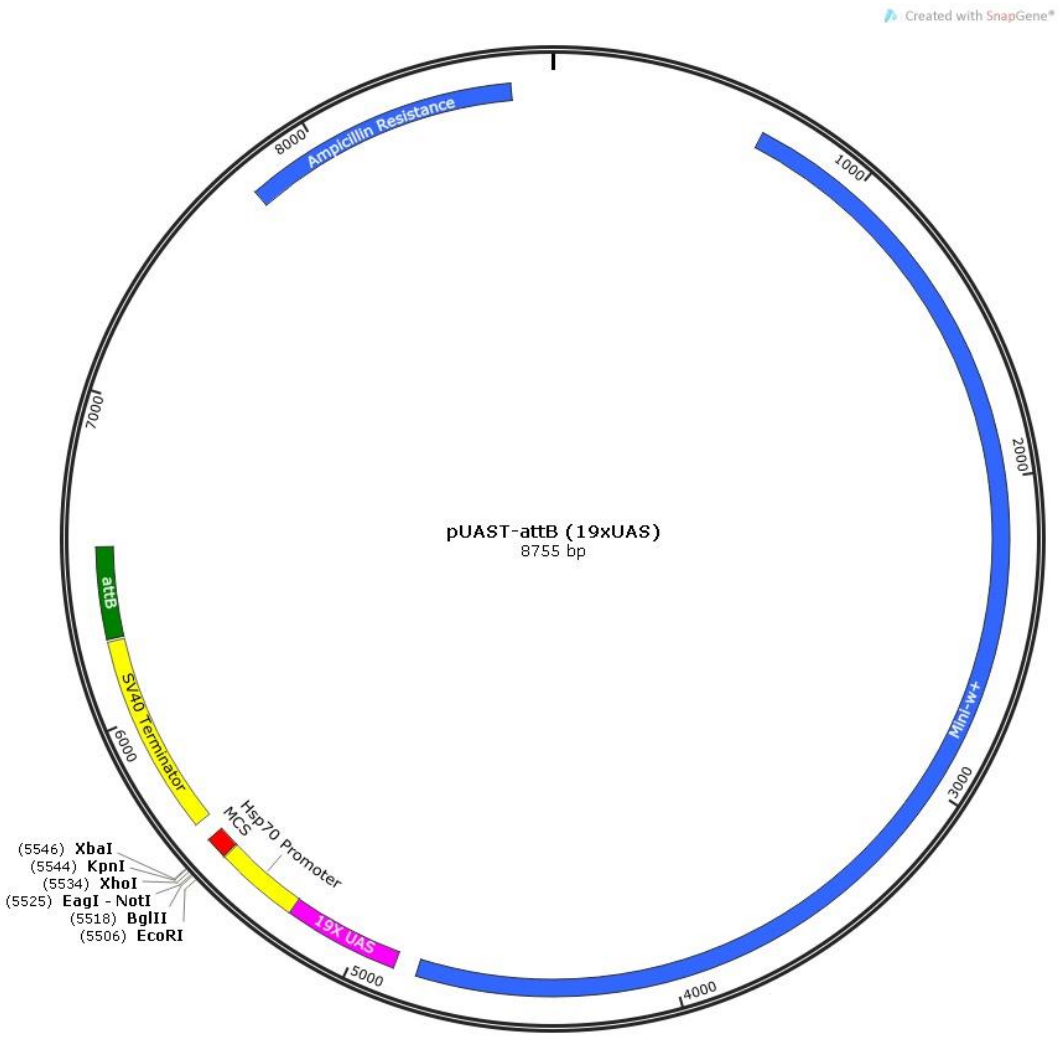

The pUAST-attB vector was originally designed to express transgenes mainly within the somatic tissue of flies using the GAL4/UAS system. The original vector was a gift from the Basler lab (Zurich, Switzerland) and contained five UAS sites. To increase transgene expressions, a HindIII fragment digested from pTiger and continaing 14X UAS sites was inserted into the pUAST-attB vector. The resulting modiefied pUAST-attB plasmid contains 19XUAS sites upstream of the multi-cloning site (MCS). The Hsp70 promoter aids transgene expression in the soma. The SV40 terminator ensures transcription termination and polyadenylation of the transgene cloned into the MCS. The attB site allows the vector to be integrated into attP landing sites within the fly genome through the PhiC31 system (materials & methods). The mini *white* gene (w+) encodes an eye pigment transporter that restores eye colour in flies lacking the white gene, to screen adult flies for positive integration events. The β-lactamase ampicillin resistance gene allows for bacteria positive selection.

Appendix 3.3: Map of the pBlueScript II (pBS) KS+ cloning vector.

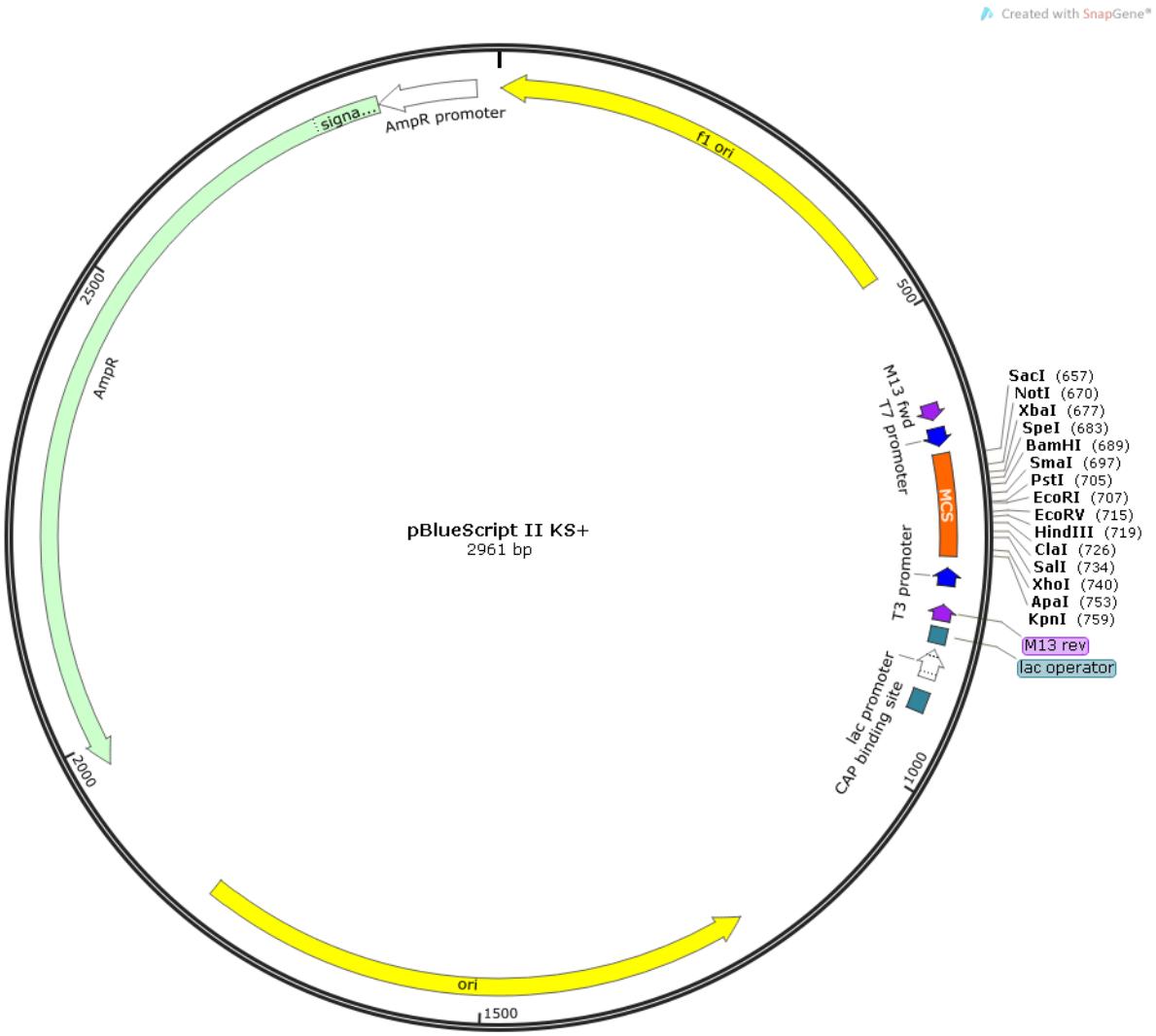

The pBS-KS+ vector (Stratagene) was used as an intermediate cloning step to build complex constructs before they were cloned into the final expression vector, or to clone sequences required to generate probes for *in situ* hybridisation. The pBS-KS+ vector contains T7 and T3 promoters on either side of the multi-cloning site (MCS), allowing for *in vitro* transcription of cloned sequences from these promoters. The vector also contains the ampicillin resistance gene for bacteria selection.

Appendix 3.4: Map of the pBlueScript II (pBS) SK+ cloning vector.

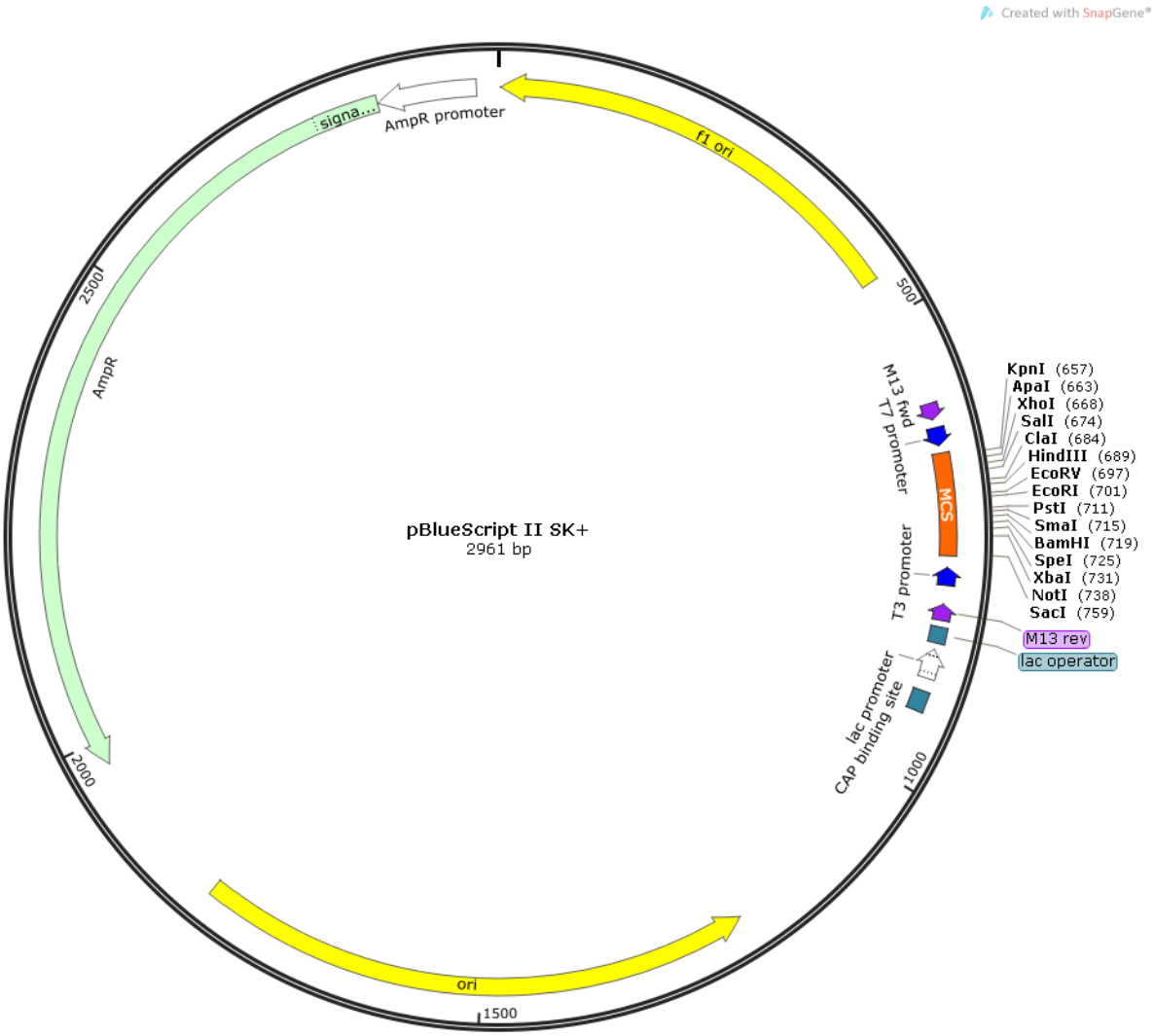

As for pBS-KS+ (see Appendix 3.3), but the multi-cloning site (MCS) is orientated in the opposite direction.

Appendix 3.5: Map of pENTR-TOPO cloning vector.

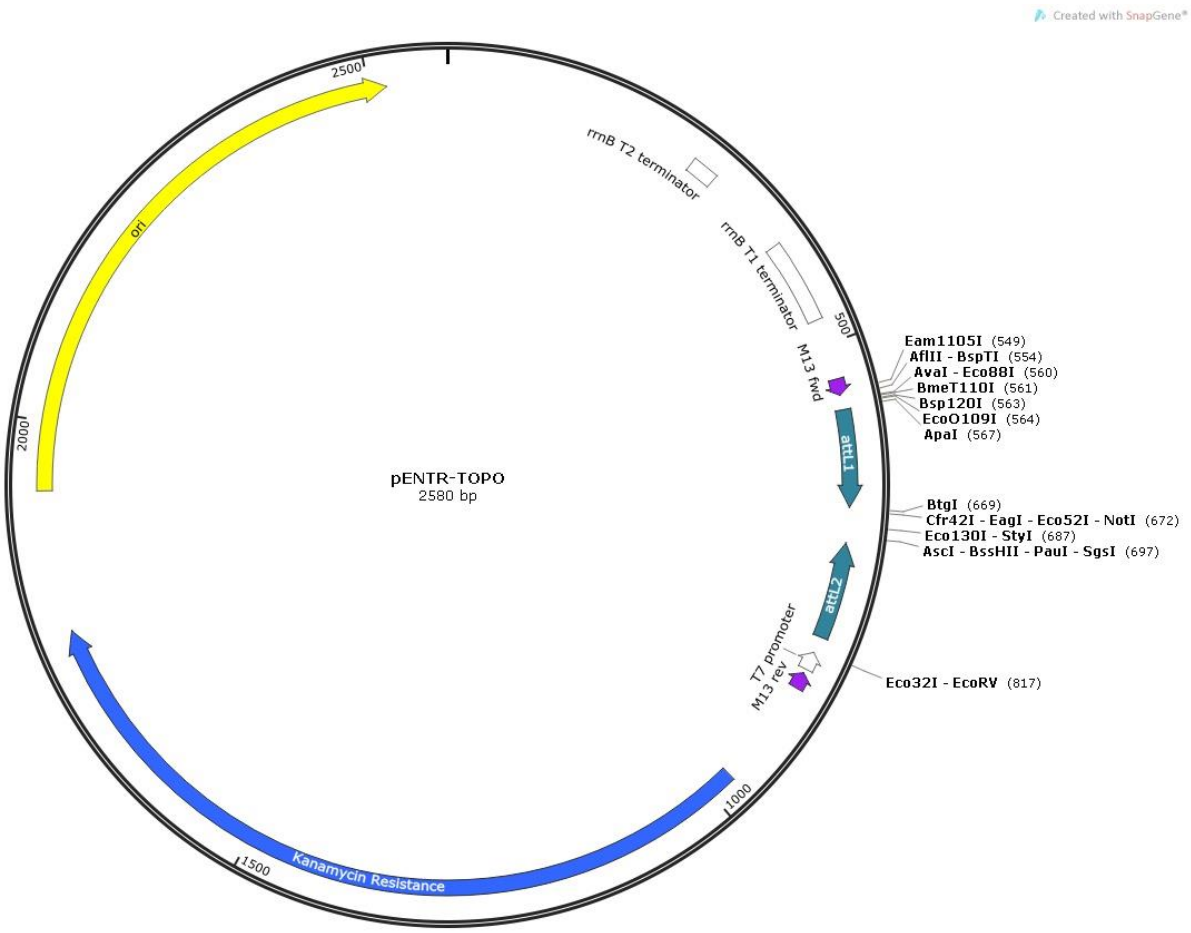

pENTR-TOPO (Invitrogen) was used to insert the genomic regions encoding for the candidate mRNAs after PCR amplification. The vector contains the kanamycin resistance gene to produce aminoglycoside phosphotransferase so that bacteria could be screened for the presence of the construct. The attL1 and attL2 sites, positioned either side of the transgene insertion site, allow recombination of the transgene into a destination vector containing a Gateway cassette (methods & materials). In our case, the destination vector is a modified version of the pTiger plasmid in which a cassette containing 18X MS2 hairpin repeats were inserted upstream of the Gateway cassette (see Appendix 4.1).

Appendix 3.6: Map of pJet1.2 cloning vector.

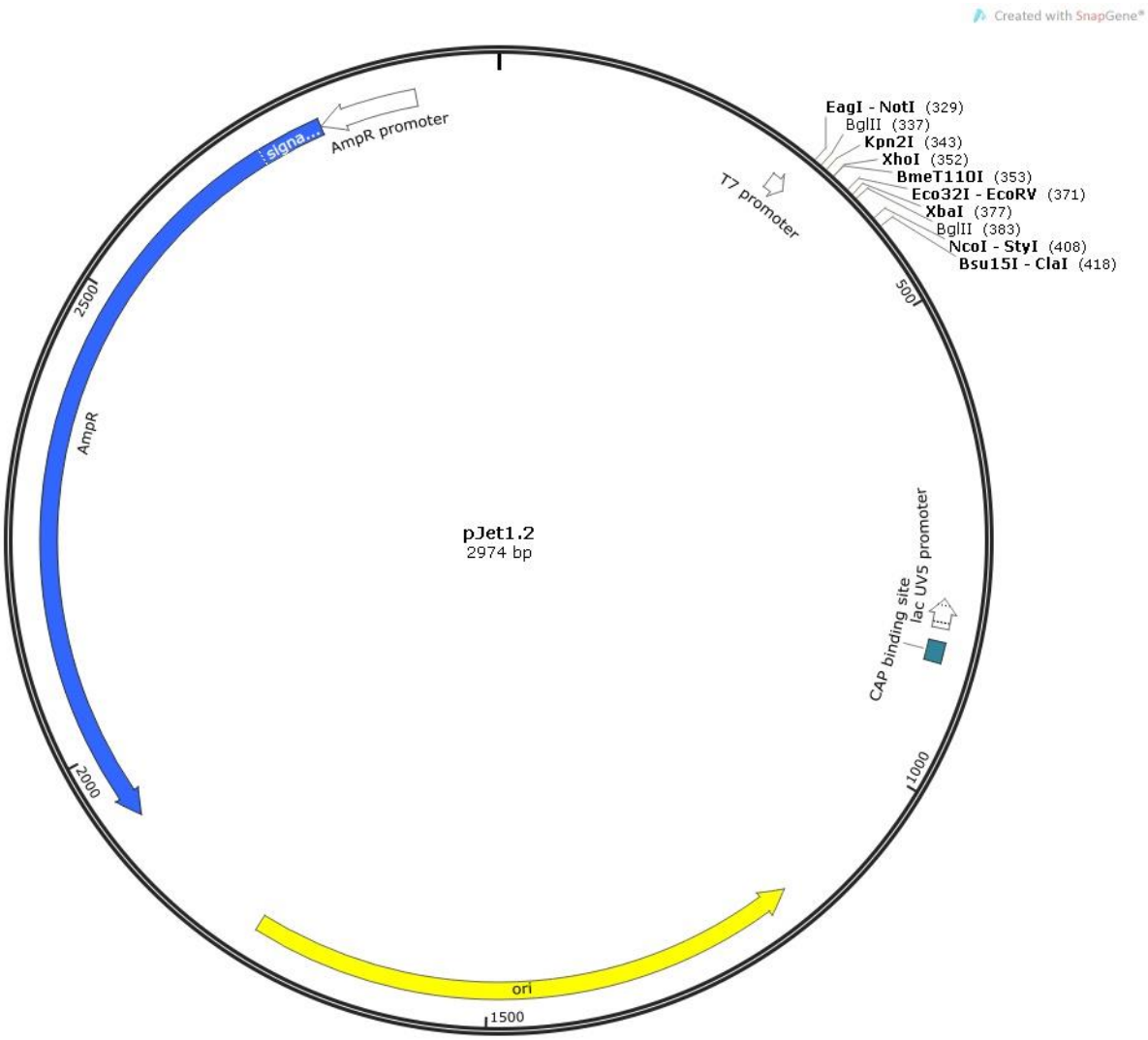

pJet1.2 (ThermoScientific) was used in some cases as an intermediate vector to insert PCR products before their subsequent cloning into the final destination vector. The pJet1.2 vector allows the cloning of PCR products with either 3'-dA overhangs or blunt-ended products when used with the thermostable DNA blunting enzyme (CloneJET PCR Cloning Kit – Thermo Scientific). The PCR fragments inserted into pJet1.2 were released by restriction enzyme digestion for their ligation into the final expression vector.

Appendix 4: Vector maps of constructs generated within this project

Appendix 4.1: Vector map of the 18 hairpin MS2 binding site repeats cloned into pTiger

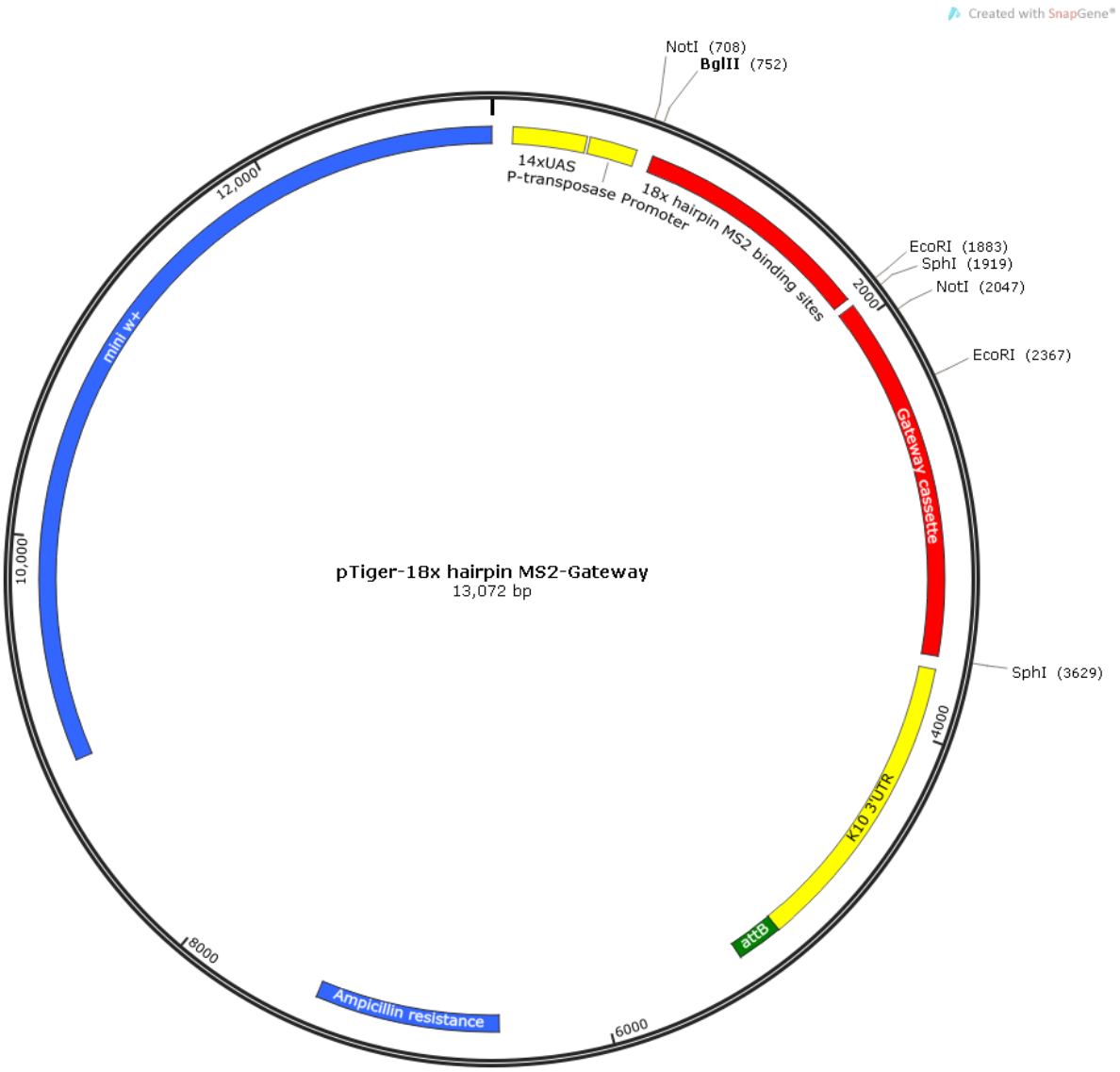

The 18 repeats of the hairpin MS2 binding sites were first cloned into pTiger (pUASp-14xUAS-attB) from BglII (5')-EcoRI (3'). The Gateway cassette was then PCR using primers that introduced SphI restriction sites at both the 5' and 3' and was ligated into this vector using SphI. The Gateway cassette was oriented in the construct using both an EcoRI and a NotI diagnostic digest. Candidate mRNA sequences were then recombined into the Gateway cassette to tag them with the 18x hairpin MS2 sites.

Appendix 4.2: Vector map of pTiger-NLS-MCP-eGFP/mCherry

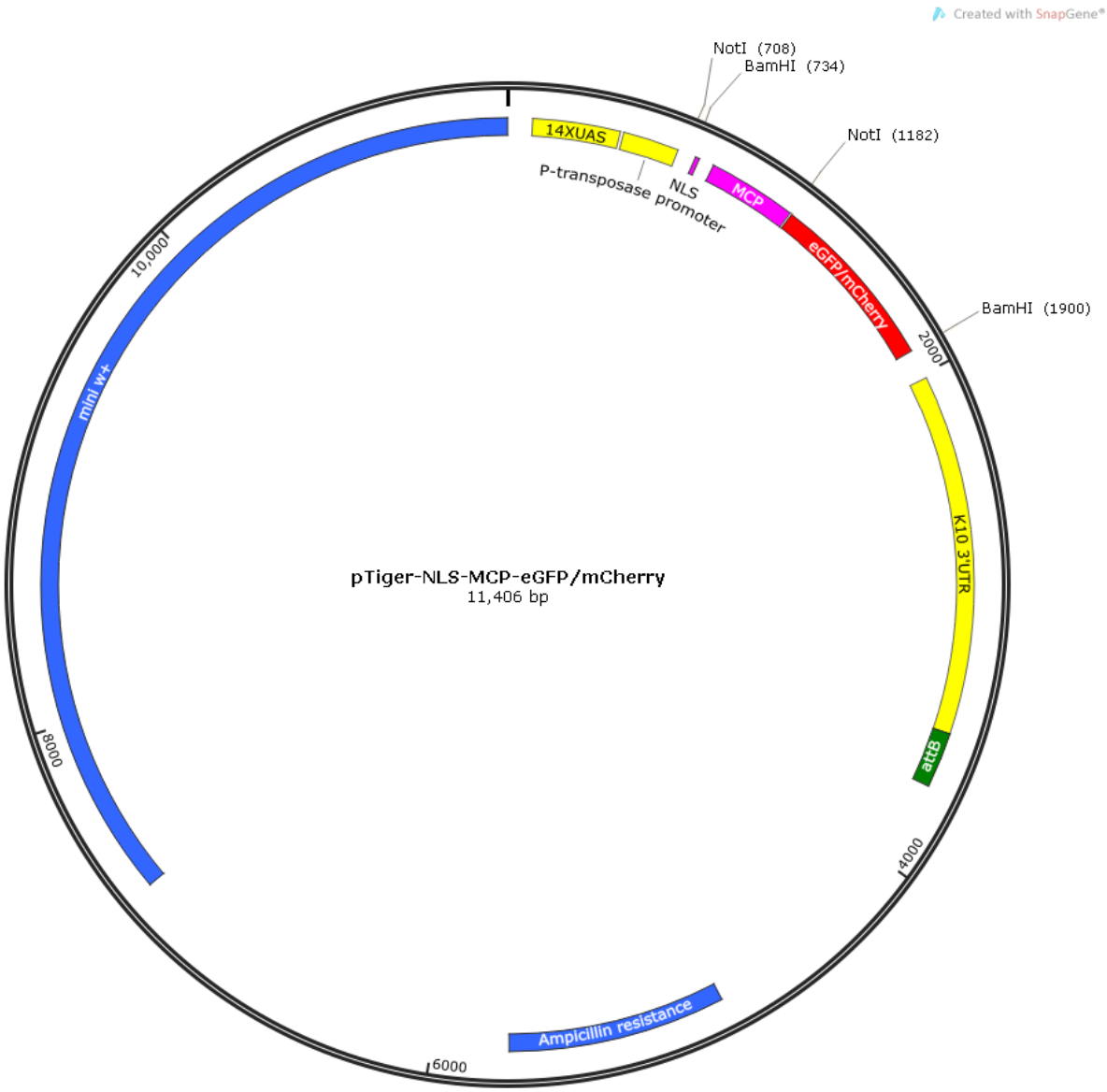

A single copy of the MCP sequence was cloned into pTiger and fused to both mCherry and eGFP. The sequence encoding NLS-MCP-eGFP/mCherry was first constructed in the pBS-SK+ vector (see materials and methods and map in appendix 3.3) and was released from pBS with a BamHI digest and the NLS-MCP-eGFP/mCherry cassette cloned into pTiger via BamHI.

Appendix 4.3: Vector map of pTiger-NLS-tandemMCP-mCherry/eGFP

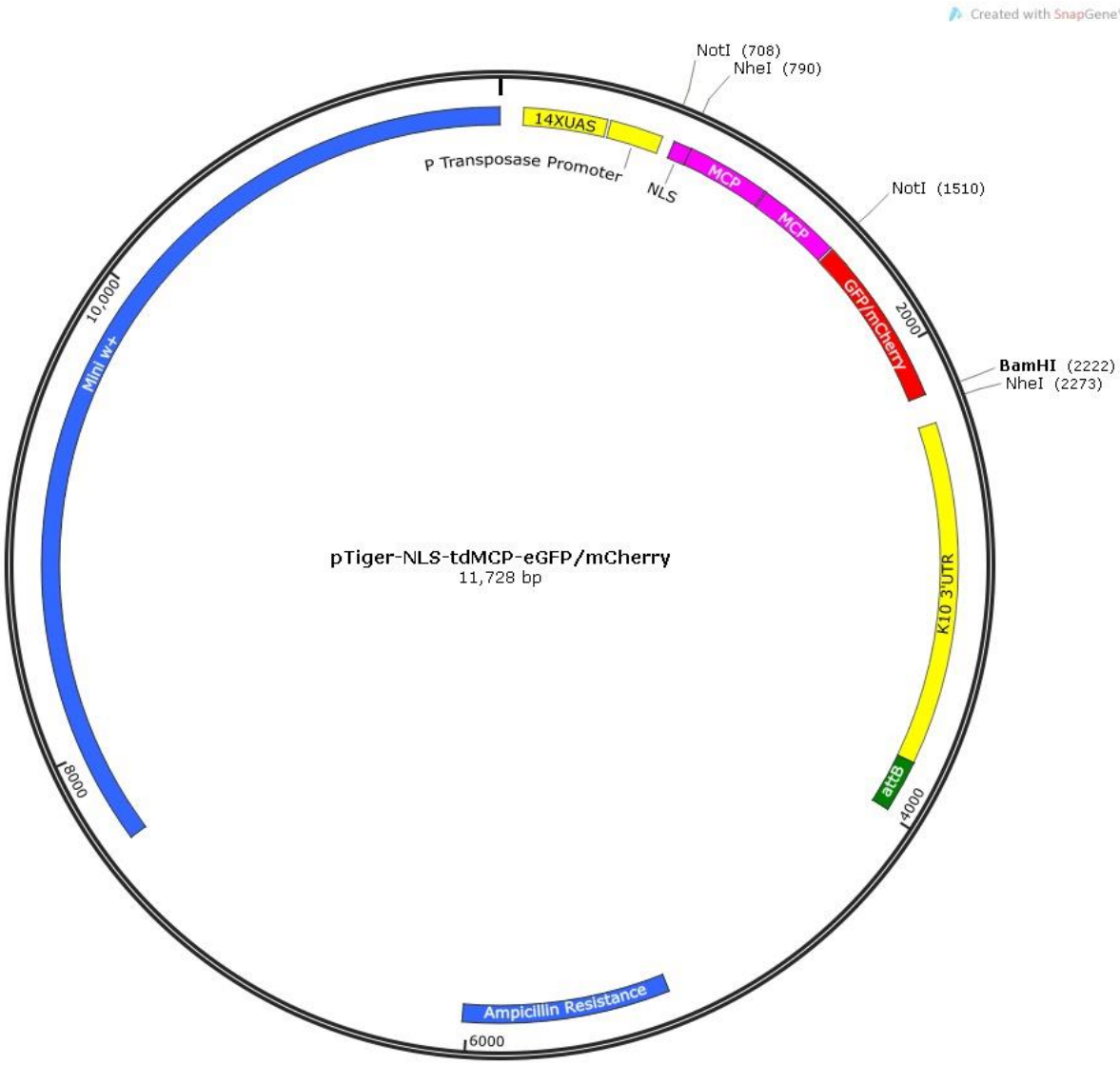

The NLS-tdMCP sequence was PCR amplified from an existing construct (UbC NLS-HA-MCP-YFP - Addgene plasmid 31230) and cloned into pTiger-mCherry- and eGFP via NotI, which were previously generated in the lab. A NheI restriction digest was used to orient the NLS-td-MCP fragment in pTiger-eGFP/mCherry.

Appendix 4.4: pUAST-*serpent*-Gal4::VP16 (UAS sites removed)

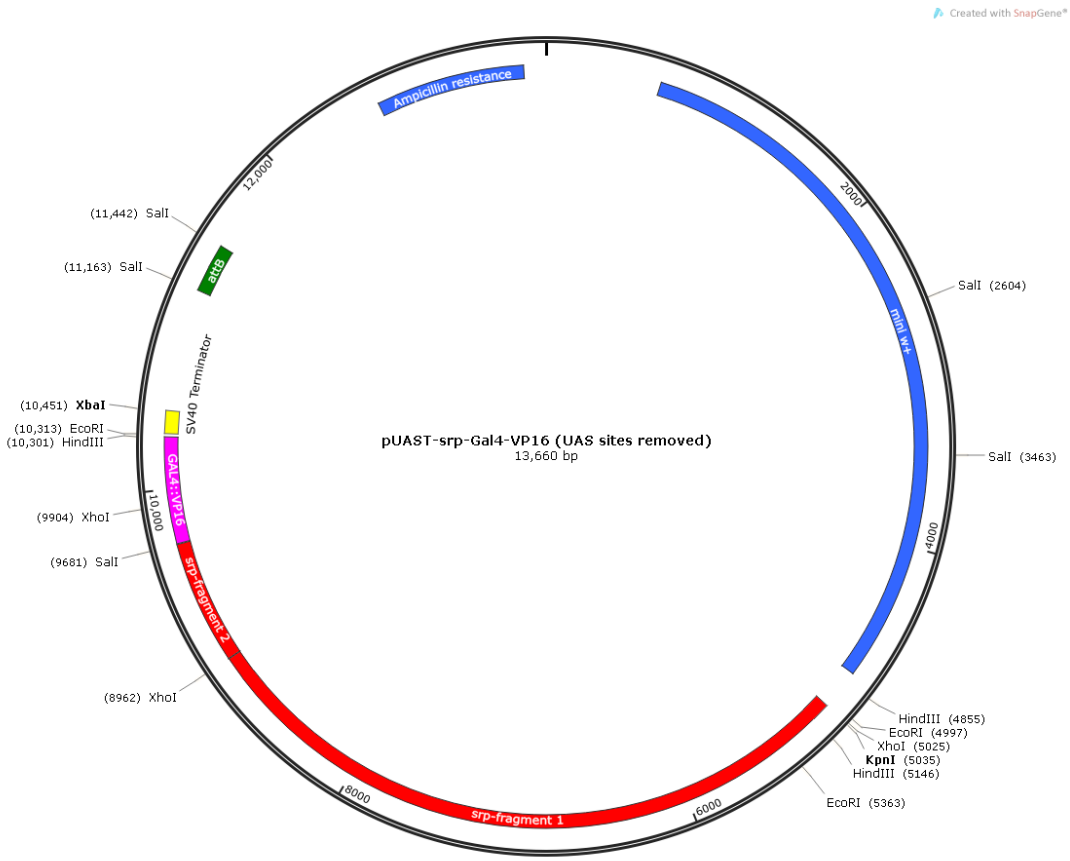

The *serpent*-Gal4::VP16 cassette was first constructed in pBS-SK+ (see appendix 3.3). Each individual component, including two fragments to generate the *srp* promoter, GAL4::VP16 and the SV40 terminator, were PCR amplified from either genomic or plasmid DNA and the relevant restriction sites added to the ends of each fragment (see materials and methods). The UAS sites were first removed from the pUAST-attB (19xUAS) vector *via* PstI digestion. The completed *srp* cassette was released from the pBS vector using KpnI and XbaI and cloned into the pUAST without UAS sites, digested with KpnI and XbaI.

Appendix 4.5: Vector map of pTiger-Imp-eGFP/mCherry

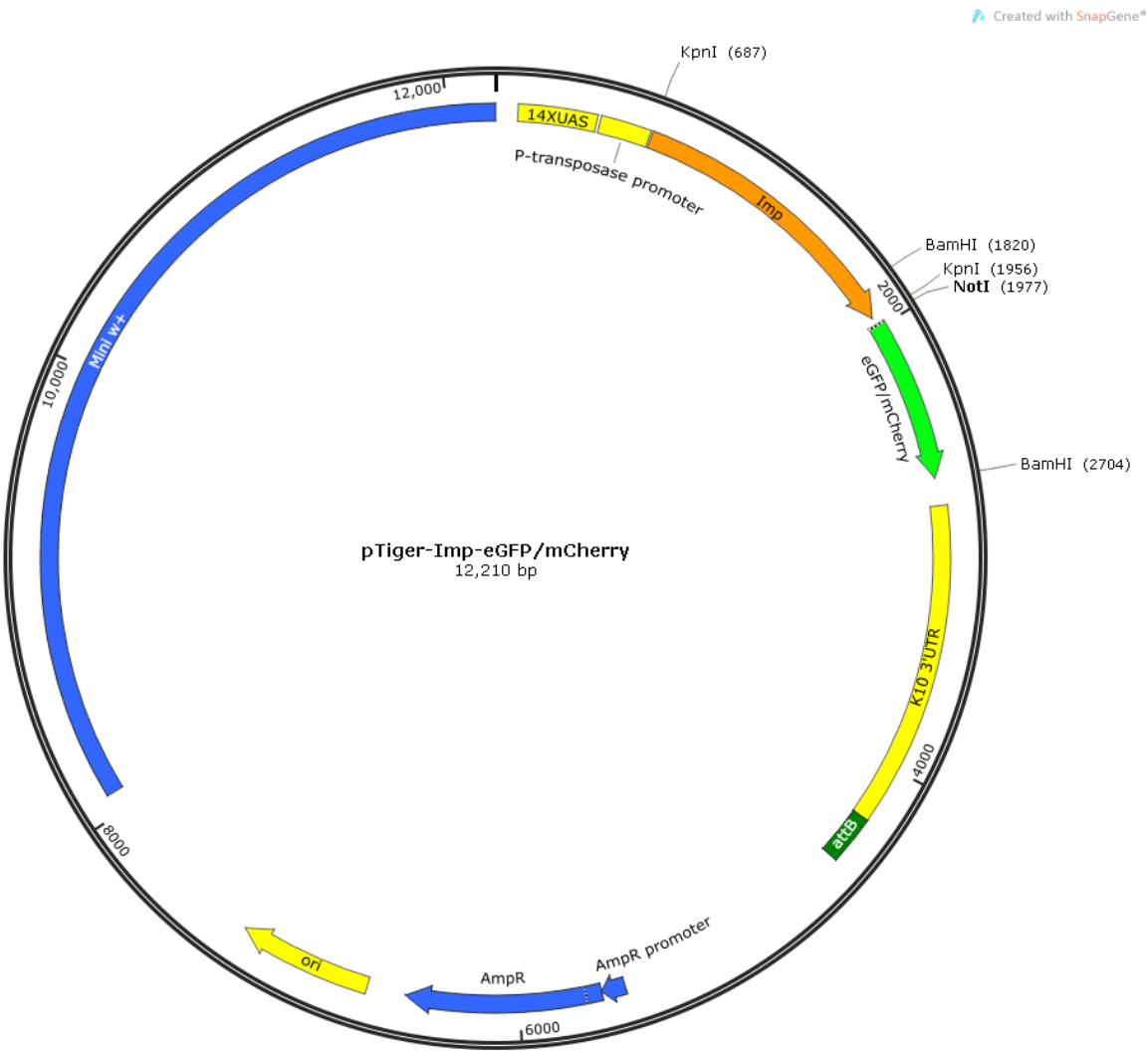

An identical cloning strategy was used to fluorescently-tag Imp, Hrp48 and PTB at their C-terminal end. The coding region of Imp was amplified from cDNA, while Hrp48 and PTB were PCR amplified using plasmid templates containing their coding regions. KpnI restriction sites were introduced at both the 5' and 3' ends of the coding sequences and they were ligated into both pTiger-eGFP and –mCherry via KpnI.

Appendix 5: Fly Stocks used in this project

Genotype	From	Reference
Haemocyte-specific Gal4 drivers		
w; serpent-Gal4 (*srp*Gal4)	Gift from Will Wood, University of Bristol	Brückner *et al*. 2004
w; serpent-Gal4, UAS-eGFP	Gift from Will Wood, University of Bristol	Brückner *et al*. 2004 ; Yeh *et al*. 1995
w; serpent-Gal4, UAS-mCherry-moesin	Gift from Will Wood, University of Bristol	Brückner *et al*. 2004; Millard & Martin. 2008
w; serpent-Gal4, UAS-eGFP-moesin (GMA)	Gift from Will Wood, University of Bristol	Brückner *et al*. 2004; Dutta *et al*. 2002
w; croquemort-Gal4, UAS-eGFP-moesin	Gift from Will Wood, University of Bristol	Stramer *et al*. 2005 ; Dutta *et al*. 2002
w; serpent-Gal4, UAS-eGFP; *croquemort*-Gal4, UAS-eGFP	Gift from Will Wood, University of Bristol	Brückner *et al*. 2004 ; Stramer *et al*. 2005
w; serpent-Gal4, UAS-mCherry-moesin; *croquemort*-Gal4, UAS-mCherry-moesin	Gift from Will Wood, University of Bristol	Brückner *et al*. 2004; Millard & Martin 2008
w; serpent-Gal4, UAS-eGFP-moesin; *croquemort*-Gal4, UAS-eGFP-moesin	Generated in lab from existing stocks – see methods	Brückner *et al*. 2004 ; Stramer *et al*. 2005
w; serpent-Gal4, UAS-Clip170; *Dr*/TM6B*dfd*	Gift from Will Wood, University of Bristol	Stramer *et al*. 2010
w; serpent-Gal4::VP16	Constructed in this thesis	Design based on Brückner *et al*. 2004
Border cell-specific Gal4 drivers		
*w; slowbordercells(slbo-)*Gal4/CyO	Gift from Daimark Bennett, University of Liverpool	Rørth *et al*. 1998
w; slbo-Gal4, UAS-CD8::eGFP/CyO	Gift from Daimark Bennett, University of Liverpool	Rørth *et al*. 1998
w;; slbo-lifeAct::eGFP	Bloomington Stock 58364	Riedl *et al*. 2008; Cai *et al*. 2014
Maternal Gal4 drivers		

w; P(mat-tub-GAL4)mat67	Bloomington Stock 7062	Bossing *et al*. 2002; Staller *et al.* 2013.
w;; P(mat-tub-GAL4),mat67	Bloomington Stock 7063	Bossing *et al*. 2002; Staller *et al.* 2013.
UAS-driven transgenes (fluorescently-labelled RBPs & MS2 System reagents)		
w; UAS-eGFP-PTB	Constructed in this thesis	Design based on Besse *et al*. 2009
w; UAS-PTB-eGFP	Constructed in this thesis	Tested in this project
w;;UAS-PTB-eGFP	Constructed in this thesis	Tested in this project
w;;UAS-Hrp48-mCherry	Constructed in this thesis	Tested in this project
w;;UAS-Hrp48-GFP	Constructed in this thesis	Tested in this project
w;;UAS-Imp-mCherry	Constructed in this thesis	Tested in this project
w;;UAS-Imp-GFP	Constructed in this thesis	Tested in this project
w;;UAS-GFP-Imp	Gift from Florence Besse, Institute of Biology Valrose (Nice)	Medioni *et al*. 2014
w; UAS-NLS-MCP-mCherry	Constructed in this thesis	Tested in this project
w; UAS-NLS-MCP-eGFP	Constructed in this thesis	Tested in this project
w; UAS-NLS-tandemMCP-mCherry	Constructed in this thesis	Tested in this project
w; UAS-NLS-tandemMCP-eGFP	Constructed in this thesis	Tested in this project
w;;UAS-18x hairpin MS2 binding sites-*actin42a*	Constructed in this thesis	Tested in this project
w;;UAS-18xMS2-*actin5c*	Constructed in this thesis	Tested in this project
w;; UAS-18xMS2-*arp14D*	Constructed in this thesis	Tested in this project
w;;UAS-18xMS2-*arp66B*	Constructed in this thesis	Tested in this project
w; UAS-βPS-integrin (Myospheroid)	Gift from Will Wood, University of Bristol	Martin-Bermudo & Brown 1996
RNAi lines		
w; if/CyO; Walium20-PTB	Generated in SLQ lab	Unpublished
w; Walium20-PTB; TM3*sb*/TM6B	Generated in SLQ lab	Unpublished

w; Walium20-PTB; Walium20-PTB	Generated in SLQ lab	Unpublished
w; if/CyO; Walium22-Hrp48	Generated in SLQ lab	Unpublished
w; Walium22-Hrp48; TM3*sb*;TM6B	Generated in SLQ lab	Unpublished
w; if/CyO; Walium22-Hrp48	Generated in SLQ lab	Unpublished
w; if/CyO; Walium22-Imp	Generated in SLQ lab	Unpublished
w; Walium22-Imp; Walium22-Imp	Generated in SLQ lab	Unpublished
w;; Walium22-Sexlethal	Generated in SLQ lab	Unpublished
w; if/CyO; Valium20-Imp	Bloomington Stock Center (BL34977)	TRiP RNAi Project (HMS01168)
w; if/CyO; Valium20-Hrp48	Bloomington Stock Center (BL33716)	TRiP RNAi Project (HMS00597)
w;; Imp-GD	Vienna *Drosophila* RNAi Center (VDRC) Stock Center	VDRC Stock Center (20321)
w; Hrp48-KK	VDRC Stock Center	VDRC Stock Center (101555)
w;; Hrp48-GD	VDRC Stock Center	VDRC Stock Center (16041)
w;; Valium20-Cdc42	Bloomington Stock Center (BL35756)	TRiP RNAi Project (HMS01502)
W;; Valium20-Rac1	Bloomington Stock Center (BL34910)	TRiP RNAi Project (HMS01258)
Mosaic analysis with a repressible cell marker (MARCM) stocks		
w-FRT19A, hs-Flp*, tub*-Gal80	Gift from Florence Besse, Institute of Biology Valrose (Nice)	Xu & Rubin 1993.
w-FRT19A	Gift from *Joaquín* de Navascués, Cardiff University	Medioni *et al*. 2014
w-FRT19A, imp^{8}	Gift from Florence Besse, Institute of Biology Valrose (Nice)	Medioni *et al*. 2014
w-FRT19A, imp^{7}	Gift from Florence Besse, Institute of Biology Valrose (Nice)	Medioni *et al*. 2014

Protein trap lines			
Fly stock identifier	**Gene trapped**	**From**	**Reference**
CPTI 00030	*heph* (PTB)	Cambridge Protein Trap Project	Lowe *et al.* 2014 http://www.flyprot.org/
CC00664	*heph* (PTB)	Spradling Lab, Carnegie Institute, Washington	Besse *et al*. 2009
CPTI 4117	*imp*	Cambridge Protein Trap Project	Lowe *et al.* 2014 http://www.flyprot.org/
G80	*imp*	Cooley Lab, Yale, USA	Quiñones-Coello *et al*. 2007

Appendix 6: Western blot to detect β-integrin in S2R+ cells

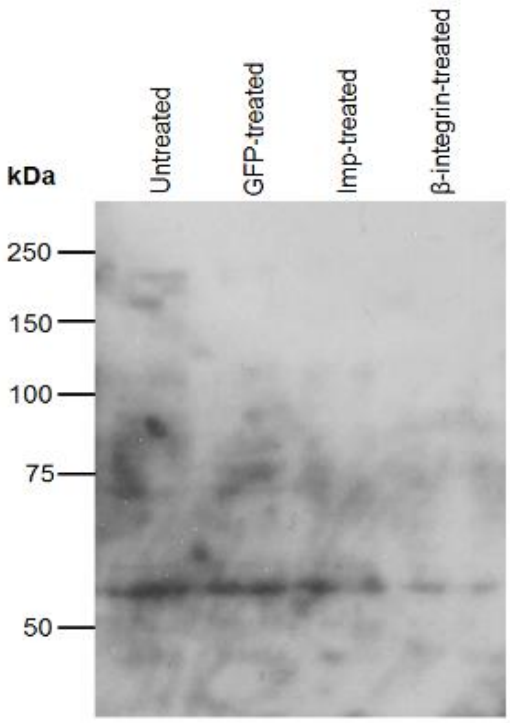

Appendix 6: Western blot to detect β-integrin
Western blots were carried out with anti-β-integrin (1:50 dilution) to detect β-integrin levels in dsRNA treated S2R+ cells. The predicted size of β-integrin is 90kDa. Each S2R+ cell extract was generated using a total of 750,000 cells. Anti-hrp secondary antibody was used at a 1:3000 dilution. No clear bands were detectable in the 90kDa range.

Appendix 7: qPCR fold-change values of RNA-immunoprecipitations

RNA-immunoprecipitation from whole embryos:

Replicate 1: Fold change in Imp-GFP & MCP-GFP relative to wt in haemocytes			
Gene	**wt**	**Imp-GFP**	**MCP-GFP**
rp49	1	0.69	0.36
H2A	1	0.77	0.08
actin42A	1	0.72	0.74
β-integrin (*mys*)	1	0.06	0.04
profilin	1	0.95	0.86
arp2	1	0	0
arp3	1	0.13	0.1

Replicate 2: Fold change in Imp-GFP & MCP-GFP relative to in haemocytes			
Gene	**wt**	**Imp-GFP**	**MCP-GFP**
rp49	1	8.94	1.9
H2A	1	11.96	5.71
actin42A	1	10.85	6.68
β-integrin (*mys*)	1	5.33	6.79
profilin	1	0.82	0.95
arp2	1	2.03	0.82
arp3	1	2.4	1.19

RNA-immunoprecipitation from ovaries:

Replicate 1: Fold change in Imp-GFP & MCP-GFP relative to wt in ovaries				
Gene	**wt**	**Imp-GFP**	**PTB-GFP**	**MCP-GFP**
rp49	1	10.73	7.66	3.48
H2A	1	77.17	80.08	7.09
tubulin67C	1	23.48	32.37	0.92
bicoid	1	101.83	206.26	53.32
oskar	1	52.59	672.47	5.84
gurken	1	33.67	135.92	2.37
act42A	1	18.85	74.72	1.09
profilin	1	1.02	0.53	0.93

Replicate 2: Fold change in Imp-GFP & MCP-GFP relative to wt in ovaries				
Gene	**wt**	**Imp-GFP**	**PTB-GFP**	**MCP-GFP**
rp49	1	2.49	18.17	2.28
H2A	1	5.66	2.92	2.43
tubulin67C	1	0.93	1.21	1.48
bicoid	1	0.07	108.38	3.08
oskar	1	3.53	464.65	2.27
gurken	1	6.39	11.63	1.19
act42A	1	4.52	16.45	2.26
profilin	1	0.90	0.91	0.55

END